UNIVERSITA' VITA-SALUTE SAN RAFFAELE

CORSO DI DOTTORATO DI RICERCA INTERNAZIONALE IN MEDICINA MOLECOLARE

CURRICULUM IN NEUROSCIENZE E NEUROLOGIA SPERIMENTALE

INVESTIGATING HEALTHY AND PATHOLOGICAL AGING THROUGH MULTIMODAL MRI CONNECTOMICS

DoS: Prof.ssa Federica Agosta

Second Supervisor: Prof. Jorge Sepulcre

Tesi di DOTTORATO di RICERCA di Camilla Cividini

matr. 013830

Ciclo di dottorato XXXIV

SSD MED/26

Anno Accademico 2020/2021

CONSULTAZIONE TESI DI DOTTORATO DI RICERCA

Il/la sottoscritto/*I*	CAMILLA CIVIDINI
Matricola/*registration number*	013830
nata/ *born at*	PONTE SAN PIETRO (BG)
il/*on*	22-03-1991

autore della tesi di Dottorato di ricerca dal titolo / *author of the PhD Thesis titled*

INVESTIGATING HEALTHY AND PATHOLOGICAL AGING THROUGH MULTIMODAL MRI CONNECTOMICS

☐ AUTORIZZA la Consultazione della tesi / AUTHORIZES *the public release of the thesis*

X NON AUTORIZZA la Consultazione della tesi per …… mesi /DOES NOT AUTHORIZE *the public release of the thesis for …… months*

a partire dalla data di conseguimento del titolo e precisamente / *from the PhD thesis date, specifically*

Dal / *from* ……/……/……   Al / *to* ……/……/……

Poiché /*because*:

☐ l'intera ricerca o parti di essa sono potenzialmente soggette a brevettabilità/ *The whole project or part of it might be subject to patentability;*

X ci sono parti di tesi che sono già state sottoposte a un editore o sono in attesa di pubblicazione/ *Parts of the thesis have been or are being submitted to a publisher or are in press;*

☐ la tesi è finanziata da enti esterni che vantano dei diritti su di esse e sulla loro pubblicazione/ *the thesis project is financed by external bodies that have rights over it and on its publication.*

Si rende noto che parti della tesi sono indisponibili in relazione all'utilizzo di dati tutelati da segreto industriale **(da lasciare solo se applicabile)** /*Please Note: some parts of the thesis are not available in relation to the norm of the use of information protected by trade secret **(To leave only if relevant)***

E' fatto divieto di riprodurre, in tutto o in parte, quanto in essa contenuto / *Copyright the contents of the thesis in whole or in part is forbidden*

Data /Date 31/01/2022   Firma/Signature   *Camilla Cividini*
.

DECLARATION

This thesis has been composed by myself and has not been used in any previous application for a degree. Throughout the text I use both 'I' and 'We' interchangeably.

All the results presented here were obtained by myself, except for:

1. Basaia, et al., Neurology 2020; Cividini et al., Neurology 2021; and the preliminary study reported in Chapter 4.2: Patient recruitment has been performed by Dr. Riva, Dr. Magnani and collaborators, Department of Neurology; and the MRI acquisition in collaboration with Prof. Falini and his group, Department of Neuroradiology, San Raffaele Scientific Institute, Vita-Salute San Raffaele University, Milan, Italy.

2. Basaia et al., Neurology 2020: Contribution to patient recruitment performed by Prof. Chiò and collaborators, Rita Levi Montalcini Department of Neuroscience, ALS Center, University of Turin, Turin, Italy; Prof. Tedeschi and collaborators, Università degli Studi della Campania "Luigi Vanvitelli", Naples, Italy.

3. The studies reported in Basaia et al., Neurology 2020 and Cividini et al., Neurology 2021 are the results of a joint effort with Dr Edoardo Gioele Spinelli, another PhD candidate at University Vita-Salute San Raffaele. Although study design and manuscript drafting were performed by both candidates, Dr Spinelli (neurologist) was mostly focused on data acquisition and analysis and critical interpretation of results in a clinical context, whereas I gave my contribution as a bioengineer for developing and performing MRI post-processing and statistical analysis.

All sources of information are acknowledged by means of reference.

ABSTRACT

Neurodegenerative disorders and aging share two main characteristics: an insidious progression and a selective predilection in the breakdown of specific brain regions. Irreversibility and steady progression of clinical manifestations are also common features between brain aging and neurodegenerative conditions. The most recent evidence suggests that selective regional vulnerability exists and defines the clinical features of different neurodegenerative diseases, as well as aging seems to affect specific brain regions paving the way (additive effect) to the onset of neurodegenerative diseases. Recent magnetic resonance imaging (MRI) advanced techniques, including diffusion tensor imaging and resting state functional MRI, allow to explore the role of structural and functional alterations in aging and neurodegenerative diseases and to shed light on the interplay between healthy aging and pathological conditions.

In this thesis, firstly I have applied graph theory-based approaches and connectomics to explore brain structural and functional changes across Frontotemporal dementia – amyotrophic lateral sclerosis (FTD-ALS) spectrum, as a model of neurodegeneration, with the goal of mapping spatiotemporal patterns of degeneration in these conditions. In the second part, I moved the focus on healthy aging to identify structural and functional brain signs of vulnerability.

Results within the FTD-ALS spectrum revealed a considerable motor and extra-motor network degeneration in ALS patients and an even more widespread damage in primary lateral sclerosis patients. Moreover, a maladaptive role of functional rearrangements in ALS with cognitive/behavioral impairment concomitantly with similar structural alterations compared to ALS cognitively normal was found when I investigated the neural correlates of cognitive impairment. This seems to support the hypothesis that ALS with cognitive/behavioral impairment might be considered as a phenotypic variant of ALS, rather than a consequence of disease worsening. Focusing on the role played by aging, our findings showed potential functional and structural pattern of vulnerability. Finally, the application of a recent technique to investigate white matter integrity using the NODDI model in a cohort of young and older adults showed that the fibers of frontal regions are characterized by greater damage and are the most vulnerable to aging, followed by the parietal and temporal fibers.

Taken together, our studies suggest that the assessment of network connectivity through graph-based analyses, connectomics and novel diffusion MRI model in aging and neurodegenerative disorders is useful in order to answer the question of whether neurodegeneration-related patterns of damage represent accelerated aging or a distinct process.

TABLE OF CONTENTS

ACRONYMS AND ABBREVIATIONS

AD=Alzheimer's disease; ALS=amyotrophic lateral sclerosis; ALS-cn= amyotrophic lateral sclerosis cognitively normal; ALS-ci= amyotrophic lateral sclerosis with cognitive impairment; ALS-bi= amyotrophic lateral sclerosis with behavioral impairment; ALS-cbi= amyotrophic lateral sclerosis with cognitive and behavioral impairment; ALSFRS-R= ALS functional rating scale revised; bvFTD= behavioral variant of frontotemporal dementia; CSF= cerebrospinal fluid; DLB= dementia with Lewy bodies; DMN= default mode network; DT= diffusion tensor; DTI= diffusion tensor imaging; FA= fractional anisotropy; fMRI= functional magnetic resonance imaging; FTD= frontotemporal dementia; FTLD= frontotemporal lobar degeneration; HC= healthy controls; ICVF= intra-cellular volume fraction; ISO= isotropic water diffusion; LMN= lower motor neuron; MD= mean diffusivity; MND= motor neuron disease; MRI= magnetic resonance imaging; NBS= network based statistics; NFT= Neurofibrillary tangles (; NODDI= Neurite orientation dispersion and density imaging; ODI= orientation dispersion index; PLS= primary lateral sclerosis; PMA= progressive muscular atrophy; PPA= primary progressive aphasia; RS fMRI= resting-state functional magnetic resonance imaging; SD= semantic dementia; SFC= stepwise functional connectivity; UMN= upper motor neuron; VBM= voxel=based morphometry.

1. AGING AND NEURODEGENERATIVE DISEASES

1.1 AGING

As the elderly population is increasing, aging itself constitutes a consistent burden, becoming a challenge to societies worldwide and a greatest risk factor for a majority of chronic diseases (Kennedy *et al*, 2014). Trends show that life expectancy has almost doubled in the last 150 years. About 10% of the population was 65 or older in the mid-1950s, with only 1-3% being older than 80 (Atella *et al*, 2019), while in the last 60 years, in countries like Italy, the proportion of elderly people (>65 years old) has more than doubled (21.5%), and it is predicted to reach the 33% in 2050 tripling the proportion of the 85+ (5.9%), which will become the 14% in the mid-2050s (Atella *et al.*, 2019).

Aging is characterized by molecular and physiological deregulations that are often accompanied by subsequent pathological consequences such as diabetes, cancer, cardiovascular and among others neurodegenerative diseases. It seems therefore critical to understand the events of the aging process. Unsurprisingly, a key challenge in current research is to understand and recognize aging determinants, along with defining its characteristics and biomarkers (Flatt & Partridge, 2018).

Accordingly, this chapter will focus on the molecular and physiological alterations in aging and specifically the cellular markers in brain aging. Then, the focus will be on cognitive decline as aging-related effect, risk and protective factors in aging and, finally, changes observed in neuroimaging studies, to define the structural and functional magnetic resonance imaging (MRI) key features that follow elderly's brains. The recognition of such features may pave the way toward a deeper understanding of brain aging and hence of what might arise in concomitance with such complex process, notably neurodegenerative diseases, that will be explored in the second part of this chapter.

1.1.1 Biological Aging

Several molecular regulatory processes that have major effects on longevity and influence the structural and functional changes with advancing age, have been well-established and comprehensively synthesized by López-Otin et al. as the 'hallmarks of aging' (Lopez-Otin *et al*, 2013). These are common cellular and molecular denominators contributing to the aging process that together determine the aging phenotype. The hallmark phenomena are in some way intermingled with the processes that occur in neurodegeneration and probably represent the groundwork of age-related

neurodegenerative diseases. These nine hallmarks are categorized into primary, antagonistic and integrative hallmarks (Figure 1).
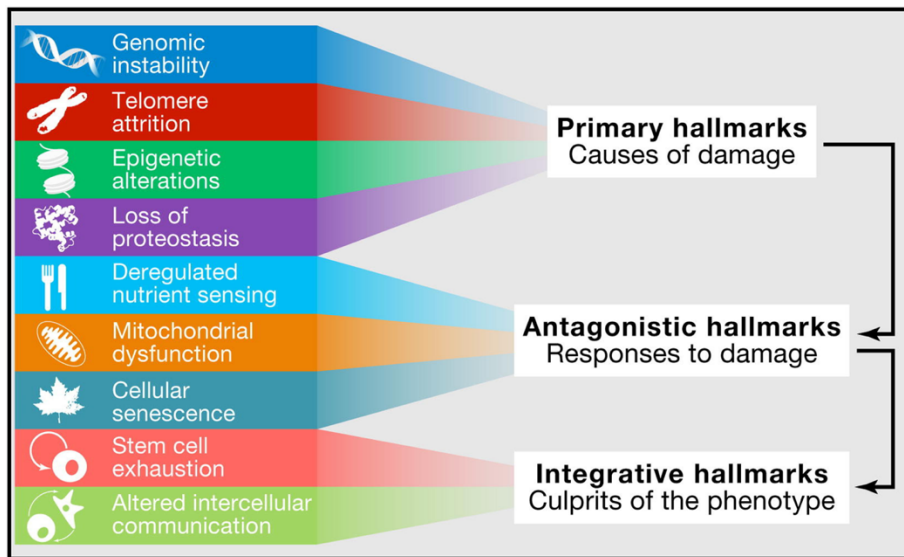
Figure 1. Functional Interconnections between the Hallmarks of Aging. The proposed nine hallmarks of aging are grouped into three categories. In the top, those hallmarks considered to be the primary causes of cellular damage. In the middle, those considered to be part of compensatory or antagonistic responses to the damage. These responses initially mitigate the damage, but eventually, if chronic or exacerbated, they become deleterious themselves. In the bottom, there are integrative hallmarks that are the result of the previous two groups of hallmarks and are ultimately responsible for the functional decline associated with aging. Figure from (Lopez-Otin *et al.*, 2013).

Primary hallmarks of aging

Genomic instability. It refers to high-frequency mutations within the genome. Progressively, genomic instability might trigger neuronal death, accelerate aging, and increase susceptibility to age-related neurodegenerative diseases. Indeed, oxidative damages are believed to be early events in Alzheimer's disease (AD), promoting the hyperphosphorylation of tau and mitochondrial dysfunction, leading to the formation of NFTs, a known pathological signature of AD (Bhatia & Sharma, 2021;Luque-Contreras *et al*, 2014).

Telomere attrition. It is a natural mechanism whereby cells in our body shorten at each cell division, up to the point where a limit is reached (Hayflick's limit), triggering cellular senescence. Since microglial cells retain the ability to undergo cell divisions in adulthood, they are therefore more susceptible to this process. The microglial senescent phenotype implies loss of neuroprotection, thus favoring neuronal degeneration. This

might play a role in NFT deposition and the so-called amyloid/neuroinflammation cascade hypothesis in AD (Bussian *et al*, 2018; Streit *et al*, 2021).

Epigenetic alterations. Epigenetic changes may occur in genes involved in protein folding and metabolism, as well as in the regulation of cytokines release and microglia, that have a role in the inflammation processes. There is emerging evidence that many genes involved in neurodegeneration also undergo this type of influence.

Loss of proteostasis. The balance between protein synthesis and degradation is the most intriguing observation, and probably the molecular cornerstone underlying neurodegeneration. Impaired regulation of protein homeostasis underlies the abnormal deposition of aggregated hyperphosphorylated tau, β-amyloid, α-synuclein, the nuclear to cytoplasmic translocation of TDP-43 and the formation of neural inclusions (e.g., NFT, Lewy bodies, amyloid plaques) in older individuals. This consideration has led to prototyping most neurodegenerative diseases as proteinopathies (protein aggregation syndromes) (Bourdenx *et al*, 2017).

Antagonistic hallmarks of aging

The antagonistic hallmarks are thought to be at initial phase compensatory responses but then become antagonistic and deleterious.

Deregulated nutrient sensing and altered metabolism. Dysregulated metabolism promotes the aging processes and represents major risk factors for the development of the neurodegenerative diseases associated with aging (Johnson & Stolzing, 2019).

Mitochondrial dysfunction. It is the major and early contributor of the aging process. As stated in the "free radical theory" of aging (Barja, 2014), the gradual accumulation of damage during aging is primarily driven by dysfunctional mitochondria, responsible for cellular energy deficit, production of reactive oxygen species, and progressive accumulation of free radicals. Moreover, degradation of dysfunctional mitochondria has received particular attention because of its key role in preventing age-related disease(Arotcarena *et al*, 2019; Fivenson *et al*, 2017). In the context of neurodegeneration, oxidative stress triggers compensatory mechanisms, that may fail turning into pathological processes.

Cellular senescence. This mechanism implies an arrest in the stress-induced stable cell cycle. It aims at maintaining survival of healthy cells and removing damaged cells

by autophagy. Age-dependent functional decline of autophagy is thought to give a significant contribution towards disease development and/or progression (Klaips *et al*, 2018). For instance, the impaired autophagy of Aβ plaques and tau tangles is present in the pathogenesis of AD and frontotemporal dementia (FTD), favoring protein aggregation (Wong *et al*, 2020).

Integrative hallmarks of aging

Integrative hallmarks arise because of cumulative damage induced by the primary and antagonistic hallmarks and are ultimately responsible for the functional cellular decline associated with aging.

Altered intercellular communication and inflammation. An important feature of the aging process is a chronic progressive increase in the proinflammatory status, originally called "inflamm-aging" (Franceschi *et al*, 2000). The sustained elevation of inflammation exacerbates tau phosphorylation, Aβ deposition, and both α-synuclein truncation and aggregation (Chen *et al*, 2016).

Stem cells exhaustion. The progressive decline in stem cell function and proliferative capacity over the lifespan plays a major role in the majority of body tissues that progressively lose their ability to repair damage through replication. Such process occurs, although less persistently, in the brain.

1.1.2 Brain aging

There are several effects of aging in the brain, which like our whole body, changes as we age. One of the most prevalent cellular changes is deposition of beta-amyloid (Aβ) plaques in many brain regions (Rodrigue *et al*, 2012). Aβ is a protein fragment that is deposited on the brain in the form of sticky, starch-like plaques, which can be found in the brains of elderly individuals who are not even cognitively impaired (Mufson *et al*, 2016). Amyloid PET studies have found Aβ aggregates in the frontal and parietal cortex, precuneus, and posterior cingulate gyrus approximately in 20–30% of healthy elderly (Rodrigue *et al.*, 2012). Aβ aggregates are a characteristic feature of all patients with AD and, in subjects with mild cognitive impairment, it is an important predictor for the conversion to AD (Rodrigue *et al*, 2009). In addition,

microstructural brain alterations are routinely observed in elderly brains. These include deposition of substances, tissue alterations and characteristic lesions in brain parenchyma. For instance, a significant increase in the level of iron, which plays an important role in myelination and remyelination, has been shown in aging (Kennedy & Raz, 2015). Indeed, the accumulation of free iron in brain structures causes axonal injury and accelerates cellular apoptosis (Kennedy & Raz, 2015). As a consequence, other brain changes such as brain shrinkage and white matter damage occur in conjunction with iron depositions. Among all, white matter lesions are the most frequent alterations encountered in elderly brains. Their prevalence in elderly individuals can range from 5% to above 90% and their origin is thought to be linked to vascular and ischemic changes (Grajauskas *et al*, 2019). Furthermore, detection of "micro-scale" changes of a microvascular nature has been reported with advancing age, including dilated perivascular spaces, micro-infarcts (tiny areas of necrotic tissue due to ischemia), microbleeds (brain areas of blood break-down products) and lacunes (fluid-filled cavities due to an occlusion or atherosclerosis) (Grajauskas *et al.*, 2019).

If we evaluate changes in brain at a macroscopic level, the most common and widely recognized sign is atrophy. Brain atrophy results from a reduction of brain parenchymal tissue volume and comes with several associated morphological variations. Most studies of post-mortem human brains indicate that after 60 years of age there is a consistent loss of brain tissue (Ho *et al*, 1980). It has been shown that brain weight loss occurs after the third and fourth decades of life, with a rate of 0.1–0.2% per year from college age onward and increases at about 0.3–0.5% per year in the 70s (Esiri, 2007). Brain volume reduction is associated with mild sulcal widening, gyral narrowing, and mild blunting of the lateral ventricular angles. Moreover, tissue loss leads to a consequential enlargement of ventricles, sulci, and other cerebrospinal fluid spaces. The loss in brain weight and brain shrinkage can be addressed to structural alterations of both gray matter and white matter. Alterations in gray matter result most likely from significant reductions in the mean dendritic diameters and dendritic spine densities, and from a loss of synapses and dendrites in neuronal cells (Benavides-Piccione *et al*, 2013). White matter density also declines with age explaining by the less efficient myelin production by oligodendrocytes with aging, resulting in thinner myelin sheaths and shorter internodes (Marner *et al*, 2003).

1.1.3 Cognitive decline

Loss of synapses along with impairment in function of the remaining ones are important contributors to age-related cognitive decline. However, age-related worsening in mental abilities is nonetheless highly variable. Indeed, it is well-established that some cognitive capacities decline significantly with age while others are quite spared. The main functions that suffer a worsening of the performances during aging regard information processing (e.g., attention, perception, short-term memory) (Park & Reuter-Lorenz, 2009) and, definitively, the processing speed along with working memory function which translates into motor slowdown and decision-making tasks (Eckert *et al*, 2010). To these are added other aspects as executive or control processes (e.g., inhibitory functions, set shifting, monitoring), which become less efficient over time, probably due to a decline in attentional resources (Stuss & Craik, 2019). On the other hand, other aspects of cognitive function such as implicit memory, knowledge storage, vocabulary, information, and comprehension are protected and relatively resistant to cognitive aging (Park & Reuter-Lorenz, 2009).

The variability and discrepancies of cognitive decline in aging might be explained by the concept of "reserve", defined as the capacity to preserve cognitive function (Groot *et al*, 2018). The "brain reserve" can be divided into two main components: the cognitive reserve and the brain reserve. Cognitive reserve acts by recruiting alternate neural networks or existing networks more efficiently to deal with the normal cognitive decline and it usually derived from educational gain. Meanwhile, brain reserve represents a higher quantity of neural resources to better tolerate aging or emerging neuropathology (Groot *et al.*, 2018).

1.1.4 Risk and Protective factors in aging

Lifestyle, sociodemographic, behavioral and genetic factors have been suggested as impacting elements on the course of age-related neural changes. Such factors may help in contributing to a qualitative better aging, also defined as "successful aging" (Urtamo *et al*, 2019) and provide means that slow, delay, or prevent age-related diseases.

These factors can be classified in those with a detrimental effect, favoring pathological changes in the brain and cognitive decline, and those with a protective role a "successful aging". The first are cardiovascular risk factors (i.e., hypertension, diabetes, and obesity), psychosocial factors (i.e., depression and social isolation), and unhealth behaviors (i.e., physical inactivity, smoking, alcohol abuse) (Kralj *et al*, 2018). Among non-modifiable risk factors APOE allelic ε4 variant, known to be a genetic risk factor for AD, is more associated with higher memory decline in the elderlies even in the absence of cognitive impairment (Brathen *et al*, 2021). On the other side of the coin, protective factors include diet and caloric restriction appears as the most successful interventions to extend lifespan and prevents age-associated diseases. Dietary restriction ameliorates brain aging by downregulating oxidative stress, upregulating anti-inflammatory responses, promoting neurogenesis, and increasing synaptic plasticity (Fusco & Pani, 2013). Performing physical activity has positive effects on cognitive functions. The explanation of such neuroprotective role in brain effects lies on several underlying mechanisms, including increased brain blood flow, angiogenesis, immune regulation, and induction of neurotrophic factors, contrasting grey matter loss and white matter lesions formation (Domingos *et al*, 2021). Furthermore, cognitive reserve allows to counteract the age-related cognitive decline and to mitigate the cognitive impairment caused by brain pathology (Stern *et al*, 2019). Therefore, high-level education and midlife and late-life cognitive stimulation have undoubtedly a positive impact on aging effects (Stern *et al.*, 2019).

1.1.5 Imaging

Neuroimaging has significantly contributed to understand the process of brain aging, allowing us to track and assess changes during normal aging and neurological conditions (Grajauskas *et al.*, 2019). Among neuroimaging techniques, MRI is nowadays the most widely available imaging modality, thanks to its properties of non-invasiveness, cost-effectiveness, and in vivo applicability.

Structural MRI allows to study grey matter integrity. In particular, grey matter changes are usually assessed by using probabilistic (i.e., voxel- based morphometry, VBM) or quantitative tools (i.e. cortical thickness). Morphological studies, which investigated grey matter changes on T1-weighted scans by using the aforementioned techniques, showed a

linear age-related brain volume reduction across the entire brain (Good *et al*, 2001). A consistent result is that age-related morphometric changes are widespread across the cortex, although there are specific regions with a major and non-linear grey matter losses over time (Terribilli *et al*, 2011). Gray matter decline appears more prominent in frontal, parietal and temporal lobes, specifically in inferior prefrontal cortex, insula, superior parietal gyrus, and supramarginal gyrus, central and cingulate sulci and insular areas than in other cortical areas (Salat *et al*, 2004) (Bourisly *et al*, 2015; Galluzzi *et al*, 2008). In addition, substantial evidence showed a linear and slow decline in amygdala, thalamus, nucleus accumbens and caudate, whereas the atrophy rates accelerate at older ages in other brain regions, especially entorhinal cortex, hippocampus, putamen and precentral gyrus (Grajauskas *et al.*, 2019). Furthermore, a longitudinal study investigating changes over time in a cohort of 66 older adults with a mean follow up of 8 years highlighted that frontoparietal regions exhibit greater rates of decline than temporal and occipital regions, supporting the hypothesis of the anterior-posterior gradient of cortical thinning (Thambisetty *et al*, 2010).

When investigating the functional behavior of human brain, functional MRI (fMRI) is one of the most used imaging methods with the advantage to be an indirect and non-invasive technique in comparison with other functional neuroimaging exams. fMRI is based on the measurement of fluctuations in blood flow and BOLD (blood-oxygenation level dependent) contrast, exploiting the paramagnetic properties of the blood. The assessment of functional activity in resting condition (resting-state fMRI (RS fMRI)) has provided important insights into brain functional organization and revealed age-related connectivity changes in the brain. The most consistent finding across all studies is the reduction of functional connectivity in regions of the default mode network (DMN) in older adults compared to younger adults (Damoiseaux *et al*, 2007). The regions of this large-scale brain network are primarily the medial prefrontal cortex, posterior cingulate cortex/precuneus and angular gyrus, as well as additional subsystems, including medial temporal structures (Buckner *et al*, 2008). Of note, in older adults, the reduced functional connectivity in the DMN regions was found associated with lower episodic memory, executive function and processing speed scores, reinforcing the hypothesis that brain normally loses functional integrity during advanced aging (Esposito *et al*, 2008) (Staffaroni *et al*, 2018). Furthermore, anterior regions of the DMN appear more

12

susceptible than posterior regions; for instance, the medial prefrontal cortex shows lower activation than other regions of the DMN alongside aging (Galiano *et al*, 2020).

Age-related differences in functional connectivity have also been observed in other brain networks such as the salience, dorsal attention and sensorimotor networks (Damoiseaux, 2017; Onoda *et al*, 2012)(Damoiseaux, 2017). These networks are responsible for communication and social behavior (Menon, 2015), attention and working memory (Zhou *et al*, 2018), motor and coordinating tasks, respectively. Both the salience and dorsal attention networks appear to have a diminished functional connectivity strength with advancing age (Ferreira & Busatto, 2013; Li *et al*, 2020; Tomasi & Volkow, 2012) (Oschmann & Gawryluk, 2020). An opposite trend was observed in networks involved in primary information processing, such as the sensorimotor and visual, where the functional connectivity was even found increased with age (Li *et al.*, 2020).

Such findings suggest a general trend in functional connectivity characterized by a decrease within networks along with an increase inter networks to maintain the efficient communication implementing compensatory mechanisms as well as dedifferentiation processes.

1.2 THE LINK BETWEEN AGING AND NEURODEGENERATION

The aging process itself is by far one of the most impacting among the many predisposing factors for neurodegeneration. Given that neurodegenerative dementia is especially common in old individuals, the hypothesis that brain aging might form a continuum with neurodegeneration has been considered. Gowers in 1902 (Gowers, 1902) explained for the first time what is degeneration and devised a new term "abiotrophy", which identified a lack of "vital endurance". However, this hypothesis arises a question: if the human being lived another 50 years beyond the current expectation, would all nervous structures show the changes of neurodegenerative disease? The answer is probably "no", as there are distinctive cellular and subcellular features of degenerative diseases that are different from the programmed loss of cells that is due to aging. On one hand, neurodegenerative mechanisms could be interpreted as a manifestation of accelerated aging, on the other hand they might be determined by a substrate of genetic and environmental factors, and thus the divergency from physiological aging. The question of whether characteristic cellular and subcellular features represent lesser

aspects of brain aging or whether they are the harbingers of neurodegenerative diseases remains largely unexplained (Wyss-Coray, 2016). Therefore, the goal here is to detect what is the link and why aging is the most prominent risk factor associated with neurodegenerative dementia.

Neurodegenerative diseases and aging have two common characteristics: a relentless progression and a selective preference in the breakdown of specific brain regions (Han, 2009). Indeed, regional vulnerability defines the clinical features of different neurodegenerative diseases; similarly, specific brain alterations provide different cognitive decline in aging. Evidently, these two shared features identify different consequences, which are the extremes of a demarcation zone between a physiological and pathological process. However, the separation line is shadowy since the aging and the neurodegenerative processes are intermingled.

1.3 FRONTOTEMPORAL LOBAR DEGENERATION

1.3.1 FRONTOTEMPORAL DEMENTIA

FTD is an umbrella term that included several neurodegenerative syndromes and neuropathologically heterogeneous disorders characterized by progressive prominent changes in behavior and executive functions, or language, accompanied by degeneration of the frontal and/or temporal lobes with a relative sparing of posterior brain regions (Bang *et al*, 2015). FTD is a common type of dementia, even though less common than AD and dementia with Lewy bodies (DLB), with an average age of symptoms onset in the sixth decade, its prevalence is around 3-26% of cases with an expected onset early than 65 years (Bang *et al.*, 2015).

Along with age, family history is a major risk factor for FTD (Niccoli *et al*, 2017). The expansion of a non-coding GGGGCC hexanucleotide repeat in the *C9orf72* gene is the most common cause of inherited FTD (DeJesus-Hernandez *et al*, 2011). Inherited mutation of the *MAPT* gene, coding for tau, accounts for 5 to 10% of all cases of FTD and less than 25% of familial cases. Another associated mutation is in the *GRN* gene, leading to haploinsufficiency and loss of functional progranulin concentrations in the serum and cerebrospinal fluid (CSF). Mutations in other genes, namely *TARDBP* (encoding for TDP-43), *FUS*, *VCP,* or *CHMP2B* are rarer and are mainly associated with familial amyotrophic lateral sclerosis (ALS) with or without FTD (Bang *et al.*, 2015).

14

1.3.1.1 Neuropathology

It is not surprising that the neuropathology underlying clinical FTD (i.e., frontotemporal lobar degeneration, FTLD) is also heterogeneous. Indeed, neuropathological subtypes have been associated with characteristic patterns of abnormal protein deposition following the prion-like propagation models (Figure 2) (Hofmann *et al*, 2019). The corresponding pathological subtypes of FTLD include tau protein (FTLD-tau) for approximately 40% whose spreading is hypothesized to follow a prion-like model (Sieben *et al*, 2012). The remaining majority (~ 50% of cases) of tau negative FTLD are positive for ubiquinated TDP-43 inclusions (FTLD-TDP) (Mackenzie *et al*, 2010). Finally, around 5% of patients are both tau and TDP-43 negative, showing aggregates of other proteins such as FUS (FTLD -FUS) (Mackenzie *et al.*, 2010).
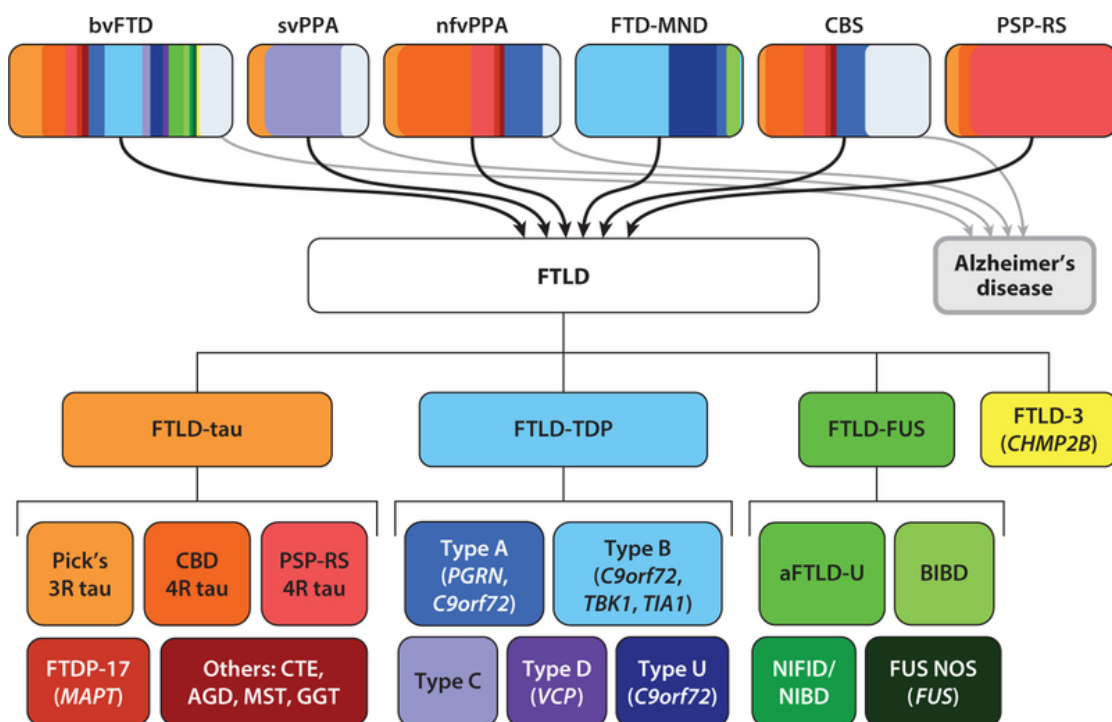
Figure 2. Summary of the complex variety of clinical syndromes, neuropathology, and genetics of FTD. The main six clinical syndromes include bvFTD, svPPA, nfvPPA, FTD-MND, CBS, and PSPS are reported, inserting the information that a small number of patients with bvFTD, svPPA, nfvPPA, or CBS have Alzheimer's disease as the underlying pathology. Based on the proteinopathy involved, the neuropathology of clinical syndromes of FTLD can be classified in FTLD-tau, FTLD-TDP, or FTLD-FUS. Finally, genetic mutations associated with each molecular subtype are italicized (Hofmann *et al.*, 2019).

Most common clinical variants of FTD are the behavioral variant of frontotemporal dementia (bvFTD) and the language variant, termed primary progressive aphasia (PPA). The latter can be further subclassified into non-fluent variant PPA, characterized by impaired speech production, and semantic variant PPA (also referred to as semantic dementia, SD), characterized by impaired word comprehension and semantic memory (Bang *et al.*, 2015).

1.3.1.2 Behavioral Variant Frontotemporal Dementia

bvFTD is the most common clinical variant and accounts approximately for 70% of all FTD cases. In general, the most marked symptoms of bvFTD include behavioral changes and executive dysfunction, personality changes, a mixture of disinhibition and lack of embarrassment, apathy, and loss of sympathy or empathy (Rohrer, 2011). All these can result in tactless and socially inappropriate behavior, impulsive or careless actions, reduced interest in work, hobbies, social interaction, and hygiene. Furthermore, patients may show compulsive and ritualistic behaviors, e.g., repetitive movements, and repetitive use of verbal phrases. Binge eating, increased consumption of sweets or alcohol, and weight gain are different aspects of the characteristic hyperorality in this type of dementia. Moreover, anosognosia is usually prominent and patients often show deficits in various executive tasks, although their visuospatial skills are normal at first.

Diagnostic criteria

Despite the recent advances in the characterization of bvFTD, the diagnosis of the syndrome remains challenging, due to the absence of definitive biomarkers for an early and accurate differential diagnosis. To date, the diagnosis of bvFTD is dependent on clinical diagnostic criteria, whose latest diagnostic version has been established in 2011 (Rascovsky *et al*, 2011). According to the latter, the diagnosis might be:

Possible bvFTD: based solely on the clinical syndrome and aims to identify patients at the mildest stages of disease. This classification relies on the flexible combination of three of six clinically discriminating features: disinhibition, apathy/inertia, loss of sympathy/empathy, perseverative/compulsive behaviors, hyperorality and a dysexecutive neuropsychological profile (Rascovsky *et al.*, 2011).

Probable bvFTD: based on the clinical syndrome, plus demonstrable functional

decline and the frontotemporal imaging findings that reflect the principal anatomical location of neurodegeneration in bvFTD. Furthermore, a diagnosis of probable bvFTD may be withheld if other biomarkers are strongly indicative of AD or other degenerative processes.

bvFTD with definite FTLD pathology: patients who exhibit the bvFTD clinical syndrome and who also have a pathogenic mutation or histopathological evidence of FTLD.

Neuroimaging in bvFTD

Structural MRI

There is a considerable body of research employing MRI in bvFTD to investigate the pattern and distribution of grey matter loss. bvFTD is generally characterized by frontotemporal atrophy, showing an antero-posterior gradient with the involvement of medial orbitofrontal, anterior cingulate, insular and anterior temporal cortices and relative sparing of the parietal and occipital lobes (Rosen *et al*, 2002; Seeley *et al*, 2008). Furthermore, atrophy, although commonly bilateral, is generally asymmetrical (Barkhof & van Buchem, 2016). Subcortical structures like the striatum, thalamus, hypothalamus and brainstem are often involved (Du *et al*, 2007; Seeley *et al.*, 2008).
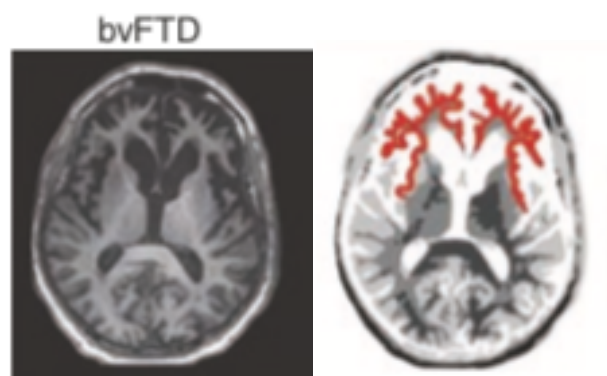
Figure 3. Characteristic patterns of gray matter atrophy (highlighted in red) in frontotemporal dementia (FTD). Patients with bvFTD exhibit prominent frontal, insular, and anterior cingulate atrophy. Figure adapted from Meeter et al., 2017 (Meeter *et al*, 2017).

Several studies have been aimed at improving differential diagnosis distinguishing FTD from AD. Indeed, cortical thinning of the anterior temporal and frontal lobes is indicative of bvFTD, whereas atrophy of the posterior cingulate gyrus, parietal lobe and

frontal pole suggests an AD pathology (Canu *et al*, 2017; Du *et al.*, 2007). Moreover, the pattern of gray matter atrophy can distinguish to some degree clinical and pathological FTD syndromes (Agosta *et al*, 2015). Compared to cognitively normal subjects, FTD patients have a thinner cortex in bilateral frontal and temporal regions and some thinning in inferior parietal regions and the posterior cingulate (Du *et al.*, 2007), and frontal atrophy (most evident in medial portions) is somewhat more exacerbated in bvFTD subjects compared to the decline observed in normal aging individuals (Manera *et al*, 2019). Noteworthy, another study investigated the relation between aging and bvFTD, suggesting that there is an overlap in atrophy among healthy elderly and bvFTD. Specifically, atrophy in dorsolateral frontal and orbitofrontal regions seen in normal aging is severe enough to match that of bvFTD patients at a mild stage of the disease (Chow *et al*, 2008).

To investigate white matter tracts organization, different diffusion tensor imaging (DTI) analyses can be applied. DTI is sensitive to the direction and extent of water movement to provide a measure of the integrity of white matter tracts. The diffusion tensor permits to extract two measures such as fractional anisotropy (FA) and mean diffusivity (MD), which are indirect indices of white matter integrity. Indeed, intact white matter will restrict diffusion of water molecules parallel to the main fiber direction (leading to higher FA and lower MD), whereas damage to white matter will cause diffusivity to be less restricted (i.e., lower FA and higher MD) (Basser *et al*, 1994). Analysis of DTI metrics can be performed using ROI approaches, or whole-brain voxel-wise methods such as VBM-style analysis or tract-based spatial statistics (TBSS) (Smith *et al*, 2006).

In patients with bvFTD, DTI studies showed an involvement of the major frontal white matter tracts (anterior cingulum, genu of the corpus callosum, and superior longitudinal fasciculus) and those travelling through the temporal lobes (uncinate, inferior longitudinal fasciculus , and inferior fronto-occipital fasciculus) (Whitwell *et al*, 2010; Agosta *et al*, 2012a; Mahoney *et al*, 2014). White matter abnormalities, however, have been identified also in posterior regions, including the posterior portions of inferior longitudinal fasciculus and posterior cingulum (Whitwell *et al.*, 2010; Agosta *et al.*, 2012a; Mahoney *et al.*, 2014). DTI can be helpful in differentiating bvFTD from AD cases due to the fact

that bvFTD is associated to greater damage especially in frontal regions (Canu *et al.*, 2017; Mahoney *et al.*, 2014).

<u>Functional MRI</u>

Several studies have explored functional brain connectivity in patients with bvFTD using RS fMRI analyses. Studies focusing on the assessment of resting-state networks have shown that bvFTD patients feature a recurrent attenuation of within-resting-state network connectivity of the salience network (Farb *et al*, 2013; Filippi *et al*, 2013; Zhou *et al*, 2010). This altered pattern is not unexpected, since the regions known to harbor the neuropathological changes of bvFTD, such as the fronto-insular and anterior cingulate areas, are central regions of the salience network.
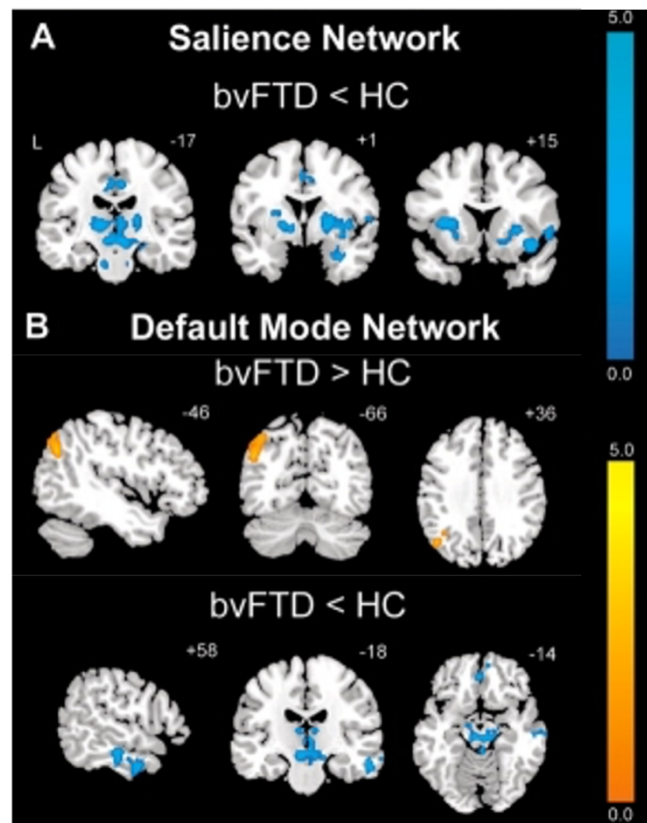
Figure 4. In the Salience Network (A), patients with bvFTD showed distributed connectivity reductions compared to healthy controls (HC). In the DMN (B), patients with bvFTD showed increased left angular gyrus connectivity relative to HC and a further focal brainstem connectivity disruption within the DMN. Figure adapted from Zhou J. et al., 2010 (Zhou *et al.*, 2010).

Moreover, given their role in processing socially relevant information and behavior, attenuated salience network connectivity is unsurprisingly predictive of worsening

behavioral symptoms and correlates with both clinical dementia ratings and behavioral test scores (Day *et al*, 2013; Filippi *et al.*, 2013). Altered connectivity has been observed in other functional networks: increased functional connectivity has been reported in the attention/working memory network, and in the medial parietal components of the DMN (Farb *et al.*, 2013; Filippi *et al.*, 2013; Whitwell *et al*, 2011; Zhou *et al.*, 2010).

This contrasting pattern of altered functional connectivity in the DMN and salience network may be useful to differentiate bvFTD patients from patients with AD, which typically show reduced connectivity in the DMN and posterior brain nodes (Canu *et al.*, 2017).

1.3.1.3 Motor Neuron Disease

Motor neuron disease (MND) encompasses several phenotypes all of which are relentlessly progressive and ultimately fatal. The involvement of the upper motor neurons (UMN) and/or lower motor neurons (LMN) defines different clinical phenotypes, including ALS, primary lateral sclerosis (PLS) and progressive muscular atrophy (PMA) (Norris *et al*, 1993). ALS is the most common clinical presentation of MND and is characterized by the progressive degeneration of both UMN and LMN. PLS is characterized by the progressive degeneration of UMN only, while PMA by degeneration of LMN only. Clinically, patients with MND greatly differ in terms of site of onset, differential UMN and LMN involvement, presence and severity of extra-motor impairment (e.g., cognitive impairment), and disease progression, delineating a wide spectrum of syndromes partially overlapping with FTD with different prognostic impact at the individual level (Swinnen & Robberecht, 2014).

Epidemiology

Epidemiological studies in MND are a challenging task, because of the difficulties in determining disease onset and the delay between onset and clinical manifestations. An Italian-study provided that the MND incidence in Europe is 2.08/100,000 individuals, corresponding to an estimated 15,355 cases (Chio *et al*, 2013). Prevalence is 5.40/100,000 individuals (about 39,863 prevalent cases). The mean age at onset is approximately 60 years (Chio *et al.*, 2013). Survival time generally ranges between 2 and 5 years from onset

(Chio *et al*, 2009; del Aguila *et al*, 2003) and only 5–10% of patients survive longer than 10 years (Chio *et al.*, 2009). The most common cause of death is respiratory failure.

Neuropathology

Up to 98% of MND cases show aggregates of ubiquitin-positive TDP-43 as molecular hallmark of disease pathology (Neumann *et al*, 2006), spreading in a prion-like way hypothesized by Brettschneider and colleagues (Brettschneider *et al*, 2013). The staging of TDP-43 protein starts from the primary motor cortex, supplementary motor area brainstem motor nuclei and spinal cord (stage I). Pathological process also expands into contiguous portions of the premotor and prefrontal regions (stage II), moving to medial and lateral orbitofrontal cortex, postcentral gyrus, caudate nucleus, putamen and nucleus accumbens (stage III). Patients with most extensive patterns of neuropathology involved entorhinal cortex and the hippocampus (stage IV).

Most MND cases are sporadic, however genetic alterations are reported in up to 10% of patients (Renton *et al*, 2014). Among all genetic alterations, the most common mutation is the hexanucleotide expansion in the *C9orf72* gene, which is associated with greater prevalence of cognitive deficits and full-blown FTD. Since such mutation is found in a large proportion of FTD patients, this mutation can be considered as the link between MND and FTD (Robberecht & Philips, 2013). Other involved genes are *SOD1*, *TARDBP* – encoding for the TDP-43 protein –, *FUS*, *OPTN*, and *VCP*.

Clinical presentation and diagnostic criteria

Based on the differential UMN and LMN involvement, patients can be classified into different phenotypes:

Progressive muscular atrophy (PMA) is characterized by clinical and electrophysiological evidence of progressive LMN involvement without evidence of UMN disease. The disorder, constituting about 5% of MND cases, is usually asymmetric and distal and/or proximal onset can occur (Garg *et al*, 2017).

Flail arm and flail leg syndromes are both characterized by a predominant involvement of LMN and mild alterations of UMN. The flail arm variant symptoms include progressive, predominantly proximal, weakness and wasting in the upper limbs with possible development of Hoffman sign in the upper limbs. On the other hand, flail

leg syndrome is characterized by weakness and wasting in the lower limbs and possible occurrence of Babinski sign with disease progression(Chio *et al*, 2011).

Predominant UMN ALS is characterized by LMN signs, such as muscle weakness and wasting, but with a prevalence of UMN features comprising spastic paresis in association with one or more of the following symptoms: Babinski or Hoffmann sign, hyperactive reflexes, clonic jaw jerk, dysarthric speech and pseudobulbar affect.

Primary lateral sclerosis (PLS) is reported in 5% of MND cases. It presents a selective UMN involvement without LMN disturbances after 4 years from disease onset (Gordon *et al*, 2006). In contrast with classic ALS, PLS prognosis is more favorable (Gordon *et al*, 2009) and survival time is longer (Gordon *et al.*, 2006).

Diagnosis of the different MND phenotypes is based on specific diagnostic criteria.

ALS is diagnosed with the revised El Escorial criteria (Brooks *et al*, 2000), which requires the presence of clinical, electrophysiological or neuropathologic evidence of LMN degeneration and clinical evidence of UMN degeneration, the progression of signs within a region or to other regions. Such evidence has to be combined with the absence of other diseases or neuroimaging evidence able to explain the observed signs.
PLS diagnosis is usually based on the Pringle's criteria (Pringle *et al*, 1992), while PMA is carried out with the criteria by van den Berg-Vos et al. (van den Berg-Vos *et al*, 2003).

MND progression can be monitored using the revised version of the ALS Functional Rating Scale (ALSFRS-R) (Cedarbaum *et al*, 1999), that is currently the most widely used measurement tool. Patients are scored from 0 (maximum disability) to 48 points (normal functioning) for bulbar and limb symptoms, mobility, and respiratory function.

Cognitive impairment
The traditional idea that MND is only a purely neuromuscular disease, as depicted by Jean-Martin Charcot in the 1869 (Ferrari *et al*, 2011), is now outdated. Indeed, it is well-established that nearly 50% of MND patients manifests cognitive and behavioral impairment, ranging from mild impairment to a full-blown dementia syndrome (Phukan *et al*, 2012). The revised Strong criteria (Strong *et al*, 2017) have established a recognized nomenclature for the MND clinical continuum. Such criteria classify from MND cognitively normal (ALS-cn) to MND with frontotemporal dementia (ALS-FTD),

including MND with cognitive impairment (ALSci), MND with behavioural impairment (ALSbi) and MND with combined cognitive and behavioural impairment (ALS-cbi). MND-FTD can be diagnosed when a patient meets Rascovsky criteria (Rascovsky *et al.*, 2011) for the behavioral variant or Gorno-Tempini criteria (Gorno-Tempini *et al*, 2011) for the linguistic (i.e., semantic and non-fluent) variants of FTD, even if more rarely (Phukan *et al.*, 2012). The diagnosis of ALSci is based on the presence of execution dysfunction or language dysfunction or the combination of the two, evaluated as cognitive scores on standardized neuropsychological tests falling or below the 5th percentile, compared to age- and education-matched healthy individuals. For ALSbi, the diagnosis is defined by the detection of apathy with or without behavioral changes or the presence of two or more of the following behavioral symptoms: a) disinhibition, b) loss of sympathy and empathy, c) perseverative, stereotyped, or compulsive behavior, d) hyperorality/dietary change, e) loss of insight (see above), f) psychotic symptoms (e.g., somatic delusions, hallucinations, irrational beliefs) (Strong *et al.*, 2017). ALScbi is classified including patients who fulfil criteria for both ALSci and ALSbi. Finally, ALS-FTD is diagnosed by the evidence of progressive deterioration of behavior and/or cognition and the presence of at least three of the behavioral/cognitive symptoms according to Rascovsky criteria (Rascovsky *et al.*, 2011). Alternatively, ALS-FTD can be defined by the presence of at least two of those behavioral/cognitive symptoms, together with loss of insight and/or psychotic symptoms, or even the presence of language impairment, that may coexist with behavioral/cognitive symptoms meeting criteria for semantic dementia/semantic variant PPA or non-fluent variant PPA, defined by Neary et al. (Neary *et al*, 1998) or Gorno-Tempini et al. (Gorno-Tempini *et al.*, 2011).

Neuroimaging in Motor Neuron Disease

Traditionally, the use of conventional MRI in patients suspected of having ALS has been restricted to exclude other causes of symptoms of MND (Filippi *et al*, 2010). There is a growing body of evidence that recognized MRI as a powerful tool to detect in vivo brain alterations associated with MND pathology (Chio *et al*, 2014), providing potential markers of disease activity.

There are many studies in literature that investigated the grey matter loss in patients with ALS using VBM technique on high-resolution 3D T1-weighted MRI scans. Such

studies show diverging results, on one hand detecting focal atrophy in motor/premotor regions (Agosta *et al*, 2007; Turner *et al*, 2007), on the other highlighting widespread frontotemporal atrophy sparing the motor cortex (Mezzapesa *et al*, 2007), or even no significant atrophy (Abrahams *et al*, 2005). Such variability might be explained by the differences in imaging processing pipelines and statistical approaches applied. Evaluating longitudinal structural changes, a significant decrease in grey matter volume over a 6-month follow-up was found in motor and extra-motor frontotemporal cortex, thalami, and caudate nucleus, associated with clinical and cognitive decline (Menke *et al*, 2014).

Another method to assess grey matter changes is the surface-based morphometry that estimates cortical thickness. Studies, which performed such methodological framework, have systematically reported in patients with ALS significant cortical thinning in the primary motor areas (Agosta *et al*, 2012b; Verstraete *et al*, 2010), along with extra-motor involvement more severe in ALS patients with cognitive/behavioral deficits (Agosta *et al*, 2016; Schuster *et al*, 2014). Moreover, the specific investigation of subcortical structures has revealed the involvement of caudate nucleus, accumbens (Bede *et al*, 2013) and thalamus (Menke *et al.*, 2014), consistent with the neuropathological studies(Brettschneider *et al.*, 2013).

Numerous studies assessed white matter tract integrity in patients with ALS using DTI. From current literature it is consistently reported a "signature" of white matter alterations (i.e., decreased FA and increased M) in corticospinal tracts (CSTs) and in the corpus callosum, specifically middle and posterior parts (Muller *et al*, 2016). Additionally, white matter damage, similarly to the grey matter atrophy, has also been revealed in extra-motor frontotemporal tracts, more evidently in patients with cognitive or neuropsychiatric impairment (Agosta *et al.*, 2016; Lillo *et al*, 2014).

Although ALS is the most common phenotype of MND and, for such reason the most studied, some studies put their effort in evaluating microstructural integrity in patients with PLS. Widespread damage in both motor and extra-motor areas correlated with the severity of cognitive deficits (Agosta *et al*, 2014b). On the contrary, there are neuroimaging studies that observed the least diffuse white matter damage in patients with predominant LMN involvement, with diverging results from literature (Spinelli *et al*, 2016; Prudlo *et al*, 2012; Rosenbohm *et al*, 2016).

Regarding fMRI, several studies showed decreased functional connectivity of the

sensorimotor network in ALS patients (Mohammadi *et al*, 2009), whereas others found increased connectivity (Douaud *et al*, 2011), or complex regional patterns of decreased and increased functional connectivity (Zhou *et al*, 2014). Functional brain networks involved in cognition and behavior, namely the DMN and frontoparietal network, were also found to be altered (Agosta *et al*, 2013; Luo *et al*, 2012). What emerges from RS fMRI studies is that an increase in functional connectivity might be explained by a compensatory mechanism in earlier disease stages, followed by functional failure as the pathology worsens. In agree with such hypothesis, patients with less white matter damages in CST were characterized by increased functional connectivity (Agosta *et al*, 2011), associated with lower rate of disease progression, shorter disease duration (Luo *et al.*, 2012). Furthermore, Menke and colleagues, in a two-year longitudinal study, showed a reduction of RS functional connectivity in the sensorimotor and thalamic networks, arguably supporting the neuroanatomical and clinical decline in patients with ALS (Menke *et al*, 2018). Conversely, other studies demonstrated an increase of functional connectivity in regions known to be affected by ALS pathology correlating with a higher disease progression rate (Douaud *et al.*, 2011), and a worsening of clinical manifestations and executive cognitive functions (Agosta *et al*, 2014a).

REFERENCES

Abrahams S, Leigh PN, Goldstein LH (2005) Cognitive change in ALS: a prospective study. *Neurology* 64: 1222-1226

Agosta F, Canu E, Inuggi A, Chio A, Riva N, Silani V, Calvo A, Messina S, Falini A, Comi G *et al* (2014a) Resting state functional connectivity alterations in primary lateral sclerosis. *Neurobiol Aging* 35: 916-925

Agosta F, Canu E, Valsasina P, Riva N, Prelle A, Comi G, Filippi M (2013) Divergent brain network connectivity in amyotrophic lateral sclerosis. *Neurobiol Aging* 34: 419-427

Agosta F, Ferraro PM, Riva N, Spinelli EG, Chio A, Canu E, Valsasina P, Lunetta C, Iannaccone S, Copetti M *et al* (2016) Structural brain correlates of cognitive and behavioral impairment in MND. *Hum Brain Mapp* 37: 1614-1626

Agosta F, Galantucci S, Magnani G, Marcone A, Martinelli D, Antonietta Volonte M, Riva N, Iannaccone S, Ferraro PM, Caso F *et al* (2015) MRI signatures of the frontotemporal lobar degeneration continuum. *Hum Brain Mapp* 36: 2602-2614

Agosta F, Galantucci S, Riva N, Chio A, Messina S, Iannaccone S, Calvo A, Silani V, Copetti M, Falini A *et al* (2014b) Intrahemispheric and interhemispheric structural network abnormalities in PLS and ALS. *Hum Brain Mapp* 35: 1710-1722

Agosta F, Pagani E, Rocca MA, Caputo D, Perini M, Salvi F, Prelle A, Filippi M (2007) Voxel-based morphometry study of brain volumetry and diffusivity in amyotrophic lateral sclerosis patients with mild disability. *Hum Brain Mapp* 28: 1430-1438

Agosta F, Scola E, Canu E, Marcone A, Magnani G, Sarro L, Copetti M, Caso F, Cerami C, Comi G *et al* (2012a) White matter damage in frontotemporal lobar degeneration spectrum. *Cereb Cortex* 22: 2705-2714

Agosta F, Valsasina P, Absinta M, Riva N, Sala S, Prelle A, Copetti M, Comola M, Comi G, Filippi M (2011) Sensorimotor functional connectivity changes in amyotrophic lateral sclerosis. *Cereb Cortex* 21: 2291-2298

Agosta F, Valsasina P, Riva N, Copetti M, Messina MJ, Prelle A, Comi G, Filippi M (2012b) The cortical signature of amyotrophic lateral sclerosis. *PLoS One* 7: e42816

Arotcarena ML, Teil M, Dehay B (2019) Autophagy in Synucleinopathy: The Overwhelmed and Defective Machinery. *Cells* 8

Atella V, Piano Mortari A, Kopinska J, Belotti F, Lapi F, Cricelli C, Fontana L (2019) Trends in age-related disease burden and healthcare utilization. *Aging Cell* 18: e12861

Bang J, Spina S, Miller BL (2015) Frontotemporal dementia. *Lancet* 386: 1672-1682

Barja G (2014) The mitochondrial free radical theory of aging. *Prog Mol Biol Transl Sci* 127: 1-27

Barkhof F, van Buchem MA (2016) Neuroimaging in dementia. In: *Diseases of the Brain, Head and Neck, Spine 2016-2019*, pp. 79-85. Springer:

Basser PJ, Mattiello J, LeBihan D (1994) MR diffusion tensor spectroscopy and imaging. *Biophysical journal* 66: 259-267

Bede P, Elamin M, Byrne S, McLaughlin RL, Kenna K, Vajda A, Pender N, Bradley DG, Hardiman O (2013) Basal ganglia involvement in amyotrophic lateral sclerosis. *Neurology* 81: 2107-2115

Benavides-Piccione R, Fernaud-Espinosa I, Robles V, Yuste R, DeFelipe J (2013) Age-based comparison of human dendritic spine structure using complete three-dimensional reconstructions. *Cereb Cortex* 23: 1798-1810

Bhatia V, Sharma S (2021) Role of mitochondrial dysfunction, oxidative stress and autophagy in progression of Alzheimer's disease. *J Neurol Sci* 421: 117253

Bourdenx M, Koulakiotis NS, Sanoudou D, Bezard E, Dehay B, Tsarbopoulos A (2017) Protein aggregation and neurodegeneration in prototypical neurodegenerative diseases: Examples of amyloidopathies, tauopathies and synucleinopathies. *Prog Neurobiol* 155: 171-193

Bourisly AK, El-Beltagi A, Cherian J, Gejo G, Al-Jazzaf A, Ismail M (2015) A voxel-based morphometric magnetic resonance imaging study of the brain detects age-related gray matter volume changes in healthy subjects of 21-45 years old. *Neuroradiol J* 28: 450-459

Brathen ACS, De Lange AG, Fjell AM, Walhovd KB (2021) Risk- and protective factors for memory plasticity in aging. *Neuropsychol Dev Cogn B Aging Neuropsychol Cogn* 28: 201-217

Brettschneider J, Del Tredici K, Toledo JB, Robinson JL, Irwin DJ, Grossman M, Suh E, Van Deerlin VM, Wood EM, Baek Y *et al* (2013) Stages of pTDP-43 pathology in amyotrophic lateral sclerosis. *Annals of neurology* 74: 20-38

Brooks BR, Miller RG, Swash M, Munsat TL, World Federation of Neurology Research Group on Motor Neuron D (2000) El Escorial revisited: revised criteria for the diagnosis of amyotrophic lateral sclerosis. *Amyotroph Lateral Scler Other Motor Neuron Disord* 1: 293-299

Buckner RL, Andrews-Hanna JR, Schacter DL (2008) The brain's default network: anatomy, function, and relevance to disease. *Ann N Y Acad Sci* 1124: 1-38

Bussian TJ, Aziz A, Meyer CF, Swenson BL, van Deursen JM, Baker DJ (2018) Clearance of senescent glial cells prevents tau-dependent pathology and cognitive decline. *Nature* 562: 578-582

Canu E, Agosta F, Mandic-Stojmenovic G, Stojkovic T, Stefanova E, Inuggi A, Imperiale F, Copetti M, Kostic VS, Filippi M (2017) Multiparametric MRI to distinguish early onset Alzheimer's disease and behavioural variant of frontotemporal dementia. *Neuroimage Clin* 15: 428-438

Cedarbaum JM, Stambler N, Malta E, Fuller C, Hilt D, Thurmond B, Nakanishi A (1999) The ALSFRS-R: a revised ALS functional rating scale that incorporates assessments of respiratory function. BDNF ALS Study Group (Phase III). *J Neurol Sci* 169: 13-21

Chen WW, Zhang X, Huang WJ (2016) Role of neuroinflammation in neurodegenerative diseases (Review). *Mol Med Rep* 13: 3391-3396

Chio A, Calvo A, Moglia C, Mazzini L, Mora G, group Ps (2011) Phenotypic heterogeneity of amyotrophic lateral sclerosis: a population based study. *J Neurol Neurosurg Psychiatry* 82: 740-746

Chio A, Logroscino G, Hardiman O, Swingler R, Mitchell D, Beghi E, Traynor BG, Eurals C (2009) Prognostic factors in ALS: A critical review. *Amyotroph Lateral Scler* 10: 310-323

Chio A, Logroscino G, Traynor BJ, Collins J, Simeone JC, Goldstein LA, White LA (2013) Global epidemiology of amyotrophic lateral sclerosis: a systematic review of the published literature. *Neuroepidemiology* 41: 118-130

Chio A, Pagani M, Agosta F, Calvo A, Cistaro A, Filippi M (2014) Neuroimaging in amyotrophic lateral sclerosis: insights into structural and functional changes. *Lancet Neurol* 13: 1228-1240

Chow TW, Binns MA, Freedman M, Stuss DT, Ramirez J, Scott CJ, Black S (2008) Overlap in frontotemporal atrophy between normal aging and patients with frontotemporal dementias. *Alzheimer Dis Assoc Disord* 22: 327-335

Damoiseaux JS (2017) Effects of aging on functional and structural brain connectivity. *NeuroImage* 160: 32-40

Damoiseaux JS, Beckmann CF, Arigita EJS, Barkhof F, Scheltens P, Stam CJ, Smith SM, Rombouts SARB (2007) Reduced resting-state brain activity in the "default network" in normal aging. *Cerebral Cortex* 18: 1856-1864

Day GS, Farb NA, Tang-Wai DF, Masellis M, Black SE, Freedman M, Pollock BG, Chow TW (2013) Salience network resting-state activity: prediction of frontotemporal dementia progression. *JAMA Neurol* 70: 1249-1253

DeJesus-Hernandez M, Mackenzie IR, Boeve BF, Boxer AL, Baker M, Rutherford NJ, Nicholson AM, Finch NA, Flynn H, Adamson J *et al* (2011) Expanded GGGGCC hexanucleotide repeat in noncoding region of C9ORF72 causes chromosome 9p-linked FTD and ALS. *Neuron* 72: 245-256

del Aguila MA, Longstreth WT, Jr., McGuire V, Koepsell TD, van Belle G (2003) Prognosis in amyotrophic lateral sclerosis: a population-based study. *Neurology* 60: 813-819

Domingos C, Pego JM, Santos NC (2021) Effects of physical activity on brain function and structure in older adults: A systematic review. *Behav Brain Res* 402: 113061

Douaud G, Filippini N, Knight S, Talbot K, Turner MR (2011) Integration of structural and functional magnetic resonance imaging in amyotrophic lateral sclerosis. *Brain* 134: 3470-3479

Du AT, Schuff N, Kramer JH, Rosen HJ, Gorno-Tempini ML, Rankin K, Miller BL, Weiner MW (2007) Different regional patterns of cortical thinning in Alzheimer's disease and frontotemporal dementia. *Brain* 130: 1159-1166

Eckert MA, Keren NI, Roberts DR, Calhoun VD, Harris KC (2010) Age-related changes in processing speed: unique contributions of cerebellar and prefrontal cortex. *Front Hum Neurosci* 4: 10

Esiri MM (2007) Ageing and the brain. *J Pathol* 211: 181-187

Esposito F, Aragri A, Pesaresi I, Cirillo S, Tedeschi G, Marciano E, Goebel R, Di Salle F (2008) Independent component model of the default-mode brain function: combining

individual-level and population-level analyses in resting-state fMRI. *Magn Reson Imaging* 26: 905-913

Farb NA, Grady CL, Strother S, Tang-Wai DF, Masellis M, Black S, Freedman M, Pollock BG, Campbell KL, Hasher L *et al* (2013) Abnormal network connectivity in frontotemporal dementia: evidence for prefrontal isolation. *Cortex; a journal devoted to the study of the nervous system and behavior* 49: 1856-1873

Ferrari R, Kapogiannis D, Huey ED, Momeni P (2011) FTD and ALS: a tale of two diseases. *Curr Alzheimer Res* 8: 273-294

Ferreira LK, Busatto GF (2013) Resting-state functional connectivity in normal brain aging. *Neurosci Biobehav Rev* 37: 384-400

Filippi M, Agosta F, Abrahams S, Fazekas F, Grosskreutz J, Kalra S, Kassubek J, Silani V, Turner MR, Masdeu JC *et al* (2010) EFNS guidelines on the use of neuroimaging in the management of motor neuron diseases. *Eur J Neurol* 17: 526-e520

Filippi M, Agosta F, Scola E, Canu E, Magnani G, Marcone A, Valsasina P, Caso F, Copetti M, Comi G *et al* (2013) Functional network connectivity in the behavioral variant of frontotemporal dementia. *Cortex; a journal devoted to the study of the nervous system and behavior* 49: 2389-2401

Fivenson EM, Lautrup S, Sun N, Scheibye-Knudsen M, Stevnsner T, Nilsen H, Bohr VA, Fang EF (2017) Mitophagy in neurodegeneration and aging. *Neurochem Int* 109: 202-209

Flatt T, Partridge L (2018) Horizons in the evolution of aging. *BMC biology* 16: 1-13

Franceschi C, Bonafe M, Valensin S, Olivieri F, De Luca M, Ottaviani E, De Benedictis G (2000) Inflamm-aging. An evolutionary perspective on immunosenescence. *Ann N Y Acad Sci* 908: 244-254

Fusco S, Pani G (2013) Brain response to calorie restriction. *Cell Mol Life Sci* 70: 3157-3170

Galiano A, Mengual E, Garcia de Eulate R, Galdeano I, Vidorreta M, Recio M, Riverol M, Zubieta JL, Fernandez-Seara MA (2020) Coupling of cerebral blood flow and functional connectivity is decreased in healthy aging. *Brain Imaging Behav* 14: 436-450

Galluzzi S, Beltramello A, Filippi M, Frisoni GB (2008) Aging. *Neurol Sci* 29 Suppl 3: 296-300

Garg N, Park SB, Vucic S, Yiannikas C, Spies J, Howells J, Huynh W, Matamala JM, Krishnan AV, Pollard JD *et al* (2017) Differentiating lower motor neuron syndromes. *J Neurol Neurosurg Psychiatry* 88: 474-483

Good CD, Johnsrude IS, Ashburner J, Henson RN, Friston KJ, Frackowiak RS (2001) A voxel-based morphometric study of ageing in 465 normal adult human brains. *NeuroImage* 14: 21-36

Gordon PH, Cheng B, Katz IB, Mitsumoto H, Rowland LP (2009) Clinical features that distinguish PLS, upper motor neuron-dominant ALS, and typical ALS. *Neurology* 72: 1948-1952

Gordon PH, Cheng B, Katz IB, Pinto M, Hays AP, Mitsumoto H, Rowland LP (2006) The natural history of primary lateral sclerosis. *Neurology* 66: 647-653

Gorno-Tempini ML, Hillis AE, Weintraub S, Kertesz A, Mendez M, Cappa SF, Ogar JM, Rohrer JD, Black S, Boeve BF *et al* (2011) Classification of primary progressive aphasia and its variants. *Neurology* 76: 1006-1014

Gowers WR (1902) *A Lecture on Abiotrophy: Diseases from Defect of Life*. John Bale, Sons and Danielsson, Limited

Grajauskas LA, Siu W, Medvedev G, Guo H, D'Arcy RCN, Song X (2019) MRI-based evaluation of structural degeneration in the ageing brain: Pathophysiology and assessment. *Ageing Res Rev* 49: 67-82

Groot C, van Loenhoud AC, Barkhof F, van Berckel BNM, Koene T, Teunissen CC, Scheltens P, van der Flier WM, Ossenkoppele R (2018) Differential effects of cognitive reserve and brain reserve on cognition in Alzheimer disease. *Neurology* 90: e149-e156

Han MH, 2009. Adams and Victor's Principles of Neurology. American Association of Neuropathologists, Inc.

Ho KC, Roessmann U, Straumfjord JV, Monroe G (1980) Analysis of brain weight. I. Adult brain weight in relation to sex, race, and age. *Arch Pathol Lab Med* 104: 635-639

Hofmann JW, Seeley WW, Huang EJ (2019) RNA Binding Proteins and the Pathogenesis of Frontotemporal Lobar Degeneration. *Annu Rev Pathol* 14: 469-495

Johnson AA, Stolzing A (2019) The role of lipid metabolism in aging, lifespan regulation, and age-related disease. *Aging Cell* 18: e13048

Kennedy BK, Berger SL, Brunet A, Campisi J, Cuervo AM, Epel ES, Franceschi C, Lithgow GJ, Morimoto RI, Pessin JE *et al* (2014) Geroscience: linking aging to chronic disease. *Cell* 159: 709-713

Kennedy K, Raz N (2015) Normal aging of the brain.

Klaips CL, Jayaraj GG, Hartl FU (2018) Pathways of cellular proteostasis in aging and disease. *J Cell Biol* 217: 51-63

Kralj C, Daskalopoulou C, Rodríguez-Artalejo F, García-Esquinas E, Cosco T, Prince M, Prina A (2018) Healthy ageing: A systematic review of risk factors. *King's Global Health Institute Reports* 2018: 1

Li Q, Dong C, Liu T, Chen X, Perry A, Jiang J, Cheng J, Niu H, Kochan NA, Brodaty H *et al* (2020) Longitudinal Changes in Whole-Brain Functional Connectivity Strength Patterns and the Relationship With the Global Cognitive Decline in Older Adults. *Front Aging Neurosci* 12: 71

Lillo P, Matamala JM, Valenzuela D, Verdugo R, Castillo JL, Ibanez A, Slachevsky A (2014) [Overlapping features of frontotemporal dementia and amyotrophic lateral sclerosis]. *Revista medica de Chile* 142: 867-879

Lopez-Otin C, Blasco MA, Partridge L, Serrano M, Kroemer G (2013) The hallmarks of aging. *Cell* 153: 1194-1217

Luo C, Chen Q, Huang R, Chen X, Chen K, Huang X, Tang H, Gong Q, Shang HF (2012) Patterns of spontaneous brain activity in amyotrophic lateral sclerosis: a resting-state FMRI study. *PLoS One* 7: e45470

Luque-Contreras D, Carvajal K, Toral-Rios D, Franco-Bocanegra D, Campos-Pena V (2014) Oxidative stress and metabolic syndrome: cause or consequence of Alzheimer's disease? *Oxid Med Cell Longev* 2014: 497802

Mackenzie IR, Neumann M, Bigio EH, Cairns NJ, Alafuzoff I, Kril J, Kovacs GG, Ghetti B, Halliday G, Holm IE *et al* (2010) Nomenclature and nosology for neuropathologic subtypes of frontotemporal lobar degeneration: an update. *Acta Neuropathol* 119: 1-4

Mahoney CJ, Ridgway GR, Malone IB, Downey LE, Beck J, Kinnunen KM, Schmitz N, Golden HL, Rohrer JD, Schott JM *et al* (2014) Profiles of white matter tract pathology in frontotemporal dementia. *Hum Brain Mapp* 35: 4163-4179

Manera AL, Dadar M, Collins DL, Ducharme S, Frontotemporal Lobar Degeneration Neuroimaging I (2019) Deformation based morphometry study of longitudinal MRI changes in behavioral variant frontotemporal dementia. *Neuroimage Clin* 24: 102079

Marner L, Nyengaard JR, Tang Y, Pakkenberg B (2003) Marked loss of myelinated nerve fibers in the human brain with age. *J Comp Neurol* 462: 144-152

Meeter LH, Kaat LD, Rohrer JD, van Swieten JC (2017) Imaging and fluid biomarkers in frontotemporal dementia. *Nat Rev Neurol* 13: 406-419

Menke RA, Korner S, Filippini N, Douaud G, Knight S, Talbot K, Turner MR (2014) Widespread grey matter pathology dominates the longitudinal cerebral MRI and clinical landscape of amyotrophic lateral sclerosis. *Brain* 137: 2546-2555

Menke RAL, Proudfoot M, Talbot K, Turner MR (2018) The two-year progression of structural and functional cerebral MRI in amyotrophic lateral sclerosis. *Neuroimage Clin* 17: 953-961

Menon V (2015) Large-scale functional brain organization. *Brain mapping: An encyclopedic reference* 2: 449-459

Mezzapesa DM, Ceccarelli A, Dicuonzo F, Carella A, De Caro MF, Lopez M, Samarelli V, Livrea P, Simone IL (2007) Whole-brain and regional brain atrophy in amyotrophic lateral sclerosis. *AJNR American journal of neuroradiology* 28: 255-259

Mohammadi B, Kollewe K, Samii A, Krampfl K, Dengler R, Munte TF (2009) Changes of resting state brain networks in amyotrophic lateral sclerosis. *Exp Neurol* 217: 147-153

Mufson EJ, Malek-Ahmadi M, Perez SE, Chen K (2016) Braak staging, plaque pathology, and APOE status in elderly persons without cognitive impairment. *Neurobiol Aging* 37: 147-153

Muller HP, Turner MR, Grosskreutz J, Abrahams S, Bede P, Govind V, Prudlo J, Ludolph AC, Filippi M, Kassubek J *et al* (2016) A large-scale multicentre cerebral diffusion tensor imaging study in amyotrophic lateral sclerosis. *J Neurol Neurosurg Psychiatry* 87: 570-579

Neary D, Snowden JS, Gustafson L, Passant U, Stuss D, Black S, Freedman M, Kertesz A, Robert PH, Albert M *et al* (1998) Frontotemporal lobar degeneration: a consensus on clinical diagnostic criteria. *Neurology* 51: 1546-1554

Neumann M, Sampathu DM, Kwong LK, Truax AC, Micsenyi MC, Chou TT, Bruce J, Schuck T, Grossman M, Clark CM *et al* (2006) Ubiquitinated TDP-43 in frontotemporal lobar degeneration and amyotrophic lateral sclerosis. *Science* 314: 130-133

Niccoli T, Partridge L, Isaacs AM (2017) Ageing as a risk factor for ALS/FTD. *Hum Mol Genet* 26: R105-R113

Norris F, Shepherd R, Denys E, U K, Mukai E, Elias L, Holden D, Norris H (1993) Onset, natural history and outcome in idiopathic adult motor neuron disease. *J Neurol Sci* 118: 48-55

Onoda K, Ishihara M, Yamaguchi S (2012) Decreased functional connectivity by aging is associated with cognitive decline. *J Cogn Neurosci* 24: 2186-2198

Oschmann M, Gawryluk JR (2020) A Longitudinal Study of Changes in Resting-State Functional Magnetic Resonance Imaging Functional Connectivity Networks During Healthy Aging. *Brain connectivity* 10: 377-384

Park DC, Reuter-Lorenz P (2009) The adaptive brain: aging and neurocognitive scaffolding. *Annu Rev Psychol* 60: 173-196

Phukan J, Elamin M, Bede P, Jordan N, Gallagher L, Byrne S, Lynch C, Pender N, Hardiman O (2012) The syndrome of cognitive impairment in amyotrophic lateral sclerosis: a population-based study. *J Neurol Neurosurg Psychiatry* 83: 102-108

Pringle CE, Hudson AJ, Munoz DG, Kiernan JA, Brown WF, Ebers GC (1992) Primary lateral sclerosis. Clinical features, neuropathology and diagnostic criteria. *Brain* 115 (Pt 2): 495-520

Prudlo J, Bissbort C, Glass A, Grossmann A, Hauenstein K, Benecke R, Teipel SJ (2012) White matter pathology in ALS and lower motor neuron ALS variants: a diffusion tensor imaging study using tract-based spatial statistics. *J Neurol* 259: 1848-1859

Rascovsky K, Hodges JR, Knopman D, Mendez MF, Kramer JH, Neuhaus J, van Swieten JC, Seelaar H, Dopper EG, Onyike CU *et al* (2011) Sensitivity of revised diagnostic criteria for the behavioural variant of frontotemporal dementia. *Brain* 134: 2456-2477

Renton AE, Chio A, Traynor BJ (2014) State of play in amyotrophic lateral sclerosis genetics. *Nat Neurosci* 17: 17-23

Robberecht W, Philips T (2013) The changing scene of amyotrophic lateral sclerosis. *Nat Rev Neurosci* 14: 248-264

Rodrigue KM, Kennedy KM, Devous MD, Sr., Rieck JR, Hebrank AC, Diaz-Arrastia R, Mathews D, Park DC (2012) beta-Amyloid burden in healthy aging: regional distribution and cognitive consequences. *Neurology* 78: 387-395

Rodrigue KM, Kennedy KM, Park DC (2009) Beta-amyloid deposition and the aging brain. *Neuropsychol Rev* 19: 436-450

Rohrer JD (2011) Behavioural variant frontotemporal dementia--defining genetic and pathological subtypes. *J Mol Neurosci* 45: 583-588

Rosen HJ, Gorno-Tempini ML, Goldman WP, Perry RJ, Schuff N, Weiner M, Feiwell R, Kramer JH, Miller BL (2002) Patterns of brain atrophy in frontotemporal dementia and semantic dementia. *Neurology* 58: 198-208

Rosenbohm A, Muller HP, Hubers A, Ludolph AC, Kassubek J (2016) Corticoefferent pathways in pure lower motor neuron disease: a diffusion tensor imaging study. *J Neurol* 263: 2430-2437

Salat DH, Buckner RL, Snyder AZ, Greve DN, Desikan RS, Busa E, Morris JC, Dale AM, Fischl B (2004) Thinning of the cerebral cortex in aging. *Cereb Cortex* 14: 721-730

Schuster C, Kasper E, Dyrba M, Machts J, Bittner D, Kaufmann J, Mitchell AJ, Benecke R, Teipel S, Vielhaber S *et al* (2014) Cortical thinning and its relation to cognition in amyotrophic lateral sclerosis. *Neurobiol Aging* 35: 240-246

Seeley WW, Crawford R, Rascovsky K, Kramer JH, Weiner M, Miller BL, Gorno-Tempini ML (2008) Frontal paralimbic network atrophy in very mild behavioral variant frontotemporal dementia. *Arch Neurol* 65: 249-255

Sieben A, Van Langenhove T, Engelborghs S, Martin JJ, Boon P, Cras P, De Deyn PP, Santens P, Van Broeckhoven C, Cruts M (2012) The genetics and neuropathology of frontotemporal lobar degeneration. *Acta Neuropathol* 124: 353-372

Smith SM, Jenkinson M, Johansen-Berg H, Rueckert D, Nichols TE, Mackay CE, Watkins KE, Ciccarelli O, Cader MZ, Matthews PM *et al* (2006) Tract-based spatial statistics: voxelwise analysis of multi-subject diffusion data. *NeuroImage* 31: 1487-1505

Spinelli EG, Agosta F, Ferraro PM, Riva N, Lunetta C, Falzone YM, Comi G, Falini A, Filippi M (2016) Brain MR Imaging in Patients with Lower Motor Neuron-Predominant Disease. *Radiology* 280: 545-556

Staffaroni AM, Brown JA, Casaletto KB, Elahi FM, Deng J, Neuhaus J, Cobigo Y, Mumford PS, Walters S, Saloner R *et al* (2018) The Longitudinal Trajectory of Default Mode Network Connectivity in Healthy Older Adults Varies As a Function of Age and Is Associated with Changes in Episodic Memory and Processing Speed. *J Neurosci* 38: 2809-2817

Stern Y, Barnes CA, Grady C, Jones RN, Raz N (2019) Brain reserve, cognitive reserve, compensation, and maintenance: operationalization, validity, and mechanisms of cognitive resilience. *Neurobiol Aging* 83: 124-129

Streit WJ, Khoshbouei H, Bechmann I (2021) The Role of Microglia in Sporadic Alzheimer's Disease. *J Alzheimers Dis* 79: 961-968

Strong MJ, Abrahams S, Goldstein LH, Woolley S, McLaughlin P, Snowden J, Mioshi E, Roberts-South A, Benatar M, HortobaGyi T *et al* (2017) Amyotrophic lateral sclerosis - frontotemporal spectrum disorder (ALS-FTSD): Revised diagnostic criteria. *Amyotrophic lateral sclerosis & frontotemporal degeneration* 18: 153-174

Stuss DT, Craik FI (2019) Alterations in executive functions with aging. *Cognitive changes and the aging brain*: 168-187

Swinnen B, Robberecht W (2014) The phenotypic variability of amyotrophic lateral sclerosis. *Nat Rev Neurol* 10: 661-670

Terribilli D, Schaufelberger MS, Duran FL, Zanetti MV, Curiati PK, Menezes PR, Scazufca M, Amaro E, Jr., Leite CC, Busatto GF (2011) Age-related gray matter volume changes in the brain during non-elderly adulthood. *Neurobiol Aging* 32: 354-368

Thambisetty M, Wan J, Carass A, An Y, Prince JL, Resnick SM (2010) Longitudinal changes in cortical thickness associated with normal aging. *NeuroImage* 52: 1215-1223

Tomasi D, Volkow ND (2012) Aging and functional brain networks. *Molecular psychiatry* 17: 471, 549-458

Turner MR, Hammers A, Allsop J, Al-Chalabi A, Shaw CE, Brooks DJ, Leigh PN, Andersen PM (2007) Volumetric cortical loss in sporadic and familial amyotrophic lateral sclerosis. *Amyotroph Lateral Scler* 8: 343-347

Urtamo A, Jyvakorpi SK, Strandberg TE (2019) Definitions of successful ageing: a brief review of a multidimensional concept. *Acta Biomed* 90: 359-363

van den Berg-Vos RM, Visser J, Franssen H, de Visser M, de Jong JM, Kalmijn S, Wokke JH, van den Berg LH (2003) Sporadic lower motor neuron disease with adult onset: classification of subtypes. *Brain* 126: 1036-1047

Verstraete E, van den Heuvel MP, Veldink JH, Blanken N, Mandl RC, Hulshoff Pol HE, van den Berg LH (2010) Motor network degeneration in amyotrophic lateral sclerosis: a structural and functional connectivity study. *PLoS One* 5: e13664

Whitwell JL, Avula R, Senjem ML, Kantarci K, Weigand SD, Samikoglu A, Edmonson HA, Vemuri P, Knopman DS, Boeve BF *et al* (2010) Gray and white matter water diffusion in the syndromic variants of frontotemporal dementia. *Neurology* 74: 1279-1287

Whitwell JL, Josephs KA, Avula R, Tosakulwong N, Weigand SD, Senjem ML, Vemuri P, Jones DT, Gunter JL, Baker M *et al* (2011) Altered functional connectivity in asymptomatic MAPT subjects: a comparison to bvFTD. *Neurology* 77: 866-874

Wong SQ, Kumar AV, Mills J, Lapierre LR (2020) Autophagy in aging and longevity. *Hum Genet* 139: 277-290

Wyss-Coray T (2016) Ageing, neurodegeneration and brain rejuvenation. *Nature* 539: 180-186

Zhou F, Xu R, Dowd E, Zang Y, Gong H, Wang Z (2014) Alterations in regional functional coherence within the sensory-motor network in amyotrophic lateral sclerosis. *Neuroscience letters* 558: 192-196

Zhou J, Greicius MD, Gennatas ED, Growdon ME, Jang JY, Rabinovici GD, Kramer JH, Weiner M, Miller BL, Seeley WW (2010) Divergent network connectivity changes in behavioural variant frontotemporal dementia and Alzheimer's disease. *Brain* 133: 1352-1367

Zhou Y, Friston KJ, Zeidman P, Chen J, Li S, Razi A (2018) The Hierarchical Organization of the Default, Dorsal Attention and Salience Networks in Adolescents and Young Adults. *Cereb Cortex* 28: 726-737

2. HUMAN BRAIN CONNECTOME

A human brain comprises about 100 billion neurons connected by about 100 trillion synapses, which are anatomically organized over multiple scales of space and functionally interactive over multiple scales of time (Fornito, 2016). Attempts to comprehensively map the neural connections are motivated by brain is not rigid architecture organized in individual regions, but rather its functioning is based on interaction patterns across the entire network (Filippi *et al*, 2013). Indeed, brain is a

macroscopic network of white matter pathways, that enable functional communication between distinct and anatomically separated regions of the brain. Cognitive and behavioral functions rely on these interaction patterns. Recent advances in neuroscience have enabled initiatives and collaborative projects to map brain networks more comprehensively and in greater detail, focusing on quantifying, visualizing, and understanding brain network organization not only in a healthy condition but also in pathological one. In the latter context, this might provide some help in clarifying fundamental pathophysiological aspects of neurological and psychiatric disorders and, in the near future, such knowledge might even help to develop new individualized therapeutic/rehabilitative strategies.

In order to better understand how brain works, useful and powerful approaches are network science and graph theory, a branch of mathematics dealing with the formal description and analysis of graphs, which are defined as sets of nodes or vertices linked by connections or edges. Network science and graph theory methods might help in understanding brain architecture, its function and dysfunction (Bullmore & Sporns, 2009; Griffa *et al*, 2013) and, in addition, in exploring how cognitive processes are related to the morphological substrates evaluating the linkage between structural changes and functional derangement (Sporns *et al*, 2005).

The human brain is probably the most highly complex, nonlinear and parallel information processing system in nature, with the ability to build its own rules based on experience and consisting of a multitude of interconnected networks. It presents an intractable computational problem, a constant challenge in revealing its operation, to such an extent that the ''network science of the brain'' remains a very recent challenging field. The network science defines the whole set of connections within the human brain as "Connectome".

The term "connectome" was proposed in 2005 by Dr. Olaf Sporns and refers to the full set of elements and connections comprising a nervous system (Sporns *et al.*, 2005). "Connectomics" is a scientific research field that includes all those approaches that study the connectome as the description of the functional and structural connectivity patterns of the human brain by mapping neural units and their connections at individual or group level (Sporns *et al.*, 2005). There are many advantages of such analysis approach:

1. Complex network analysis promises to reliably quantify brain networks with a

small number of neurobiologically meaningful and easily computable measures (Sporns & Zwi, 2004).

2. Network analysis allow to explore structural–functional connectivity relationship (Honey *et al*, 2009; Schmidt *et al*, 2014; Suarez *et al*, 2020).

3. Comparisons of structural or functional network organization in case-control studies are likely to reveal connectivity abnormalities in neurological and psychiatric disorders (Griffa *et al.*, 2013; Pievani *et al*, 2014; Wang *et al*, 2009).

2.1 GRAPH THEORETICAL MODEL

Graph theory is a field of mathematics that allows to model and simplify the complex nature of processes in different fields in order to investigate and better understand such phenomena. When describing a real-world system, a graph provides an abstract representation of the system's elements and their interactions (Bullmore & Sporns, 2009; Sporns, 2018). One of the most interesting applications of such approach can be found in network neuroscience, where graphs provide a theoretical framework to model pairwise communications between the elements of a network and allows the analysis of its topology.

The brain network is represented by nodes, i.e., brain regions, linked by edges, expressing structural or functional connections between the nodes. Mathematically, a network might be considered as a matrix, where each row and column represent different nodes (brain regions) and the cells of matrix carried the information on the interaction (structural or functional) of pairwise nodes.

A graph may be classified as undirected or directed depending on whether links have directions or not (Figure 5) (Farahani *et al*, 2019). Weighted links can represent the size or the density of anatomical tracts in the structural architecture of the network, while in the functional network they represent the strength of correlation or causal interactions. Unweighted (binary) networks indicated the only existence or absence of connection. Weighted network analysis can provide a more informative description of the structural and functional brain architecture, which has led to a greater interest and investigation over the years (Telesford *et al*, 2011).

A Binary graph (Undirected)

B Weighted graph (Undirected)

C Binary graph (Directed)

D Weighted graph (Directed)
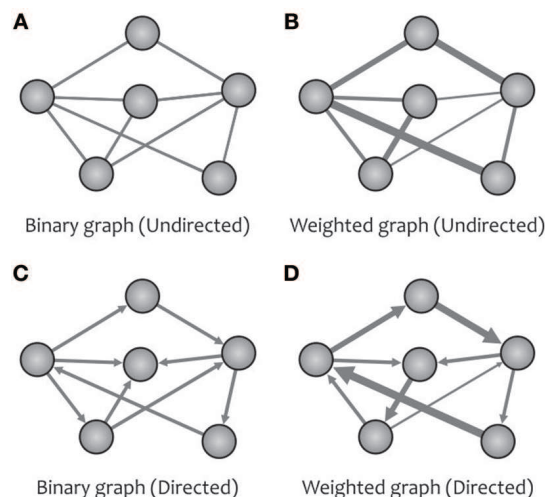
Figure 5: A network can be designed as **A)** binary (unweighted) **B)** weighted graphs and might represent the direction of causal effects in different regions **(C, D)** (Farahani *et al.*, 2019).

The architecture of the brain network can be described as a "small world" network (Figure 6-C) in which most nodes are not near each other but can be reached from every other node by a small number of steps (Farahani *et al.*, 2019; Sporns & Honey, 2006). Small-world property is characterized by the shortest path between each pair of nodes in the network using the minimum number of edges (Figure 6-B) and the highest clustering coefficient (Figure 6-A) to satisfy the balance between minimizing the resource cost and maximizing the flow of information among the network components (Farahani *et al.*, 2019; Sporns & Honey, 2006). Such architecture is crucial for healthy brain function and has an important role in cognitive abilities (van den Heuvel *et al*, 2009). On the other hand, disruption of the connectome, likely affects both network topological organization and function (Filippi *et al.*, 2013).
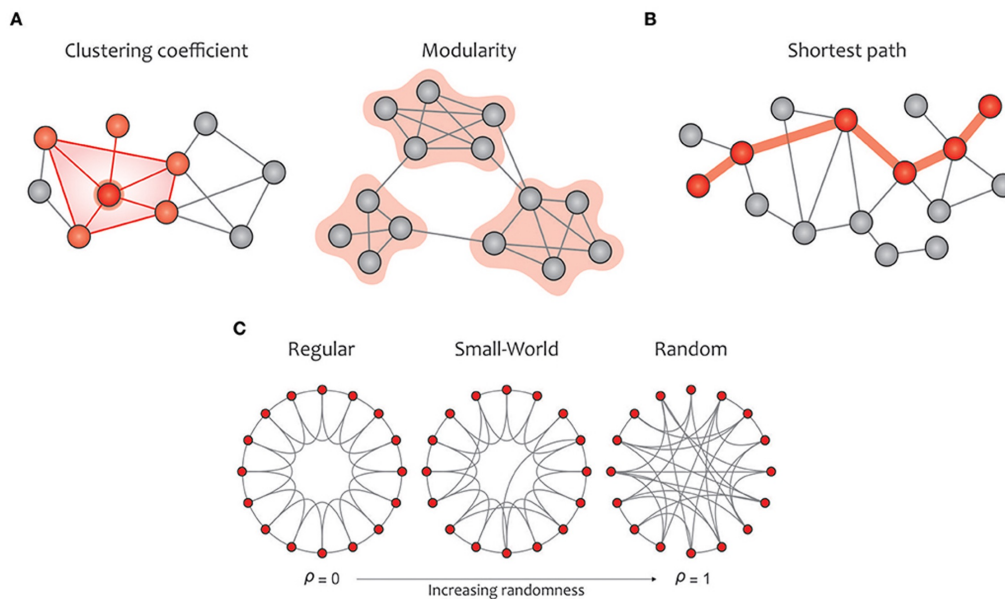
Figure 6: Summary of global graph measures. **(A)** Clustering coefficient quantifies how much neighbors of a given node are interconnected; modularity is related to clusters of nodes that have dense interconnectivity within clusters but sparse connections with nodes in other clusters. **(B)** characteristic path length determined as the average shortest path length across all pairs of nodes. **(C)** A regular network (left) displays a high clustering coefficient and a long average path length, while a random network (right) displays a low clustering coefficient and a short average path length. A small-world network (middle) illustrates an intermediate balance between regular and random networks, reflecting a high clustering coefficient and a short path length. Adapted from (Farahani *et al.*, 2019).

2.1.1 Graph metrics

As abovementioned, graph theory can be applied to model, simplify, and abstract the complex nature of brain and to describe several properties of network brain architecture from both structural and functional point of view. Although it is not yet established which measures are most appropriate for the analysis of brain networks, the most examined graph metrics in brain connectomics include degree, clustering, global efficiency and modularity (Figure 7).

The degree of a node is defined as the node's number of connections and provides a metric of the effect that a node has on the overall network infrastructure. Nodes with high degrees and an overall central position in a network's topological organization are often described as hubs (Filippi *et al.*, 2013). The level of clustering or local efficiency expresses the level of local connectedness of a network. The shortest path length describes the minimum number of steps needed to travel between two nodes. Global efficiency, calculated as the inverse of this measure, expresses the capacity of the network to communicate between remote regions.
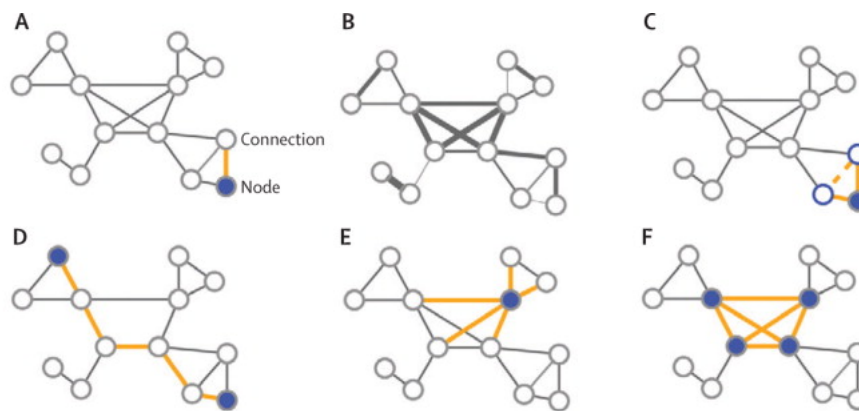
Figure 7. Summary of the main measures estimated with graph analysis. **(A)** A graph is a mathematical description of a network, consisting of a collection of nodes and connections. **(B)** A weighted graph includes information about the strength of the connections. **(C–F)** Local and global metrics can provide insight into the topological organization of a network. **(C)** The clustering coefficient describes the tendency of nodes to form local triangles, providing insight into the local organization of the network. **(D)** The shortest path length describes the minimum number of steps needed to travel between two nodes and describe the network capacity to communicate between distant regions. **(E)** The degree of a node describes its number of connections. **(F)** High-level connectivity between nodes (Filippi *et al.*, 2013).

Recent evidence suggests that a stable property of cortical brain network architecture is represented by central regions interconnecting distinct, functionally specialized

systems (i.e., regions displaying disproportionately numerous connections with other brain areas), known as hubs (Filippi *et al.*, 2013; van den Heuvel & Hulshoff Pol, 2010). Hubs are defined as heavily connected nodes in a network. Accordingly, hubs have a high node degree and a stronger potential effect on the overall network infrastructure. Hubs can be distinguished in "connector" or "provincial" according to their participation coefficient, high or low respectively. Connector hubs are usually those nodes that potentially play a role in between-module communication and in interconnecting nodes of the network (Bertolero *et al*, 2015). On the other hand, provincial hubs are thought to serve as hubs that integrate information within modules to support the functional specialization (Bertolero *et al.*, 2015). Hubs of a network tend to be more densely connected among themselves than nodes of a lower degree, organizing as a "rich club" network (van den Heuvel & Sporns, 2011).

2.1.2 Network Based Statistics

Network-based statistic (NBS) (Zalesky *et al*, 2010) is a powerful statistical approach to identify connections in brain network that may be associated with a pathological status in case-control studies. The purpose of the NBS in these studies is to identify any pairwise associations that are significantly different between groups. Such approach is a method to control the family-wise error (FWE) rate when mass-univariate testing is performed at every connection comprising the graph.

Specifically, the test statistic independently computed for each link is thresholded to construct a set of suprathreshold links. Connections comprising this set represent potential candidates for a statistical difference between groups, although at this stage statistical significance cannot be established. Such connections are stored and topological clusters, i.e., connected graph components, are identified within the suprathresholded connection step. The presence of a component might be the evidence of a non-chance structure for which the null hypothesis can be rejected, but such framework is not applicable for any individual connection. Finally, permutation testing is used to assign FWE-corrected p-value to each connected component based on its size.

NBS results in a more powerful tool than link-based controlling procedures (i.e., false discovery rate), as long as connectivity differences were structured in such a way that they formed connective components. Furthermore, its advantageous lies on its

applicability in the context of graph-based models where there is a massive number of multiple comparisons, arising when it is of interest evaluating every connection. The potential gain offered by NBS comes at a price: the null hypothesis can only be rejected on a component-by-component basis. This meaning that, with the NBS, it is never possible to declare individual links as being significant, only the component to which they belong can be declared significant.

2.2 STRUCTURAL AND FUNCTIONAL BRAIN NETWORKS

2.2.1 Structural brain network

According to graph theory, structural brain networks can be described as graphs that are composed of nodes, such as brain regions, that are linked by edges representing structural connections. Although graph theory emphasizes topological connectivity patterns, the topological and physical distances between elements in brain networks are often intricately related.

Graph theory allows to map white matter tracts individually using DTI. Maps of structural connectivity are created following the following steps:

1. *Identification of nodes*: network nodes are identified by applying a selected atlas of GM structures to the brain.

2. *Reconstruction of white matter tracts:* once brain regions are defined, white matter tracts between such regions are reconstructed using DTI.

3. *Identification of Streamlines:* streamlines touching each couple of the segmented grey matter nodes are selected and the number of streamlines is calculated for each white matter tract and inserted into a matrix, defining structural connections.

4. *Extraction of microstructural integrity measures:* for each structural connection, mean fractional anisotropy, mean diffusivity, radial diffusion and axial diffusion values are extracted as common measures of microstructural integrity.

5. *Creation of structural connectome:* finally, all values of such measures are inserted in different matrices, separately.

Analyzing the matrices, it is possible to provide information concerning the topological organization of network architecture (Stam & van Straaten, 2012).

2.2.2 Functional brain network

Although analyzing structural networks helps us to understand the fundamental architecture of the brain, it is also interesting to study functional networks in order to elucidate how the brain architecture supports neurophysiological dynamics.

Maps of functional connectivity are created following the following steps:

1. *Identification of nodes*: network nodes are identified by applying a selected atlas of grey matter structures to the brain.

2. *Extraction of mean RS fMRI time-series:* a mean RS fMRI time-series are obtained averaging the time-series of all voxels contained in each brain region. Likewise, a mean RS fMRI time-series are obtained for each region.

3. *Creation of functional connectome:* the Pearson correlation coefficient between these mean time-series, indicating the level of functional connectivity between pairwise regions, are entered into cell *c(i,j)* of an association matrix. Moreover, negative correlation coefficients, reflecting functional distinct brain regions, will be set to 0 to mark these brain regions as unconnected.

Graph-based approach might be applied to the association matrix of functional connectivity to provide information concerning the functional organization of brain architecture (Stam & van Straaten, 2012).

The functional connectivity matrix is used to be often "thresholded", meaning that only those connections that reach a specific value are considering. Thresholding is a commonly applied approach in studying functional connectome to remove spurious connections and to obtain connected matrices with a stronger biological interpretation, even though some studies suggested that this operation may ignore potentially valuable information in the functional network reconstruction (Gallos *et al*, 2012; Santarnecchi *et al*, 2014). Some most commonly applied approaches to perform this thresholding include the "absolute threshold" and the "proportional threshold" approach. The first approach describes the selection of those network edges that exceed an absolute threshold T 'a priori' defined. Another approach includes the selection of a pre-defined number of strongest connections as network edges, ensuring equal network density across datasets (van den Heuvel *et al*, 2017). Finally, another approach involves masking functional connectivity matrices with a comprehensive structural healthy connectome. Indeed, the healthy connectome might ideally represent all the possible structural connections existing in the human brain, in contrast to the pathological condition which might have already altered the structural connectome. Such framework allows not only to avoid taking into account false-positive functional connections, enhancing the biological interpretation of the results, but also to minimize the risk of including spurious functional connections (Filippi *et al*, 2017; Migliaccio *et al*, 2020; Schmidt *et al.*, 2014).

Effective connectivity models, that are specific functional connectivity approach for generating directed graphs, aim to estimate causal influence that each element of the

network exerts on the other elements. Among such models the most commonly applied are dynamic causal modelling (Friston *et al*, 2003) or Granger causality (Brovelli *et al*, 2004).

2.3 STATE OF ART IN NEURODEGENERATIVE DISEASES AND AGING

The application of the abovementioned graph theoretical approach has opened new avenues toward studying the functional and structural brain topological organization in order to identify the underpinning mechanisms to healthy aging and pathological conditions as neurodegenerative diseases.

Common findings among RS fMRI studies have indicated that aging affects the functional modular organization and functional hubs of the human brain (Zhang *et al*, 2020). In particular, aging is accompanied by changes in balance of network's cost of wiring and communication efficiency (defined as the minimum path length between regions) that implies decreasing local efficiency within networks and requires multi-step less efficient paths between regions mainly in frontal and temporal cortical regions (Betzel *et al*, 2014; Chan *et al*, 2014; Geerligs *et al*, 2015). This underlies an overall shift in the functional connectome topology, moving towards a predominance of long-range rather than short-range communication.

Overall, the most consistent findings of functional changes involve particularly higher-order networks specialized for cognition, such as the DMN (Geerligs *et al.*, 2015; Betzel *et al.*, 2014; Siman-Tov *et al*, 2016). Age-related functional differences have also been observed in other brain networks such as dorsal attention and the salience network (Grady *et al*, 2016; Tomasi & Volkow, 2012). These networks appear the most affected resting-state network in aging, with weakened within-network functional connectivity in different studies using graph theory (Grady *et al.*, 2016). In general, the idea is that intra-modular connectivity becomes weak during aging while inter-modular connections keep developing to balance the modular structure in the brain network (Spreng *et al*, 2016). Finally, among lifespan, there is greater recruitment of hubs in old subjects compared to young and middle age groups in the left hemisphere (Zhang *et al.*, 2020), supporting the right hemi-aging model, according to which age-related declines preferentially affect functions attributed to the right hemisphere than those associated with the left hemisphere

(Dolcos *et al*, 2002).

Regarding to structural connectivity, one of the main findings is that the topological efficiency of the white matter structural networks shows an inverted U-shaped trajectory across lifespan, with the peak age at approximately the third decade (Zhao *et al*, 2015). Indeed, in old age the structural organization eventually altered greatly, shifting to a more localized organization: such phenomena might be explained by increased shortest path length and clustering coefficient (Otte *et al*, 2015), but also by the opposite trend of the local and global efficiency: the local efficiency decreased, at first, but then increased, whereas global efficiency increased and then decreased with aging (Wu *et al*, 2012). Moreover, the hub integration decreased linearly with age, especially accompanied by the loss of frontal hubs and their connections (Zhao *et al.*, 2015). Moreover, the most prominent structural changes were found in frontal and temporal cortices (Coelho *et al*, 2021; Zhao *et al.*, 2015), consistent with the last-in-first-out hypothesis which posits that brain regions that reach full maturation later are more vulnerable to age-related atrophy.

Graph theory-based methods have found application also in the field of neurodegenerative diseases, which can be described as dysconnectivity syndromes, since their clinical manifestations might be related to disrupted integration of spatially distributed regions of the brain, part of large-scale networks. By applying such methods, it is possible to characterize the structural and functional brain topological organization in patients with different neurological disorders, as mild cognitive impairment, AD, bvFTD and MND.

Abnormal topological properties have been described in the structural brain networks of patients with AD (Filippi *et al*, 2020; Tijms *et al*, 2013). Studies suggested a greater segregation and a disrupted integration of topological organization in AD based on the network construction (He *et al*, 2008). Moreover, studies of structural brain networks in patients with AD showed increased inter-regional correlations within the local brain lobes and disrupted long-distance inter-regional correlations (Yao *et al*, 2010) and found an association between abnormal patterns of white matter connectivity and cognitive deficits.

Graph analysis has also been used to analyze RS fMRI data of patients with AD (Sanz-Arigita *et al*, 2010) and bvFTD (Agosta *et al*, 2013; Saba *et al*, 2019). In these studies, it emerges that altered functional connectivity involved brain regions closely associated

with neuropathological changes of such disorders, including posterior cingulate cortex and precuneus, the inferior parietal lobule, and the medial frontal cortex (components of default mode network) for AD (Zhao *et al*, 2012), and frontotemporal lobes and subcortical regions for bvFTD (Agosta *et al.*, 2013). Furthermore, through the reconstruction of functional connectome in patients with bvFTD, a global fragmentation of the functional brain network with severe disruption of the information-flow highways was observed in these patients, showing above all that the frontotemporal areas were less compact, more isolated, and concentrated in less integrated structures, compared to healthy controls (Saba *et al.*, 2019). Moreover, graph analysis and connectomics turn out to be useful tools to differentiate early onset AD from bvFTD, revealing disease-specific patterns of functional network topology and connectivity alterations (Filippi *et al.*, 2017). In addition, graph theory metrics have demonstrated their strength in the differentiation of individuals across the AD spectrum (Filippi *et al.*, 2020; Hojjati *et al*, 2017; Khazaee *et al*, 2015).

Graph analysis and connectomics were also applied to investigate ALS. Evaluating structural brain network in ALS, the most consistent finding is the reduced WM connectivity, centered around the primary motor connections as well as secondary motor connections (frontal cortex) (Fortanier *et al*, 2019; Verstraete *et al*, 2011). In addition, overall efficiency and clustering coefficient were found to be decreased in ALS patients(Verstraete *et al.*, 2011). Moreover, since ALS is now recognized as a system failure, involving not only clinical motor symptoms but also cognitive symptoms, a recent study applied a connectomic approach to better characterized ALS patients with cognitive/behavioral deficits revealing widespread cerebral white matter changes affecting frontotemporal regions in ALS with mild cognitive deficits relative to ALS with only motor impairment (van der Burgh *et al*, 2020). Few studies applied network-based analyses to the assessment of functional alterations in ALS patients using RS fMRI (Geevasinga *et al*, 2017; Zhou *et al*, 2016), demonstrating complex connectivity alterations encompassing frontal, temporal and occipital regions.

On the other hand, there is a paucity in literature of studies that applying connectomic approaches in MND variants such as PLS and PMA. Up to date, the study from our group (Basaia *et al*, 2020) is the first and only study that applied graph theory in these MND phenotypes, highlighting that PLS patients are characterized by widespread structural and

functional alterations encompassing both motor and extra-motor areas with a pattern resembling classic ALS patients in line with previous studies (Agosta *et al*, 2014; Muller *et al*, 2018). By contrast, PMA patients did not show any structural or functional damage relative to healthy controls, in line with previous studies (Rosenbohm *et al*, 2016; Spinelli *et al*, 2016), even using a technique that is highly sensitive to local disruptions in the brain networks.

2.4 NOVEL GRAPH THEORY METRICS (STEPWISE)

While most graph theory MRI studies emphasize the separation and isolation of networks in the brain, recent studies focused attention on how brain systems are bound together. In order to address this question, a novel graph method called 'stepwise connectivity' (SFC) has specifically developed to explore the convergence and interactions of sensory systems at the connectivity level (Sepulcre *et al*, 2012). SFC analysis aims to characterize regions that connect to specific seed brain areas at different levels of link-step distances. A step is referred to the number of links (edges) that belongs to a path connecting a node to the seed area.

Many graph theory metrics are based on the direct strength or number of connections that a given region or voxel displays, without taking into account of the position or distance of a given node from other proximal and distal regions. Recently, to overcome this caveat, graph theory metric based on SFC analysis has been developed. This metric calculates the relative network distance of every voxel in the brain and quantifies the precise or optimal location of that voxel with reference to all other voxels (Gao *et al*, 2018; Qian *et al*, 2018). In other words, the optimal connectivity distance metric captures the distance at which two nodes reach their maximal degree of connectivity.

2.5 ADVANCED DIFFUSION MRI MODEL

Diffusion MRI provides unique insight into tissue microstructure and is, without a doubt, the most promising technique for in vivo quantification of neurite morphology. The principle behind it is the measurement of the displacement of water molecules undergoing diffusion. Indeed, the water displacement pattern is influenced by tissue microarchitecture and, consequently, diffusion MRI measures support inferences on tissue microstructural integrity (Alexander *et al*, 2019; Zhang *et al*, 2012).

Currently, DTI is the most common MRI-based neuroimaging technique that allows to investigate white matter microstructural changes (Assaf & Cohen, 2000). This diffusion model allows to obtain indirect measures of microstructural white matter changes such as FA, MD, radial and axial diffusivity, not only in a condition of normal brain aging, but also in presence of neurodegenerative diseases or psychiatric disorders (Goveas *et al*, 2015; Wassenaar *et al*, 2019; Pasternak *et al*, 2018).

Despite its simple implementation and its microstructural sensitivity, the model underlying DTI is unspecific to biological changes. Indeed, reduction in FA might be caused by a decrease in neurite density but also by a dispersion of neurite orientation distribution (Zhang *et al.*, 2012). To better understand the direct neurobiological relevance from diffusion MRI, multicompartment biophysical models are needed.

The recent research in diffusion MRI is developing more advanced tools that can better model tissue microstructure and extract microstructural integrity features directly. A successful model of white matter microstructure consists of designing glial cells, axons, and extra-cellular space as individual compartments, since they show different diffusion behavior. Such approach is called Neurite orientation dispersion and density imaging (NODDI) and allows to investigate the exchange of water between the intra-cellular and extra-cellular compartments (Zhang *et al.*, 2012).

2.5.1 NODDI model

At the state-of-art, a novel model for the estimation of microstructural integrity is the NODDI (Parker *et al*, 2021; Zhang *et al.*, 2012). It is a multi-compartment model that enables the evaluation of three key aspects of neural tissue at each voxel: intra-cellular, extra-cellular, and CSF compartments. The intra-neurite compartment considers the tissue component of axons and dendrites, the extra-neurite compartment considers the

tissue component of cell bodies and glial cells, and the non-tissue comportment (e.g., CSF) accounts for free water (Figure 8)(Tariq *et al*, 2016).
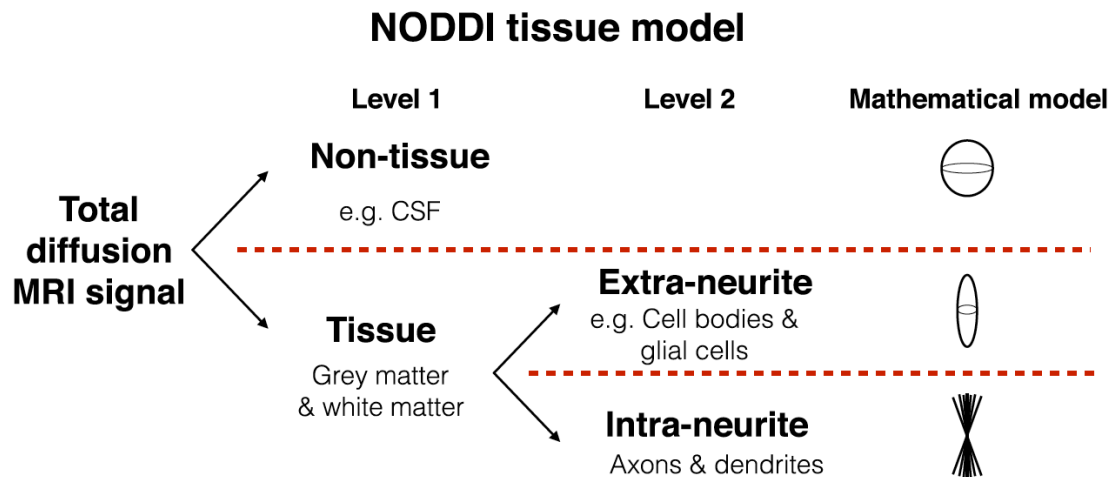
NODDI tissue model

Figure 8. Breakdown of the total normalized diffusion MRI signal as modelled by NODDI. The contributions of the tissue and non-tissue components of the brain are modelled separately. The tissue signal is further broken down to account for the signal originating from the highly restricted neurites and the hindered space outside the neurites. The non-tissue compartment is modelled by isotropic Gaussian diffusion. The intra-neurite compartment models the neurites as orientationally dispersed sticks, while the space around the neurites is prescribed an anisotropic diffusion model (Tariq *et al.*, 2016).

Such model considers the behavior of water diffusion within the environment (e.g., brain) in a more detailed and complex way and gives rise to a separate normalized MR signal. NODDI allows to estimate the density and the orientation dispersion of neurites by calculating tissue and non-tissue metrics such as neurite density index, also called intra-cellular volume fraction (ICVF), orientation dispersion index (ODI) and CSF volume fraction, also called isotropic water diffusion (ISO) (Tariq *et al.*, 2016; Zhang *et al.*, 2012). ICVF and ODI are strictly related to the density and the structural integrity of axons in white matter and dendrites in grey matter, that are fundamental for neural communication and might provide useful biomarkers of brain function in aging and neurodegenerative diseases(Parker *et al.*, 2021). Indeed, alterations in such metrics have been revealed in healthy aging (Kodiweera *et al*, 2016) and in neurological phenotypes, as amyotrophic lateral sclerosis (Gatto *et al*, 2018), frontotemporal dementia (Wen *et al*,

2019a), Alzheimer's disease (Colgan *et al*, 2016; Fu *et al*, 2020; Parker *et al*, 2018; Slattery *et al*, 2017; Wen *et al*, 2019b) and Parkinson's disease (Kamagata *et al*, 2018).

REFERENCES

Agosta F, Canu E, Inuggi A, Chio A, Riva N, Silani V, Calvo A, Messina S, Falini A, Comi G *et al* (2014) Resting state functional connectivity alterations in primary lateral sclerosis. *Neurobiol Aging* 35: 916-925

Agosta F, Sala S, Valsasina P, Meani A, Canu E, Magnani G, Cappa SF, Scola E, Quatto P, Horsfield MA *et al* (2013) Brain network connectivity assessed using graph theory in frontotemporal dementia. *Neurology* 81: 134-143

Alexander DC, Dyrby TB, Nilsson M, Zhang H (2019) Imaging brain microstructure with diffusion MRI: practicality and applications. *NMR Biomed* 32: e3841

Assaf Y, Cohen Y (2000) Assignment of the water slow-diffusing component in the central nervous system using q-space diffusion MRS: implications for fiber tract imaging. *Magn Reson Med* 43: 191-199

Basaia S, Agosta F, Cividini C, Trojsi F, Riva N, Spinelli EG, Moglia C, Femiano C, Castelnovo V, Canu E *et al* (2020) Structural and functional brain connectome in motor neuron diseases: A multicenter MRI study. *Neurology* 95: e2552-e2564

Bertolero MA, Yeo BT, D'Esposito M (2015) The modular and integrative functional architecture of the human brain. *Proc Natl Acad Sci U S A* 112: E6798-6807

Betzel RF, Byrge L, He Y, Goni J, Zuo XN, Sporns O (2014) Changes in structural and functional connectivity among resting-state networks across the human lifespan. *NeuroImage* 102 Pt 2: 345-357

Brovelli A, Ding M, Ledberg A, Chen Y, Nakamura R, Bressler SL (2004) Beta oscillations in a large-scale sensorimotor cortical network: directional influences revealed by Granger causality. *Proc Natl Acad Sci U S A* 101: 9849-9854

Bullmore E, Sporns O (2009) Complex brain networks: graph theoretical analysis of structural and functional systems. *Nat Rev Neurosci* 10: 186-198

Chan MY, Park DC, Savalia NK, Petersen SE, Wig GS (2014) Decreased segregation of brain systems across the healthy adult lifespan. *Proc Natl Acad Sci U S A* 111: E4997-5006

Coelho A, Fernandes HM, Magalhaes R, Moreira PS, Marques P, Soares JM, Amorim L, Portugal-Nunes C, Castanho T, Santos NC *et al* (2021) Reorganization of brain structural networks in aging: A longitudinal study. *J Neurosci Res* 99: 1354-1376

Colgan N, Siow B, O'Callaghan JM, Harrison IF, Wells JA, Holmes HE, Ismail O, Richardson S, Alexander DC, Collins EC *et al* (2016) Application of neurite orientation dispersion and density imaging (NODDI) to a tau pathology model of Alzheimer's disease. *NeuroImage* 125: 739-744

Dolcos F, Rice HJ, Cabeza R (2002) Hemispheric asymmetry and aging: right hemisphere decline or asymmetry reduction. *Neurosci Biobehav Rev* 26: 819-825

Farahani FV, Karwowski W, Lighthall NR (2019) Application of Graph Theory for Identifying Connectivity Patterns in Human Brain Networks: A Systematic Review. *Frontiers in neuroscience* 13: 585

Filippi M, Basaia S, Canu E, Imperiale F, Magnani G, Falautano M, Comi G, Falini A, Agosta F (2020) Changes in functional and structural brain connectome along the Alzheimer's disease continuum. *Molecular psychiatry* 25: 230-239

Filippi M, Basaia S, Canu E, Imperiale F, Meani A, Caso F, Magnani G, Falautano M, Comi G, Falini A *et al* (2017) Brain network connectivity differs in early-onset neurodegenerative dementia. *Neurology* 89: 1764-1772

Filippi M, van den Heuvel MP, Fornito A, He Y, Hulshoff Pol HE, Agosta F, Comi G, Rocca MA (2013) Assessment of system dysfunction in the brain through MRI-based connectomics. *Lancet Neurol* 12: 1189-1199

Fornito A, Zalesky, A., Bullmore, E. (2016) *Fundamentals of brain network analysis*. Elsevier Academic Press

Fortanier E, Grapperon AM, Le Troter A, Verschueren A, Ridley B, Guye M, Attarian S, Ranjeva JP, Zaaraoui W (2019) Structural Connectivity Alterations in Amyotrophic Lateral Sclerosis: A Graph Theory Based Imaging Study. *Frontiers in neuroscience* 13: 1044

Friston KJ, Harrison L, Penny W (2003) Dynamic causal modelling. *NeuroImage* 19: 1273-1302

Fu X, Shrestha S, Sun M, Wu Q, Luo Y, Zhang X, Yin J, Ni H (2020) Microstructural White Matter Alterations in Mild Cognitive Impairment and Alzheimer's Disease : Study Based on Neurite Orientation Dispersion and Density Imaging (NODDI). *Clin Neuroradiol* 30: 569-579

Gallos LK, Makse HA, Sigman M (2012) A small world of weak ties provides optimal global integration of self-similar modules in functional brain networks. *Proc Natl Acad Sci U S A* 109: 2825-2830

Gao Q, Yu Y, Su X, Tao Z, Zhang M, Wang Y, Leng J, Sepulcre J, Chen H (2018) Adaptation of brain functional stream architecture in athletes with fast demands of sensorimotor integration. *Hum Brain Mapp*

Gatto RG, Mustafi SM, Amin MY, Mareci TH, Wu YC, Magin RL (2018) Neurite orientation dispersion and density imaging can detect presymptomatic axonal degeneration in the spinal cord of ALS mice. *Functional neurology* 33: 155-163

Geerligs L, Renken RJ, Saliasi E, Maurits NM, Lorist MM (2015) A Brain-Wide Study of Age-Related Changes in Functional Connectivity. *Cereb Cortex* 25: 1987-1999

Geevasinga N, Korgaonkar MS, Menon P, Van den Bos M, Gomes L, Foster S, Kiernan MC, Vucic S (2017) Brain functional connectome abnormalities in amyotrophic lateral sclerosis are associated with disability and cortical hyperexcitability. *Eur J Neurol* 24: 1507-1517

Goveas J, O'Dwyer L, Mascalchi M, Cosottini M, Diciotti S, De Santis S, Passamonti L, Tessa C, Toschi N, Giannelli M (2015) Diffusion-MRI in neurodegenerative disorders. *Magn Reson Imaging* 33: 853-876

Grady C, Sarraf S, Saverino C, Campbell K (2016) Age differences in the functional interactions among the default, frontoparietal control, and dorsal attention networks. *Neurobiol Aging* 41: 159-172

Griffa A, Baumann PS, Thiran JP, Hagmann P (2013) Structural connectomics in brain diseases. *NeuroImage* 80: 515-526

He Y, Chen Z, Evans A (2008) Structural insights into aberrant topological patterns of large-scale cortical networks in Alzheimer's disease. *J Neurosci* 28: 4756-4766

Hojjati SH, Ebrahimzadeh A, Khazaee A, Babajani-Feremi A, Alzheimer's Disease Neuroimaging I (2017) Predicting conversion from MCI to AD using resting-state fMRI, graph theoretical approach and SVM. *J Neurosci Methods* 282: 69-80

Honey CJ, Sporns O, Cammoun L, Gigandet X, Thiran JP, Meuli R, Hagmann P (2009) Predicting human resting-state functional connectivity from structural connectivity. *Proc Natl Acad Sci U S A* 106: 2035-2040

Kamagata K, Zalesky A, Hatano T, Di Biase MA, El Samad O, Saiki S, Shimoji K, Kumamaru KK, Kamiya K, Hori M *et al* (2018) Connectome analysis with diffusion MRI in idiopathic Parkinson's disease: Evaluation using multi-shell, multi-tissue, constrained spherical deconvolution. *Neuroimage Clin* 17: 518-529

Khazaee A, Ebrahimzadeh A, Babajani-Feremi A (2015) Identifying patients with Alzheimer's disease using resting-state fMRI and graph theory. *Clinical neurophysiology : official journal of the International Federation of Clinical Neurophysiology* 126: 2132-2141

Kodiweera C, Alexander AL, Harezlak J, McAllister TW, Wu YC (2016) Age effects and sex differences in human brain white matter of young to middle-aged adults: A DTI, NODDI, and q-space study. *NeuroImage* 128: 180-192

Migliaccio R, Agosta F, Basaia S, Cividini C, Habert MO, Kas A, Montembeault M, Filippi M (2020) Functional brain connectome in posterior cortical atrophy. *Neuroimage Clin* 25: 102100

Muller HP, Agosta F, Gorges M, Kassubek R, Spinelli EG, Riva N, Ludolph AC, Filippi M, Kassubek J (2018) Cortico-efferent tract involvement in primary lateral sclerosis and amyotrophic lateral sclerosis: A two-centre tract of interest-based DTI analysis. *Neuroimage Clin* 20: 1062-1069

Otte WM, van Diessen E, Paul S, Ramaswamy R, Subramanyam Rallabandi VP, Stam CJ, Roy PK (2015) Aging alterations in whole-brain networks during adulthood mapped with the minimum spanning tree indices: the interplay of density, connectivity cost and life-time trajectory. *NeuroImage* 109: 171-189

Parker CS, Veale T, Bocchetta M, Slattery CF, Malone IB, Thomas DL, Schott JM, Cash DM, Zhang H, Alzheimer's Disease Neuroimaging I (2021) Not all voxels are created equal: Reducing estimation bias in regional NODDI metrics using tissue-weighted means. *NeuroImage* 245: 118749

Parker TD, Slattery CF, Zhang J, Nicholas JM, Paterson RW, Foulkes AJM, Malone IB, Thomas DL, Modat M, Cash DM *et al* (2018) Cortical microstructure in young onset Alzheimer's disease using neurite orientation dispersion and density imaging. *Hum Brain Mapp* 39: 3005-3017

Pasternak O, Kelly S, Sydnor VJ, Shenton ME (2018) Advances in microstructural diffusion neuroimaging for psychiatric disorders. *NeuroImage* 182: 259-282

Pievani M, Filippini N, van den Heuvel MP, Cappa SF, Frisoni GB (2014) Brain connectivity in neurodegenerative diseases--from phenotype to proteinopathy. *Nat Rev Neurol* 10: 620-633

Qian J, Diez I, Ortiz-Teran L, Bonadio C, Liddell T, Goni J, Sepulcre J (2018) Positive Connectivity Predicts the Dynamic Intrinsic Topology of the Human Brain Network. *Frontiers in systems neuroscience* 12: 38

Rosenbohm A, Muller HP, Hubers A, Ludolph AC, Kassubek J (2016) Corticoefferent pathways in pure lower motor neuron disease: a diffusion tensor imaging study. *J Neurol* 263: 2430-2437

Saba V, Premi E, Cristillo V, Gazzina S, Palluzzi F, Zanetti O, Gasparotti R, Padovani A, Borroni B, Grassi M (2019) Brain Connectivity and Information-Flow Breakdown Revealed by a Minimum Spanning Tree-Based Analysis of MRI Data in Behavioral Variant Frontotemporal Dementia. *Frontiers in neuroscience* 13: 211

Santarnecchi E, Galli G, Polizzotto NR, Rossi A, Rossi S (2014) Efficiency of weak brain connections support general cognitive functioning. *Hum Brain Mapp* 35: 4566-4582

Sanz-Arigita EJ, Schoonheim MM, Damoiseaux JS, Rombouts SA, Maris E, Barkhof F, Scheltens P, Stam CJ (2010) Loss of 'small-world' networks in Alzheimer's disease: graph analysis of FMRI resting-state functional connectivity. *PLoS One* 5: e13788

Schmidt R, Verstraete E, de Reus MA, Veldink JH, van den Berg LH, van den Heuvel MP (2014) Correlation between structural and functional connectivity impairment in amyotrophic lateral sclerosis. *Hum Brain Mapp* 35: 4386-4395

Sepulcre J, Sabuncu MR, Yeo TB, Liu H, Johnson KA (2012) Stepwise connectivity of the modal cortex reveals the multimodal organization of the human brain. *J Neurosci* 32: 10649-10661

Siman-Tov T, Bosak N, Sprecher E, Paz R, Eran A, Aharon-Peretz J, Kahn I (2016) Early Age-Related Functional Connectivity Decline in High-Order Cognitive Networks. *Front Aging Neurosci* 8: 330

Slattery CF, Zhang J, Paterson RW, Foulkes AJM, Carton A, Macpherson K, Mancini L, Thomas DL, Modat M, Toussaint N *et al* (2017) ApoE influences regional white-matter axonal density loss in Alzheimer's disease. *Neurobiol Aging* 57: 8-17

Spinelli EG, Agosta F, Ferraro PM, Riva N, Lunetta C, Falzone YM, Comi G, Falini A, Filippi M (2016) Brain MR Imaging in Patients with Lower Motor Neuron-Predominant Disease. *Radiology* 280: 545-556

Sporns O (2018) Graph theory methods: applications in brain networks. *Dialogues Clin Neurosci* 20: 111-121

Sporns O, Honey CJ (2006) Small worlds inside big brains. *Proc Natl Acad Sci U S A* 103: 19219-19220

Sporns O, Tononi G, Kotter R (2005) The human connectome: A structural description of the human brain. *PLoS Comput Biol* 1: e42

Sporns O, Zwi JD (2004) The small world of the cerebral cortex. *Neuroinformatics* 2: 145-162

Spreng RN, Stevens WD, Viviano JD, Schacter DL (2016) Attenuated anticorrelation between the default and dorsal attention networks with aging: evidence from task and rest. *Neurobiol Aging* 45: 149-160

Stam CJ, van Straaten EC (2012) The organization of physiological brain networks. *Clinical neurophysiology : official journal of the International Federation of Clinical Neurophysiology* 123: 1067-1087

Suarez LE, Markello RD, Betzel RF, Misic B (2020) Linking Structure and Function in Macroscale Brain Networks. *Trends Cogn Sci* 24: 302-315

Tariq M, Schneider T, Alexander DC, Gandini Wheeler-Kingshott CA, Zhang H (2016) Bingham-NODDI: Mapping anisotropic orientation dispersion of neurites using diffusion MRI. *NeuroImage* 133: 207-223

Telesford QK, Simpson SL, Burdette JH, Hayasaka S, Laurienti PJ (2011) The brain as a complex system: using network science as a tool for understanding the brain. *Brain connectivity* 1: 295-308

Tijms BM, Wink AM, de Haan W, van der Flier WM, Stam CJ, Scheltens P, Barkhof F (2013) Alzheimer's disease: connecting findings from graph theoretical studies of brain networks. *Neurobiol Aging* 34: 2023-2036

Tomasi D, Volkow ND (2012) Aging and functional brain networks. *Molecular psychiatry* 17: 471, 549-458

van den Heuvel MP, de Lange SC, Zalesky A, Seguin C, Yeo BTT, Schmidt R (2017) Proportional thresholding in resting-state fMRI functional connectivity networks and consequences for patient-control connectome studies: Issues and recommendations. *NeuroImage* 152: 437-449

van den Heuvel MP, Hulshoff Pol HE (2010) Exploring the brain network: a review on resting-state fMRI functional connectivity. *Eur Neuropsychopharmacol* 20: 519-534

van den Heuvel MP, Sporns O (2011) Rich-club organization of the human connectome. *J Neurosci* 31: 15775-15786

van den Heuvel MP, Stam CJ, Kahn RS, Hulshoff Pol HE (2009) Efficiency of functional brain networks and intellectual performance. *J Neurosci* 29: 7619-7624

van der Burgh HK, Westeneng HJ, Walhout R, van Veenhuijzen K, Tan HHG, Meier JM, Bakker LA, Hendrikse J, van Es MA, Veldink JH *et al* (2020) Multimodal longitudinal study of structural brain involvement in amyotrophic lateral sclerosis. *Neurology* 94: e2592-e2604

Verstraete E, Veldink JH, Mandl RC, van den Berg LH, van den Heuvel MP (2011) Impaired structural motor connectome in amyotrophic lateral sclerosis. *PLoS One* 6: e24239

Wang L, Zhu C, He Y, Zang Y, Cao Q, Zhang H, Zhong Q, Wang Y (2009) Altered small-world brain functional networks in children with attention-deficit/hyperactivity disorder. *Hum Brain Mapp* 30: 638-649

Wassenaar TM, Yaffe K, van der Werf YD, Sexton CE (2019) Associations between modifiable risk factors and white matter of the aging brain: insights from diffusion tensor imaging studies. *Neurobiol Aging* 80: 56-70

Wen J, Zhang H, Alexander DC, Durrleman S, Routier A, Rinaldi D, Houot M, Couratier P, Hannequin D, Pasquier F *et al* (2019a) Neurite density is reduced in the presymptomatic phase of C9orf72 disease. *J Neurol Neurosurg Psychiatry* 90: 387-394

Wen Q, Mustafi SM, Li J, Risacher SL, Tallman E, Brown SA, West JD, Harezlak J, Farlow MR, Unverzagt FW *et al* (2019b) White matter alterations in early-stage Alzheimer's disease: A tract-specific study. *Alzheimers Dement (Amst)* 11: 576-587

Wu K, Taki Y, Sato K, Kinomura S, Goto R, Okada K, Kawashima R, He Y, Evans AC, Fukuda H (2012) Age-related changes in topological organization of structural brain networks in healthy individuals. *Hum Brain Mapp* 33: 552-568

Yao Z, Zhang Y, Lin L, Zhou Y, Xu C, Jiang T, Alzheimer's Disease Neuroimaging I (2010) Abnormal cortical networks in mild cognitive impairment and Alzheimer's disease. *PLoS Comput Biol* 6: e1001006

Zalesky A, Fornito A, Bullmore ET (2010) Network-based statistic: identifying differences in brain networks. *NeuroImage* 53: 1197-1207

Zhang H, Schneider T, Wheeler-Kingshott CA, Alexander DC (2012) NODDI: practical in vivo neurite orientation dispersion and density imaging of the human brain. *NeuroImage* 61: 1000-1016

Zhang Y, Wang Y, Chen N, Guo M, Wang X, Chen G, Li Y, Yang L, Li S, Yao Z *et al* (2020) Age-Associated Differences of Modules and Hubs in Brain Functional Networks. *Front Aging Neurosci* 12: 607445

Zhao T, Cao M, Niu H, Zuo XN, Evans A, He Y, Dong Q, Shu N (2015) Age-related changes in the topological organization of the white matter structural connectome across the human lifespan. *Hum Brain Mapp* 36: 3777-3792

Zhao X, Liu Y, Wang X, Liu B, Xi Q, Guo Q, Jiang H, Jiang T, Wang P (2012) Disrupted small-world brain networks in moderate Alzheimer's disease: a resting-state FMRI study. *PLoS One* 7: e33540

Zhou C, Hu X, Hu J, Liang M, Yin X, Chen L, Zhang J, Wang J (2016) Altered Brain Network in Amyotrophic Lateral Sclerosis: A Resting Graph Theory-Based Network Study at Voxel-Wise Level. *Frontiers in neuroscience* 10: 204

3. AIMS OF THE WORK

Neurodegenerative diseases have two main characteristics: an insidious progression and a selective predilection in the breakdown of specific brain regions. Both aspects are also shared with aging process. Irreversibility and steady progression of clinical manifestations are common features between brain aging and neurodegeneration conditions. Moreover, selective regional vulnerability defines the clinical features of different neurodegenerative diseases, as well as aging seems to affect specific brain regions paving the way (additive effect) to the onset of neurodegenerative diseases (Bischof *et al*, 2019; Pandya & Patani, 2020; Pichet Binette *et al*, 2020). Defining this separation line is however shadowy, as the aging and the neurodegenerative processes are intermingled.

In order to shed light on brain changes related to aging and those caused by neurodegenerative diseases, MRI advanced techniques, such as connectome-based approaches, represent valuable in vivo technical innovation. Connectomics allow to model better the complex organizational nature of the brain in order to understand the underlying brain circuitry and the underpinnings mechanisms with a network-based approach, relying on the interplay between segregation and integration properties (Sporns, 2013). This has paved the way to investigate comprehensively several neurodegenerative diseases, including ALS and FTD. A growing body of evidence supports the notion of clinical, pathological and genetic overlap between ALS and the wide spectrum of FTD (Burrell *et al*, 2016; Devenney *et al*, 2015).

During my PhD studies, I have applied graph theory-based approaches and connectomics to explore brain structural and functional changes across FTD-ALS spectrum with the goal of mapping spatiotemporal patterns of degeneration in these conditions. Moreover, I applied novel advanced MRI techniques on healthy aging to identify specific structural and functional brain changes in order to answer the question of whether neurodegeneration-related patterns of damage represent accelerated aging or a distinct process.

The studies are described in chapters 4 and 5, and the results are jointly discussed in chapter 6.

Specific aims of the project included:

1.   Investigating structural and functional brain network architecture in MND clinical phenotypes (chapter 4.1). The global topology and regional effects on the structural and functional brain connectome were investigated in patients with ALS, PLS and PMA.

2.   Chapter 4.2 was focused on the specific and more common phenotype of MND (i.e., ALS). The aim of the present study was to investigate structural and functional network correlates of cognitive/behavioral impairment in patients within the ALS-FTD continuum. Using up-to-date MRI approaches, I assessed distinctive patterns of network disruption (i.e., "ALS-cn-like pattern" and "bvFTD-like pattern") that may prove useful for accurate classification at a single-patient level.

3.   In Chapter 5, I put my effort in understanding the role played by healthy aging in neurodegenerative diseases, studying the age-related vulnerability of the human brain connectome (chapter 5.1). The goal here was to better understand how aging might pave the way to the onset of neurodegenerative diseases, as dementia.

4.   Finally, in chapter 5.2 I assessed white matter integrity using novel and advanced diffusion metrics, able to identify the tracts affected during aging. The identification of such changes might help to understand the substrate and the regional variability of age-related degeneration.

5.   Chapter 7 listed other studies and projects I have played an active role and participated in their implementation during my PhD.

REFERENCES

Bischof GN, Ewers M, Franzmeier N, Grothe MJ, Hoenig M, Kocagoncu E, Neitzel J, Rowe JB, Strafella A, Drzezga A *et al* (2019) Connectomics and molecular imaging in neurodegeneration. *Eur J Nucl Med Mol Imaging* 46: 2819-2830

Burrell JR, Halliday GM, Kril JJ, Ittner LM, Gotz J, Kiernan MC, Hodges JR (2016) The frontotemporal dementia-motor neuron disease continuum. *Lancet* 388: 919-931

Damoiseaux JS (2017) Effects of aging on functional and structural brain connectivity. *NeuroImage* 160: 32-40

Devenney E, Vucic S, Hodges JR, Kiernan MC (2015) Motor neuron disease-frontotemporal dementia: a clinical continuum. *Expert Rev Neurother* 15: 509-522

Pandya VA, Patani R (2020) Decoding the relationship between ageing and amyotrophic lateral sclerosis: a cellular perspective. *Brain* 143: 1057-1072

Pichet Binette A, Gonneaud J, Vogel JW, La Joie R, Rosa-Neto P, Collins DL, Poirier J, Breitner JCS, Villeneuve S, Vachon-Presseau E *et al* (2020) Morphometric network differences in ageing versus Alzheimer's disease dementia. *Brain* 143: 635-649

Sporns O (2013) Structure and function of complex brain networks. *Dialogues Clin Neurosci* 15: 247-262

4. APPLICATIONS OF ADVANCED MRI TECNIQUES IN MOTOR NEURON DISEASE - FRONTOTEMPORAL DEGENERATION SPECTRUM

4.1. STRUCTURAL AND FUNCTIONAL BRAIN CONNECTOME IN MOTOR NEURON DISEASES: A MULTICENTER MRI STUDY

Structural and functional brain connectome in motor neuron diseases
A multicenter MRI study

Silvia Basaia, PhD, Federica Agosta, MD, PhD, Camilla Cividini, MSc, Francesca Trojsi, MD, PhD,
Nilo Riva, MD, PhD, Edoardo G. Spinelli, MD, Cristina Moglia, MD, PhD, Cinzia Femiano, MD,
Veronica Castelnovo, MSc, Elisa Canu, PhD, Yuri Falzone, MD, Maria Rosaria Monsurrò, MD, Andrea Falini, MD,
Adriano Chiò, MD, Gioacchino Tedeschi, MD, and Massimo Filippi, MD

Correspondence
Prof. Filippi
filippi.massimo@hsr.it

Abstract

Objective
To investigate structural and functional neural organization in amyotrophic lateral sclerosis (ALS), primary lateral sclerosis (PLS), and progressive muscular atrophy (PMA).

Methods
A total of 173 patients with sporadic ALS, 38 patients with PLS, 28 patients with PMA, and 79 healthy controls were recruited from 3 Italian centers. Participants underwent clinical, neuropsychological, and brain MRI evaluations. Using graph analysis and connectomics, global and lobar topologic network properties and regional structural and functional brain connectivity were assessed. The association between structural and functional network organization and clinical and cognitive data was investigated.

Results
Compared with healthy controls, patients with ALS and patients with PLS showed altered structural global network properties, as well as local topologic alterations and decreased structural connectivity in sensorimotor, basal ganglia, frontal, and parietal areas. Patients with PMA showed preserved global structure. Patient groups did not show significant alterations of functional network topologic properties relative to controls. Increased local functional connectivity was observed in patients with ALS in the precentral, middle, and superior frontal areas, and in patients with PLS in the sensorimotor, basal ganglia, and temporal networks. In patients with ALS and patients with PLS, structural connectivity alterations correlated with motor impairment, whereas functional connectivity disruption was closely related to executive dysfunction and behavioral disturbances.

Conclusions
This multicenter study showed widespread motor and extramotor network degeneration in ALS and PLS, suggesting that graph analysis and connectomics might represent a powerful approach to detect upper motor neuron degeneration, extramotor brain changes, and network reorganization associated with the disease. Network-based advanced MRI provides an objective in vivo assessment of motor neuron diseases, delivering potential prognostic markers.

From the Neuroimaging Research Unit, Institute of Experimental Neurology, Division of Neuroscience, (S.B., F.A., C.C., E.G.S., V.C., E.C., M.F.), Neurorehabilitation Unit (N.R.), Neurology Unit (Y.F., M.F.), Neurophysiology Unit (M.F.), and Department of Neuroradiology and CERMAC (A.F.), IRCCS San Raffaele Scientific Institute; Vita-Salute San Raffaele University (F.A., C.C., E.G.S., V.C., Y.F., A.F., M.F.), Milan; Department of Advanced Medical and Surgical Sciences (F.T., C.F., M.R.M., G.T.), University of Campania "Luigi Vanvitelli," Naples; and ALS Center (C.M., A.C.), "Rita Levi Montalcini" Department of Neuroscience, University of Torino, Italy.

INTRODUCTION

Motor neuron diseases (MND) are progressive neurodegenerative conditions characterized by the breakdown of the motor system. The involvement of the upper motor neurons (UMN) and/or lower motor neurons (LMN) defines different clinical phenotypes, including amyotrophic lateral sclerosis (ALS), primary lateral sclerosis (PLS) and progressive muscular atrophy (PMA)(Norris *et al*, 1993). Compared with ALS, PLS and PMA patients are characterized by a slower rate of progression and a more benign prognosis(Chio *et al*, 2011).

Validation of noninvasive biomarkers to characterize different MND phenotypes is a challenge of growing importance in order to recognize subjects known to be at risk of more rapid progression (i.e., conversion to the ALS phenotype) prior to the appearance of clinically apparent disease. Brain magnetic resonance imaging (MRI) has shown to be promising, over the last decades, to detect in vivo structural and functional brain abnormalities and to monitor degeneration within the central nervous system of MND patients (Basaia *et al*, 2019). To date, it is of great relevance to evaluate whether MRI biomarkers are suitable and reliable in a multicenter context.

In ALS patients, many diffusion tensor (DT) MRI studies have consistently identified structural alterations in a "signature" white matter (WM) region involving the corticospinal tract (CST) and the middle and posterior parts of the corpus callosum (Muller *et al*, 2016). DT MRI has proven useful in distinguishing MND variants (Agosta *et al*, 2014b; Rosenbohm *et al*, 2016; Spinelli *et al*, 2016), as PLS patients showed more widespread DT MRI damage compared to ALS (Agosta *et al.*, 2014b), whereas the least diffuse WM damage was observed in patients with predominant LMN involvement (Rosenbohm *et al.*, 2016; Spinelli *et al.*, 2016).

In ALS, resting-state functional MRI (RS fMRI) studies reported inconsistent results, showing either decreased or increased functional connectivity in the premotor, motor and subcortical regions (Agosta *et al*, 2014a; Menke *et al*, 2016). To date, other MND phenotypes are yet to be explored using RS fMRI, as only one study reported increased functional connectivity within the sensorimotor, frontal, and left frontoparietal networks of PLS patients (Agosta *et al.*, 2014a), and no studies assessed brain functional underpinnings of PMA.

In the last decade, neuroimaging research has zeroed in on the study of changes in structural and functional connectivity at a whole-brain-system level, rather than on alterations in single brain regions (Bullmore & Sporns, 2009), applying the 'graph theory' analysis (Tijms *et al*, 2013). It has been widely demonstrated that this approach is a powerful tool to measure structural and functional reorganization in neurodegenerative diseases (van den Heuvel & Sporns, 2019), including ALS (Geevasinga *et al*, 2017; Verstraete *et al*, 2014). To date, no studies used graph analysis and connectomics to investigate structural and functional networks in different phenotypes of MND. In addition, previous network-based studies involved single-center cohorts, thus limiting the generalizability of findings.

Considering this background, the aim of the present study was to investigate structural and functional neural organization in ALS, PLS and PMA patients using graph analysis and connectomics. One of the main novelties of our study was the use of data from different centers, neuroimaging protocols and scanners, in order to reach both reliability and reproducibility of results.

METHODS

The present work is a prospective and multicenter study. Subjects were recruited and clinically evaluated at three Italian ALS centers (San Raffaele Scientific Institute, Milan; Azienda Ospedaliera Città della Salute e della Scienza, Turin; and Università degli Studi della Campania "Luigi Vanvitelli", Naples) from 2009 to 2017 in the framework of a large, observational study. MRI scans were obtained from all participants using two 3T scanners: Philips Medical Systems Intera machine (for Milan and Turin patients) and GE Signa HDxt machine (for Naples patients). All MRI data were analyzed at the Neuroimaging Research Unit, Division of Neuroscience, San Raffaele Scientific Institute and Vita-Salute San Raffaele University, Milan, Italy.

Participants

239 sporadic MND patients (173 cases with classic ALS, 38 with PLS, and 28 with PMA) were consecutively recruited from those routinely evaluated at the three clinical centers (Table 1). Classic ALS patients (131 from Milan/Turin and 42 from Naples) met a diagnosis of probable or definite ALS according to the revised El Escorial criteria

(Brooks *et al*, 2000). Thirty-eight patients (all from the Milan/Turin dataset) were diagnosed as PLS according to Pringle's criteria at the last available clinical follow up (Pringle *et al*, 1992). Twenty-eight patients had PMA (all from the Milan/Turin dataset) (van den Berg-Vos *et al*, 2003). All patients were receiving riluzole at study entry. Seventy-nine age- and sex-matched healthy controls (61 from Milan/Turin and 18 from Naples) were recruited by word of mouth (Table 1), based on the following criteria: normal neurological assessment; mini mental state examination (MMSE) score ≥28; no family history of neurodegenerative diseases. Exclusion criteria for all subjects (i.e., patients and healthy controls) were: medical illnesses or substance abuse that could interfere with cognitive functioning; any (other) major systemic, psychiatric, or neurological diseases; other causes of brain damage, including lacunae and extensive cerebrovascular disorders at MRI.

Disease severity was assessed using the ALS Functional Rating Scale-revised (ALSFRS-r) (Cedarbaum *et al*, 1999). The baseline rate of disease progression was defined according to the following formula: (48–ALSFRS-r score)/time between symptom onset and first visit. Muscular strength was assessed by manual muscle testing based on the Medical Research Council (MRC) scale, and clinical upper motor neuron (UMN) involvement was graded by totaling the number of pathological UMN signs on examination (Turner *et al*, 2004). For the UMN score, we also considered the presence of non-definite UMN signs such as reduced, but still evocable reflexes in muscles with LMN signs, which were detected in few PMA individuals.

Standard Protocol Approvals, Registrations, and Patient Consents

Local ethical standards committee on human experimentation approved the study protocol and all participants provided written informed consent (Ethical committee numbers: RF-2011-02351193 and ConnectALS).

Neuropsychological assessment

Neuropsychological assessments were performed by experienced neuropsychologists unaware of the MRI results (data available from Appendix, E-Table 1). The following cognitive functions were evaluated: global cognitive functioning with the MMSE (Folstein *et al*, 1975); long and short term verbal memory with the Rey Auditory Verbal

Learning Test (Carlesimo *et al*, 1996) and the digit span forward (Orsini *et al*, 1987), respectively; executive functions with the digit span backward (Monaco *et al*, 2013). the Stroop interference test (Barbarotto *et al*, 1998), the Cognitive Estimation Task (Della Sala *et al*, 2003), the Weigl's Sorting test (Tognoni, 1987), the Wisconsin Card Sorting Test (Laiacona *et al*, 2000) or the Modified Card Sorting Test (Caffarra *et al*, 2004), and the Raven's coloured progressive matrices (Basso *et al*, 1987); fluency with the phonemic and semantic fluency tests (Carlesimo *et al.*, 1996; Novelli, 1986; Tognoni, 1987) and the relative fluency indices (controlling for individual motor disabilities) (Abrahams *et al*, 2000); language with the Italian battery for the assessment of aphasic disorders (Miceli *et al*, 1994). Mood was evaluated with the Hamilton depression rating scale (Hamilton, 1960) or Beck Depression Inventory (Beck *et al*, 1961). The presence of behavioral disturbances was assessed with the Frontal Behavioral Inventory (Alberici *et al*, 2007) and the Amyotrophic Lateral Sclerosis-Frontotemporal Dementia-Questionnaire (ALS-FTD-Q) (Raaphorst *et al*, 2012) administered to patients' caregivers. Healthy controls underwent the entire assessment except for the Stroop interference test, the Cognitive Estimation Task and the Weigl's Sorting test.

Cognitive test scores were not available for all patients. Data available from Appendix (E-Table 1) reports the number of patients that performed each cognitive test.

MRI analysis

Using two 3T MR scanners, T1-weighted, T2-weighted, fluid-attenuated inversion recovery, DT MRI and RS fMRI sequences were obtained from all participants (data available from Appendix, E-Table 2 for MRI sequence parameters). An experienced observer, blinded to participants' identity and diagnosis, performed MRI analysis. Grey matter (GM) was parcellated into 220 similarly-sized brain regions, which included cerebral cortex and basal ganglia but excluded the cerebellum (figure 1-Ia) (Filippi *et al*, 2017). DT MRI and RS fMRI pre-processing and construction of brain structural and functional connectome have been described previously (Filippi *et al*, 2020) (figure 1-Ia and Ib).

Global brain and lobar network analysis

Global and mean lobar structural and functional network characteristics were explored using the Brain Connectivity Matlab toolbox (http://www.brain-connectivity-toolbox.net). Network metrics, including nodal strength, characteristic path length, local efficiency and clustering coefficient were assessed to characterize the topological organization of global brain and lobar networks in patients and healthy controls (figure 1-II) (Sporns & Zwi, 2004). In order to investigate the network characteristics in different areas of the brain, the 220 regions of interest (ROIs) from both hemispheres were grouped into six anatomical macro-areas (hereafter referred to as brain lobes): temporal, parietal, occipital, fronto-insular, basal ganglia, and sensorimotor areas (Filippi et al., 2017). Structural network properties were generated according to fractional anisotropy (FA) values, while analysis of brain network function was based on functional connectivity strength values (z-transformed Pearson's correlation coefficients). Global and lobar metrics were compared between groups using age-, sex- and MR scanner-adjusted ANOVA models, followed by post-hoc pairwise comparisons, Bonferroni-corrected for multiple comparisons (p<0.05, SPSS Statistics 22.0). In addition, to evaluate the effect of the full-blown dementia patients into the results, the analyses were performed also without the eight ALS-FTD patients. Furthermore, the comparison between ALS and controls subjects, recruited only from Milan/Turin centers, was performed in order to assess the reproducibility of the findings when MRI were obtained using a single MR scanner.

Connectivity analysis

Network Based Statistics (NBS) (Zalesky et al, 2010a) were performed to assess regional FA and functional connectivity strength network data in patients and controls at the level of significance p<0.05 (figure 1-III). The largest (or principal) connected component and the smaller clusters of altered connections, which were not included in the principal component, were studied (Galantucci et al, 2017; Zalesky et al., 2010a). A corrected p value in the direct comparison between ALS patients and healthy controls (both provided by Milan/Turin and Naples centers) was calculated for each component using an age-, sex-, and MR scanner-adjusted permutation analysis (10000 permutations). Regarding the other comparisons, only MND patients and controls from Milan/Turin centers were included in the age- and sex-adjusted permutation analysis. In line with

previous global and lobar network analysis, NBS was performed also excluding ALS-FTD patients and ALS/controls subjects recruited at the Naples center.

Correlation analysis

To assess the relationship between structural and functional brain network properties and clinical and neuropsychological variables, correlation analysis was performed in each patient group. Partial correlations between MRI measures (exhibiting significant differences between patients and controls), clinical variables and cognitive data were estimated using Pearson's correlation coefficient (R), at the level of significance $p<0.05$ (figure 1-IV). Correlation analyses were adjusted for age, sex (in PLS patients) and age, sex, and MR scanner (in ALS patients). Relationship with neuropsychological data were also adjusted for education and ALSFRS-r. Correlation analyses at global/lobar and regional level were also controlled for multiple comparisons, applying respectively Bonferroni and false discovery rate (FDR) adjustment.

Data availability

The dataset used and analyzed during the current study will be made available by the corresponding author upon request to qualified researchers (i.e., affiliated to a university or research institution/hospital). Additional Tables and Figures are available from Appendix (E-Tables 1-7 and Additional figures 1-2).

RESULTS

A summary of structural and functional altered metrics at global, lobar and regional levels in the different MND phenotypes has been reported in figure 2.

Patients with ALS vs healthy controls

Compared to healthy controls, ALS patients showed altered structural global network properties (lower mean local efficiency) (data available from Appendix, E-Table 3). ALS patients showed a reduced mean structural local efficiency in the sensorimotor, basal ganglia and frontal networks and longer path length in basal ganglia, frontal and temporal networks relative to healthy controls (figure 3; data available from Appendix, E-Table 4). They showed also reduced mean nodal strength in frontal and temporal regions relative

to controls (figure 3; data available from Appendix, E-Table 4). ALS patients had preserved global and lobar functional nodal properties compared to controls (data available from Appendix, E-Tables 3 and 4). NBS showed structural changes in ALS patients relative to controls: decreased FA in the sensorimotor networks, including precentral and postcentral gyri, supplementary motor area and basal ganglia, and among the connections of the medial and lateral prefrontal cortex (figure 4A). ALS patients showed also increased functional connectivity compared to controls involving precentral gyrus, middle and superior frontal gyri (figure 4B). The listed results were confirmed excluding from the analysis ALS-FTD patients (data available from Appendix, E-Table 5 and figure 1) or ALS and healthy controls acquired at the Naples center (data available from Appendix, E-Table 6 and figure 3).

Patients with PLS vs healthy controls

Compared to healthy controls, PLS patients showed altered structural global network properties (lower mean local efficiency and clustering coefficient, longer mean path length) (data available from Appendix, E-Table 3). PLS patients showed a reduced mean structural local efficiency and clustering coefficient and longer path length in the sensorimotor, basal ganglia, frontal and parietal areas relative to healthy controls (figure 3; data available from Appendix, E-Table 4). PLS patients had a relatively preserved global and lobar functional nodal properties compared to controls (figure 3; data available from Appendix, E-Tables 3 and 4). Using NBS, widespread structural changes were observed in PLS patients relative to controls: decreased FA within the sensorimotor networks, including precentral and postcentral gyri, supplementary motor area and basal ganglia, and among connections within temporal and occipito-parietal areas (figure 4A). NBS analysis showed that PLS patients had higher functional connectivity in the sensorimotor, basal ganglia and temporal networks relative to controls (figure 4B). PLS structural and functional damage mimics the one observed in classical ALS (figure 5).

Patients with PMA vs healthy controls

PMA patients did not show differences in structural and functional graph and connectivity properties at both global and regional level (figures 3 and 4; data available from Appendix, E-Tables 3 and 4).

Patients with ALS vs patients with PLS

ALS and PLS patients did not show differences in structural and functional graph properties at global level (data available from Appendix, E-Table 3). PLS patients demonstrated altered local structural, but not functional, alterations in sensorimotor network relative to ALS group (longer path length) (figure 3; data available from Appendix, E-Table 4). NBS did not show differences between ALS and PLS patients (figure 4). These findings were confirmed excluding ALS-FTD patients from the analysis (data available from Appendix, E-Table 5 and figure 1).

Patients with ALS vs patients with PMA

ALS and PMA patients did not show differences in structural and functional graph properties at both global and lobar level (figure 3; Additional data available from Appendix, E-Tables 3 and 4). However, ALS patients showed decreased FA relative to PMA cases within the sensorimotor network including precentral and postcentral gyri and frontal network (figure 4A). NBS did not show functional connectivity differences between ALS and PMA patients (figure 4B). The presented results have been validated excluding ALS-FTD patients from the analysis (data available from Appendix, E-Table 5 and figure 1).

Patients with PLS vs patients with PMA

PLS and PMA patients did not show differences in structural and functional graph properties at global level (data available from Appendix, E-Table 3). PLS patients demonstrated altered local structural, but not functional, alterations in sensorimotor and frontal networks relative to PMA group (lower mean local efficiency and clustering coefficient and longer mean path length) (figure 3; data available from Appendix, E-Table 4). In the NBS analysis, PLS patients showed decreased FA relative to PMA cases in the connections within and among sensorimotor network basal ganglia, frontal and parieto-occipital areas (figure 4A). NBS did not show functional connectivity differences between PLS and PMA patients (figure 4B).

Correlation analysis

70

In ALS patients, graph analysis structural brain changes mostly correlated with clinical disease severity (figure 6A). Indeed, a longer path length was related to disease progression rate (Δdp) both at the global (R= 0.25, p= 0.01) and lobar levels, particularly within sensorimotor (R= 0.23, p= 0.01), basal ganglia (R= 0.22, p= 0.02) and frontal-insular (R= 0.22, p= 0.02) networks. Moreover, structural local efficiency in parietal network correlated negatively with Δdp (R= -0.20, p= 0.03) and positively with ALSFRS-r score (R= 0.29, p< 0.001). Regarding regional analysis, in ALS patients, a decreased FA of the connections within temporal network correlated with a worse performance in global cognition (R= 0.36, p=0.03), while a higher disruption within the sensorimotor areas correlated with longer disease duration (R ranging from -0.51 to -0.28, p <0.05) and greater disease severity (R ranging from -0.34 to 0.30, p <0.05). In ALS patients, functional connectivity changes within basal ganglia network and connections between basal ganglia and premotor areas correlated with disease progression (R ranging from -0.60 to 0.24, p <0.05). Moreover, higher functional connectivity, within extra-motor areas (temporo-frontal network), correlated with worse performance at executive (R= 0.37, p= 0.01) and behavioral tests (R= 0.50, p= 0.04). In PLS patients, disrupted structural connections within motor and premotor areas correlated with lower ALSFRS-r scores (R= 0.56, p=0.02) (figure 6B). On the other hand, functional connectivity alterations were more related to cognitive performance. Particularly, functional clustering coefficient correlated with executive dysfunctions within basal ganglia network (R= -0.65, p= 0.04). Moreover, higher functional connectivity of the connections among temporal and frontal areas correlated with a worse performance at behavioral test (R ranging from 0.65 to 0.72, p <0.05). Correlations were not assessed in the PMA group since no significance structural and functional differences were found in the previous analyses relative to controls.

DISCUSSION

Using graph analysis and connectomics to explore structural and functional brain networks, the present multicenter study showed that clinical variants within the MND spectrum result in different patterns of brain network changes. ALS patients showed altered structural global and lobar network properties and regional connectivity, with a specific involvement of sensorimotor, basal ganglia, frontal and temporal areas. On the

same line, the structural damage in the PLS group was found in the sensorimotor network, together with a more widespread damage in extra-motor regions, such as the parietal lobe. On the contrary, PMA patients showed preserved structural and functional connectomes. Finally, in both ALS and PLS groups, alterations in structural connectivity correlated with measures of motor impairment, while functional connectivity disruptions were mostly related to executive dysfunctions and behavioral disturbances. These results proved to be independent of the presence of full-blown dementia, being confirmed also excluding eight ALS-FTD patients from the analyses.

To date, several MRI studies have highlighted structural (Muller *et al.*, 2016; Spinelli *et al.*, 2016) and/or functional (Agosta *et al.*, 2014a; Menke *et al.*, 2016) 'signatures' of different phenotypes within the MND spectrum. However, while DT MRI studies have described consistent results, the literature of functional studies have reported inconsistent findings. Moreover, the above-mentioned studies have zeroed in on the study of structural and functional alterations at a voxel or regional level, rather than on alterations at brain-system level (Bullmore & Sporns, 2009). In order to overcome this limitation, the present study has applied advanced network-based neuroimaging techniques, aiming to provide information about how networks are embedded and interact in the brain of different phenotypes within the MND spectrum, deepening previous findings of standard MRI techniques. Whereas whole-brain approaches might detect alterations at voxel or regional level, connectome analysis considers the relationships between degenerating connections and is able to provide connectivity information about the integrated nature of brain (Crossley *et al*, 2014). Another advantage of this new approach is that it may help in bridging the gap between different types of data, such as anatomical and functional connectivity. In fact, the use of a common parcellating system and the same statistical approach allows a straightforward comparison between the two types of information.

Up to date, graph analysis and connectomics have already been applied to characterize structural and functional damage in ALS patients. Particularly, our findings are consistent with previous DT MRI studies that reported the presence of an impaired subnetwork including bilateral primary motor regions, supplementary motor areas and basal ganglia (Buchanan *et al*, 2015). Furthermore, our study highlights that affected extra-motor regions are structurally connected to the sensorimotor network, known to be the "epicenter" of the degenerative process of the disease (Brettschneider *et al*, 2013). This

hypothesis is consistent with the pattern of progression of TDP-43 pathological burden described by Brettschneider et al. (Brettschneider *et al.*, 2013) in post mortem tissue, and supports a network-based degeneration model in ALS (Seeley *et al*, 2009), although longitudinal MRI studies are needed to validate this hypothesis.

On the other hand, very few RS fMRI studies applied network-based analyses on ALS patients, demonstrating complex connectivity alterations encompassing frontal, temporal, occipital and subcortical regions (Geevasinga *et al.*, 2017; Zhou *et al*, 2016). In our study, we found increased functional connectivity in sensorimotor, basal ganglia and frontal areas in ALS patients. Our results are mostly consistent with previous studies, although showing more focal functional rearrangements, possibly due to differences in disease stage and methodology (as in our study only functional edges with existing structural connections were considered). Although our study confirms previous findings, our strength is the application of advanced neuroimaging techniques in an unprecedented number of ALS patients due to the fact that is a multicenter study. In light of this, the great number of patients have a strong impact on the statistical power of the analysis and influenced the quality and reliability of our results. Of note, this is the first study that applied graph theory in patients with PLS and PMA. Particularly, PLS patients showed widespread structural and functional alterations encompassing both motor and extra-motor areas with a pattern resembling classic ALS patients (figure 4), in line with previous studies (Agosta *et al.*, 2014b; Muller *et al*, 2018). By contrast, PMA patients did not show any structural or functional damage relative to healthy controls. These findings are in line with previous studies that could not demonstrate central nervous system damage in PMA patients (Rosenbohm *et al.*, 2016; Spinelli *et al.*, 2016), even using a technique that is highly sensitive to local disruptions in the brain networks. Therefore, here we have demonstrated the high sensitivity of graph-based analysis to detect different disease related disconnection patterns and its potential use to facilitate clinical diagnosis and offer new insights into syndromes' clinical diversity.

Noteworthy, ALS and PLS patients are characterized by more widespread structural than functional damage relative to healthy controls (figure 3). The presence of functionally unaffected, but structurally impaired nodes and connections in both groups suggests that structural alterations may be earlier in the course of the disease compared with functional network abnormalities. In keeping with the network-based hypothesis

(Jucker & Walker, 2013), pathological alterations physically spread along neuroanatomical connections in the brain; therefore, it is reasonable to speculate that functional connectivity alterations may follow the structural disruption of the brain network. These findings are also in line with those recently observed in other neurodegenerative diseases (Filippi *et al.*, 2020). However, it should also be considered that this cross-sectional study cannot fully address the temporal sequence or causal relationships between structural and functional abnormalities, and different techniques (i.e., DT MRI and RS fMRI) may intrinsically show different sensitivities to underlying biological processes.

In the present study, the regional (i.e., NBS) analysis showed greater sensitivity for the detection of structural and, particularly, functional damage of brain networks, compared with the evaluation of single network properties. Moreover, the results of the global/lobar structural analysis provided some apparent inconsistencies across different network measures. For example, although structural nodal strength did not show significant alterations in the sensorimotor regions of MND patients compared with healthy controls, all other graph theoretical measures (i.e., local efficiency, clustering coefficient and path length) did. Given the inter-dependence of these measures, and the fact that nevertheless nodal strength was on average lower than healthy controls in all MND groups, we argue that nodal strength might simply be less sensitive than other measures to the structural disruption of the sensorimotor network in our cohort. This might differ in other anatomical areas with different topological organization, such as the temporal regions (which are also affected in MND (Verstraete *et al.*, 2014)), where nodal strength and path length were significantly altered in ALS patients, in contrast with the sparing of other network properties. Therefore, our results support the utility of graph theoretical measures used in combination, rather than as single measures, also considering the current impossibility of establishing a clear-cut neuropathological substrate for each of these.

Concerning the correlation analysis, our findings suggest that the presence of structural damage in ALS patients in motor, premotor and parietal regions, key elements for the correct programming and processing/execution of the movement, is specifically related to clinical measures of motor impairment, rate of progression and disease duration. Particularly, the rate of progression was more closely related to global and lobar

alterations, while measures of disease severity and duration were associated with regional connectivity disruption, although correlation coefficients were generally moderate in size (0.2 to 0.4). By contrast, the (possibly, maladaptive) increase of functional connectivity in frontal and temporal regions was related to executive dysfunctions and behavioral impairment, as previously shown (Agosta *et al.*, 2014a). PLS patients showed a similar pattern of correlations, although with a lower number of significant findings, partly due to the small sample size. Nevertheless, a strong relationship between functional connectivity in extra-motor areas and behavioral impairment was found, to point out that the cognitive profile in PLS patients traced the one in ALS patients, with more prominent deficits in the behavioral domain.

One of the most important caveats of previous studies is the single-center origin of imaging data that limits the generalizability of findings. In light of this, one of the main novelties of our study was including data from different centers, neuroimaging protocols and scanners. Although MRI protocols were not harmonized between the two acquisition centers, the obtained results proved to be solid (as shown by the single-center sub-analysis) and the approach was easily reproducible despite protocol differences. On the other hand, this study is not without limitations. First, the PLS and PMA groups were relatively small, affecting the statistical power of the results. In particular, the absence of differences between PMA patients and healthy controls might partially depend on the relatively small sample size. However, PMA also showed significant structural sparing compared with both ALS and PLS patients, consistent with previous studies performed using different techniques (Rosenbohm *et al.*, 2016; Spinelli *et al.*, 2016), as well as with the common notion of PMA as a predominant lower motor neuron disease. Second, cognitive test scores were not available for all patients. However, we selected tests for which patient samples were sufficiently represented. Third, healthy controls showed higher education than ALS and PLS patients, although the analyses involving neuropsychological data were adjusted for education. Fourth, we chose arbitrarily to parcellate the brain into 220 similarly sized regions based on the Automated Anatomical Labeling (AAL) atlas, excluding the cerebellum. Technically, network science applied to the human brain has yet to reach consensus regarding the best way to divide the brain into its most relevant anatomical units (Zalesky *et al*, 2010b) as well as to threshold connectivity matrices (van den Heuvel *et al*, 2017). The definition of an optimal

framework has not yet been reached in the neuroscience community, and the field of network data analysis remains an area of active methodological development. However, it is generally acknowledged that similarly sized regions of interest avoid larger regions to have higher connectivity because of their larger surface. The exclusion of the cerebellum was motivated by the fact that the AAL atlas is rather inaccurate to segment this anatomical region, and other, unbiased ad-hoc methods should be preferred in future studies. Fifth, although RS-fMRI data were carefully registered to and masked with GM maps to avoid a regional atrophy influence, a possible partial volume effect on our results cannot be excluded. Finally, this is a cross-sectional study. Longitudinal studies are needed to evaluate structural and functional changes along with the disease progression over time and are warranted in order to confirm the role of MRI network-based analysis for a differential diagnosis and prognosis of MND in a clinical context, as well to support the hypothesis of a single continuum from ALS to FTD.

In conclusion, this study showed a considerable motor and extra-motor network degeneration in ALS patients and an even more widespread damage in PLS patients, suggesting that graph analysis and connectomics might represent a powerful approach to detect overlapping and specific regions of damage in different MND phenotypes. Importantly, these techniques have proven robust and suitable to manage the multicenter setting variability. Network-based advanced MRI analyses hold the promise to provide an objective in vivo assessment of MND-related pathological changes, delivering potential prognostic markers.

REFERENCES

Abrahams S, Leigh PN, Harvey A, Vythelingum GN, Grise D, Goldstein LH (2000) Verbal fluency and executive dysfunction in amyotrophic lateral sclerosis (ALS). *Neuropsychologia* 38: 734-747

Agosta F, Canu E, Inuggi A, Chio A, Riva N, Silani V, Calvo A, Messina S, Falini A, Comi G *et al* (2014a) Resting state functional connectivity alterations in primary lateral sclerosis. *Neurobiol Aging* 35: 916-925

Agosta F, Galantucci S, Riva N, Chio A, Messina S, Iannaccone S, Calvo A, Silani V, Copetti M, Falini A *et al* (2014b) Intrahemispheric and interhemispheric structural network abnormalities in PLS and ALS. *Hum Brain Mapp* 35: 1710-1722

Alberici A, Geroldi C, Cotelli M, Adorni A, Calabria M, Rossi G, Borroni B, Padovani A, Zanetti O, Kertesz A (2007) The Frontal Behavioural Inventory (Italian version) differentiates frontotemporal lobar degeneration variants from Alzheimer's disease. *Neurol Sci* 28: 80-86

Barbarotto R, Laiacona M, Frosio R, Vecchio M, Farinato A, Capitani E (1998) A normative study on visual reaction times and two Stroop colour-word tests. *Ital J Neurol Sci* 19: 161-170

Basaia S, Filippi M, Spinelli EG, Agosta F (2019) White Matter Microstructure Breakdown in the Motor Neuron Disease Spectrum: Recent Advances Using Diffusion Magnetic Resonance Imaging. *Front Neurol* 10: 193

Basso A, Capitani E, Laiacona M (1987) Raven's coloured progressive matrices: normative values on 305 adult normal controls. *Functional neurology* 2: 189-194

Beck AT, Ward CH, Mendelson M, Mock J, Erbaugh J (1961) An inventory for measuring depression. *Arch Gen Psychiatry* 4: 561-571

Brettschneider J, Del Tredici K, Toledo JB, Robinson JL, Irwin DJ, Grossman M, Suh E, Van Deerlin VM, Wood EM, Baek Y *et al* (2013) Stages of pTDP-43 pathology in amyotrophic lateral sclerosis. *Annals of neurology* 74: 20-38

Brooks BR, Miller RG, Swash M, Munsat TL, World Federation of Neurology Research Group on Motor Neuron D (2000) El Escorial revisited: revised criteria for the diagnosis of amyotrophic lateral sclerosis. *Amyotroph Lateral Scler Other Motor Neuron Disord* 1: 293-299

Buchanan CR, Pettit LD, Storkey AJ, Abrahams S, Bastin ME (2015) Reduced structural connectivity within a prefrontal-motor-subcortical network in amyotrophic lateral sclerosis. *Journal of magnetic resonance imaging : JMRI* 41: 1342-1352

Bullmore E, Sporns O (2009) Complex brain networks: graph theoretical analysis of structural and functional systems. *Nat Rev Neurosci* 10: 186-198

Caffarra P, Vezzadini G, Dieci F, Zonato F, Venneri A (2004) Modified Card Sorting Test: normative data. *Journal of clinical and experimental neuropsychology* 26: 246-250

Carlesimo GA, Caltagirone C, Gainotti G (1996) The Mental Deterioration Battery: normative data, diagnostic reliability and qualitative analyses of cognitive

impairment. The Group for the Standardization of the Mental Deterioration Battery. *Eur Neurol* 36: 378-384

Cedarbaum JM, Stambler N, Malta E, Fuller C, Hilt D, Thurmond B, Nakanishi A (1999) The ALSFRS-R: a revised ALS functional rating scale that incorporates assessments of respiratory function. BDNF ALS Study Group (Phase III). *J Neurol Sci* 169: 13-21

Chio A, Calvo A, Moglia C, Mazzini L, Mora G, group Ps (2011) Phenotypic heterogeneity of amyotrophic lateral sclerosis: a population based study. *J Neurol Neurosurg Psychiatry* 82: 740-746

Crossley NA, Mechelli A, Scott J, Carletti F, Fox PT, McGuire P, Bullmore ET (2014) The hubs of the human connectome are generally implicated in the anatomy of brain disorders. *Brain* 137: 2382-2395

Della Sala S, MacPherson SE, Phillips LH, Sacco L, Spinnler H (2003) How many camels are there in Italy? Cognitive estimates standardised on the Italian population. *Neurol Sci* 24: 10-15

Filippi M, Basaia S, Canu E, Imperiale F, Magnani G, Falautano M, Comi G, Falini A, Agosta F (2020) Changes in functional and structural brain connectome along the Alzheimer's disease continuum. *Molecular psychiatry* 25: 230-239

Filippi M, Basaia S, Canu E, Imperiale F, Meani A, Caso F, Magnani G, Falautano M, Comi G, Falini A *et al* (2017) Brain network connectivity differs in early-onset neurodegenerative dementia. *Neurology* 89: 1764-1772

Folstein MF, Folstein SE, McHugh PR (1975) "Mini-mental state". A practical method for grading the cognitive state of patients for the clinician. *J Psychiatr Res* 12: 189-198

Galantucci S, Agosta F, Stefanova E, Basaia S, van den Heuvel MP, Stojkovic T, Canu E, Stankovic I, Spica V, Copetti M *et al* (2017) Structural Brain Connectome and Cognitive Impairment in Parkinson Disease. *Radiology* 283: 515-525

Geevasinga N, Korgaonkar MS, Menon P, Van den Bos M, Gomes L, Foster S, Kiernan MC, Vucic S (2017) Brain functional connectome abnormalities in amyotrophic lateral sclerosis are associated with disability and cortical hyperexcitability. *Eur J Neurol* 24: 1507-1517

Hamilton M (1960) A rating scale for depression. *J Neurol Neurosurg Psychiatry* 23: 56-62

Jucker M, Walker LC (2013) Self-propagation of pathogenic protein aggregates in neurodegenerative diseases. *Nature* 501: 45-51

Laiacona M, Inzaghi MG, De Tanti A, Capitani E (2000) Wisconsin card sorting test: a new global score, with Italian norms, and its relationship with the Weigl sorting test. *Neurol Sci* 21: 279-291

Menke RA, Proudfoot M, Wuu J, Andersen PM, Talbot K, Benatar M, Turner MR (2016) Increased functional connectivity common to symptomatic amyotrophic lateral sclerosis and those at genetic risk. *J Neurol Neurosurg Psychiatry* 87: 580-588

Miceli G, neuropsicologia UcdSCSd, psicologia CndrId (1994) *Batteria per l'analisi dei deficit afasici B.A.D.A*. Servizio di neuropsicologia, Università cattolica del S. Cuore

Monaco M, Costa A, Caltagirone C, Carlesimo GA (2013) Forward and backward span for verbal and visuo-spatial data: standardization and normative data from an Italian adult population. *Neurol Sci* 34: 749-754

Muller HP, Agosta F, Gorges M, Kassubek R, Spinelli EG, Riva N, Ludolph AC, Filippi M, Kassubek J (2018) Cortico-efferent tract involvement in primary lateral sclerosis and amyotrophic lateral sclerosis: A two-centre tract of interest-based DTI analysis. *Neuroimage Clin* 20: 1062-1069

Muller HP, Turner MR, Grosskreutz J, Abrahams S, Bede P, Govind V, Prudlo J, Ludolph AC, Filippi M, Kassubek J *et al* (2016) A large-scale multicentre cerebral diffusion tensor imaging study in amyotrophic lateral sclerosis. *J Neurol Neurosurg Psychiatry* 87: 570-579

Norris F, Shepherd R, Denys E, U K, Mukai E, Elias L, Holden D, Norris H (1993) Onset, natural history and outcome in idiopathic adult motor neuron disease. *J Neurol Sci* 118: 48-55

Novelli G, Laiacona M, Papagno C, Vallar G, Capitani E, Cappa SF (1986) Three clinical tests to research and rate the lexical performance of normal subjects. *Arch Psicol Neurol Psichiatr* 47: 477-506

Orsini A, Grossi D, Capitani E, Laiacona M, Papagno C, Vallar G (1987) Verbal and spatial immediate memory span: normative data from 1355 adults and 1112 children. *Ital J Neurol Sci* 8: 539-548

Pringle CE, Hudson AJ, Munoz DG, Kiernan JA, Brown WF, Ebers GC (1992) Primary lateral sclerosis. Clinical features, neuropathology and diagnostic criteria. *Brain* 115 (Pt 2): 495-520

Raaphorst J, Beeldman E, Schmand B, Berkhout J, Linssen WH, van den Berg LH, Pijnenburg YA, Grupstra HF, Weikamp JG, Schelhaas HJ *et al* (2012) The ALS-FTD-Q: a new screening tool for behavioral disturbances in ALS. *Neurology* 79: 1377-1383

Rosenbohm A, Muller HP, Hubers A, Ludolph AC, Kassubek J (2016) Corticoefferent pathways in pure lower motor neuron disease: a diffusion tensor imaging study. *J Neurol* 263: 2430-2437

Seeley WW, Crawford RK, Zhou J, Miller BL, Greicius MD (2009) Neurodegenerative diseases target large-scale human brain networks. *Neuron* 62: 42-52

Spinelli EG, Agosta F, Ferraro PM, Riva N, Lunetta C, Falzone YM, Comi G, Falini A, Filippi M (2016) Brain MR Imaging in Patients with Lower Motor Neuron-Predominant Disease. *Radiology* 280: 545-556

Sporns O, Zwi JD (2004) The small world of the cerebral cortex. *Neuroinformatics* 2: 145-162

Tijms BM, Wink AM, de Haan W, van der Flier WM, Stam CJ, Scheltens P, Barkhof F (2013) Alzheimer's disease: connecting findings from graph theoretical studies of brain networks. *Neurobiol Aging* 34: 2023-2036

Tognoni HSaG (1987) *Standardizzazione e Taratura Italiana di Test Neuropsicologici*

Turner MR, Cagnin A, Turkheimer FE, Miller CC, Shaw CE, Brooks DJ, Leigh PN, Banati RB (2004) Evidence of widespread cerebral microglial activation in amyotrophic lateral sclerosis: an [11C](R)-PK11195 positron emission tomography study. *Neurobiol Dis* 15: 601-609

van den Berg-Vos RM, Visser J, Franssen H, de Visser M, de Jong JM, Kalmijn S, Wokke JH, van den Berg LH (2003) Sporadic lower motor neuron disease with adult onset: classification of subtypes. *Brain* 126: 1036-1047

van den Heuvel MP, de Lange SC, Zalesky A, Seguin C, Yeo BTT, Schmidt R (2017) Proportional thresholding in resting-state fMRI functional connectivity networks and consequences for patient-control connectome studies: Issues and recommendations. *NeuroImage* 152: 437-449

van den Heuvel MP, Sporns O (2019) A cross-disorder connectome landscape of brain dysconnectivity. *Nat Rev Neurosci* 20: 435-446

Verstraete E, Veldink JH, van den Berg LH, van den Heuvel MP (2014) Structural brain network imaging shows expanding disconnection of the motor system in amyotrophic lateral sclerosis. *Hum Brain Mapp* 35: 1351-1361

Zalesky A, Fornito A, Bullmore ET (2010a) Network-based statistic: identifying differences in brain networks. *NeuroImage* 53: 1197-1207

Zalesky A, Fornito A, Harding IH, Cocchi L, Yucel M, Pantelis C, Bullmore ET (2010b) Whole-brain anatomical networks: does the choice of nodes matter? *NeuroImage* 50: 970-983

Zhou C, Hu X, Hu J, Liang M, Yin X, Chen L, Zhang J, Wang J (2016) Altered Brain Network in Amyotrophic Lateral Sclerosis: A Resting Graph Theory-Based Network Study at Voxel-Wise Level. *Frontiers in neuroscience* 10: 204

Table 1. Demographic and clinical features of ALS, PLS and PMA patients and matched healthy controls.

	HC	ALS	PLS	PMA	p ALS vs HC	p PLS vs HC	p PMA vs HC	p ALS vs PLS	p ALS vs PMA	p PLS vs PMA
N	79	173	38	28						
Age [years]	61.84 ± 8.82 (42.00 - 81.81)	61.56 ± 10.64 (28.47 - 86.12)	63.20 ± 7.89 (43.87 - 80.26)	58. 44 ± 8.99 (39.62 - 73.91)	1.00	1.00	0.69	1.00	0.71	0.31
Sex [women/men]	46/33	72/101	20/18	8/20	**0.02**	0.69	**0.01**	0.28	0.22	0.08
Education [years]	12.87± 4.38 (5 - 24)	10.41 ± 4.42 (3 - 24)	10.40 ± 4.43 (2 - 18)	10.82 ± 4.81 (5 - 24)	**<0.001**	**0.03**	0.23	1.00	1.00	1.00
Onset [limb/bulbar]	-	128/45	33/5	27/1	-	-	-	0.10	0.01	0.23
Disease duration [months]	-	18.97 ± 17.66 (2 - 136)	79.32 ± 60.46 (8 - 247)	69.14 ± 98.61 (4 - 457)	-	-	-	**<0.001**	**<0.001**	1.00
ALSFRS-r [0-48]	-	37.92 ± 6.95 (11 - 47)	37.16 ± 5.72 (22 - 44)	40.14 ± 6.00 (25 - 48)	-	-	-	1.00	0.31	0.22
UMN score	-	9.82 ± 4.75 (0 - 16)	13.67 ± 2.11 (10 - 16)	2.14 ± 1.70 (0 - 5)	-	-	-	**0.001**	**<0.001**	**<0.001**
MRC global score	-	96.04 ± 23.86 (5 - 148)	112.86 ± 10.43 (80 - 121)	96.25 ± 17.73 (51 - 119)	-	-	-	**0.004**	1.00	0.04
Disease progression rate	-	0.78 ± 0.70 (0.04 - 4.11)	0.31 ± 0.49 (0.03 - 2.89)	0.33 ± 0.42 (0 - 2.00)	-	-	-	**<0.001**	**0.002**	1.00

Values are numbers or means ± standard deviations (range). Disease duration was defined as months from onset to date of MRI scan. P values refer to ANOVA models, followed by post-hoc pairwise comparisons (Bonferroni-corrected for multiple comparisons), or Chi-squared test. Abbreviations: ALS= Amyotrophic lateral sclerosis; ALSFRS-r= Amyotrophic lateral sclerosis functional rating scale revised; HC= healthy controls; MRC= Medical Research Council; N= Number; PLS= Primary lateral sclerosis; PMA= Progressive muscular atrophy; UMN= Upper motor neuron.
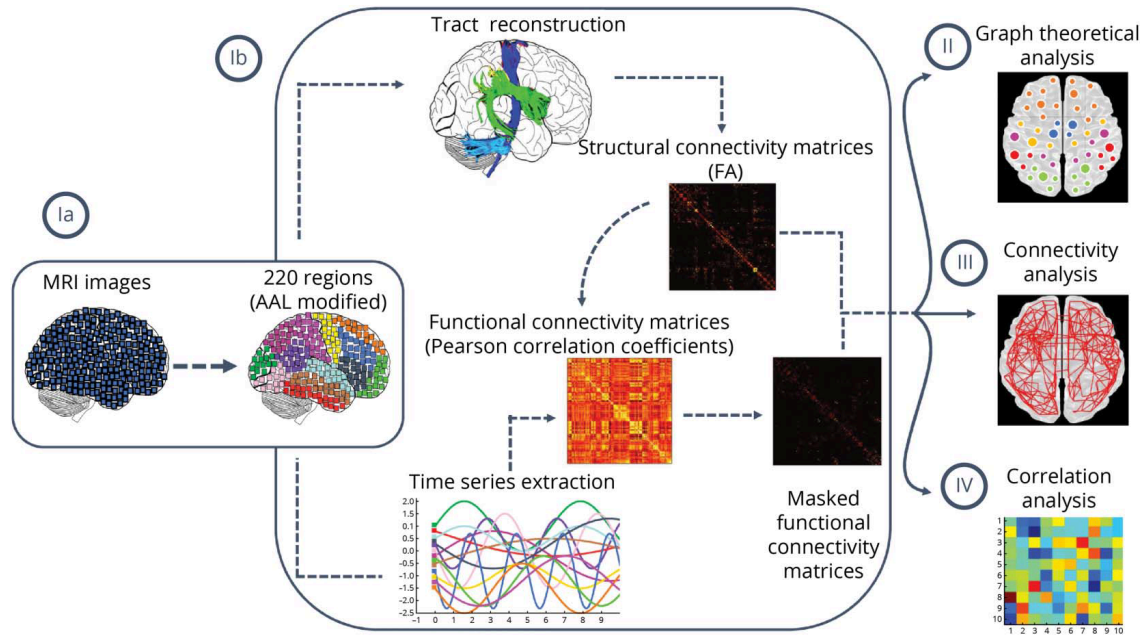
Figure 1. MRI processing pipeline. **(IA)** Grey matter was parcellated in 220 similarly-sized brain regions, which included cerebral cortex and basal ganglia but excluded the cerebellum. **(IB)** Diagram reported diffusion-tensor MRI and resting-state functional MRI pre-processing steps and construction of brain structural and functional connectomes. Structural and functional matrices were the input for three distinctive analyses: **(II)** Global and lobar graph analysis; **(III)** Connectivity analysis; and **(IV)** Correlation analysis. Abbreviations: AAL= automated anatomical labeling; FA= fractional anisotropy; MRI= magnetic resonance imaging.

Structural connectivity (FA)

Global brain analysis	Whole brain

| Lobar network analysis | Fronto-insular | Temporal | Parietal | Occipital | Basal ganglia | Sensorimotor |

| Connectivity analysis | FI T P O BG S | FI T P O BG S | FI T P O BG S | FI T P O BG S | FI T P O BG S | FI T P O BG S |

ALS

Functional connectivity

Global brain analysis	Whole brain

| Lobar network analysis | Fronto-insular | Temporal | Parietal | Occipital | Basal ganglia | Sensorimotor |

| Connectivity analysis | FI T P O BG S | FI T P O BG S | FI T P O BG S | FI T P O BG S | FI T P O BG S | FI T P O BG S |

Structural connectivity (FA)

Global brain analysis	Whole brain

| Lobar network analysis | Fronto-insular | Temporal | Parietal | Occipital | Basal ganglia | Sensorimotor |

| Connectivity analysis | FI T P O BG S | FI T P O BG S | FI T P O BG S | FI T P O BG S | FI T P O BG S | FI T P O BG S |

PLS

Functional connectivity

Global brain analysis	Whole brain

| Lobar network analysis | Fronto-insular | Temporal | Parietal | Occipital | Basal ganglia | Sensorimotor |

| Connectivity analysis | FI T P O BG S | FI T P O BG S | FI T P O BG S | FI T P O BG S | FI T P O BG S | FI T P O BG S |

Figure 2. Summary of altered structural and functional metrics in the different MND variants. Three shades of green color were used to define the severity of damage in terms of percentage of altered metrics (global and lobar analyses) and percentage of altered connections between two lobes (connectivity analysis). The three shades of green depicted the following ranks: 1-25% (light green), 26-50% (medium green) and 51-75% (dark green). White background represents the absence of alterations. Abbreviations: ALS= Amyotrophic Lateral Sclerosis; BG= basal ganglia; FA= fractional anisotropy; FI= fronto-insular; O= occipital; P= parietal; PLS= Primary Lateral Sclerosis; S= sensorimotor; T= temporal.
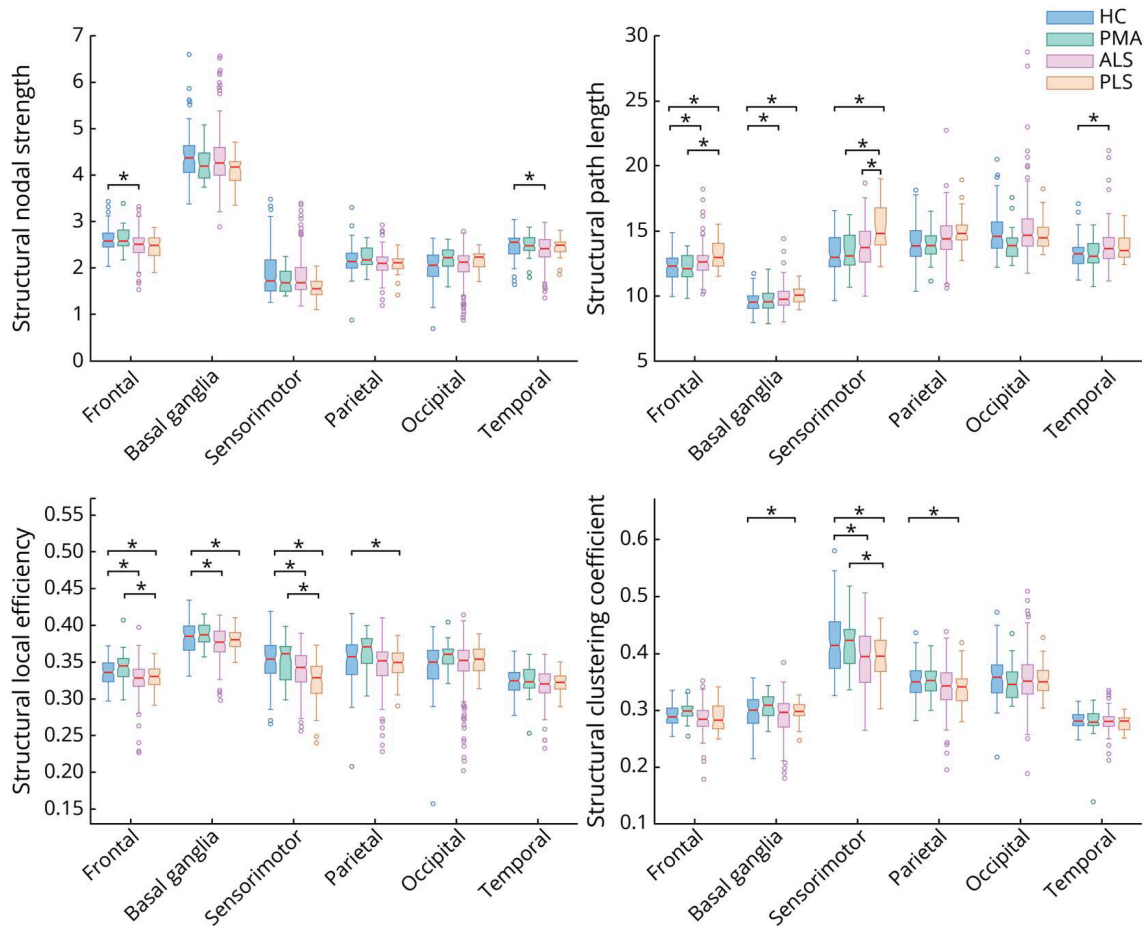
Figure 3. Graph analysis properties of brain lobar networks in ALS, PLS and PMA patients and healthy controls. Box plot of structural nodal strength, path length, local efficiency and clustering coefficient of each brain lobe are shown for patient groups and matched healthy controls. The red horizontal line in each box plot represents the median, the two lines just above and below the median represent the 25th and 75th percentiles, whiskers represent the minimum and maximum values, and all the dots outside the confidence interval are considered as outliers. *p<0.05. All the comparisons were adjusted for age, sex and MR scanner. Abbreviations: ALS= Amyotrophic Lateral Sclerosis; HC= healthy controls; PLS= Primary Lateral Sclerosis; PMA= Progressive Muscular Atrophy.
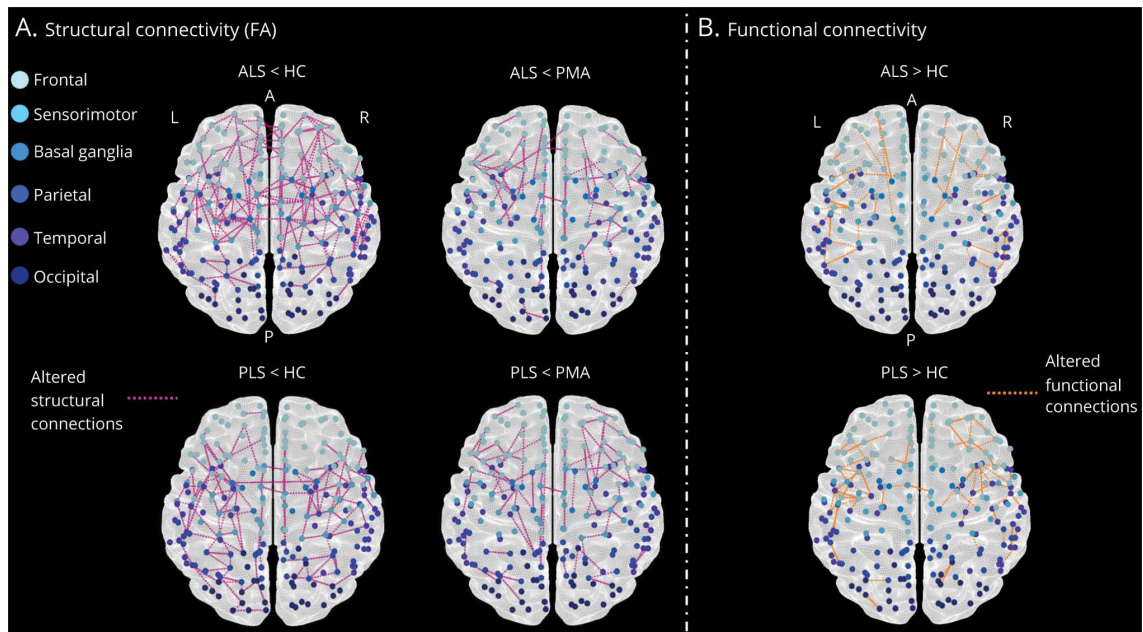
Figure 4. Subnetworks showing altered structural and functional connectivity in ALS, PLS and PMA patients relative to healthy controls and between patient groups. Altered structural (A) and functional (B) connections are represented in magenta and orange, respectively. All the comparisons were adjusted for age, sex and MR scanner. Six shades of blue color were used to define the belonging of each node to different lobes starting with light blue (frontal lobe) to dark blue (posterior lobe, i.e., occipital). Abbreviations: A= anterior; ALS= Amyotrophic Lateral Sclerosis; FA= fractional anisotropy; HC= healthy controls; L= left; P= posterior; PLS= Primary Lateral Sclerosis; PMA= Progressive Muscular Atrophy; R= right.
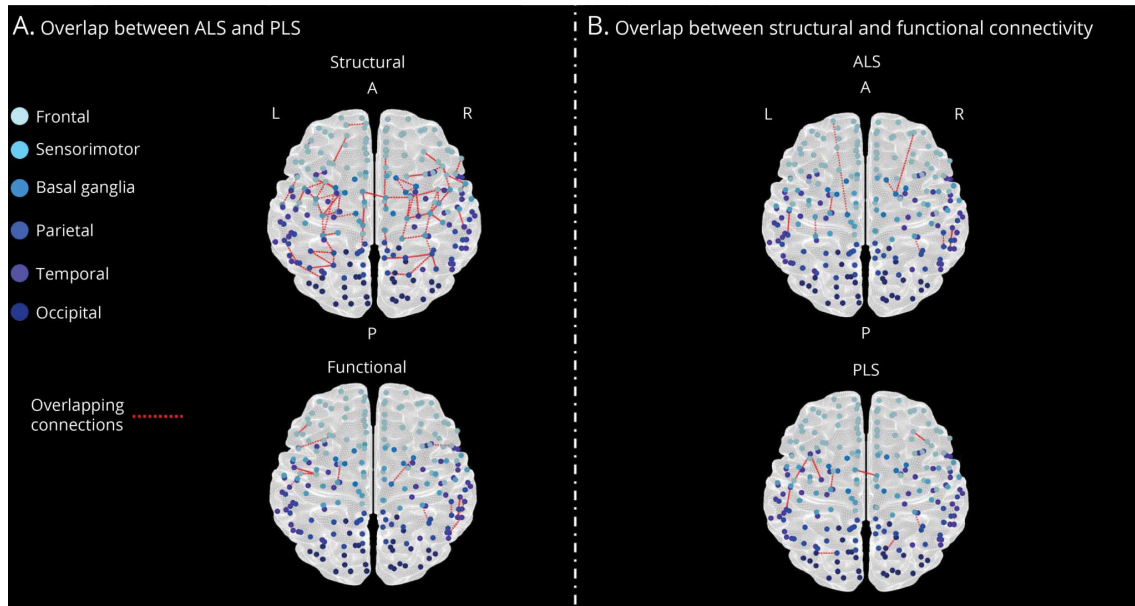
Figure 5. Subnetworks showing overlapping affected connections. Overlapping affected connections in ALS and PLS patients in structural and functional MRI (A) and overlapping structural and functional affected connections within the two groups (B) are represented in red. Six shades of blue color were used to define the belonging of each node to different lobes starting with light blue (frontal lobe) to dark blue (posterior lobe, i.e., occipital). Abbreviations: A= anterior; ALS= Amyotrophic Lateral Sclerosis; FA= fractional anisotropy; HC= healthy controls; L= left; P = posterior; PLS= Primary Lateral Sclerosis; R= right.
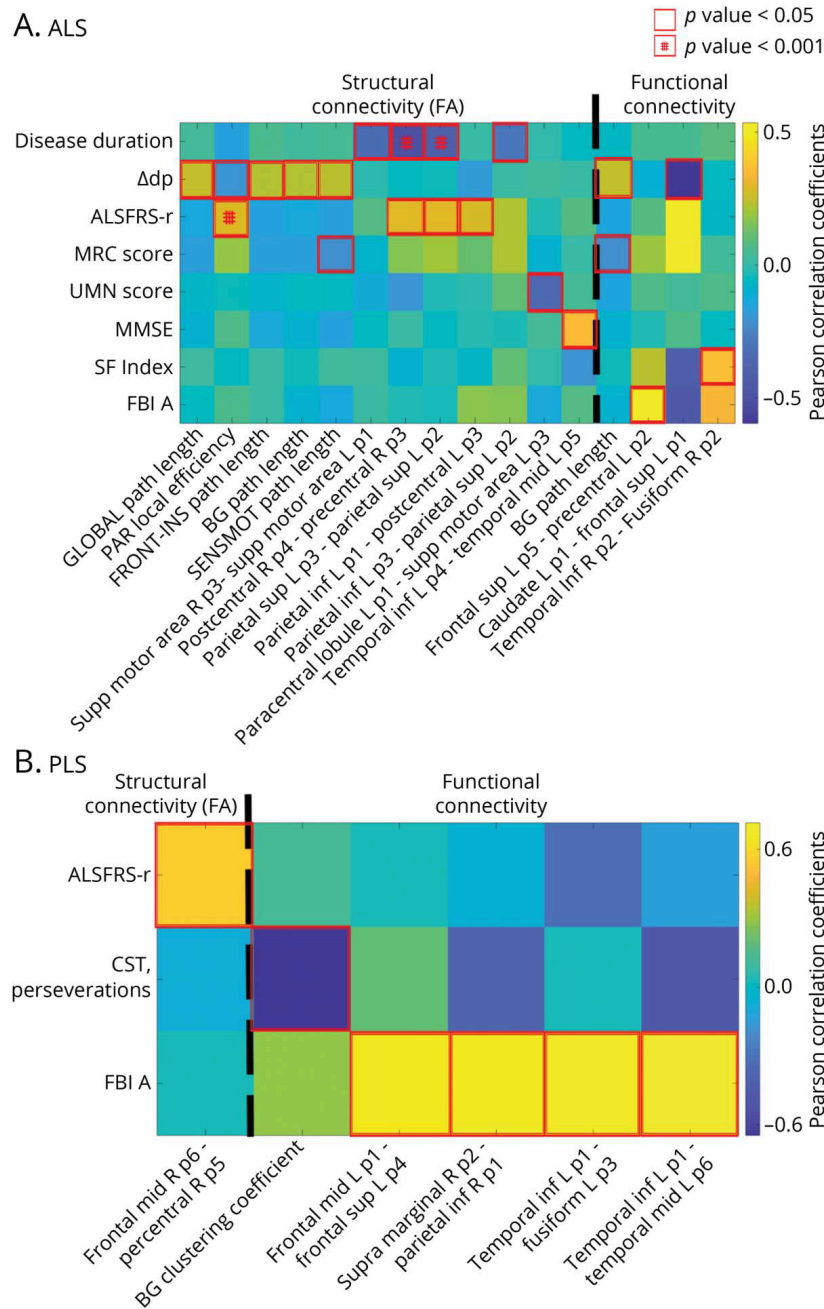
Figure 6. Characterization of the relationship between structural and functional MRI metrics and clinical/cognitive data in ALS and PLS patients. Each row shows structural and functional brain proprieties (data available from Appendix, E-Table 7 for details on brain parcellation) and each column clinical and cognitive scores in ALS (A) and PLS (B) patients. Color scale represents Pearson's correlation coefficient. Red square alone or with a hash indicate statistical significance, respectively, at a threshold of $p<0.05$ and $p<0.001$. Abbreviations: $\Delta dp=$ disease progression rate; ALS= Amyotrophic Lateral Sclerosis; ALSFRS-r= Amyotrophic Lateral Sclerosis functional rating scale revised; BG= basal ganglia; CST= Card Sorting Test; FA= fractional anisotropy; FBI= Frontal Behavioral Inventory; FRONT-INS= fronto-insular; Inf= inferior; L= left; Mid= middle; MMSE= Mini-Mental state examination; MRC= Medical Research Council; p=part; PAR= parietal; PLS= Primary Lateral Sclerosis; R= right; SENSMOT= sensorimotor; SF= semantic fluency; Sup= superior; Supp= supplementary; UMN= upper motor neuron.

E-Table 1. Neuropsychological features of ALS, PLS and PMA patients and matched healthy controls.

	HC	ALS	PLS	PMA	p ALS vs HC	p PLS vs HC	p PMA vs HC	p ALS vs PLS	p ALS vs PMA	p PLS vs PMA
Global cognition										
MMSE*	n 41 0.98 ± 0.03 (0.87 - 1.00)	n 129 0.94 ± 0.07 (0.67 - 1.00)	n 31 0.97 ± 0.04 (0.83 - 1.00)	n 21 0.95 ± 0.05 (0.83 - 1.00)	**0.03**	1.00	0.35	**0.03**	1.00	0.32
Memory										
Digit span forward	n 40 5.95 ± 0.96 (4.00 - 9.00)	n 101 5.17 ± 0.95 (3.00 - 9.00)	n 31 5.77 ± 1.41 (3.00 - 9.00)	n 20 5.65 ± 0.81 (4.00 - 7.00)	**<0.001**	1.00	0.59	**0.003**	0.38	0.95
RAVLT immediate	n 40 46.08 ± 9.43 (26.00 - 62.00)	n 102 39.69 ± 12.04 (11.00 - 64.00)	n 31 39.77 ± 9.94 (23.00 - 55.00)	n 19 43.00 ± 11.26 (14.00 - 60.00)	0.50	0.66	1.00	1.00	0.98	0.92
RAVLT delayed	n 40 9.23 ± 3.25 (3.00 - 15.00)	n 102 8.19 ± 3.35 (0.00 - 15.00)	n 31 7.81 ± 3.25 (0.00 - 14.00)	n 19 7.47 ± 3.44 (0.00 - 13.00)	1.00	1.00	0.68	1.00	0.38	1.00
Executive function										
CPM	n 37 30.43 ± 3.79 (22.00 - 36.00)	n 99 27.53 ± 5.16 (14.00 - 36.00)	n 32 29.03 ± 3.89 (21.00 - 35.00)	n 20 28.30 ± 7.41 (6.00 - 36.00)	0.06	1.00	0.94	0.36	1.00	1.00
Digit span backward	n 33 4.45 ± 1.09 (2.00 - 7.00)	n 97 3.52 ± 1.17 (0.00 - 6.00)	n 30 4.33 ± 1.16 (2.00 - 6.00)	n 20 4.15 ± 0.88 (3.00 - 6.00)	**0.001**	1.00	1.00	**0.001**	0.07	1.00
Stroop interference (seconds)	-	n 65 42.31 ± 34.26 (6.00 - 196.00)	n 22 42.47 ± 24.81 (10.00 - 98.00)	n 19 43.30 ± 20.47 (12.00 - 93.00)	-	-	-	1.00	1.00	1.00

CET	-	n 90 14.34 ± 4.08 (6.00 - 25.00)	n 27 14.63 ± 2.88 (10.00 - 22.00)	n 18 13.06 ± 3.75 (6.00 - 20.00)	-	-	-	1.00	0.70	0.79
Test di Weigl	-	n 86 10.85 ± 3.36 (1.00 - 15.00)	n 26 13.04 ± 2.11 (7.00 - 15.00)	n 17 11.53 ± 4.02 (0.00 - 15.00)	-	-	-	**0.002**	1.00	0.20
CST, perseverations**	n 33 0.11 ± 0.15 (0.00 - 0.83)	n 85 0.17 ± 0.13 (0.01 - 0.73)	n 24 0.12 ± 0.10 (0.02 - 0.30)	n 17 0.18 ± 0.19 (0.03 - 0.80)	0.56	1.00	0.79	0.38	1.00	0.92
Language										
BADA (noun)	n 22 29.73 ± 0.63 (28.00 - 30.00)	n 99 28.78 ± 2.12 (13.00 - 30.00)	n 31 29.39 ± 0.72 (28.00 - 30.00)	n 19 29.21 ± 1.08 (27.00 - 30.00)	0.16	1.00	1.00	0.33	1.00	1.00
BADA (action)	n 22 27.68 ± 0.57 (26.00 - 28.00)	n 99 26.63 ± 2.22 (17.00 - 28.00)	n 30 26.57 ± 1.48 (23.00 - 28.00)	n 19 26.32 ± 2.52 (20.00 - 28.00)	0.11	0.25	**0.04**	1.00	0.98	1.00
Fluency										
Index PF***	n 29 4.82 ± 2.17 (2.60 - 12.05)	n 102 8.07 ± 7.99 (1.81 - 59.00)	n 27 7.23 ± 4.61 (3.41 - 27.19)	n 21 6.47 ± 3.88 (1.90 - 18.80)	0.44	1.00	1.00	1.00	1.00	1.00
Index SF***	n 29 4.20 ± 1.62 (2.49 - 10.90)	n 101 5.57 ± 3.51 (2.20 - 23.00)	n 27 4.88 ± 1.61 (2.61 - 8.70)	n 19 4.03 ± 1.02 (2.76 - 5.89)	0.07	1.00	1.00	0.21	0.44	1.00
Mood & Behavior										
BDI	n 25 5.00 ± 4.42 (0.00 - 15.00)	-	-	-	-	-	-	-	-	-
HDRS	-	n 80 7.33 ± 5.00 (0.00 - 23.00)	n 28 7.29 ± 5.32 (1.00 - 24.00)	n 15 4.60 ± 2.50 (0.00 - 8.00)	-	-	-	1.00	0.24	0.40
FBI A	-	n 67	n 22	n 8	-	-	-	0.13	1.00	1.00

		4.31 ± 5.07 (0.00 - 25.00)	1.77 ± 3.84 (0.00 - 16.00)	2.25 ± 2.96 (0.00 - 8.00)						
FBI B	-	n 67 1.49 ± 1.93 (0.00 - 8.00)	n 22 0.86 ± 1.88 (0.00 - 8.00)	n 8 1.38 ± 2.33 (0.00 - 6.00)	-	-	-	0.62	1.00	0.92
FBI total	-	n 73 5.74 ± 6.41 (0.00 - 32.00)	n 24 2.79 ± 5.28 (0.00 - 24.00)	n 11 3.64 ± 4.82 (0.00 - 14.00)	-	-	-	0.15	1.00	1.00
ALS-FTD-Q	-	n 62 11.79 ± 8.88 (0.00 - 35.00)	n 5 14.80 ± 17.85 (0.00 - 44.00)	n 5 20.00 ± 18.83 (5.00 - 50.00)	-	-	-	1.00	0.28	1.00

Values are numbers or means ± standard deviations (range). Differences between patient groups and healthy controls were assessed using one-way ANOVA (statistical contrasts) corrected for age, sex and education. Comparisons among patients were also corrected for ALSFRS-r. *= Ratio between the number of correct items and the maximum number of administered items; **= Perseverations are reported as the ratio between perseveration absolute number and the maximum number of cards provided during the test; ***= Verbal fluency indices were obtained as following: time for generation condition - time for control condition (reading or writing generated words)/total number of items generated. Abbreviations: ALS= Amyotrophic lateral sclerosis; ALS-FTD-Q= ALS-FTD questionnaire; BADA= Battery for aphasic deficit analysis; BDI= Beck Depression Inventory; CET= Cognitive estimation test; CPM= Colored progressive matrices; CST= Card sorting tests; FBI= Frontal Behavioral Inventory; HDRS= Hamilton Depression Rating Scale; HC= Healthy controls; MMSE= Mini-Mental state examination; PF= Phonemic fluency; PLS= Primary lateral sclerosis; PMA= Progressive muscular atrophy; RAVLT= Rey auditory verbal learning test; SF= Semantic fluency.

E-Table 2. MRI acquisition parameters.

Milan/Turin	Philips Medical System Intera 3T scan				
	*T2-*weighted SE	FLAIR	3D T1-weighted FFE	Pulsed-gradient SE echo planar with sensitivity encoding	T2*-weighted single-shot EPI sequence (resting state fMRI)
Repetition time (msec)	3500	11000	25	8986	3000
Echo time (msec)	85	120	4.6	80	35
Flip angle	90°	90°	30°	-	90°
Section thickness (mm)	5	5	-	2.5	4
No. of sections	22	22	220	55	30 for 220 volumes
Matrix	512x512	512x512	256x256	96x96	128x128
Field of view (mm²)	230x184	230x230	230x182	240x240	240x240
Diffusion gradient directions	-	-	-	32	-
b value sec/mm²	-	-	-	1000	-
Naples	GE Signa HDxt scan				
	T2-weigthed FSE	FLAIR	T1-weigthed sagittal images	Gradient echo planar imaging	T2*-weighted echo planar sequence (resting state fMRI)
Repetition time (msec)	3444	9052	7000	13000	1508
Echo time (msec)	128	122.4	2848	83.6	32
Flip angle	-	-	8°	-	90°
Section thickness (mm)	4	4	-	-	4
No. of sections	32	32	-	50	29 for 240 volumes
Matrix	512x512	512x512	256x256	128x128	64x64
Field of view (mm²)	240x240	240x240	260x260	320x320	256x256
Diffusion gradient directions	-	-	-	32	-

b value sec/mm²	-	-	-	1000	-

Abbreviations: FFE= fast field echo; FLAIR= fluid-attenuated inversion recovery; FSE= fast spin echo; MRI= magnetic resonance imaging; msec= millisecond; mm= millimeter; No= number; SE=spin echo; sec=second.

E-Table 3. Lobar graph analysis properties of structural and functional brain networks in ALS, PLS and PMA patients and matched healthy controls.

Regions	Graph analysis properties		HC	ALS	PLS	PMA	p ALS vs HC	p PLS vs HC	p PMA vs HC	p ALS vs PLS	p ALS vs PMA	p PLS vs PMA
			79	**173**	**38**	**28**						
Fronto-insular	Nodal strength	Structural (FA)	2.61 ± 0.28 (2.03 - 3.43)	2.50 ± 0.30 (1.54 - 3.33)	2.45 ± 0.23 (1.90 - 2.87)	2.62 ± 0.26 (2.17 - 3.38)	**0.01**	0.13	1.00	1.00	0.25	0.51
		Functional	2.80 ± 0.51 (1.70 - 4.26)	2.73 ± 0.59 (1.54 - 5.35)	2.71 ± 0.63 (1.72 - 4.75)	2.71 ± 0.42 (1.92 - 3.71)	1.00	1.00	0.57	1.00	1.00	1.00
	Path length	Structural (FA)	12.30 ± 1.05 (9.97 - 14.87)	12.70 ± 1.23 (10.12 - 18.18)	13.17 ± 1.07 (11.53 - 15.52)	12.20 ± 1.02 (9.79 - 13.87)	**0.045**	**0.003**	1.00	0.40	0.41	**0.03**
		Functional	11.80 ± 2.09 (7.57 - 19.53)	11.95 ± 2.30 (5.33 - 19.63)	12.05 ± 2.65 (7.07 - 20.96)	11.55 ± 1.61 (8.42 - 15.63)	1.00	0.61	1.00	1.00	1.00	1.00
	Local efficiency	Structural (FA)	0.34 ± 0.02 (0.30 - 0.37)	0.33 ± 0.02 (0.23 - 0.40)	0.33 ± 0.02 (0.29 - 0.36)	0.34 ± 0.02 (0.30 - 0.41)	**0.01**	**0.02**	1.00	1.00	0.07	**0.049**
		Functional	0.27 ± 0.06 (0.15 - 0.46)	0.27 ± 0.07 (0.12 - 0.55)	0.26 ± 0.07 (0.16 - 0.48)	0.26 ± 0.05 (0.15 - 0.39)	1.00	1.00	1.00	1.00	1.00	1.00
	Clustering coefficient	Structural (FA)	0.29 ± 0.02 (0.25 - 0.34)	0.29 ± 0.02 (0.18 - 0.35)	0.29 ± 0.02 (0.26 - 0.33)	0.30 ± 0.02 (0.25 - 0.33)	0.71	0.62	1.00	1.00	0.94	0.62
		Functional	0.17 ± 0.03 (0.10 - 0.29)	0.17 ± 0.04 (0.09 - 0.36)	0.16 ± 0.04 (0.11 - 0.28)	0.16 ± 0.03 (0.10 - 0.23)	1.00	1.00	0.63	1.00	1.00	1.00
Temporal	Nodal strength	Structural (FA)	2.49 ± 0.26 (1.65 - 3.04)	2.39 ± 0.31 (1.36 - 2.99)	2.45 ± 0.20 (1.86 - 2.81)	2.48 ± 0.25 (1.80 - 2.89)	**0.02**	0.30	0.22	1.00	1.00	1.00
		Functional	2.65 ± 0.54 (1.33 - 4.29)	2.65 ± 0.65 (1.27 - 5.27)	2.84 ± 0.56 (1.71 - 4.38)	2.73 ± 0.45 (1.83 - 3.62)	1.00	1.00	0.47	1.00	0.64	0.61
	Path length	Structural (FA)	13.29 ± 1.06 (11.24 - 17.05)	13.77 ± 1.42 (11.16 - 21.19)	13.73 ± 0.85 (12.40 - 16.20)	13.24 ± 1.03 (10.73 - 15.47)	**0.02**	0.07	1.00	1.00	1.00	1.00

		Functional	13.08 ± 2.61 (7.70 - 23.80)	13.13 ± 2.91 (5.66 - 25.69)	12.47 ± 2.32 (7.79 - 19.42)	12.37 ± 1.63 (10.02 - 17.05)	1.00	1.00	1.00	1.00	1.00	1.00
	Local Efficiency	Structural (FA)	0.32 ± .02 (0.28 - 0.37)	0.32 ± 0.02 (0.23 - 0.36)	0.32 ± 0.01 (0.29 - 0.35)	0.32 ± 0.02 (0.25 - 0.36)	0.24	0.28	0.66	1.00	1.00	1.00
		Functional	0.29 ± 0.07 (0.13 - 0.50)	0.29 ± 0.08 (0.10 - 0.62)	0.32 ± 0.08 (0.14 - 0.56)	0.30 ± 0.06 (0.17 - 0.42)	1.00	1.00	0.33	1.00	0.54	0.35
	Clustering coefficient	Structural (FA)	0.28 ± 0.01 (0.25 - 0.32)	0.28 ± 0.02 (0.21 - 0.34)	0.28 ± 0.01 (0.25 - 0.30)	0.28 ± 0.03 (0.14 - 0.32)	1.00	1.00	0.93	1.00	1.00	1.00
		Functional	0.18 ± 0.04 (0.08 - 0.28)	0.18 ± 0.05 (0.08 - 0.37)	0.20 ± 0.05 (0.10 - 0.34)	0.18 ± 0.04 (0.08 - 0.25)	1.00	1.00	0.12	1.00	0.10	0.14
Parietal	Nodal strength	Structural (FA)	2.16 ± 0.31 (0.87 - 3.29)	2.11 ± 0.27 (1.19 - 2.93)	2.09 ± 0.20 (1.41 - 2.50)	2.23 ± 0.23 (1.75 - 2.66)	0.69	0.93	1.00	1.00	0.82	0.79
		Functional	2.43 ± 0.47 (1.05 - 3.75)	2.46 ± 0.51 (1.31 - 4.80)	2.57 ± 0.56 (1.76 - 3.76)	2.46 ± 0.34 (1.67 - 2.95)	1.00	1.00	1.00	1.00	0.90	0.99
	Path length	Structural (FA)	14.06 ± 1.54 (10.38 - 18.14)	14.46 ± 1.54 (10.58 - 22.75)	14.98 ± 1.23 (12.73 - 18.94)	13.94 ± 1.18 (11.10 - 16.52)	0.24	0.07	1.00	1.00	0.42	0.10
		Functional	12.96 ± 2.70 (7.85 - 24.04)	12.97 ± 3.44 (5.76 - 36.07)	12.38 ± 2.71 (7.89 - 22.14)	12.36 ± 1.92 (9.48 - 16.70)	1.00	1.00	1.00	1.00	1.00	1.00
	Local efficiency	Structural (FA)	0.35 ± 0.03 (0.21 - 0.42)	0.35 ± 0.03 (0.23 - 0.41)	0.35 ± 0.02 (0.29 - 0.39)	0.36 ± 0.02 (0.30 - 0.40)	0.20	**0.01**	1.00	0.36	1.00	0.10
		Functional	0.23 ± 0.06 (0.08 - 0.41)	0.23 ± 0.07 (0.10 - 0.45)	0.24 ± 0.08 (0.11 - 0.38)	0.22 ± 0.05 (0.10 - 0.30)	1.00	1.00	0.30	1.00	0.13	0.48
	Clustering coefficient	Structural (FA)	0.35 ± 0.03 (0.28 - 0.44)	0.34 ± 0.04 (0.19 - 0.44)	0.34 ± 0.03 (0.28 - 0.42)	0.35 ± 0.03 (0.30 - 0.41)	0.67	**0.02**	1.00	0.20	1.00	0.83
		Functional	0.16 ± 0.04 (0.07 - 0.30)	0.17 ± 0.05 (0.07 - 0.31)	0.18 ± 0.05 (0.09 - 0.27)	0.16 ± 0.04 (0.07 - 0.24)	1.00	1.00	0.24	1.00	0.07	0.36
Occipital	Nodal strength	Structural (FA)	2.03 ± 0.34 (0.69 - 2.64)	2.02 ± 0.41 (0.87 - 2.79)	2.16 ± 0.20 (1.71 - 2.49)	2.20 ± 0.23 (1.59 - 2.62)	1.00	1.00	1.00	1.00	1.00	1.00
		Functional	2.79 ± 0.87 (1.21 - 4.97)	2.79 ± 0.97 (0.62 - 5.75)	2.94 ± 0.85 (1.47 - 5.26)	2.99 ± 0.79 (1.91 - 4.97)	1.00	1.00	1.00	1.00	1.00	1.00

94

							1.00	1.00	1.00	1.00	1.00	1.00
	Path length	Structural (FA)	14.89 ± 1.72 (12.20 - 20.48)	15.17 ± 2.34 (11.71 - 28.71)	14.66 ± 1.14 (13.18 - 18.19)	14.01 ± 1.18 (12.33 - 17.55)	1.00	1.00	1.00	1.00	1.00	1.00
		Functional	13.28 ± 3.30 (7.62 - 26.83)	13.17 ± 3.58 (6.03 - 28.63)	12.43 ± 2.61 (7.43 - 21.60)	12.29 ± 1.95 (9.31 - 16.84)	1.00	1.00	1.00	1.00	1.00	1.00
	Local efficiency	Structural (FA)	0.35 ± 0.03 (0.16 - 0.40)	0.34 ± 0.04 (0.20 - 0.41)	0.35 ± 0.02 (0.31 - 0.39)	0.36 ± 0.02 (0.32 - 0.40)	1.00	1.00	1.00	1.00	1.00	1.00
		Functional	0.30 ± 0.12 (0.06 - 0.61)	0.30 ± 0.13 (0.02 - 0.63)	0.34 ± 0.12 (0.15 - 0.74)	0.32 ± 0.11 (0.13 - 0.54)	1.00	1.00	1.00	1.00	1.00	1.00
	Clustering coefficient	Structural (FA)	0.36 ± 0.04 (0.22 - 0.47)	0.36 ± 0.04 (0.19 - 0.51)	0.35 ± 0.03 (0.30 - 0.43)	0.35 ± 0.03 (0.31 - 0.44)	1.00	1.00	1.00	1.00	1.00	1.00
		Functional	0.20 ± 0.07 (0.06 - 0.41)	0.20 ± 0.08 (0.01 - 0.44)	0.22 ± 0.08 (0.11 - 0.46)	0.21 ± 0.06 (0.10 - 0.32)	1.00	1.00	1.00	1.00	1.00	1.00
Basal ganglia	Nodal strength	Structural (FA)	4.43 ± 0.54 (3.38 - 6.59)	4.40 ± 0.67 (2.88 - 6.56)	4.12 ± 0.31 (3.36 - 4.71)	4.24 ± 0.36 (3.74 - 5.07)	1.00	1.00	1.00	1.00	1.00	1.00
		Functional	2.65 ± 0.75 (1.49 - 5.23)	2.82 ± 0.87 (1.34 - 6.27)	2.61 ± 0.67 (1.48 - 4.55)	2.75 ± 0.60 (1.70 - 3.78)	0.91	1.00	1.00	0.37	1.00	1.00
	Path length	Structural (FA)	9.57 ± 0.74 (7.94 - 11.70)	9.88 ± 0.95 (8.01 - 14.43)	10.09 ± 0.63 (8.93 - 11.53)	9.59 ± 0.78 (7.87 - 11.38)	**0.04**	**0.03**	1.00	1.00	0.97	0.32
		Functional	10.86 ± 2.21 (5.97 - 16.65)	10.86 ± 2.69 (4.15 - 26.50)	10.91 ± 2.41 (7.13 - 19.02)	10.34 ± 1.58 (7.93 - 13.62)	1.00	1.00	1.00	1.00	1.00	1.00
	Local efficiency	Structural (FA)	0.38 ± 0.02 (0.33 - 0.43)	0.38 ± 0.02 (0.30 - 0.41)	0.38 ± 0.01 (0.35 - 0.41)	0.39 ± 0.02 (0.36 - 0.42)	**0.004**	**0.03**	1.00	1.00	1.00	1.00
		Functional	0.18 ± 0.06 (0.06 - 0.36)	0.20 ± 0.07 (0.04 - 0.47)	0.18 ± 0.05 (0.08 - 0.32)	0.20 ± 0.06 (0.11 - 0.33)	0.10	1.00	1.00	0.24	1.00	1.00
	Clustering coefficient	Structural (FA)	0.29 ± 0.03 (0.22 - 0.36)	0.29 ± 0.04 (0.18 - 0.39)	0.30 ± 0.02 (0.25 - 0.33)	0.31 ± 0.02 (0.26 - 0.34)	0.05	**0.03**	1.00	1.00	1.00	0.56
		Functional	0.12 ± 0.04 (0.04 - 0.23)	0.14 ± 0.05 (0.03 - 0.32)	0.13 ± 0.03 (0.05 - 0.21)	0.14 ± 0.05 (0.06 - 0.25)	0.12	1.00	1.00	0.67	1.00	1.00
Sensorimotor	Nodal strength	Structural (FA)	1.90 ± 0.54 (1.26 - 3.49)	1.85 ± 0.48 (1.18 - 3.38)	1.55 ± 0.22 (1.11 - 2.04)	1.74 ± 0.26 (1.40 - 2.25)	0.51	0.09	1.00	1.00	1.00	0.20

		Functional	1.86 ± 0.66 (0.93 - 4.68)	1.95 ± 0.63 (0.61 - 4.41)	1.79 ± 0.61 (0.99 - 3.59)	1.84 ± 0.50 (1.04 - 2.64)	1.00	1.00	1.00	1.00	1.00	1.00
	Path length	Structural (FA)	13.27 ± 1.64 (9.67 - 16.53)	13.75 ± 1.71 (10.00 - 18.64)	15.15 ± 1.72 (12.25 - 19.02)	13.42 ± 1.39 (10.68 - 16.27)	0.10	**<0.001**	1.00	**0.004**	0.21	**<0.001**
		Functional	13.99 ± 5.05 (8.50 - 51.35)	13.47 ± 3.01 (4.72 - 21.53)	14.06 ± 3.74 (7.98 - 26.98)	13.01 ± 2.36 (9.50 - 20.04)	1.00	1.00	1.00	1.00	1.00	1.00
	Local efficiency	Structural (FA)	0.35 ± 0.03 (0.27 - 0.42)	0.34 ± 0.03 (0.26 - 0.39)	0.32 ± 0.03 (0.24 - 0.37)	0.35 ± 0.03 (0.30 - 0.40)	**0.01**	**<0.001**	1.00	0.05	0.42	**0.004**
		Functional	0.16 ± 0.09 (0.05 - 0.56)	0.17 ± 0.08 (0.02 - 0.46)	0.14 ± 0.06 (0.04 - 0.36)	0.15 ± 0.06 (0.05 - 0.32)	1.00	1.00	1.00	1.00	1.00	1.00
	Clustering coefficient	Structural (FA)	0.42 ± 0.05 (0.33 - 0.58)	0.39 ± 0.05 (0.27 - 0.51)	0.39 ± 0.04 (0.30 - 0.46)	0.42 ± 0.04 (0.34 - 0.52)	**<0.001**	**<0.001**	0.67	0.15	0.82	**0.03**
		Functional	0.12 ± 0.06 (0.04 - 0.34)	0.12 ± 0.05 (0.02 - 0.30)	0.11 ± 0.05 (0.03 - 0.25)	0.11 ± 0.04 (0.04 - 0.27)	1.00	1.00	1.00	1.00	1.00	1.00

Values are reported as mean ± standard deviation (range). Differences between patient groups and healthy controls were assessed using one-way ANOVA (statistical contrasts) corrected for age, sex and center. P-values were adjusted for multiple comparisons at significance level 0.05 using Bonferroni post-hoc test. Abbreviations: ALS= Amyotrophic lateral sclerosis; FA= Fractional anisotropy; HC= Healthy controls; PLS= Primary lateral sclerosis; PMA= Progressive muscular atrophy.

E-Table 4. Brain nodes of the network.

| N	Node	Lobe	N	Node	Lobe	N	Node	Lobe
1	Precentral_L_p1	SENSMOT	75	Insula_L_p2	FRONT-INS	149	Parietal_Inf_L_p1	PAR
2	Precentral_L_p2	SENSMOT	76	Insula_L_p3	FRONT-INS	150	Parietal_Inf_L_p2	PAR
3	Precentral_L_p3	SENSMOT	77	Insula_R_p1	FRONT-INS	151	Parietal_Inf_L_p3	PAR
4	Precentral_L_p4	SENSMOT	78	Insula_R_p2	FRONT-INS	152	Parietal_Inf_R_p1	PAR
5	Precentral_L_p5	SENSMOT	79	Cingulum_Ant_L_p1	FRONT-INS	153	Parietal_Inf_R_p2	PAR
6	Precentral_R_p1	SENSMOT	80	Cingulum_Ant_L_p2	FRONT-INS	154	SupraMarginal_L_p1	PAR
7	Precentral_R_p2	SENSMOT	81	Cingulum_Ant_R_p1	FRONT-INS	155	SupraMarginal_L_p2	PAR
8	Precentral_R_p3	SENSMOT	82	Cingulum_Ant_R_p2	FRONT-INS	156	SupraMarginal_R_p1	PAR
9	Precentral_R_p4	SENSMOT	83	Cingulum_Mid_L_p1	FRONT-INS	157	SupraMarginal_R_p2	PAR
10	Precentral_R_p5	SENSMOT	84	Cingulum_Mid_L_p2	FRONT-INS	158	SupraMarginal_R_p3	PAR
11	Frontal_Sup_L_p1	FRONT-INS	85	Cingulum_Mid_L_p3	FRONT-INS	159	Angular_L_p1	PAR
12	Frontal_Sup_L_p2	FRONT-INS	86	Cingulum_Mid_R_p1	FRONT-INS	160	Angular_L_p2	PAR
13	Frontal_Sup_L_p3	FRONT-INS	87	Cingulum_Mid_R_p2	FRONT-INS	161	Angular_R_p1	PAR
14	Frontal_Sup_L_p4	FRONT-INS	88	Cingulum_Mid_R_p3	FRONT-INS	162	Angular_R_p2	PAR
15	Frontal_Sup_L_p5	FRONT-INS	89	Cingulum_Post_L_p1	PAR	163	Precuneus_L_p1	PAR
16	Frontal_Sup_R_p1	FRONT-INS	90	Cingulum_Post_R_p1	PAR	164	Precuneus_L_p2	PAR
17	Frontal_Sup_R_p2	FRONT-INS	91	Hippocampus_L_p1	TEMP	165	Precuneus_L_p3	PAR
18	Frontal_Sup_R_p3	FRONT-INS	92	Hippocampus_R_p1	TEMP	166	Precuneus_L_p4	PAR
19	Frontal_Sup_R_p4	FRONT-INS	93	ParaHippocampal_L_p1	TEMP	167	Precuneus_L_p5	PAR
20	Frontal_Sup_R_p5	FRONT-INS	94	ParaHippocampal_R_p1	TEMP	168	Precuneus_R_p1	PAR
21	Frontal_Sup_Orb_L_p1	FRONT-INS	95	ParaHippocampal_R_p2	TEMP	169	Precuneus_R_p2	PAR
22	Frontal_Sup_Orb_R_p1	FRONT-INS	96	Amygdala_L_p1	TEMP	170	Precuneus_R_p3	PAR
23	Frontal_Mid_L_p1	FRONT-INS	97	Amygdala_R_p1	TEMP	171	Precuneus_R_p4	PAR
24	Frontal_Mid_L_p2	FRONT-INS	98	Calcarine_L_p1	OCC	172	Paracentral_Lobule_L_p1	SENSMOT
25	Frontal_Mid_L_p3	FRONT-INS	99	Calcarine_L_p2	OCC	173	Paracentral_Lobule_L_p2	SENSMOT
26	Frontal_Mid_L_p4	FRONT-INS	100	Calcarine_L_p3	OCC	174	Paracentral_Lobule_R_p1	SENSMOT
27	Frontal_Mid_L_p5	FRONT-INS	101	Calcarine_R_p1	OCC	175	Caudate_L_p1	BG
28	Frontal_Mid_L_p6	FRONT-INS	102	Calcarine_R_p2	OCC	176	Caudate_R_p1	BG
29	Frontal_Mid_L_p7	FRONT-INS	103	Calcarine_R_p3	OCC	177	Putamen_L_p1	BG
30	Frontal_Mid_R_p1	FRONT-INS	104	Cuneus_L_p1	OCC	178	Putamen_R_p1	BG
31	Frontal_Mid_R_p2	FRONT-INS	105	Cuneus_L_p2	OCC	179	Pallidum_L_p1	BG
32	Frontal_Mid_R_p3	FRONT-INS	106	Cuneus_R_p1	OCC	180	Pallidum_R_p1	BG
33	Frontal_Mid_R_p4	FRONT-INS	107	Cuneus_R_p2	OCC	181	Thalamus_L_p1	BG
34	Frontal_Mid_R_p5	FRONT-INS	108	Lingual_L_p1	OCC	182	Thalamus_R_p1	BG
35	Frontal_Mid_R_p6	FRONT-INS	109	Lingual_L_p2	OCC	183	Heschl_L_p1	TEMP
36	Frontal_Mid_R_p7	FRONT-INS	110	Lingual_L_p3	OCC	184	Heschl_R_p1	TEMP
37	Frontal_Mid_Orb_L_p1	FRONT-INS	111	Lingual_R_p1	OCC	185	Temporal_Sup_L_p1	TEMP
38	Frontal_Mid_Orb_R_p1	FRONT-INS	112	Lingual_R_p2	OCC	186	Temporal_Sup_L_p2	TEMP
39	Frontal_Inf_Oper_L_p1	FRONT-INS	113	Lingual_R_p3	OCC	187	Temporal_Sup_L_p3	TEMP
40	Frontal_Inf_Oper_R_p1	FRONT-INS	114	Occipital_Sup_L_p1	OCC	188	Temporal_Sup_R_p1	TEMP
41	Frontal_Inf_Oper_R_p2	FRONT-INS	115	Occipital_Sup_L_p2	OCC	189	Temporal_Sup_R_p2	TEMP
42	Frontal_Inf_Tri_L_p1	FRONT-INS	116	Occipital_Sup_R_p1	OCC	190	Temporal_Sup_R_p3	TEMP
43	Frontal_Inf_Tri_L_p2	FRONT-INS	117	Occipital_Sup_R_p2	OCC	191	Temporal_Sup_R_p4	TEMP
44	Frontal_Inf_Tri_L_p3	FRONT-INS	118	Occipital_Mid_L_p1	OCC	192	Temporal_Pole_Sup_L_p1	TEMP
45	Frontal_Inf_Tri_R_p1	FRONT-INS	119	Occipital_Mid_L_p2	OCC	193	Temporal_Pole_Sup_L_p2	TEMP
46	Frontal_Inf_Tri_R_p2	FRONT-INS	120	Occipital_Mid_L_p3	OCC	194	Temporal_Pole_Sup_R_p1	TEMP
47	Frontal_Inf_Tri_R_p3	FRONT-INS	121	Occipital_Mid_L_p4	OCC	195	Temporal_Pole_Sup_R_p2	TEMP
48	Frontal_Inf_Orb_L_p1	FRONT-INS	122	Occipital_Mid_R_p1	OCC	196	Temporal_Mid_L_p1	TEMP
49	Frontal_Inf_Orb_L_p2	FRONT-INS	123	Occipital_Mid_R_p2	OCC	197	Temporal_Mid_L_p2	TEMP
50	Frontal_Inf_Orb_R_p1	FRONT-INS	124	Occipital_Mid_R_p3	OCC	198	Temporal_Mid_L_p3	TEMP
51	Frontal_Inf_Orb_R_p2	FRONT-INS	125	Occipital_Inf_L_p1	OCC	199	Temporal_Mid_L_p4	TEMP
52	Rolandic_Oper_L_p1	FRONT-INS	126	Occipital_Inf_R_p1	OCC	200	Temporal_Mid_L_p5	TEMP
53	Rolandic_Oper_R_p1	FRONT-INS	127	Fusiform_L_p1	TEMP	201	Temporal_Mid_L_p6	TEMP
54	Rolandic_Oper_R_p2	FRONT-INS	128	Fusiform_L_p2	TEMP	202	Temporal_Mid_L_p7	TEMP
55	Supp_Motor_Area_L_p1	SENSMOT	129	Fusiform_L_p3	TEMP	203	Temporal_Mid_R_p1	TEMP
56	Supp_Motor_Area_L_p2	SENSMOT	130	Fusiform_R_p1	TEMP	204	Temporal_Mid_R_p2	TEMP
57	Supp_Motor_Area_L_p3	SENSMOT	131	Fusiform_R_p2	TEMP	205	Temporal_Mid_R_p3	TEMP
58	Supp_Motor_Area_R_p1	SENSMOT	132	Fusiform_R_p3	TEMP	206	Temporal_Mid_R_p4	TEMP
59	Supp_Motor_Area_R_p2	SENSMOT	133	Postcentral_L_p1	SENSMOT	207	Temporal_Mid_R_p5	TEMP

60	Supp_Motor_Area_R_p3	SENSMOT	134	Postcentral_L_p2	SENSMOT	208	Temporal_Mid_R_p6	TEMP
61	Olfactory_L_p1	FRONT-INS	135	Postcentral_L_p3	SENSMOT	209	Temporal_Pole_Mid_L_p1	TEMP
62	Olfactory_R_p1	FRONT-INS	136	Postcentral_L_p4	SENSMOT	210	Temporal_Pole_Mid_R_p1	TEMP
63	Frontal_Sup_Medial_L_p1	FRONT-INS	137	Postcentral_L_p5	SENSMOT	211	Temporal_Pole_Mid_R_p2	TEMP
64	Frontal_Sup_Medial_L_p2	FRONT-INS	138	Postcentral_R_p1	SENSMOT	212	Temporal_Inf_L_p1	TEMP
65	Frontal_Sup_Medial_L_p3	FRONT-INS	139	Postcentral_R_p2	SENSMOT	213	Temporal_Inf_L_p2	TEMP
66	Frontal_Sup_Medial_L_p4	FRONT-INS	140	Postcentral_R_p3	SENSMOT	214	Temporal_Inf_L_p3	TEMP
67	Frontal_Sup_Medial_R_p1	FRONT-INS	141	Postcentral_R_p4	SENSMOT	215	Temporal_Inf_L_p4	TEMP
68	Frontal_Sup_Medial_R_p2	FRONT-INS	142	Postcentral_R_p5	SENSMOT	216	Temporal_Inf_R_p1	TEMP
69	Frontal_Sup_Medial_R_p3	FRONT-INS	143	Parietal_Sup_L_p1	PAR	217	Temporal_Inf_R_p2	TEMP
70	Frontal_Mid_Orb_L_p2	FRONT-INS	144	Parietal_Sup_L_p2	PAR	218	Temporal_Inf_R_p3	TEMP
71	Frontal_Mid_Orb_R_p2	FRONT-INS	145	Parietal_Sup_L_p3	PAR	219	Temporal_Inf_R_p4	TEMP
72	Rectus_L_p1	FRONT-INS	146	Parietal_Sup_R_p1	PAR	220	Temporal_Inf_R_p5	TEMP
73	Rectus_R_p1	FRONT-INS	147	Parietal_Sup_R_p2	PAR			
74	Insula_L_p1	FRONT-INS	148	Parietal_Sup_R_p3	PAR			

Abbreviations: Ant= anterior; BG= basal ganglia; FRONT-INS= fronto-insular; Inf= inferior; L= left; Mid= middle; N= region number; Oper= operculum; OCC= occipital; Orb= orbital; p= part; PAR= parietal; Post= posterior; R= right; SENSMOT= sensorimotor; Sup= superior; Supp= supplementary; TEMP= temporal; Tri= triangularis.

Additional figure 1. Subnetworks showing altered structural and functional connectivity in ALS (excluding ALS-FTD patients), PLS and PMA patients and healthy controls. Altered structural (A) and functional (B) connections are represented in magenta and orange, respectively. ALS patients and healthy controls comparison was adjusted for age, sex, and MR scanner. All the other comparisons were adjusted for age and sex. Six shades of blue color were used to define the belonging of each node to different lobes starting with light blue (frontal lobe) to dark blue (posterior lobe, i.e., occipital). Abbreviations: A= anterior; ALS= Amyotrophic Lateral Sclerosis; FA= fractional anisotropy; FTD= frontotemporal dementia; HC= healthy controls; L= left; P = posterior; PMA= Progressive muscular atrophy; R= right.
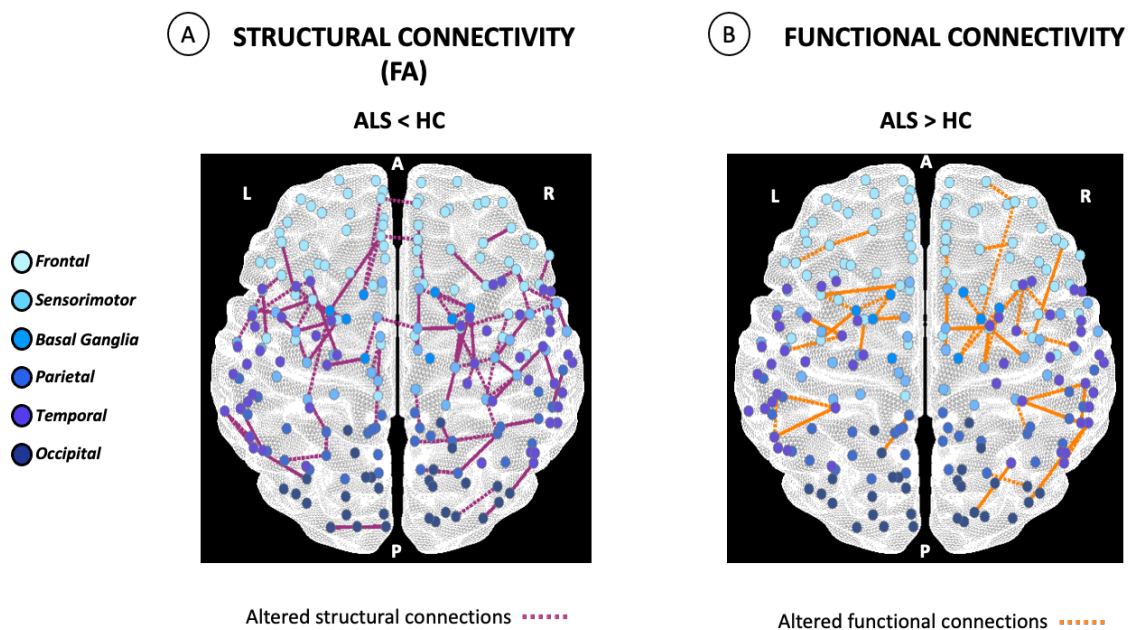
Additional figure 2. Subnetworks showing affected connections between groups acquired in Milan. Altered structural (A) and functional (B) connections are represented in magenta and orange, respectively. All the comparisons were adjusted for age and sex. Six shades of blue color were used to define the belonging of each node to different lobes starting with light blue (frontal lobe) to dark blue (posterior lobe, i.e., occipital). Abbreviations: A= anterior; ALS= Amyotrophic Lateral Sclerosis; FA= fractional anisotropy; HC= healthy controls; L= left; P = posterior; R= right.

4.2 AMYOTROPHIC LATERAL SCLEROSIS-FRONTOTEMPORAL DEMENTIA: SHARED AND DIVERGENT NEURAL CORRELATES ACROSS THE CLINICAL SPECTRUM

[1,6]Camilla Cividini, MSc, [1]Silvia Basaia, PhD, [1,6]Edoardo G. Spinelli, MD, [1]Elisa Canu, PhD, [1,6]Veronica Castelnovo, MSc, [4]Nilo Riva, MD, PhD, [1,2,6]Giordano Cecchetti, MD, [2]Francesca Caso, MD, PhD, [2]Giuseppe Magnani, MD, [5,6]Andrea Falini, MD, PhD, [1-4,6]Massimo Filippi, MD, [1,2,6]Federica Agosta, MD, PhD

[1]Neuroimaging Research Unit, Division of Neuroscience, IRCCS San Raffaele Scientific Institute, Milan, Italy; [2]Neurology Unit, IRCCS San Raffaele Scientific Institute, Milan, Italy; [3]Neurophysiology Service, IRCCS San Raffaele Scientific Institute, Milan, Italy; [4]Neurorehabilitation Unit, IRCCS San Raffaele Scientific Institute, Milan, Italy; [5]Neuroradiology Unit and CERMAC, IRCCS San Raffaele Scientific Institute, Milan, Italy; [6]Vita-Salute San Raffaele University, Milan, Italy.

Abstract

Objectives. A significant overlap between amyotrophic lateral sclerosis (ALS) and behavioral variant of frontotemporal dementia (bvFTD) has been observed at clinical, genetic and pathological levels. Within this continuum of presentations, the presence of mild cognitive and/or behavioral symptoms in ALS patients has been consistently reported, although it is unclear whether this is to be considered a distinct phenotype or, rather, a natural evolution of ALS. Here, we used mathematical modeling of MRI connectomic data to decipher common and divergent neural correlates across the ALS-FTD spectrum.

Methods. We included 83 ALS patients, 35 bvFTD patients and 61 healthy controls, who underwent clinical, cognitive and MRI assessments. ALS patients were classified according to the revised Strong criteria into 54 ALS with only motor deficits (ALS-cn), 21 ALS with cognitive and/or behavioral involvement (ALS-ci/bi), and 8 ALS with bvFTD (ALS-FTD). First, we assessed the functional and structural connectivity patterns across the ALS-FTD spectrum. Second, we investigated whether and where MRI connectivity alterations of ALS patients with any degree of cognitive impairment (i.e., ALS-ci/bi and ALS-FTD) resembled more the pattern of damage of one (ALS-cn) or the other end (bvFTD) of the spectrum, moving from group-level to single-subject analysis.

Results. As compared with controls, extensive structural and functional disruption of the frontotemporal and parietal networks characterized bvFTD (bvFTD-like pattern), while a more focal structural damage within the sensorimotor-basal ganglia areas characterized ALS-cn (ALS-cn-like pattern). ALS-ci/bi patients demonstrated an "ALS-cn-like" pattern of structural damage, diverging from ALS-cn with similar motor impairment for the presence of enhanced functional connectivity within sensorimotor areas and decreased functional connectivity within the "bvFTD-like" pattern. On the other hand, ALS-FTD patients resembled both structurally and functionally the bvFTD-like pattern of damage with, in addition, the structural ALS-cn-like damage in the motor areas.

Conclusions. Our findings suggest a maladaptive role of functional rearrangements in ALS-ci/bi concomitantly with similar structural alterations compared to ALS-cn, supporting the hypothesis that ALS-ci/bi might be considered as a phenotypic variant of ALS, rather than a consequence of disease worsening.

INTRODUCTION

Amyotrophic lateral sclerosis (ALS) is the most common clinical presentation of motor neuron disease, characterized by progressive neurodegeneration of upper and lower motor neurons. A growing body of evidence supports the notion of clinical, pathological and genetic overlap between ALS and the wide spectrum of frontotemporal dementia (FTD) (Burrell *et al*, 2016). Indeed, at least 50% of ALS patients develop cognitive symptoms – mostly affecting executive functions – and behavioral alterations along the course of the disease, leading to a full-blown diagnosis of FTD in 5-25% of cases (Saxon *et al*, 2017; Strong *et al*, 2017). Considering that comorbid cognitive impairment is a known negative prognostic factor associated with more rapid progression to death or tracheostomy in ALS patients (Calvo *et al*, 2017; Elamin *et al*, 2013), a better definition and understanding of this condition has clear clinical relevance.

The revised Strong criteria (Strong *et al.*, 2017) established a recognized nomenclature for the ALS-FTD clinical continuum ranging from ALS cognitively normal (ALS-cn) to ALS with FTD (ALS-FTD), including ALS with cognitive impairment (ALSci), ALS with behavioural impairment (ALSbi), and ALS with combined cognitive and behavioural impairment (ALS-cbi). Nevertheless, there is currently great debate regarding the pathological underpinnings distinguishing ALS-cn from ALS-ci/bi and ALS-FTD cases, and whether this is to be considered a distinct phenotype or, rather, a natural evolution of ALS. Cross-sectional studies reported an increasing percentage of ALS-ci/bi in disease stages with more severe motor impairment (Chio *et al*, 2019), and even a sequential cognitive staging system has been proposed for ALS (Lule *et al*, 2018), mirroring regions involved in pathological stages of TDP-43 deposition (Brettschneider *et al.*, 2013). However, findings of the few available longitudinal neuropsychological studies in ALS diverge, as some support a stability of cognitive and behavioral changes over time, when present (Kasper *et al*, 2015; Kilani *et al*, 2004), whereas others suggest a subtle progression of cognitive deficits (Beeldman *et al*, 2020; Castelnovo *et al*, 2021). The largest study in this context5 showed that patients who were cognitively impaired at baseline had a faster decline, in contrast with a tendency to remain cognitively intact in those who were cognitively unimpaired at study entry.

In this context, advanced magnetic resonance imaging (MRI) has provided a useful tool to investigate brain architecture in ALS and FTD. Several MRI studies evaluated

patients with behavioral variant of FTD (bvFTD), using both conventional MRI (Gordon *et al*, 2016; Seeley *et al*, 2008; Trojsi *et al*, 2015; Whitwell *et al*, 2011) and connectomic approaches (Agosta *et al*, 2013b; Filippi *et al.*, 2017), reporting specific patterns of structural and functional damage within frontoinsular and temporal networks. In ALS, widespread grey matter (GM) (Agosta *et al*, 2016; Alruwaili *et al*, 2018; Illan-Gala *et al*, 2020) and white matter (WM) damage (Agosta *et al.*, 2016; Alruwaili *et al.*, 2018; Kasper *et al*, 2014) has been shown in patients cognitively impaired relative to ALS-cn patients, involving not only motor but also extra-motor areas, including frontotemporal, parietal, insular and cingulate regions. A recent study using a connectomic approach revealed widespread cerebral WM changes affecting frontotemporal regions in ALS-ci/bi patients relative to ALS-cn patients (van der Burgh *et al*, 2020). Available functional MRI studies have reported conflicting results, as executive dysfunction and behavioral disturbances in ALS have been associated with either enhanced functional connectivity in frontoparietal and temporal networks (Basaia *et al*, 2020; Castelnovo *et al*, 2020; Schulthess *et al*, 2016) or suppressed connectivity within frontoparietal, salience and executive networks (Mohammadi *et al*, 2009; Trojsi *et al.*, 2015). However, in the current literature, there is a lack of MRI studies specifically assessing functional brain alterations in ALS with mild cognitive/behavioral decline, as only one study suggested an enhanced functional connectivity in patients with cognitive decline relative to ALS-cn (Hu *et al*, 2020).

To date, a direct evaluation of brain network reorganization in ALS-ci/bi compared with the opposite ends of the ALS-FTD spectrum (i.e., ALS-cn and full-blown FTD) is still needed. Moreover, no studies have combined the structural and functional information using graph analysis and connectomics to investigate neural correlates of cognitive and behavioral decline within patients of the spectrum. The aim of the present study was to bridge this gap, investigating structural and functional network correlates of cognitive/behavioral impairment in patients within the ALS-FTD continuum, who were fully characterized according to the revised Strong criteria (Strong *et al.*, 2017). Using up-to-date MRI approaches, we assessed distinctive patterns of network disruption (i.e., "ALS-cn-like pattern" and "bvFTD-like pattern") that may prove useful for accurate classification at a single-patient level.

METHODS

An overview of the Methods is provided in Figure 1.

Participants

Eighty-three ALS and 35 bvFTD patients were recruited at the IRCCS Ospedale San Raffaele, Milan, Italy, in the framework of an observational study (Fig. 1.I). Only sporadic patients (i.e., with no family history of dementia or motor neuron disease) who proved negative for mutations in the major genes associated with ALS/FTD (i.e., C9ORF72, GRN, MAPT, TARDBP, SOD1, FUS, TBK1, TREM2, OPTN and VCP) were included. The diagnosis of ALS was based on the revised El Escorial criteria (Brooks *et al.*, 2000), whereas bvFTD was diagnosed according to Rascovsky criteria (Rascovsky *et al*, 2011). Patients underwent a comprehensive evaluation including neurological history, clinical assessment (Table 1), neuropsychological testing (eTable 1) and MRI scan. For ALS patients, the site of disease onset was recorded; disease severity was assessed using the ALSFRS-r (Cedarbaum *et al.*, 1999); rate of disease progression was defined as [48–ALSFRS-r score]/time from symptom onset; and muscular strength was assessed by manual muscle testing based on the Medical Research Council (MRC) scale. ALS patients were receiving riluzole at study entry. For bvFTD patients, disease severity was assessed using the Clinical Dementia Rating scale (Knopman *et al*, 2008).

Sixty-one healthy controls were recruited by word of mouth, based on the following criteria: no history of neurologic and psychiatric diseases, no family history of neurodegenerative diseases, and a normal neurological assessment (Table 1).

Exclusion criteria for all subjects were: (other) significant medical illnesses or substance abuse that could interfere with cognitive functioning; any (other) major systemic, psychiatric, or neurological illnesses; and other causes of focal or diffuse brain damage, including lacunae and extensive cerebrovascular disorders at routine MRI.

Cognitive and Behavioral Assessment

Patient classification (Fig. 1.I). Comprehensive multi-domain cognitive testing was performed by trained neuropsychologists unaware of MRI results. Tested cognitive domains were: global cognitive functioning, memory, executive function, visuospatial abilities, fluency, language, mood and behaviors, as previously described (Basaia *et al.*, 2020; Filippi *et al.*, 2017) (eTable 1). According to the revised Strong criteria (Strong *et*

104

al., 2017), patients with ALS were classified into 54 cases with motor impairment only (ALS-cn), 21 cases with cognitive and/or behavioral deficits (ALS-ci/bi) and 8 ALS patients with bvFTD (ALS-FTD).

MRI acquisition and pre-processing

MRI scans were obtained using a 3T Philips Medical Systems Intera machine scan. T1-weighted, T2-weighted, fluid-attenuated inversion recovery, diffusion tensor MRI (DT MRI) and resting-state functional MRI (RS fMRI) sequences were acquired. Full details of the MRI acquisition protocol are reported in eTable 2. MRI analyses were performed by experienced observers blinded to subjects' identity.

Connectome Reconstruction (Fig. 1.II). Brain parcellation, DT MRI and RS fMRI pre-processing, and construction of brain structural and functional connectome have been described previously (Basaia *et al.*, 2020; Filippi *et al.*, 2017). Briefly, brain was parcellated into 220 similarly-sized GM cortical and subcortical regions (eTable 3). Applying a graph theoretical approach, the 220 brain regions are represented as nodes and structural/functional connections linking each pair of nodes as edges. Edges for structural connectivity are represented by fractional anisotropy (FA), whereas functional edges are represented by Pearson's correlation coefficients between each pair of nodes. Once the structural macroscale connectome was reconstructed per each subject, we applied the structural connectome of an independent healthy control group as a comprehensive brain connection mask (Filippi *et al.*, 2017). Then, the masked structural connectome of each subject was used as mask for the respective functional connectome, in order to investigate the functional alterations only where structural connections exist, enhancing the biological interpretation of the results (Schmidt *et al*, 2014).

Statistical analysis

Characterization of functional and structural connectivity across the ALS-FTD spectrum

Regional connectivity analysis (Fig. 1.III). We investigated structural and functional network features in the different subject groups at regional level. Network Based Statistic (NBS) (Zalesky *et al.*, 2010a) was performed to assess regional structural and functional connectivity strength at the level of significance $p<0.05$. All possible combinations of

comparisons between groups were performed. The largest (or principal) connected component and the smaller clusters of altered connections were identified (Basaia *et al.*, 2020; Zalesky *et al.*, 2010a). A corrected p-value was calculated for each contrast using an age-, sex-, and education-adjusted permutation analysis (10000 permutations).

Investigation of ALS-cn-like or bvFTD-like patterns of alterations in ALS-ci/bi and ALS-FTD

The following analyses were focused firstly on identifying the specific structural and functional connectivity patterns that characterize the ends of the ALS-FTD spectrum (ALS-cn and bvFTD). Secondly, we investigated whether and where ALS-ci/bi and ALS-FTD patients showed an ALS-cn-like or a bvFTD-like connectivity pattern.

Distribution analysis (Fig. 1.IV). Distribution analysis was performed to assess the structural and functional connectivity alterations in patient groups. The connectivity values of each connection for each patient were normalized relative to controls as follows:

$$Z_{ij}^s = \frac{C_{ij}^s - \mu}{\sigma}$$

where C_{ij}^s is the structural/functional connectivity value of the connection between node i and j for subject s; μ is the mean structural/functional connectivity value of the considered connection in the control group; and σ is the standard deviation of the structural/functional connectivity value of such connection in the control group. Subsequently, the 220 regions from both hemispheres were grouped into six anatomical macro-areas (hereafter referred to as brain areas): temporal, parietal, occipital, fronto-insular, basal ganglia, and sensorimotor. Per each patient group (ALS-cn, ALS-ci/bi, ALS-FTD, and bvFTD), the mean values of intra- and inter-area connectivity were calculated averaging the normalized structural/functional connections belonging to an area (intra) or linking two distinct areas (inter), respectively. The percentage of patients with connectivity value below the reference value (i.e., control mean value) was calculated per each intra- and inter-area network. Finally, the intra- and inter-area connectivity values were compared between patient groups using age-, sex-, and education-adjusted analysis of variance models, followed by post hoc pairwise comparisons, Bonferroni-corrected for multiple comparisons (p<0.05, SPSS Statistics 26.0 [SPSS Inc., Chicago, IL]).

Classification analysis (Fig. 1.V). Classification analysis was performed to define the characteristic structural/functional patterns of damage of the two ends of the spectrum (ALS-cn and bvFTD). For this purpose, we selected the structural and functional connectivity values only in those intra- and inter-area networks, where ALS-cn and bvFTD showed significantly different patterns in the distribution analysis. Receiver Operator Characteristic (ROC) curve analysis was performed in these selected networks. The area under the curve (AUC), as derived measure of accuracy, was considered to assign a specific set of structural/functional alterations to ALS-cn (ALS-cn-like pattern) or to bvFTD (bvFTD-like pattern). Per each intra- and/or inter-area connectivity value involved in one of the two patterns, Youden Index was calculated, providing the best tradeoff between sensitivity and specificity. Finally, patients of each group were classified in those with connectivity values above or below the identified optimal cut-offs.

Frequency analysis (Fig. 1.VI). Aiming to assess, at the single-subject level, whether and where ALS-ci/bi and ALS-FTD patients showed commonalities and differences with ALS-cn-like or bvFTD-like patterns, we performed a frequency analysis using the Chi-squared test ($p < 0.05$). Specifically, we identified and compared between groups the frequency of subjects with connectivity values above and below the optimal cut-offs belonging to the ALS-cn-like and the bvFTD-like pattern. ALS-cn group was excluded in the frequency analysis of the ALS-cn-like pattern, as well as the bvFTD group was not considered in the bvFTD-like pattern analysis.

Data availability

The dataset used during the current study will be made available by the corresponding author upon request to qualified researchers (i.e., affiliated to a university or research institution/hospital).

Standard Protocol Approvals, Registration, and Patient Consents

Local ethical standards committee on human experimentation approved the study protocol and all participants (or their caregivers) provided written informed consent.

RESULTS

Clinical and neuropsychological features

Demographic and clinical characteristics of study groups are reported in Table 1, while neuropsychological features in eTable 1. Relative to controls, ALS-cn and bvFTD patients showed a larger proportion of male individuals. In addition, ALS-ci/bi and bvFTD patients showed lower education relative to controls. ALS groups and bvFTD patients were different for disease duration at MRI, which was shorter in ALS patients. ALS groups were comparable in terms of disease severity, as assessed by ALSFRS-r and MRC global score, disease progression rate and site of clinical onset, although ALS-ci/bi were older than ALS-cn. The neuropsychological assessment did not reveal differences between controls and ALS-cn. bvFTD and ALS-FTD patients performed worse than controls and ALS-cn cases in all investigated cognitive domains. The ALS-ci/bi group performed worse than controls in naming (actions) and better than bvFTD and ALS-FTD patients in fluency tests, with additional higher performance in global cognition, verbal memory, and abstract reasoning compared to bvFTD group only (eTable 1).

Characterization of functional and structural connectivity across the ALS-FTD spectrum (Fig. 2)

Structural connectivity. Regional connectivity analysis showed alterations involving the connections within and among the sensorimotor network, basal ganglia, frontal, temporal and parietal areas, in addition to minimal involvement of the occipital connections, in ALS-cn patients relative to controls (p=0.01; Fig. 2A[1]). This structural pattern of damage was also found in ALS-ci/bi and ALS-FTD cases relative to controls (p=0.02 and p=0.001, Fig. 2A[2,3], respectively), with a more widespread disruption of the same networks in ALS-FTD reflecting increasing severity of impaired behavior and cognition (Fig. 2A[3]). ALS-FTD patients showed also a more severe structural damage, mainly within frontal areas, relative to ALS-cn cases (p=0.01; Fig. 2A[6]). Additionally, ALS-cn patients showed greater structural alterations relative to bvFTD (p=0.03; Fig. 2A[5]) in few connections within and among sensorimotor regions, parietal areas, and basal ganglia, especially involving thalamus and those connections from pallidum and putamen towards precentral, postcentral and precuneus bilaterally. Patients with bvFTD showed a widespread structural damage relative to controls, ALS-cn and ALS-ci/bi

patients across the whole brain (p<0.001; Fig. 2A[4,7,8], respectively). No further differences were observed in the remaining comparisons.

Functional connectivity. NBS analysis did not show differences in functional connectivity in ALS groups relative to controls, although ALS-ci/bi patients showed a trend toward an enhanced functional connectivity relative to controls within frontal and basal ganglia areas (p=0.06). On the other hand, bvFTD patients were characterized by reduced functional connectivity relative to controls (p=0.02; Fig. 2B[1]), ALS-cn (p=0.01; Fig. 2B[3]) and ALS-ci/bi (p<0.001; Fig. 2B[4]) cases, mainly involving the connections within the frontotemporal regions and between frontal and sensorimotor areas. ALS-FTD relative to ALS-ci/bi patients showed reduced functional connectivity within and between the frontal, temporal and motor areas similarly to bvFTD cases (p=0.02; Fig. 2B[2]). No further differences were observed in the remaining comparisons.

Investigation of ALS-cn-like and bvFTD-like patterns of alterations in ALS-ci/bi and ALS-FTD: structural connectivity (Fig. 3-4)

Distribution analysis. Compared with ALS-cn, bvFTD patients showed greater structural intra-area disruption within frontal, temporal and parietal areas (Fig. 3[1], Fig. 4[3,4] and eTable 4; p<0.05) and inter-area disruption in the frontal, temporal and occipital connections toward parietal lobe (p=0.01, Fig. 3[2] and Fig. 4[2,5]), in the frontal, basal ganglia and occipital connections toward temporal areas (p=0.002, p<0.001 and p=0.03, Fig. 3[3] and Fig. 4[1,6] respectively), and in the connections between frontal and basal ganglia (p<0.001) (Fig. 3[5] and eTable 4). Most of bvFTD patients (from 83 to 100%) were found severely disrupted in these networks (eTable 4). On the other hand, most of ALS-cn patients (81%) were characterized by a greater damage within the motor network, specifically among the sensorimotor – basal ganglia connections, relative to bvFTD cases (p=0.01, Fig. 3[7]). Additionally, ALS-FTD patients showed structural connectivity alterations within the motor areas, resembling the ALS-cn damage. In particular, 88% of ALS-FTD revealed a significant structural disruption in the sensorimotor-basal ganglia connections compared with bvFTD (p=0.01; Fig. 3[7] and eTable 4). Among the other brain regions, ALS-ci/bi and ALS-FTD patients behaved differently. ALS-ci/bi patients showed significant structural connectivity differences within frontal and temporal lobe (Fig. 3[1] and Fig. 4[3]) and between frontal, temporal

and basal ganglia areas compared to bvFTD (p<0.05, (Fig. 3[3,5] and Fig. 4[1]), embracing a pattern of damage more like ALS-cn. On the other hand, ALS-FTD revealed a behavior more like bvFTD, showing a greater structural disruption within frontal (p=0.03) and in frontal -sensorimotor connections (p=0.02) compared to ALS-cn (Fig. 3[1,4] and eTable 4).

Classification analysis. From ROC curve analysis, two characteristic patterns of damage were identified: the "ALS-cn-like pattern" defined by a focal structural damage within sensorimotor-basal ganglia areas that distinguished ALS-cn from bvFTD patients (accuracy [AUC]=0.67, eFigure. 1A-blue line), and the "bvFTD-like pattern" characterized by structural alterations of the frontotemporal and parietal networks that discriminated bvFTD from ALS-cn cases with AUC ranging from 0.67 and 0.88 (eFigure. 1A-red lines). The best cutoff of structural connectivity per each significant network are reported in Table 2.

Frequency analysis. The ALS-cn-like pattern was identified more frequently in ALS-ci/bi and ALS-FTD compared with bvFTD patients (ALS-ci/bi vs bvFTD p=0.04; ALS-FTD vs bvFTD non-significant trend p=0.07) (eTable 5). On the other hand, the bvFTD-like pattern was found to be more frequent neither in ALS-ci/bi nor ALS-FTD compared to ALS-cn, except for a non-significant trend (p=0.08) within frontal and among frontal-basal ganglia, temporal-occipital areas in ALS-FTD relative to ALS-cn cases (eTable 5).

Investigation of ALS-cn-like and bvFTD-like patterns of alterations in ALS-ci/bi and ALS-FTD: functional connectivity (Fig. 5)

Distribution analysis. Regarding functional connectivity distribution analysis, decreased functional connectivity within frontotemporal (p=0.001) and between sensorimotor and parietal connections (p<0.02) was found in bvFTD compared with ALS-cn patients (Fig. 5[1,2] and eTable 4). ALS-ci/bi patients showed significant enhanced functional connectivity relative to bvFTD in the frontal-sensorimotor connections (p=0.001), parietotemporal connections (p=0.03) and within sensorimotor areas (p<0.001, Fig. 5[3,4,5] and eTable 4). Additionally, ALS-ci/bi showed increased functional connectivity within sensorimotor areas relative to ALS-cn (p<0.04, Fig. 5[4] and eTable 4). Of note, most ALS-ci/bi patients (a percentage ranging from 67 to 76%) revealed normalized values of functional connectivity greater than zero in these

abovementioned networks (i.e., frontal-sensorimotor, parietotemporal and sensorimotor). Moreover, ALS-FTD patients showed a significant greater reduced functional connectivity in temporal-sensorimotor connections compared to ALS-cn (p=0.03) and ALS-ci/bi (p<0.01, Fig. 5[6] and eTable 4).

Classification analysis. The ROC curve analysis on functional connectivity data identified only a "bvFTD-like pattern" of functional damage, involving frontotemporal and sensorimotor-parietal connections, with an AUC of 0.77 and 0.67 in discriminating bvFTD from ALS-cn, respectively (eFigure. 1B-red lines). The best cutoff values of functional connectivity for each significant network are reported in Table 2.

Frequency analysis. Within frontotemporal connections, ALS-ci/bi patients were characterized by a greater proportion of cases showing bvFTD-like decreased functional connectivity compared with ALS-cn (p=0.03; eTable 5), but a lower proportion compared with ALS-FTD (p=0.02), who mostly showed a typical bvFTD-like pattern with a decreased functional connectivity relative to ALS-cn patients (p<0.001; eTable 5).

DISCUSSION

The present multiparametric MRI study provides a comprehensive characterization of the neural correlates across the spectrum of ALS-FTD clinical presentations. A connectome-based approach was adopted, first, to identify the connectivity signatures of ALS-cn and bvFTD (i.e., the two ends of this spectrum) and, subsequently, to characterize the alterations underlying mild cognitive/behavioral deficits and full-blown dementia in ALS patients, with the aid of mathematical models and single-subject analysis. An ALS-cn-like pattern was defined by a focused structural damage within the motor areas. By contrast, a bvFTD-like pattern was delineated by a widespread structural damage and decreased functional connectivity, specifically in frontal, temporal and parietal areas. ALS-ci/bi patients showed a pattern of structural damage mostly overlapping with the ALS-cn-like pattern, whereas functional data diverged from ALS-cn for the presence of enhanced functional connectivity within the sensorimotor regions and decreased functional connectivity in the frontotemporal areas (i.e., mirroring a bvFTD-like pattern). Finally, ALS-FTD resembled the bvFTD-like pattern of damage both structurally and functionally, with, in addition, the structural ALS-cn-like damage in the motor areas. Although connectivity data alone cannot fully address the homogeneity or heterogeneity

of this spectrum, our findings suggest a maladaptive role of functional rearrangements in ALS-ci/bi concomitantly with similar structural alterations compared to ALS-cn, supporting the hypothesis that ALS-ci/bi might be considered as a phenotypic variant of ALS, rather than a consequence of disease worsening.

When considering the results of the present study, some limitations should be noted. Despite the robust size of the overall ALS cohort, some subgroups were small (i.e., ALS-FTD), although this is indicative of the relative incidence of cognitive alterations. This aspect has also influenced our choice to bring together patients with mild cognitive dysfunction (i.e., ALS-ci) and patients with mild behavioral disturbances (i.e., ALS-bi), to avoid dispersion of data and the reduced statistical power that would result. Furthermore, the lack of information of a definite pathological diagnosis for bvFTD patients is an important limitation of the present study, even though the aim of the work was to explore the neural correlates of the clinical rather than the pathological heterogeneity of the ALS-FTD spectrum. Another issue lies in the cross-sectional nature of the study. In this context, longitudinal studies are warranted to verify whether cognitive/behavioral dysfunction is a stable or progressive feature of the ALS trajectory, and to assess the evolution of associated network alterations over time.

The inherent limitations of MRI connectomic should also be acknowledged(Pandya *et al*, 2017; Reyes *et al*, 2018) including, among others, the lack of an optimal framework, i.e., a reference standard for the regional parcellation of brain MR imaging. It is also important to note that the accuracy of any attempt to model the connectome is biased by the intrinsic limitations of the imaging techniques used. For example, fibre tracking based on DT MRI is known to be poor at points where only limited information about the WM fibre direction is available such as where multiple tracts cross. This results in incomplete reconstruction of tracts and a general under-representation of long-distance connections in the brain. Despite these shortcomings, our study highlights the potential of multiparametric connectome-based approaches for providing novel pathophysiological insights and biomarkers of cognitive dysfunction in the context of ALS-FTD. A key point of our study was the demonstration of characteristic brain structural damage and functional rearrangements across ALS cognitive phenotypes, as defined based on the application of revised Strong criteria to a sizeable monocentric cohort. Our conclusions were made possible by the extensive clinical and neuropsychological characterization of

the sample, as well as by the multiparametric nature of this study. Current MRI literature has generally provided results based on the assessment of structural and functional alterations separately, at voxel or regional level, without a straightforward investigation of their relationship. Conversely, a connectomic approach gave us the potential to bridge the gap of the anatomo-functional link thanks to the application of the same parcellation system, connectome reconstruction framework and statistical approach. Whereas the capability of connectome-based approach to provide information on the brain network architecture was achieved by a group-level analysis, smoothing out the inter-individual variability, a further innovative aspect of our study was the transition to the single-level analysis by the help of mathematical models. Indeed, the study framework was able to identify the ALS-cn-like or bvFTD-like patterns of damage, and to characterize the type of damage that each ALS-ci/bi and ALS-FTD patient shared with such signatures of network alterations.

The selective involvement of motor WM regions in the ALS-cn sample is largely consistent with previous literature (Basaia *et al.*, 2020; Illan-Gala *et al.*, 2020; Muller *et al*, 2021), confirming a "signature" pattern of frank decline in FA of the subnetworks connecting primary motor, supplementary motor and premotor areas, as well as basal ganglia – specifically, the thalamus (Tu *et al*, 2018). The structural disruption of the sensorimotor network supports the current view of this network as the epicenter of degenerative process of the disease, in line with proposed neuropathological and MRI-based disease staging systems (Brettschneider *et al.*, 2013; Meier *et al*, 2020). As for the functional MRI findings, the current literature counts on a number of studies reporting reduced (Mohammadi *et al.*, 2009; Trojsi *et al.*, 2015) or increased functional connectivity in ALS patients (Basaia *et al*, 2020; Castelnovo *et al*, 2020; Schulthess *et al*, 2016), or even a mixed picture (Agosta *et al*, 2013a). Nevertheless, there is a shortage of MRI studies focusing on functional brain rearrangements in ALS related to cognitive status, and our findings contribute to fill this gap. Of note, both regional (i.e., NBS) and distribution analyses suggest that ALS-cn patients are characterized by a quite preserved functional connectivity comparable to the functional healthy-brain organization.

The bvFTD-like pattern included a widespread brain structural disruption, with a predominant damage in the frontotemporoparietal network and the involvement of the striatum, and functional connectivity breakdown within the same networks. Our findings

confirm previous evidence that see the disconnection of the frontoinsular and temporal regions as hallmark of the behavioral clinical syndrome of FTD both at structural and functional levels (Agosta *et al.*, 2013b; Filippi *et al.*, 2017; Gordon *et al.*, 2016; Whitwell *et al.*, 2011). Herein, we extend these results by highlighting the relative preservation of the motor areas in bvFTD, in contrast with a widespread structural and functional involvement of the anterior frontal lobes, as well as a differential involvement of the basal ganglia circuits when compared with ALS-cn (i.e., greater involvement of striatal connections in bvFTD, in contrast with thalamic involvement in ALS-cn). These findings are in line with previous reports (Bede *et al*, 2018; Tu *et al.*, 2018), and support the notion of a diverging network vulnerability to disease pathology in the two opposite ends of the ALS-FTD spectrum.

The focus of the current study was on elucidating MRI connectomic underpinnings of mild or full-blown cognitive deficits in ALS, possibly addressing the long-standing debate on the nature of cognitive deficits in the course of the disease, as an early or, rather, a late-stage feature. Regarding the structural brain network, the presence of mild cognitive and/or behavioral impairment in ALS patients did not contribute significantly to an additional microstructural damage relative to ALS-cn with otherwise comparable clinical characteristics – including measures of motor impairment and disease duration. Although previous literature has suggested greater structural damage related to cognitive impairment in ALS (Agosta *et al.*, 2016; Alruwaili *et al.*, 2018; Illan-Gala *et al.*, 2020; Kasper *et al.*, 2014; van der Burgh *et al.*, 2020), such damage was generally subtle and possibly driven by the inclusion of ALS-FTD subjects. By contrast, our study highlighted shared structural damage between ALS-ci/bi and ALS-cn patients, involving mainly the motor networks. On the other hand, the analysis of functional connectivity alterations played an important role for the differentiation of ALS-ci/bi from ALS-cn. Indeed, ALS-ci/bi patients showed a rearrangement of the functional networks, which was divergent from ALS-cn, with enhanced functional connectivity within motor areas and decreased connectivity in the frontotemporal networks. The concomitant absence of significant structural alterations, compared with the ALS-cn group, apparently supports a maladaptive role of such functional rearrangements in ALS-ci/bi, as previously hypothesized (Basaia *et al.*, 2020; Menke *et al*, 2018). The biological underpinnings of such functional disequilibrium have been suggested to lie in the known

excitatory/inhibitory imbalance due to interneuron pathology in ALS, causing a reduction in recurring inhibition that has been associated with disease severity (Crabe *et al*, 2020; Van den Bos *et al*, 2018). We argue that functional imbalance between motor and extra-motor frontal networks might be particularly severe in ALS-ci/bi, causing mild cognitive disturbances even in early phases of the disease – consistent with the relatively short disease duration of the present cohort. Therefore, our data suggest that ALS-ci/bi might be considered as a phenotypic variant of ALS, rather than a consequence of disease worsening (Chio *et al.*, 2019; Lule *et al.*, 2018). These findings may find support in one of the few longitudinal neuropsychological studies in this context (Elamin *et al.*, 2013), in which cognition decline was faster in patients who were already cognitively impaired at baseline, while normal cognition tended to remain intact with slower motor and cognitive progression. Of note, education levels of ALS-ci/bi patients were lower than ALS-cn in our sample, consistent with the recently highlighted influence of environmental factors that collectively constitute the cognitive reserve (i.e., education, occupation and physical activity) over an early development of cognitive symptoms in ALS (Costello *et al*, 2021).

In contrast with ALS-ci/bi cases, when ALS patients had co-occurrent dementia (ALS-FTD), our study has outlined not only a pattern of microstructural damage involving the motor networks (i.e., the characteristic ALS-cn-like pattern), but also a disruption of frontal, temporal, parietal and striatal circuits, both from a structural and a functional point of view – therefore, resembling the bvFTD-like pattern (Saxon *et al*, 2020). These findings agree with the pattern of widespread hypometabolism recently demonstrated in ALS cases with severe cognitive impairment (Canosa *et al*, 2020), possibly mirroring the most advanced stages of TDP-43 neuropathological models which have been proposed both in ALS (Brettschneider *et al.*, 2013) and bvFTD (Braak *et al*, 2013), here sharing the same pathological signature (Omer *et al*, 2017; Rohrer *et al*, 2010). Similar to ALS-ci/bi, ALS-FTD patients showed similar severity of motor symptoms and disease duration when compared with ALS-cn, supporting a view of this clinical presentation as a specific phenotype within the frontotemporal lobar degeneration spectrum, characterized by a combined, severe involvement of both motor and extra-motor brain networks, rather than an evolution of either ALS or bvFTD.

REFERENCES

Agosta F, Canu E, Valsasina P, Riva N, Prelle A, Comi G, Filippi M (2013a) Divergent brain network connectivity in amyotrophic lateral sclerosis. *Neurobiol Aging* 34: 419-427

Agosta F, Ferraro PM, Riva N, Spinelli EG, Chio A, Canu E, Valsasina P, Lunetta C, Iannaccone S, Copetti M *et al* (2016) Structural brain correlates of cognitive and behavioral impairment in MND. *Hum Brain Mapp* 37: 1614-1626

Agosta F, Sala S, Valsasina P, Meani A, Canu E, Magnani G, Cappa SF, Scola E, Quatto P, Horsfield MA *et al* (2013b) Brain network connectivity assessed using graph theory in frontotemporal dementia. *Neurology* 81: 134-143

Alruwaili AR, Pannek K, Coulthard A, Henderson R, Kurniawan ND, McCombe P (2018) A combined tract-based spatial statistics and voxel-based morphometry study of the first MRI scan after diagnosis of amyotrophic lateral sclerosis with subgroup analysis. *J Neuroradiol* 45: 41-48

Basaia S, Agosta F, Cividini C, Trojsi F, Riva N, Spinelli EG, Moglia C, Femiano C, Castelnovo V, Canu E *et al* (2020) Structural and functional brain connectome in motor neuron diseases: A multicenter MRI study. *Neurology* 95: e2552-e2564

Bede P, Omer T, Finegan E, Chipika RH, Iyer PM, Doherty MA, Vajda A, Pender N, McLaughlin RL, Hutchinson S *et al* (2018) Connectivity-based characterisation of subcortical grey matter pathology in frontotemporal dementia and ALS: a multimodal neuroimaging study. *Brain Imaging Behav* 12: 1696-1707

Beeldman E, Govaarts R, de Visser M, Klein Twennaar M, van der Kooi AJ, van den Berg LH, Veldink JH, Pijnenburg YAL, de Haan RJ, Schmand BA *et al* (2020) Progression of cognitive and behavioural impairment in early amyotrophic lateral sclerosis. *J Neurol Neurosurg Psychiatry* 91: 779-780

Braak H, Brettschneider J, Ludolph AC, Lee VM, Trojanowski JQ, Del Tredici K (2013) Amyotrophic lateral sclerosis--a model of corticofugal axonal spread. *Nat Rev Neurol* 9: 708-714

Brettschneider J, Del Tredici K, Toledo JB, Robinson JL, Irwin DJ, Grossman M, Suh E, Van Deerlin VM, Wood EM, Baek Y *et al* (2013) Stages of pTDP-43 pathology in amyotrophic lateral sclerosis. *Annals of neurology* 74: 20-38

Brooks BR, Miller RG, Swash M, Munsat TL, World Federation of Neurology Research Group on Motor Neuron D (2000) El Escorial revisited: revised criteria for the diagnosis of amyotrophic lateral sclerosis. *Amyotroph Lateral Scler Other Motor Neuron Disord* 1: 293-299

Burrell JR, Halliday GM, Kril JJ, Ittner LM, Gotz J, Kiernan MC, Hodges JR (2016) The frontotemporal dementia-motor neuron disease continuum. *Lancet* 388: 919-931

Calvo A, Moglia C, Lunetta C, Marinou K, Ticozzi N, Ferrante GD, Scialo C, Soraru G, Trojsi F, Conte A *et al* (2017) Factors predicting survival in ALS: a multicenter Italian study. *J Neurol* 264: 54-63

Canosa A, Moglia C, Manera U, Vasta R, Torrieri MC, Arena V, D'Ovidio F, Palumbo F, Zucchetti JP, Iazzolino B *et al* (2020) Metabolic brain changes across

different levels of cognitive impairment in ALS: a (18)F-FDG-PET study. *J Neurol Neurosurg Psychiatry*

Castelnovo V, Canu E, Calderaro D, Riva N, Poletti B, Basaia S, Solca F, Silani V, Filippi M, Agosta F (2020) Progression of brain functional connectivity and frontal cognitive dysfunction in ALS. *Neuroimage Clin* 28: 102509

Castelnovo V, Canu E, Riva N, Poletti B, Cividini C, Fontana A, Solca F, Silani V, Filippi M, Agosta F (2021) Progression of cognitive and behavioral disturbances in motor neuron diseases assessed using standard and computer-based batteries. *Amyotrophic lateral sclerosis & frontotemporal degeneration* 22: 223-236

Cedarbaum JM, Stambler N, Malta E, Fuller C, Hilt D, Thurmond B, Nakanishi A (1999) The ALSFRS-R: a revised ALS functional rating scale that incorporates assessments of respiratory function. BDNF ALS Study Group (Phase III). *J Neurol Sci* 169: 13-21

Chio A, Moglia C, Canosa A, Manera U, Vasta R, Brunetti M, Barberis M, Corrado L, D'Alfonso S, Bersano E *et al* (2019) Cognitive impairment across ALS clinical stages in a population-based cohort. *Neurology* 93: e984-e994

Costello E, Rooney J, Pinto-Grau M, Burke T, Elamin M, Bede P, McMackin R, Dukic S, Vajda A, Heverin M *et al* (2021) Cognitive reserve in amyotrophic lateral sclerosis (ALS): a population-based longitudinal study. *J Neurol Neurosurg Psychiatry* 92: 460-465

Crabe R, Aimond F, Gosset P, Scamps F, Raoul C (2020) How Degeneration of Cells Surrounding Motoneurons Contributes to Amyotrophic Lateral Sclerosis. *Cells* 9

Elamin M, Bede P, Byrne S, Jordan N, Gallagher L, Wynne B, O'Brien C, Phukan J, Lynch C, Pender N *et al* (2013) Cognitive changes predict functional decline in ALS: a population-based longitudinal study. *Neurology* 80: 1590-1597

Filippi M, Basaia S, Canu E, Imperiale F, Meani A, Caso F, Magnani G, Falautano M, Comi G, Falini A *et al* (2017) Brain network connectivity differs in early-onset neurodegenerative dementia. *Neurology* 89: 1764-1772

Gordon E, Rohrer JD, Fox NC (2016) Advances in neuroimaging in frontotemporal dementia. *J Neurochem* 138 Suppl 1: 193-210

Hu T, Hou Y, Wei Q, Yang J, Luo C, Chen Y, Gong Q, Shang H (2020) Patterns of brain regional functional coherence in cognitive impaired ALS. *Int J Neurosci* 130: 751-758

Illan-Gala I, Montal V, Pegueroles J, Vilaplana E, Alcolea D, Dols-Icardo O, de Luna N, Turon-Sans J, Cortes-Vicente E, Martinez-Roman L *et al* (2020) Cortical microstructure in the amyotrophic lateral sclerosis-frontotemporal dementia continuum. *Neurology* 95: e2565-e2576

Kasper E, Schuster C, Machts J, Bittner D, Vielhaber S, Benecke R, Teipel S, Prudlo J (2015) Dysexecutive functioning in ALS patients and its clinical implications. *Amyotrophic lateral sclerosis & frontotemporal degeneration* 16: 160-171

Kasper E, Schuster C, Machts J, Kaufmann J, Bittner D, Vielhaber S, Benecke R, Teipel S, Prudlo J (2014) Microstructural white matter changes underlying cognitive

and behavioural impairment in ALS--an in vivo study using DTI. *PLoS One* 9: e114543

Kilani M, Micallef J, Soubrouillard C, Rey-Lardiller D, Demattei C, Dib M, Philippot P, Ceccaldi M, Pouget J, Blin O (2004) A longitudinal study of the evolution of cognitive function and affective state in patients with amyotrophic lateral sclerosis. *Amyotroph Lateral Scler Other Motor Neuron Disord* 5: 46-54

Knopman DS, Kramer JH, Boeve BF, Caselli RJ, Graff-Radford NR, Mendez MF, Miller BL, Mercaldo N (2008) Development of methodology for conducting clinical trials in frontotemporal lobar degeneration. *Brain* 131: 2957-2968

Lule D, Bohm S, Muller HP, Aho-Ozhan H, Keller J, Gorges M, Loose M, Weishaupt JH, Uttner I, Pinkhardt E *et al* (2018) Cognitive phenotypes of sequential staging in amyotrophic lateral sclerosis. *Cortex; a journal devoted to the study of the nervous system and behavior* 101: 163-171

Meier JM, van der Burgh HK, Nitert AD, Bede P, de Lange SC, Hardiman O, van den Berg LH, van den Heuvel MP (2020) Connectome-Based Propagation Model in Amyotrophic Lateral Sclerosis. *Annals of neurology* 87: 725-738

Menke RAL, Proudfoot M, Talbot K, Turner MR (2018) The two-year progression of structural and functional cerebral MRI in amyotrophic lateral sclerosis. *Neuroimage Clin* 17: 953-961

Mohammadi B, Kollewe K, Samii A, Krampfl K, Dengler R, Munte TF (2009) Changes of resting state brain networks in amyotrophic lateral sclerosis. *Exp Neurol* 217: 147-153

Muller HP, Lule D, Roselli F, Behler A, Ludolph AC, Kassubek J (2021) Segmental involvement of the corpus callosum in C9orf72-associated ALS: a tract of interest-based DTI study. *Ther Adv Chronic Dis* 12: 20406223211002969

Omer T, Finegan E, Hutchinson S, Doherty M, Vajda A, McLaughlin RL, Pender N, Hardiman O, Bede P (2017) Neuroimaging patterns along the ALS-FTD spectrum: a multiparametric imaging study. *Amyotrophic lateral sclerosis & frontotemporal degeneration* 18: 611-623

Pandya S, Kuceyeski A, Raj A, Alzheimer's Disease Neuroimaging I (2017) The Brain's Structural Connectome Mediates the Relationship between Regional Neuroimaging Biomarkers in Alzheimer's Disease. *J Alzheimers Dis* 55: 1639-1657

Rascovsky K, Hodges JR, Knopman D, Mendez MF, Kramer JH, Neuhaus J, van Swieten JC, Seelaar H, Dopper EG, Onyike CU *et al* (2011) Sensitivity of revised diagnostic criteria for the behavioural variant of frontotemporal dementia. *Brain* 134: 2456-2477

Reyes P, Ortega-Merchan MP, Rueda A, Uriza F, Santamaria-Garcia H, Rojas-Serrano N, Rodriguez-Santos J, Velasco-Leon MC, Rodriguez-Parra JD, Mora-Diaz DE *et al* (2018) Functional Connectivity Changes in Behavioral, Semantic, and Nonfluent Variants of Frontotemporal Dementia. *Behav Neurol* 2018: 9684129

Rohrer JD, Geser F, Zhou J, Gennatas ED, Sidhu M, Trojanowski JQ, Dearmond SJ, Miller BL, Seeley WW (2010) TDP-43 subtypes are associated with distinct atrophy patterns in frontotemporal dementia. *Neurology* 75: 2204-2211

Saxon JA, Thompson JC, Harris JM, Richardson AM, Langheinrich T, Rollinson S, Pickering-Brown S, Chaouch A, Ealing J, Hamdalla H *et al* (2020) Cognition and behaviour in frontotemporal dementia with and without amyotrophic lateral sclerosis. *J Neurol Neurosurg Psychiatry* 91: 1304-1311

Saxon JA, Thompson JC, Jones M, Harris JM, Richardson AM, Langheinrich T, Neary D, Mann DM, Snowden JS (2017) Examining the language and behavioural profile in FTD and ALS-FTD. *J Neurol Neurosurg Psychiatry* 88: 675-680

Schmidt R, Verstraete E, de Reus MA, Veldink JH, van den Berg LH, van den Heuvel MP (2014) Correlation between structural and functional connectivity impairment in amyotrophic lateral sclerosis. *Hum Brain Mapp* 35: 4386-4395

Schulthess I, Gorges M, Muller HP, Lule D, Del Tredici K, Ludolph AC, Kassubek J (2016) Functional connectivity changes resemble patterns of pTDP-43 pathology in amyotrophic lateral sclerosis. *Sci Rep* 6: 38391

Seeley WW, Crawford R, Rascovsky K, Kramer JH, Weiner M, Miller BL, Gorno-Tempini ML (2008) Frontal paralimbic network atrophy in very mild behavioral variant frontotemporal dementia. *Arch Neurol* 65: 249-255

Strong MJ, Abrahams S, Goldstein LH, Woolley S, McLaughlin P, Snowden J, Mioshi E, Roberts-South A, Benatar M, HortobaGyi T *et al* (2017) Amyotrophic lateral sclerosis - frontotemporal spectrum disorder (ALS-FTSD): Revised diagnostic criteria. *Amyotrophic lateral sclerosis & frontotemporal degeneration* 18: 153-174

Trojsi F, Esposito F, de Stefano M, Buonanno D, Conforti FL, Corbo D, Piccirillo G, Cirillo M, Monsurro MR, Montella P *et al* (2015) Functional overlap and divergence between ALS and bvFTD. *Neurobiol Aging* 36: 413-423

Tu S, Menke RAL, Talbot K, Kiernan MC, Turner MR (2018) Regional thalamic MRI as a marker of widespread cortical pathology and progressive frontotemporal involvement in amyotrophic lateral sclerosis. *J Neurol Neurosurg Psychiatry* 89: 1250-1258

Van den Bos MAJ, Higashihara M, Geevasinga N, Menon P, Kiernan MC, Vucic S (2018) Imbalance of cortical facilitatory and inhibitory circuits underlies hyperexcitability in ALS. *Neurology* 91: e1669-e1676

van der Burgh HK, Westeneng HJ, Walhout R, van Veenhuijzen K, Tan HHG, Meier JM, Bakker LA, Hendrikse J, van Es MA, Veldink JH *et al* (2020) Multimodal longitudinal study of structural brain involvement in amyotrophic lateral sclerosis. *Neurology* 94: e2592-e2604

Whitwell JL, Jack CR, Jr., Parisi JE, Knopman DS, Boeve BF, Petersen RC, Dickson DW, Josephs KA (2011) Imaging signatures of molecular pathology in behavioral variant frontotemporal dementia. *J Mol Neurosci* 45: 372-378

Zalesky A, Fornito A, Bullmore ET (2010a) Network-based statistic: identifying differences in brain networks. *NeuroImage* 53: 1197-1207

Table 1. Demographic and clinical features of healthy controls, bvFTD patients and ALS patient groups.

|	Healthy controls	ALS-cn	ALS-ci/bi	ALS-FTD	bvFTD
N	61	54	21	8	35
Age [years]	63.04 ± 8.46 (43.36 – 81.81)	61.08 ± 9.96 (36.38 – 81.26)	67.99 ± 11.77^ (39.89 – 86.12)	60.28 ± 10.54 (44.68 – 70.06)	63.18 ± 9.13 (45.51 – 74.83)
Sex [women/men]	36/25	19/35*	11/10	5/3	12/23*
Education [years]	12.89 ± 4.79 (5.00 – 24.00)	11.06 ± 4.52 (5.00 – 24.00)	8.38 ± 3.72* (3.00 – 18.00)	11.50 ± 5.95 (4.00 – 18.00)	9.56 ± 3.65* (4.00 – 17.00)
Onset [limb/bulbar/limb+bulbar]	-	41/12/1	16/5/0	3/5/0	-
Disease duration [months]	-	23.76 ± 23.96# (4.00 – 136.00)	16.62 ± 12.11# (4.00 – 47.00)	23.25 ± 17.06 (7.00 – 56.00)	41.00 ± 29.63 (6.87 – 144.70)
ALSFRS-r [0-48]	-	38.31 ± 5.46 (23.00 – 47.00)	39.00 ± 5.72 (28.00 – 46.00)	35.63 ± 7.84 (24.00 – 45.00)	-
UMN score	-	11.22 ± 4.39 (0.00 – 16.00)	10.45 ± 3.78 (2.00 – 16.00)	12.67 ± 5.47 (2.00 – 16.00)	-
MRC global score	-	102.94 ± 15.39 (60.00 – 148.00)	101.20 ± 17.62 (71.00 – 127.00)	108.17 ± 8.33 (98.00 - 118)	-
Disease progression rate	-	0.64 ± 0.56 (0.04 – 2.67)	0.77 ± 0.67 (0.13 – 2.86)	0.57 ± 0.22 (0.33 – 1.00)	-
ADL	-	-	-	-	5.62 ± 0.85 (2.00 – 6.00)
IADL	-	-	-	-	4.77 ± 2.29 (1.00 – 8.00)
CDR	-	-	-	-	0.96 ± 0.57 (0.50 – 2.00)
CDR SB	-	-	-	-	4.81 ± 2.53 (1.00 – 9.50)

Values are numbers or means ± standard deviations (range). Disease duration was defined as months from onset to date of MRI scan. The rate of disease progression in ALS patients was defined as follows: (48–ALSFRS-r score)/time from symptom onset. P values refer to ANOVA models, followed by post-hoc pairwise comparisons (Bonferroni-corrected for multiple comparisons), or Chi-squared test. *: $p < 0.05$ *vs* HC; #: $p < 0.05$ *vs* bvFTD; ^: $p < 0.05$ *vs* ALS-cn. Abbreviations: ADL= Activities of Daily Living; ALS-ci/bi= ALS with cognitive and/or

behavioral impairment; ALS-FTD= ALS with Frontotemporal Dementia; ALS-cn= Amyotrophic lateral sclerosis with only motor impairment; ALSFRS-r= Amyotrophic lateral sclerosis functional rating scale revised; bvFTD= behavioral variant of Frontotemporal Dementia; CDR= Clinical dementia rating; CDR sb= Clinical dementia rating sum of boxes; HC= healthy controls; IADL= Instrumental Activities of Daily Living; MRC= Medical Research Council; N= Number; UMN= Upper motor neuron.

Table 2. Classification (ROC curves) analysis for identification of the "ALS-cn-like pattern" and the "bvFTD-like pattern".
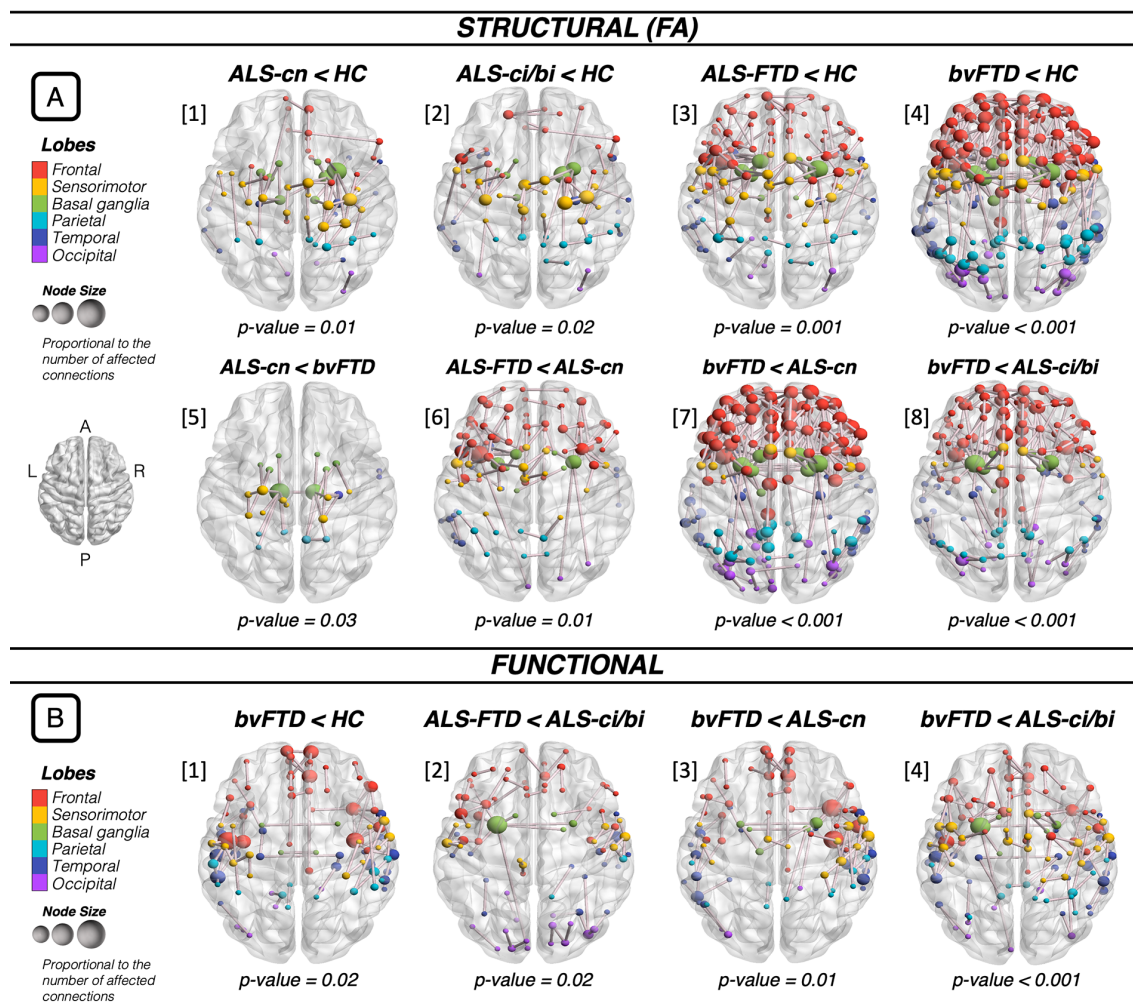
Structural Connectivity			
Intra-area and Inter-areas connections	**AUC bvFTD *vs* ALS-cn**	**AUC ALS-cn *vs* bvFTD**	**Best Cut-off (Youden's index)**
Frontal	**0.88**	0.12	-0.21 (0.68)
Frontal-Basal Ganglia	**0.82**	0.18	-0.67 (0.52)
Frontal-Parietal	**0.71**	0.29	-0.30 (0.37)
Frontal-Temporal	**0.76**	0.24	-0.20 (0.44)
Sensorimotor-Basal Ganglia	0.33	**0.67**	-0.55 (0.30)
Basal Ganglia-Temporal	**0.78**	0.22	-0.52 (0.45)
Basal Ganglia-Occipital	**0.72**	0.28	-0.47 (0.42)
Parietal	**0.67**	0.33	0.003 (0.31)
Parietal-Temporal	**0.72**	0.28	-0.36 (0.43)
Parietal-Occipital	**0.69**	0.31	-0.08 (0.35)
Temporal	**0.75**	0.25	-0.2 (0.41)
Temporal-Occipital	**0.70**	0.30	-0.40 (0.35)
Functional Connectivity			
Frontal-Temporal	**0.77**	0.23	-0.27 (0.48)
Sensorimotor-Parietal	**0.67**	0.33	-0.04 (0.34)

The Area Under the ROC curve represents the capability of the structural and functional connectivity damage within the reported intra- and inter-areas to discriminate bvFTD from ALS-cn and viceversa. Only intra-area and inter-areas connections significantly different between the two groups were considered. Bold values in the column "bvFTD vs ALS-cn" identify the "bvFTD-like pattern". Bold values in the column "ALS-cn vs bvFTD" identify the "ALS-cn-like pattern". The optimal cut-off per each connectivity distribution was calculated through the Youden's index, maximizing sensibility and specificity. Cut-off= sensibility-(1-specificity). Abbreviations: ALS-cn= Amyotrophic lateral sclerosis with only motor impairment; AUC= Area Under the ROC curve; bvFTD= behavioral variant of Frontotemporal Dementia.
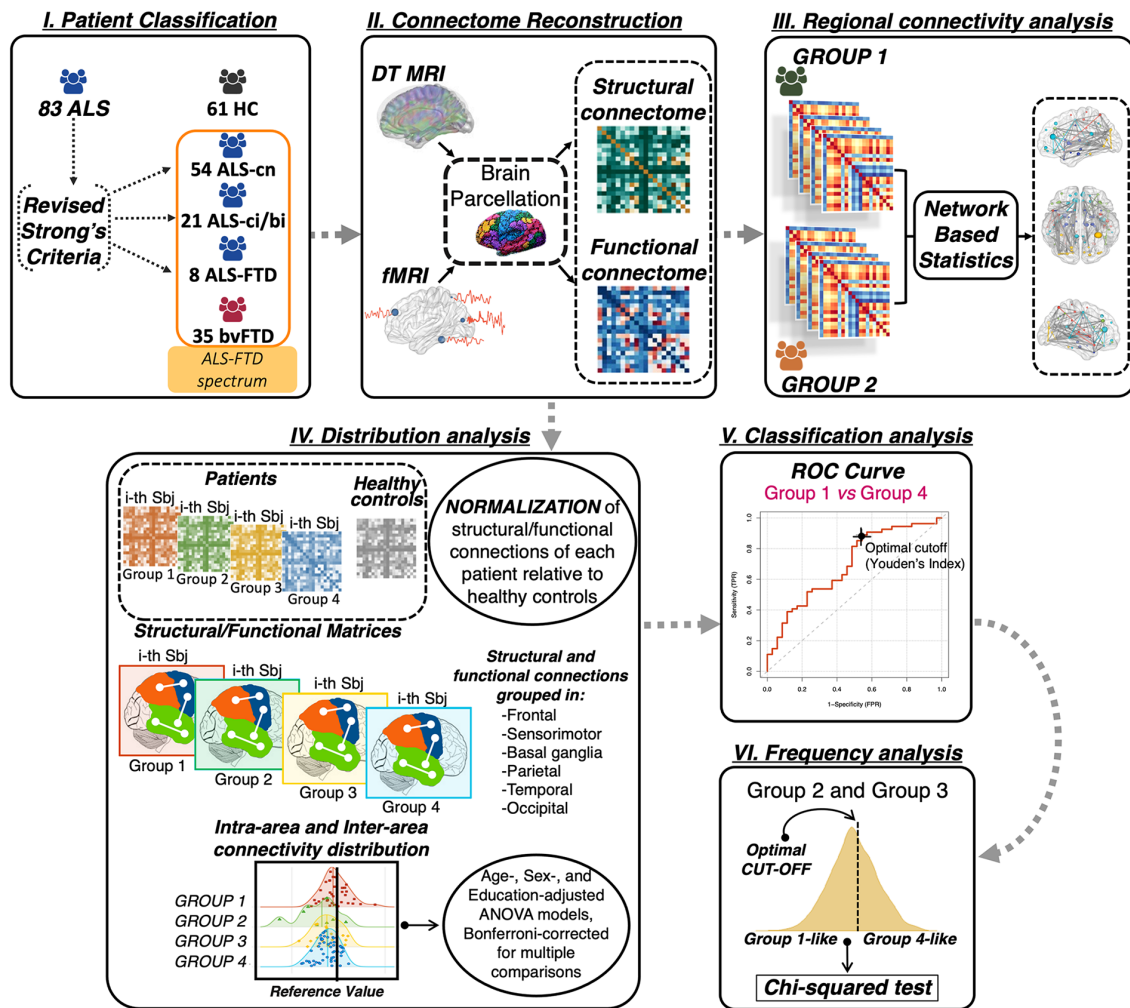
Figure 1. Study Framework. (I) Patient classification. Revised Strong's Criteria were applied to identify ALS patients with and without cognitive/behavioral impairments or dementia deficits. **(II) Connectome Reconstruction.** Connectomics was apply on DT MRI and RS fMRI, after parcellating the brain into 220 regions. Structural and functional connectomes of all subjects were reconstructed. **(III) Regional connectivity analysis.** The Network based Statistics was performed performing all possible comparisons between groups. **(IV) Distribution analysis**. After reconstructing the structural and functional connectome of each patient and control of the study, all connections per each patient were normalized relative to controls and grouped into 6 macro-areas. Intra-area and inter-area connectivity distribution were plotted and statistically compared between groups. **(V) Classification analysis.** ROC curve analysis was performed to discriminate ALS-cn from bvFTD and vice versa, considering intra and inter-area connectivity that resulted significantly different between these two groups in the distribution analysis. **(VI) Frequency analysis.** After ROC curve analysis, the optimal cut-off was identified using the Youden's index. ALS-ci/bi and ALS-FTD cases were then subdivided in those under and above the optimal cutoff. Chi-squared test was performed in order to identify the behavior of these two groups. Abbreviations: ALS= Amyotrophic lateral sclerosis; ALS-ci/bi= ALS with cognitive and/or behavioral impairment; ALS-cn= ALS with motor impairment only; ALS-FTD= ALS with Frontotemporal Dementia; bvFTD= behavioral variant of Frontotemporal Dementia; DT MRI= diffusion tensor MRI; fMRI= functional MRI; HC= healthy controls; Sbj= subject.

Figure 2. Alterations in structural and functional connectivity in ALS and bvFTD patients relative to healthy controls and each other. Altered structural (A) and functional (B) connections are represented per each significant contrast, respectively (p<0.05). The comparisons were adjusted for age, sex and education. The node color represents its belonging to specific macro-areas (frontal, sensorimotor, basal ganglia, parietal, temporal and occipital). The node size is proportional to the number of affected connections (the higher the number of disrupted connections, the bigger the node). Abbreviations: A= anterior; ALS= Amyotrophic lateral sclerosis; ALS-ci/bi= ALS with cognitive and/or behavioral impairment; ALS-cn= ALS with motor impairment only; ALS-FTD= ALS with Frontotemporal Dementia; bvFTD= behavioral variant of Frontotemporal Dementia; FA= fractional anisotropy; HC= healthy controls; L= left; P= posterior; R= right.
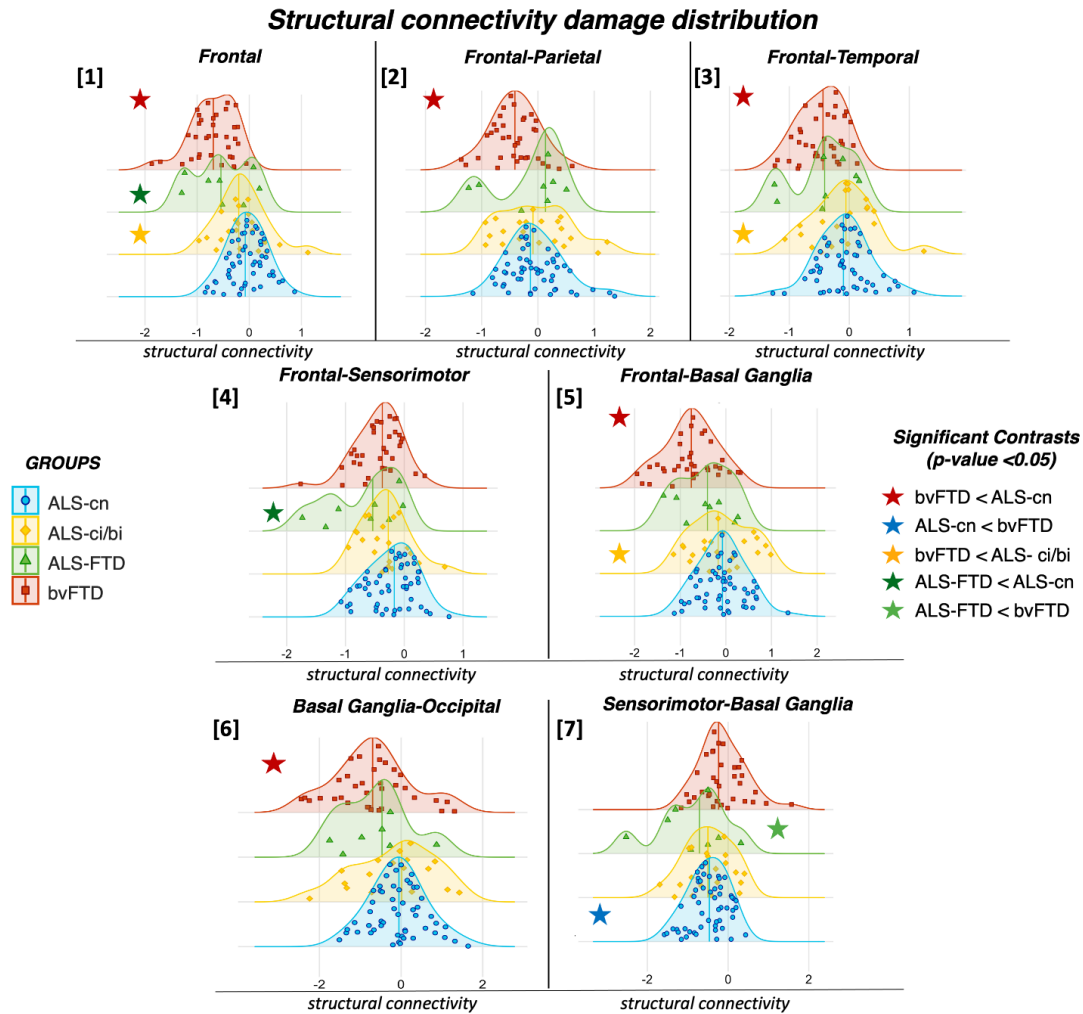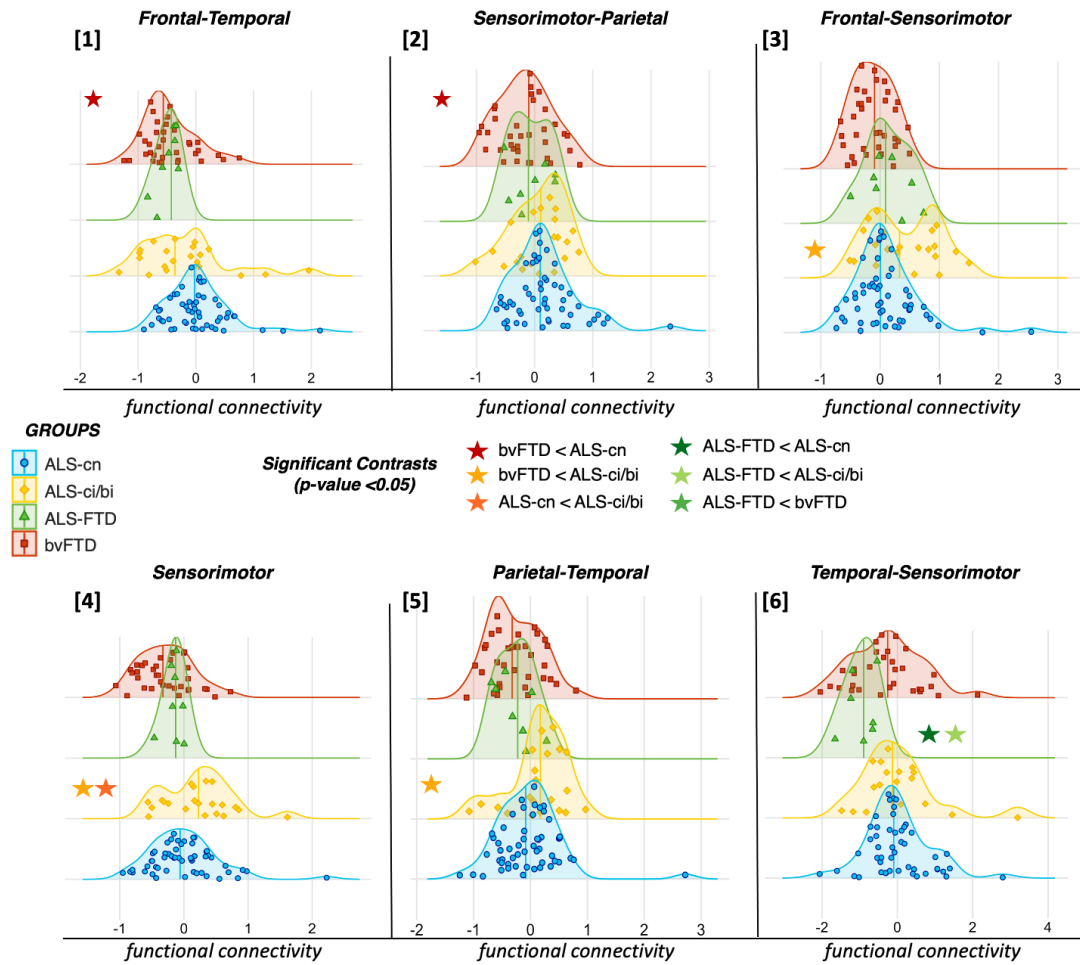
Figure 3. Distribution analysis of the structural connectivity damage in patient groups. The distribution of the structural connectivity alterations within frontal and motor areas and in the connections towards these areas is displayed. Distribution curves are normalized relative to control values. The more the curve is shifted towards negative values, the greater is the structural damage. All significant contrasts (p<0.05) – displayed with colored stars – are reported according to age-, sex- and education-adjusted ANOVA models, Bonferroni-corrected for multiple comparisons. Abbreviations: ALS= Amyotrophic lateral sclerosis; ALS-ci/bi= ALS with cognitive and/or behavioral impairment; ALS-cn= ALS with motor impairment only; ALS-FTD= ALS with Frontotemporal Dementia; bvFTD= behavioral variant of Frontotemporal Dementia.
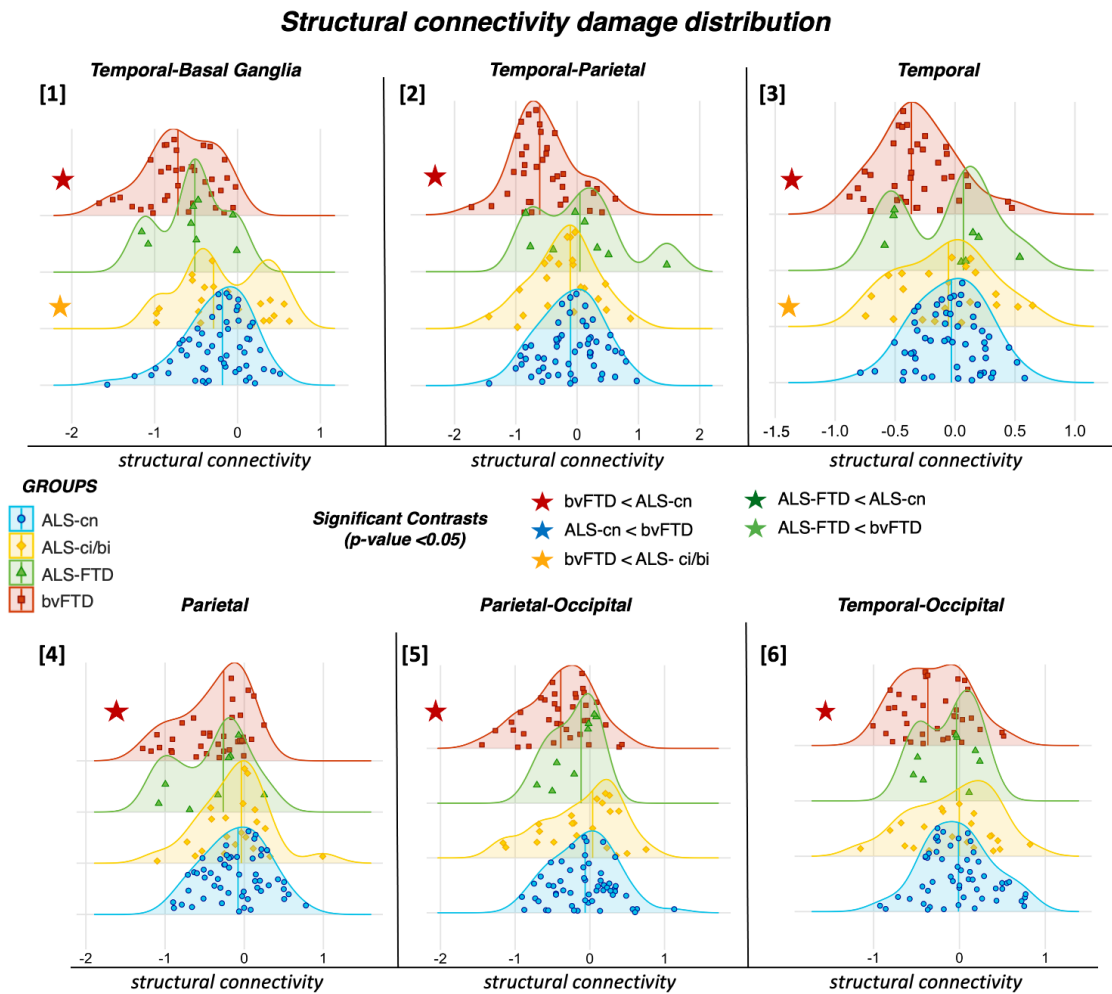
Figure 4. Distribution analysis of the structural connectivity damage in patient groups. The distribution of the structural connectivity alterations within parietal and temporal areas and in the connections towards these areas is displayed. Distribution curves are normalized relative to control values. The more the curve is shifted towards negative values, the greater is the structural damage. All significant contrasts (p<0.05) – displayed with colored stars – are reported according to age-, sex- and education-adjusted ANOVA models, Bonferroni-corrected for multiple comparisons. Abbreviations: ALS= Amyotrophic lateral sclerosis; ALS-ci/bi= ALS with cognitive and/or behavioral impairment; ALS-cn= ALS with motor impairment only; ALS-FTD= ALS with Frontotemporal Dementia; bvFTD= behavioral variant of Frontotemporal Dementia.

Figure 5. Distribution analysis of the functional connectivity damage in patient groups. Functional connectivity damage distribution within area and among areas is reported. Distribution curves are normalized relative to control values. The more the curve is shifted towards negative values, the more reduced is the functional connectivity. All significant contrasts (p<0.05) – displayed with colored stars – are reported according to age-, sex- and education-adjusted ANOVA models, Bonferroni-corrected for multiple comparisons. Abbreviations: ALS= Amyotrophic lateral sclerosis; ALS-ci/bi= ALS with cognitive and/or behavioral impairment; ALS-cn= ALS with motor impairment only; ALS-FTD= ALS with Frontotemporal Dementia; bvFTD= behavioral variant of Frontotemporal Dementia.

128

APPENDIX

eTable 1. Neuropsychological features of the healthy controls, ALS subgroups and bvFTD patients.

	HC	ALS-cn	ALS-ci/bi	ALS-FTD	bvFTD
Global cognition					
MMSE*[(Folstein et al., 1975)]	29.34 ± 0.97 (26.00 – 30.00)	28.41 ± 1.65 (21.00 – 30.00)	27.43 ± 2.52 (20.00 – 30.00)	24.75 ± 3.15$ (21.00 – 29.00)	22.81 ± 5.99$#^ (8.00 – 29.00)
Memory					
Digit span forward[(Orsini et al., 1987)]	5.97 ± 0.99 (4.00 – 9.00)	4.75 ± 0.93 (4.00 – 9.00)	27.43 ± 2.52 (3.00 – 6.00)	4.67 ± 0.82 (4.00 – 6.00)	4.55 ± 1.03$# (3.00 – 6.00)
RAVLT delayed[(Carlesimo et al., 1996)]	9.19 ± 3.32 (3.00 – 15.00)	9.02 ± 3.30 (1.00 – 15.00)	7.13 ± 2.42 (3.00 – 12.00)	5.14 ± 5.79$# (0.00 – 14.00)	3.53 ± 3.24$#^ (0.00 – 10.00)
Rey Figure recall[(Caffarra et al, 2002)]	18.37 ± 5.90 (9.50 – 33.00)	-	-	-	8.17 ± 5.73$ (0.00 – 26.00)
Executive function					
CPM[(Basso et al., 1987)]	30.91 ± 3.41 (22.00 – 36.00)	29.54 ± 4.36 (20.00 – 36.00)	26.75 ± 5.26 (16.00 – 35.00)	22.14 ± 6.62$ (14.00 – 33.00)	20.36 ± 8.08$#^ (0.00 – 32.00)
Digit span backward[(Monaco et al., 2013)]	4.57 ± 1.07 (2.00 – 7.00)	4.06 ± 0.91 (2.00 – 6.00)	3.44 ± 1.03 (2.00 – 5.00)	2.43 ± 1.81$ (0.00 – 6.00)	3.63 ± 0.96 (2.00 – 5.00)
CET[(Della Sala et al., 2003)]	-	13.66 ± 3.84 (6.00 – 24.00)	14.86 ± 4.50 (10.00 – 23.00)	19.50 ± 3.87 (14.00 – 23.00)	-
Weigl's[(Tognoni, 1987)]	-	12.45 ± 1.98 (8.00 – 15.00)	9.43 ± 4.15 (1.00 – 15.00)	7.50 ± 4.14# (4.00 – 15.00)	-
CST, perseverations**[(Caffarra et al., 2004; Laiacona et al., 2000)]	0.11 ± 0.16 (0.00 – 0.83)	0.14 ± 0.14 (0.00 –0.73)	0.16 ± 0.13 (0.04 –0.40)	0.20 ± 0.18 (0.01 – 0.46)	-
Visuospatial Abilities					
Rey Figure copy [(Caffarra et al., 2002)]	33.13 ± 2.46 (27.00 – 36.00)	-	-		19.35 ± 9.77$ (1.50 – 36.00)
Language					
BADA (noun)[(Miceli et al., 1994)]	29.79 ± 0.54 (28.00 – 30.00)	29.22 ± 0.99 (27.00 – 30.00)	28.00 ± 1.97 (24.00 – 30.00)	25.71 ± 5.94$# (13.00 – 30.00)	-
BADA (action)[(Miceli et al., 1994)]	27.68 ± 0.58 (26.00 – 28.00)	27.22 ± 1.07 (24.00 – 28.00)	24.88 ± 2.60$ (20.00 – 28.00)	23.14 ± 4.48$# (17.00 – 28.00)	-
Token Test[(De Renzi & Vignolo, 1962)]	33.20 ± 2.10 (29.00 – 36.00)	-	-		27.47 ± 5.25$ (13.00 – 36.00)
Fluency					
Phonemic fluency [(Novelli, 1986)]	38.50 ± 9.55 (18.00 – 55.00)	31.67 ± 9.71 (16.00 – 59.00)	26.55 ± 11.89 (5.00 – 55.00)	11.80 ± 5.54$# (4.00 – 28.00)	14.38 ± 11.22$#^ (0.00 – 37.00)
Index PF***[(Abrahams et al., 2000)]	4.68 ± 2.17 (2.60 – 12.05)	5.75 ± 2.54 (2.76 – 12.42)	9.34 ± 8.52 (2.64 – 35.00)	19.83 ± 12.56$#^ (7.17 – 37.20)	-

Semantic fluency[(Novelli, 1986)]	43.74 ± 8.83 (27.00 − 60.00)	40.38 ± 9.04 (26.00 − 66.00)	34.20 ± 9.45 (20.00 − 55.00)	21.60 ± 4.88$# (16.00 − 27.00)	22.59 ± 11.44$#^ (0.00 − 48.00)
Index SF*** [(Abrahams et al., 2000)]	3.89 ± 0.96 (2.49 − 6.50)	4.14 ± 1.43 (2.20 − 8.04)	6.73 ± 4.93 (2.63− 22.22)	13.57 ± 6.85$#^ (6.91 − 23.00)	-
Mood & Behavior					
BDI[(Beck et al., 1961)]	5.00 ± 4.42 (0.00 − 15.00)	-	-	-	-
HDRS[(Hamilton, 1960)]	-	6.34 ± 4.69 (0.00 − 22.00)	4.77 ± 3.44 (0.00 − 11.00)	6.60 ± 2.70 (3.00 − 10.00)	-
FBI total[(Alberici et al., 2007)]	-	2.11 ± 1.83 (0.00 − 7.00)	6.75 ± 7.21 (0.00 − 23.00)	9.75 ± 6.02 (4.00 − 18.00)	-
ALS-FTD-Q[(Raaphorst et al., 2012)]	-	8.35 ± 5.71 (2.00 − 20.00)	20.23 ± 14.29 (2.00 − 50.00)	5.00 ± 6.06 (1.00 − 14.00)	-
NPI[(Cummings et al, 1994)]	-	-	-	-	27.00 ± 15.83 (11.00 − 60.00)

Values are numbers or means ± standard deviations (range). Differences between patient groups and healthy controls were assessed using one-way ANOVA (statistical contrasts) corrected for age, sex and education. The number of patients performing each test is reported in table. $: p<0.05 vs. HC; #: p < 0.05 vs. ALS-cn; ^: p < 0.05 vs. ALS-ci/bi. *= Ratio between the number of correct items and the maximum number of administered items; **= Perseverations are reported as the ratio between perseveration absolute number and the maximum number of cards provided during the test; ***= Verbal fluency indices were obtained as following: time for generation condition - time for control condition (reading or writing generated words)/total number of items generated. Abbreviations: ALS= Amyotrophic lateral sclerosis; ALS-ci/bi= ALS with cognitive/behavioral impairment; ALS-FTD= ALS with frontotemporal dementia; ALS-cn= ALS only with motor impairment; ALS-FTD-Q= ALS-FTD-questionnaire; BADA= Battery for aphasic deficit analysis; BDI= Beck Depression Inventory; bvFTD= behavioral variant of frontotemporal dementia; CET= Cognitive estimation test; CPM= Colored progressive matrices; CST= Card sorting tests; FBI= Frontal Behavioral Inventory; HDRS= Hamilton Depression Rating Scale; HC= Healthy controls; MMSE= Mini-Mental state examination; NPI= Neuropsychiatric inventory; PF= Phonemic fluency; RAVLT= Rey auditory verbal learning test; SF= Semantic fluency.

E-REFERENCES

Abrahams S, Leigh PN, Harvey A, Vythelingum GN, Grise D, Goldstein LH (2000) Verbal fluency and executive dysfunction in amyotrophic lateral sclerosis (ALS). *Neuropsychologia* 38: 734-747

Alberici A, Geroldi C, Cotelli M, Adorni A, Calabria M, Rossi G, Borroni B, Padovani A, Zanetti O, Kertesz A (2007) The Frontal Behavioural Inventory (Italian version) differentiates frontotemporal lobar degeneration variants from Alzheimer's disease. *Neurol Sci* 28: 80-86

Basso A, Capitani E, Laiacona M (1987) Raven's coloured progressive matrices: normative values on 305 adult normal controls. *Functional neurology* 2: 189-194

Beck AT, Ward CH, Mendelson M, Mock J, Erbaugh J (1961) An inventory for measuring depression. *Arch Gen Psychiatry* 4: 561-571

Caffarra P, Vezzadini G, Dieci F, Zonato F, Venneri A (2002) Rey-Osterrieth complex figure: normative values in an Italian population sample. *Neurol Sci* 22: 443-447

Caffarra P, Vezzadini G, Dieci F, Zonato F, Venneri A (2004) Modified Card Sorting Test: normative data. *Journal of clinical and experimental neuropsychology* 26: 246-250

Carlesimo GA, Caltagirone C, Gainotti G (1996) The Mental Deterioration Battery: normative data, diagnostic reliability and qualitative analyses of cognitive impairment. The Group for the Standardization of the Mental Deterioration Battery. *Eur Neurol* 36: 378-384

Cummings JL, Mega M, Gray K, Rosenberg-Thompson S, Carusi DA, Gornbein J (1994) The Neuropsychiatric Inventory: comprehensive assessment of psychopathology in dementia. *Neurology* 44: 2308-2314

De Renzi E, Vignolo LA (1962) The token test: A sensitive test to detect receptive disturbances in aphasics. *Brain* 85: 665-678

Della Sala S, MacPherson SE, Phillips LH, Sacco L, Spinnler H (2003) How many camels are there in Italy? Cognitive estimates standardised on the Italian population. *Neurol Sci* 24: 10-15

Folstein MF, Folstein SE, McHugh PR (1975) "Mini-mental state". A practical method for grading the cognitive state of patients for the clinician. *J Psychiatr Res* 12: 189-198

Hamilton M (1960) A rating scale for depression. *J Neurol Neurosurg Psychiatry* 23: 56-62

Laiacona M, Inzaghi MG, De Tanti A, Capitani E (2000) Wisconsin card sorting test: a new global score, with Italian norms, and its relationship with the Weigl sorting test. *Neurol Sci* 21: 279-291

Miceli G, neuropsicologia UcdSCSd, psicologia CndrId (1994) *Batteria per l'analisi dei deficit afasici B.A.D.A.* Servizio di neuropsicologia, Università cattolica del S. Cuore

Monaco M, Costa A, Caltagirone C, Carlesimo GA (2013) Forward and backward span for verbal and visuo-spatial data: standardization and normative data from an Italian adult population. *Neurol Sci* 34: 749-754

Novelli G, Laiacona M, Papagno C, Vallar G, Capitani E, Cappa SF (1986) Three clinical tests to research and rate the lexical performance of normal subjects. *Arch Psicol Neurol Psichiatr* 47: 477-506

Orsini A, Grossi D, Capitani E, Laiacona M, Papagno C, Vallar G (1987) Verbal and spatial immediate memory span: normative data from 1355 adults and 1112 children. *Ital J Neurol Sci* 8: 539-548

Raaphorst J, Beeldman E, Schmand B, Berkhout J, Linssen WH, van den Berg LH, Pijnenburg YA, Grupstra HF, Weikamp JG, Schelhaas HJ *et al* (2012) The ALS-FTD-Q: a new screening tool for behavioral disturbances in ALS. *Neurology* 79: 1377-1383

Tognoni HSaG (1987) *Standardizzazione e Taratura Italiana di Test Neuropsicologici*

eTable 2. MRI acquisition parameters.

	Philips Medical System Intera 3T scan				
	*T2-*weighted SE	FLAIR	3D T1-weighted FFE	Pulsed-gradient SE echo planar with sensitivity encoding	T2*-weighted single-shot EPI sequence (Resting state fMRI)
Repetition time (msec)	3500	11000	25	8986	3000
Echo time (msec)	85	120	4.6	80	35
Flip angle	90°	90°	30°	-	90°
Section thickness (mm)	5	5	-	2.5	4
No. of sections	22	22	220	55	30 for 220 volumes
Matrix	512x512	512x512	256x256	96x96	128x128
Field of view (mm²)	230x184	230x230	230x182	240x240	240x240
Diffusion gradient directions	-	-	-	32	-
***b* value sec/mm²**	-	-	-	1000	-

Abbreviations: FFE= fast field echo; FLAIR= fluid-attenuated inversion recovery; FSE= fast spin echo; MRI= magnetic resonance imaging; msec= millisecond; mm= millimeter; No= number; SE=spin echo; sec=second

eTable 3. Brain nodes of the network.

N	Node	Lobe	N	Node	Lobe	N	Node	Lobe
1	Precentral_L_p1	SENSMOT	75	Insula_L_p2	FRONT-INS	149	Parietal_Inf_L_p1	PAR
2	Precentral_L_p2	SENSMOT	76	Insula_L_p3	FRONT-INS	150	Parietal_Inf_L_p2	PAR
3	Precentral_L_p3	SENSMOT	77	Insula_R_p1	FRONT-INS	151	Parietal_Inf_L_p3	PAR
4	Precentral_L_p4	SENSMOT	78	Insula_R_p2	FRONT-INS	152	Parietal_Inf_R_p1	PAR
5	Precentral_L_p5	SENSMOT	79	Cingulum_Ant_L_p1	FRONT-INS	153	Parietal_Inf_R_p2	PAR
6	Precentral_R_p1	SENSMOT	80	Cingulum_Ant_L_p2	FRONT-INS	154	SupraMarginal_L_p1	PAR
7	Precentral_R_p2	SENSMOT	81	Cingulum_Ant_R_p1	FRONT-INS	155	SupraMarginal_L_p2	PAR
8	Precentral_R_p3	SENSMOT	82	Cingulum_Ant_R_p2	FRONT-INS	156	SupraMarginal_R_p1	PAR
9	Precentral_R_p4	SENSMOT	83	Cingulum_Mid_L_p1	FRONT-INS	157	SupraMarginal_R_p2	PAR
10	Precentral_R_p5	SENSMOT	84	Cingulum_Mid_L_p2	FRONT-INS	158	SupraMarginal_R_p3	PAR
11	Frontal_Sup_L_p1	FRONT-INS	85	Cingulum_Mid_L_p3	FRONT-INS	159	Angular_L_p1	PAR
12	Frontal_Sup_L_p2	FRONT-INS	86	Cingulum_Mid_R_p1	FRONT-INS	160	Angular_L_p2	PAR
13	Frontal_Sup_L_p3	FRONT-INS	87	Cingulum_Mid_R_p2	FRONT-INS	161	Angular_R_p1	PAR
14	Frontal_Sup_L_p4	FRONT-INS	88	Cingulum_Mid_R_p3	FRONT-INS	162	Angular_R_p2	PAR
15	Frontal_Sup_L_p5	FRONT-INS	89	Cingulum_Post_L_p1	PAR	163	Precuneus_L_p1	PAR
16	Frontal_Sup_R_p1	FRONT-INS	90	Cingulum_Post_R_p1	PAR	164	Precuneus_L_p2	PAR
17	Frontal_Sup_R_p2	FRONT-INS	91	Hippocampus_L_p1	TEMP	165	Precuneus_L_p3	PAR
18	Frontal_Sup_R_p3	FRONT-INS	92	Hippocampus_R_p1	TEMP	166	Precuneus_L_p4	PAR
19	Frontal_Sup_R_p4	FRONT-INS	93	ParaHippocampal_L_p1	TEMP	167	Precuneus_L_p5	PAR
20	Frontal_Sup_R_p5	FRONT-INS	94	ParaHippocampal_R_p1	TEMP	168	Precuneus_R_p1	PAR
21	Frontal_Sup_Orb_L_p1	FRONT-INS	95	ParaHippocampal_R_p2	TEMP	169	Precuneus_R_p2	PAR
22	Frontal_Sup_Orb_R_p1	FRONT-INS	96	Amygdala_L_p1	TEMP	170	Precuneus_R_p3	PAR
23	Frontal_Mid_L_p1	FRONT-INS	97	Amygdala_R_p1	TEMP	171	Precuneus_R_p4	PAR
24	Frontal_Mid_L_p2	FRONT-INS	98	Calcarine_L_p1	OCC	172	Paracentral_Lobule_L_p1	SENSMOT
25	Frontal_Mid_L_p3	FRONT-INS	99	Calcarine_L_p2	OCC	173	Paracentral_Lobule_L_p2	SENSMOT
26	Frontal_Mid_L_p4	FRONT-INS	100	Calcarine_L_p3	OCC	174	Paracentral_Lobule_R_p1	SENSMOT
27	Frontal_Mid_L_p5	FRONT-INS	101	Calcarine_R_p1	OCC	175	Caudate_L_p1	BG
28	Frontal_Mid_L_p6	FRONT-INS	102	Calcarine_R_p2	OCC	176	Caudate_R_p1	BG
29	Frontal_Mid_L_p7	FRONT-INS	103	Calcarine_R_p3	OCC	177	Putamen_L_p1	BG
30	Frontal_Mid_R_p1	FRONT-INS	104	Cuneus_L_p1	OCC	178	Putamen_R_p1	BG
31	Frontal_Mid_R_p2	FRONT-INS	105	Cuneus_L_p2	OCC	179	Pallidum_L_p1	BG
32	Frontal_Mid_R_p3	FRONT-INS	106	Cuneus_R_p1	OCC	180	Pallidum_R_p1	BG
33	Frontal_Mid_R_p4	FRONT-INS	107	Cuneus_R_p2	OCC	181	Thalamus_L_p1	BG
34	Frontal_Mid_R_p5	FRONT-INS	108	Lingual_L_p1	OCC	182	Thalamus_R_p1	BG
35	Frontal_Mid_R_p6	FRONT-INS	109	Lingual_L_p2	OCC	183	Heschl_L_p1	TEMP
36	Frontal_Mid_R_p7	FRONT-INS	110	Lingual_L_p3	OCC	184	Heschl_R_p1	TEMP
37	Frontal_Mid_Orb_L_p1	FRONT-INS	111	Lingual_R_p1	OCC	185	Temporal_Sup_L_p1	TEMP
38	Frontal_Mid_Orb_R_p1	FRONT-INS	112	Lingual_R_p2	OCC	186	Temporal_Sup_L_p2	TEMP
39	Frontal_Inf_Oper_L_p1	FRONT-INS	113	Lingual_R_p3	OCC	187	Temporal_Sup_L_p3	TEMP
40	Frontal_Inf_Oper_R_p1	FRONT-INS	114	Occipital_Sup_L_p1	OCC	188	Temporal_Sup_R_p1	TEMP
41	Frontal_Inf_Oper_R_p2	FRONT-INS	115	Occipital_Sup_L_p2	OCC	189	Temporal_Sup_R_p2	TEMP
42	Frontal_Inf_Tri_L_p1	FRONT-INS	116	Occipital_Sup_R_p1	OCC	190	Temporal_Sup_R_p3	TEMP
43	Frontal_Inf_Tri_L_p2	FRONT-INS	117	Occipital_Sup_R_p2	OCC	191	Temporal_Sup_R_p4	TEMP
44	Frontal_Inf_Tri_L_p3	FRONT-INS	118	Occipital_Mid_L_p1	OCC	192	Temporal_Pole_Sup_L_p1	TEMP
45	Frontal_Inf_Tri_R_p1	FRONT-INS	119	Occipital_Mid_L_p2	OCC	193	Temporal_Pole_Sup_L_p2	TEMP
46	Frontal_Inf_Tri_R_p2	FRONT-INS	120	Occipital_Mid_L_p3	OCC	194	Temporal_Pole_Sup_R_p1	TEMP
47	Frontal_Inf_Tri_R_p3	FRONT-INS	121	Occipital_Mid_L_p4	OCC	195	Temporal_Pole_Sup_R_p2	TEMP
48	Frontal_Inf_Orb_L_p1	FRONT-INS	122	Occipital_Mid_R_p1	OCC	196	Temporal_Mid_L_p1	TEMP
49	Frontal_Inf_Orb_L_p2	FRONT-INS	123	Occipital_Mid_R_p2	OCC	197	Temporal_Mid_L_p2	TEMP
50	Frontal_Inf_Orb_R_p1	FRONT-INS	124	Occipital_Mid_R_p3	OCC	198	Temporal_Mid_L_p3	TEMP
51	Frontal_Inf_Orb_R_p2	FRONT-INS	125	Occipital_Inf_L_p1	OCC	199	Temporal_Mid_L_p4	TEMP
52	Rolandic_Oper_L_p1	FRONT-INS	126	Occipital_Inf_R_p1	OCC	200	Temporal_Mid_L_p5	TEMP
53	Rolandic_Oper_R_p1	FRONT-INS	127	Fusiform_L_p1	TEMP	201	Temporal_Mid_L_p6	TEMP
54	Rolandic_Oper_R_p2	FRONT-INS	128	Fusiform_L_p2	TEMP	202	Temporal_Mid_L_p7	TEMP
55	Supp_Motor_Area_L_p1	SENSMOT	129	Fusiform_L_p3	TEMP	203	Temporal_Mid_R_p1	TEMP
56	Supp_Motor_Area_L_p2	SENSMOT	130	Fusiform_R_p1	TEMP	204	Temporal_Mid_R_p2	TEMP
57	Supp_Motor_Area_L_p3	SENSMOT	131	Fusiform_R_p2	TEMP	205	Temporal_Mid_R_p3	TEMP
58	Supp_Motor_Area_R_p1	SENSMOT	132	Fusiform_R_p3	TEMP	206	Temporal_Mid_R_p4	TEMP
59	Supp_Motor_Area_R_p2	SENSMOT	133	Postcentral_L_p1	SENSMOT	207	Temporal_Mid_R_p5	TEMP

60	Supp_Motor_Area_R_p3	SENSMOT	134	Postcentral_L_p2	SENSMOT	208	Temporal_Mid_R_p6	TEMP
61	Olfactory_L_p1	FRONT-INS	135	Postcentral_L_p3	SENSMOT	209	Temporal_Pole_Mid_L_p1	TEMP
62	Olfactory_R_p1	FRONT-INS	136	Postcentral_L_p4	SENSMOT	210	Temporal_Pole_Mid_R_p1	TEMP
63	Frontal_Sup_Medial_L_p1	FRONT-INS	137	Postcentral_L_p5	SENSMOT	211	Temporal_Pole_Mid_R_p2	TEMP
64	Frontal_Sup_Medial_L_p2	FRONT-INS	138	Postcentral_R_p1	SENSMOT	212	Temporal_Inf_L_p1	TEMP
65	Frontal_Sup_Medial_L_p3	FRONT-INS	139	Postcentral_R_p2	SENSMOT	213	Temporal_Inf_L_p2	TEMP
66	Frontal_Sup_Medial_L_p4	FRONT-INS	140	Postcentral_R_p3	SENSMOT	214	Temporal_Inf_L_p3	TEMP
67	Frontal_Sup_Medial_R_p1	FRONT-INS	141	Postcentral_R_p4	SENSMOT	215	Temporal_Inf_L_p4	TEMP
68	Frontal_Sup_Medial_R_p2	FRONT-INS	142	Postcentral_R_p5	SENSMOT	216	Temporal_Inf_R_p1	TEMP
69	Frontal_Sup_Medial_R_p3	FRONT-INS	143	Parietal_Sup_L_p1	PAR	217	Temporal_Inf_R_p2	TEMP
70	Frontal_Mid_Orb_L_p2	FRONT-INS	144	Parietal_Sup_L_p2	PAR	218	Temporal_Inf_R_p3	TEMP
71	Frontal_Mid_Orb_R_p2	FRONT-INS	145	Parietal_Sup_L_p3	PAR	219	Temporal_Inf_R_p4	TEMP
72	Rectus_L_p1	FRONT-INS	146	Parietal_Sup_R_p1	PAR	220	Temporal_Inf_R_p5	TEMP
73	Rectus_R_p1	FRONT-INS	147	Parietal_Sup_R_p2	PAR			
74	Insula_L_p1	FRONT-INS	148	Parietal_Sup_R_p3	PAR			

Abbreviations: Ant= anterior; BG= basal ganglia; FRONT-INS= fronto-insular; Inf= inferior; L= left; Mid= middle; N= region number; Oper= operculum; OCC= occipital; Orb= orbital; p= part; PAR= parietal; Post= posterior; R= right; SENSMOT= sensorimotor; Sup= superior; Supp= supplementary; TEMP= temporal; Tri= triangularis

eTable 4. Structural and functional distribution measures of the normalized inter- and intra-area connectivity values in patient groups.

Structural Connectivity										
Intra-area and Inter-area connections	**ALS-cn**	**ALS-ci/bi**	**ALS-FTD**	**bvFTD**	**p value ALS-cn vs bvFTD**	**p value ALS-cn vs ALS-ci/bi**	**p value ALS-cn vs ALS-FTD**	**p value ALS-ci/bi vs bvFTD**	**p value ALS-ci/bi vs ALS-FTD**	**p value ALS-FTD vs bvFTD**
Frontal	-0.05 ± 0.37 (56%)	-0.13 ± 0.48 (67%)	-0.53 ± 0.56 (75%)	-0.70 ± 0.42 (100%)	**<0.001**	1.00	**0.03**	**<0.001**	0.09	1.00
Frontal-Sensorimotor	-0.22 ± 0.41 (65%)	-0.32 ± 0.39 (81%)	-0.70 ± 0.63 (100%)	-0.45 ± 0.40 (94%)	0.21	1.00	**0.02**	1.00	0.10	0.59
Frontal-Basal Ganglia	-0.09 ± 0.51 (61%)	-0.09 ± 0.64 (57%)	-0.48 ± 0.59 (75%)	-0.78 ± 0.57 (91%)	**<0.001**	1.00	0.44	**<0.001**	0.45	1.00
Frontal-Parietal	-0.06 ± 0.50 (63%)	-0.05 ±0.63 (52%)	-0.17 ± 0.64 (38%)	-0.41 ± 0.43 (86%)	**0.01**	1.00	1.00	0.07	1.00	1.00
Frontal-Temporal	-0.09 ± 0.45 (59%)	-0.11 ± 0.52 (67%)	-0.44 ± 0.54 (75%)	-0.48 ± 0.36 (92%)	**0.002**	1.00	0.27	**0.01**	0.22	1.00
Sensorimotor-Basal Ganglia	-0.50 ± 0.48 (81%)	-0.49 ± 0.57 (81%)	-0.90 ± 0.88 (88%)	-0.13 ± 0.57 (66%)	**0.01**	1.00	0.48	0.17	0.47	**0.01**
Basal Ganglia-Temporal	-0.25 ± 0.42 (67%)	-0.16 ± 0.51 (57%)	-0.55 ± 0.41 (100%)	-0.68 ± 0.42 (100%)	**<0.001**	1.00	0.46	**<0.001**	0.11	1.00
Basal Ganglia-Occipital	-0.07 ± 0.68 (54%)	-0.17 ± 1.00 (43%)	-0.61 ± 0.87 (75%)	-0.69 ± 0.94 (80%)	**0.01**	1.00	0.77	0.20	1.00	1.00
Parietal	-0.11 ± 0.40 (59%)	-0.12 ± 0.44 (57%)	-0.41 ± 0.47 (88%)	-0.38 ± 0.42 (89%)	**0.04**	1.00	0.36	0.11	0.38	1.00
Parietal-Temporal	-0.11 ± 0.51 (57%)	-0.22 ± 0.55 (71%)	0.05 ± 0.75 (50%)	-0.53 ± 0.52 (83%)	**0.01**	1.00	1.00	0.14	1.00	0.052
Parietal-Occipital	-0.08 ± 0.42 (59%)	-0.12 ± 0.53 (48%)	-0.22 ± 0.30 (75%)	-0.40 ± 0.45 (89%)	**0.01**	1.00	1.00	0.14	1.00	1.00
Temporal	-0.05 ± 0.29	-0.09 ± 0.39	-0.07 ± 0.41	-0.31 ± 0.32	**0.01**	1.00	1.00	**0.03**	1.00	0.51

	(54%)	(57%)	(38%)	(86%)						
Temporal-Occipital	-0.02 ± 0.40 (56%)	-0.08 ± 0.50 (52%)	-0.12 ± 0.31 (63%)	-0.30 ± 0.39 (77%)	**0.03**	1.00	1.00	0.28	1.00	1.00
Functional Connectivity										
Frontal-Sensorimotor	0.11 ± 0.56 (48%)	0.41 ± 0.59 (33%)	0.14 ± 0.40 (50%)	-0.12 ± 0.33 (63%)	0.21	0.09	1.00	**0.001**	1.00	0.70
Frontal-Temporal	0.03 ± 0.55 (52%)	-0.19 ± 0.78 (67%)	-0.49 ± 0.19 (100%)	-0.45 ± 0.45 (83%)	**0.001**	1.00	0.13	0.06	0.44	1.00
Sensorimotor	0.003± 0.54 (53%)	0.23 ± 0.54 (29%)	-0.15 ± 0.14 (88%)	-0.28 ± 0.41 (74%)	0.12	**0.04**	1.00	**<0.001**	0.15	1.00
Sensorimotor-Parietal	0.17 ± 0.55 (37%)	0.06 ± 0.47 (43%)	-0.07 ± 0.34 (50%)	-0.17 ± 0.45 (69%)	**0.02**	1.00	1.00	0.34	1.00	1.00
Sensorimotor-Temporal	0.005± 0.83 (54%)	0.03 ± 1.06 (48%)	-0.98 ±0.41 (88%)	-0.28 ± 0.94 (60%)	1.00	1.00	**0.03**	0.48	**0.01**	0.18
Parietal-Temporal	-0.04 ± 0.58 (52%)	0.13 ± 0.51 (24%)	-0.25 ± 0.33 (75%)	-0.28 ±0.45 (71%)	0.26	1.00	1.00	**0.03**	0.35	1.00

Values are numbers or means ± standard deviations (percentage of people with normalized connectivity value below 0). Inter- and intra-area connectivity values significantly different in at least one comparison are reported. P values refer to ANOVA models, followed by post-hoc pairwise comparisons (Bonferroni-corrected for multiple comparisons). Significant p value < 0.05. Abbreviations: ALS-ci/bi= Amyotrophic lateral sclerosis with cognitive and/or behavioral impairment; ALS-FTD= ALS with frontotemporal dementia; ALS-cn= Amyotrophic lateral sclerosis with only motor impairment; bvFTD= behavioral variant of Frontotemporal Dementia

eTable 5. Frequency analysis for the identification of ALS-cn-like or bvFTD-like patterns in ALS-ci/bi and ALS-FTD patients.

Intra-area and Inter-area connections	N ALS-cn below cutoff (%)	N ALS-ci/bi below cutoff (%)	N ALS-FTD below cutoff (%)	N bvFTD below cutoff (%)	p: ALS-ci/bi vs ALS-cn	p ALS-ci/bi vs bvFTD	p: ALS-FTD vs ALS-cn	p: ALS-FTD vs bvFTD	p: ALS-ci/bi vs ALS-FTD
Structural Connectivity									
Frontal	16 (30%)	10 (48%)	5 (63%)	-	0.12	-	0.08	-	0.38
Frontal-Basal Ganglia	6 (11%)	5 (24%)	3 (38%)	-	0.15	-	0.08	-	0.38
Frontal-Parietal	14 (26%)	8 (38%)	2 (25%)	-	0.22	-	0.66	-	0.42
Frontal-Temporal	18 (33%)	9 (43%)	5 (63%)	-	0.31	-	0.12	-	0.43
Sensorimotor-Basal Ganglia	-	9 (43%)	4 (50%)	6 (17%)	-	**0.04**	-	0.07	0.53
Basal Ganglia-Temporal	11 (20%)	5(24%)	4 (50%	-	0.48	-	0.09	-	0.18
Basal Ganglia-Occipital	15 (28%)	7 (33%)	3 (38%)	-	0.42	-	0.42	-	0.58
Parietal	31 (57%)	12 (57%)	7 (88%)		0.59	-	0.10	-	0.14
Parietal-Temporal	14 (26%)	8 (38%)	3 (38%)	-	0.22	-	0.38	-	0.66
Parietal-Occipital	23 (43%)	10 (48%)	4 (50%)	-	0.45	-	0.49	-	0.62
Temporal	15 (28%)	7 (33%)	3 (38%)	-	0.42	-	0.42	-	0.58
Temporal-Occipital	6 (11%)	6 (29%)	3 (38%)	-	0.07	-	0.08	-	0.48
Functional Connectivity									

138

Frontal-Temporal	14 (26%)	11 (52%)	8 (100%)	-	**0.03**	-	**<0.001**	-	**0.02**
Sensorimotor-Parietal	17 (31%)	8 (38%)	4 (50%)	-	0.39	-	0.26	-	0.43

Per each group, the number (**N**) and the respective percentage (%) of patients with structural/ functional connectivity values below the optimal cutoff are reported. Within 'bvFTD-like pattern', frequency analysis, using Chi-squared test was performed only between ALS groups, excluding the. Within 'ALS-cn-like pattern', frequency analysis was performed between bvFTD, ALS-ci/bi and ALS FTD, excluding ALS-cn group. Significant results are highlight in bold. Abbreviations: ALS-ci/bi= Amyotrophic lateral sclerosis with cognitive and/or behavioral impairment; ALS-FTD= ALS with frontotemporal dementia; ALS-cn= ALS with only motor impairment; AUC= Area Under the ROC curve; bvFTD= behavioral variant of Frontotemporal Dementia.
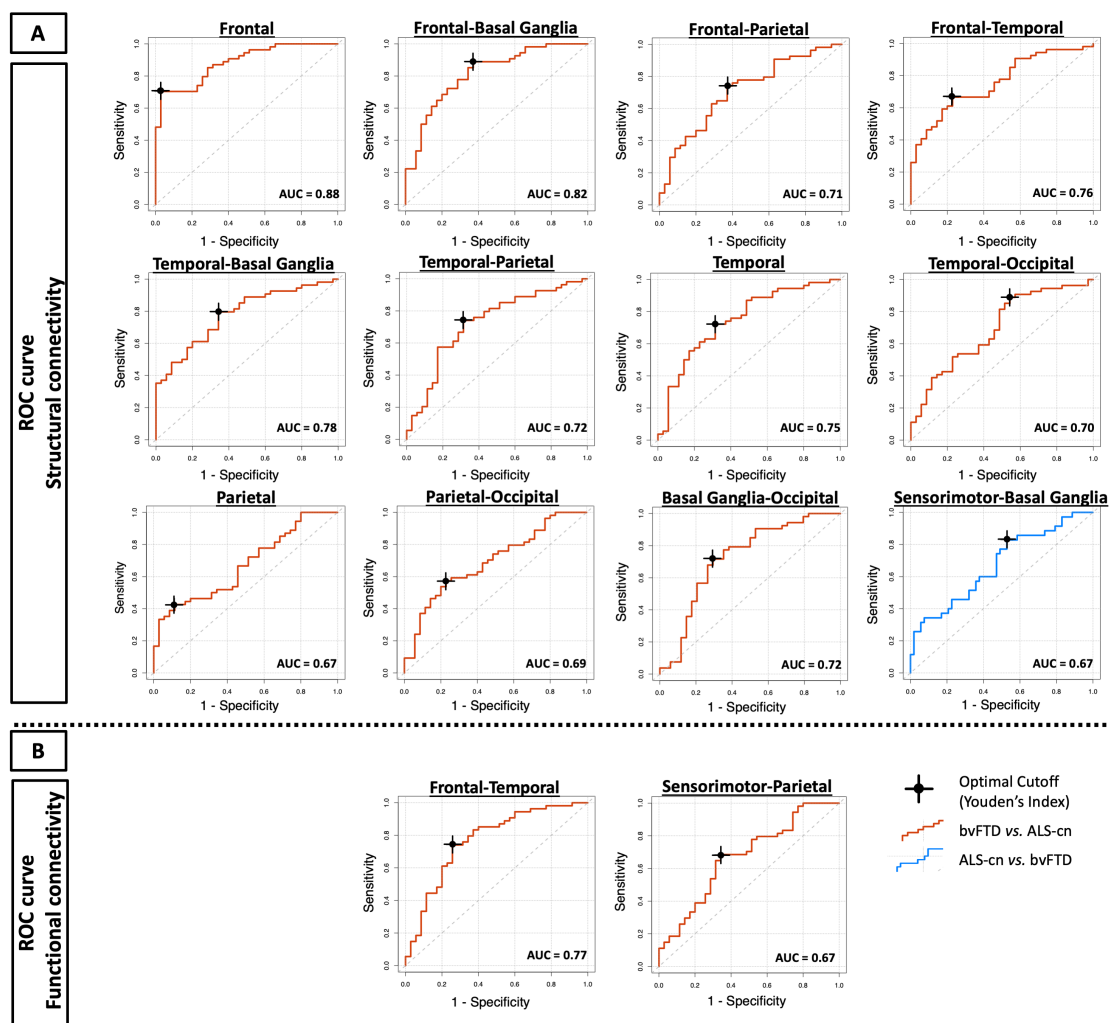
eFigure 1. Classification analysis. The ROC curves for the identification of the structural (A) and functional (B) characteristic patterns (ALS-cn-like and bvFTD-like) are shown. The curves in red represent the discriminative capability to distinguish bvFTD from ALS-cn (lower values of structural inter- and intra-area connectivity better identified bvFTD), while the curves in blue represent the opposite discriminative capability (lower values of structural inter- and intra-area connectivity better identified ALS-cn from bvFTD). Per each ROC curve, the area under the curve is reported as well as the optimal cutoff, obtained as Youden's index. Abbreviations: ALS-cn= ALS with motor impairment only; AUC= Area under the curve; bvFTD= behavioral variant of Frontotemporal Dementia.

5. EXPLORING THE FACES OF BRAIN AGING

5.1 AGE-RELATED VULNERABILITY OF THE HUMAN BRAIN CONNECTOME

Abstract

Introduction. Aging is the main risk factor for most neurodegenerative diseases and results in complex transformations of the network brain organization. The study aim was to investigate whether and how the brain functional connectome architecture relates with structural brain changes due to aging.

Methods. The study cohort included 128 healthy individuals (young [yC] age range: 20-30 years and old [oC] age range: 41-84 years), who underwent an MRI scan. Subsequently, we estimated

The brain functional matrix for each yC was reconstructed using resting-state functional MRI. Stepwise functional connectivity (SFC) analysis was applied to characterize regions that connect to specific seed brain areas at different levels of link-step distances. Eight well-known hubs of the human connectome were selected as seeds: middle frontal gyrus, rostral anterior and posterior cingulate cortex, precuneus, inferior parietal, middle temporal (DMN hubs) and lingual gyri and pericalcarine cortex (occipital hubs). Per each seed region, the functional brain network architecture was evaluated in yC to identify highly functionally connected regions with hubs. Then, structural changes in all the cortical regions across lifespan were measured on 3DT1-weighted images. For each region, cortical thickness trajectories with advancing age were modelled using Gaussian Process Regression, including sex and education as covariates, and regional changes over time were calculated. As such, positive values of change reflected regions with the highest change rate over time, while negative values present regions with less change. Finally, spatial similarity between functional pattern in yC and cortical atrophy in oC was estimated for each hub.

Results. Functional findings in yC revealed that seeds known to be part of the DMN showed distributed intra-network direct connections (within DMN regions). On the other hand, occipital hubs showed only local connectivity distribution within occipital lobe and to sensorimotor areas. Furthermore, at indirect steps, a spatial overlap was observed in SFC maps of different hubs reaching a common pattern. Structurally, greater cortical thinning was observed in the DMN hubs, while occipital hubs showed small atrophy changes across lifespan. Also, additional regions belonging to temporal lobe (parahippocampal, entorhinal, superior temporal and fusiform), frontal lobe (lateral orbitofrontal, superior and inferior frontal, including pars triangularis and opercularis), parietal lobe (the isthmus of cingulate and supramarginal) and the insular cortex showed cortical thinning with aging. Significant positive correlation was found between the functional pattern in yC of middle frontal hub and the cortical thinning in oC, while significant negative correlation emerged between the functional network organization of lingual and pericalcarine hubs and the cortical thinning in oC.

Conclusions. We observed that cortical regions functionally close to the DMN hubs, but far from the occipital hubs, became the more atrophic during aging. Our findings revealed potential pattern of vulnerability to the onset of neurodegeneration. This might hold the promise to understand the additive role of aging in modelling neurodegenerative progression trajectories in future longitudinal studies.

Supported by: European Research Council (StG-2016_714388_NeuroTRACK).

INTRODUCTION

Aging is a complex biological process characterized by an accumulation of molecular and cellular damages over the lifespan (Lopez-Otin *et al*, 2013). It can be depicted as a progressive functional decline, or a gradual deterioration of biological functions. Brain is a very efficient and integrative system with many different regions having their own function, but continuously sharing information with each other (van den Heuvel & Hulshoff Pol, 2010). Aging inevitably implies loss of viability among brain regions, and increase in susceptibility to death. Thus, the brain changes as we age, and these changes can be associated with cognitive decline and neuronal loss.

In recent years, magnetic resonance imaging (MRI) has become a powerful tool to explore alterations in the aging brain (Damoiseaux, 2017). Overall, the most consistent finding is that certain networks, above all the default mode network (DMN), showed to be particularly susceptible to aging, revealing a decreased functional connectivity in older adults relative to younger (Damoiseaux *et al*, 2007; Onoda *et al*, 2012; Tomasi & Volkow, 2012).

Aging also shows its effects on grey matter structure resulting from loss of unmyelinated axons, dendrites, and glial cell, shrinking of neural bodies, changes of dendritic morphology or decreased synaptic density. The brain shrinks in volume and the ventricular system expands in healthy aging (Fjell & Walhovd, 2010). A consistent result is that age-related morphometric changes are widespread across the cortex, although there are specific regions with a major and non-linear grey matter losses over time (Terribilli *et al*, 2011). Regionally, structural decline appears more prominent in frontal, parietal and temporal cortices (Coelho *et al*, 2021; Li *et al*, 2018; Zhang *et al*, 2020), consistent with the last-in-first-out hypothesis, which posits that brain regions that reach full maturation later are more vulnerable to age-related atrophy (Fjell *et al*, 2014a).

Moreover, by applying up-to-date MRI techniques, such as graph analysis and connectomics, it has been shown that the effect of age on functional brain connectome leads to reorganization of the human brain (Bertolero *et al*, 2015; Geerligs *et al*, 2015; Cao *et al*, 2014; Spreng *et al*, 2016). As the highways are more important than smaller routes in facilitating traffic, so hubs are nodes (brain regions) with special importance in the brain network thanks to their central position in the network's topological organization and their many connections (Power *et al*, 2013). These hubs are pivotal

structures of the core neurocognitive functional networks such as the DMN, dorsal-attention, central-executive, that often result more vulnerable, thereby supporting the idea of selective vulnerability to attack (Power *et al.*, 2013). Indeed, a recent study reported a greater reorganization of hubs in old subjects compared to young and middle age groups, to maintain communication efficiency (Zhang *et al.*, 2020). Moreover, in connectivity-related studies, aging altered brain networks differently. DMN is typically characterized by a decreasing trend in functional connectivity with age (Song *et al*, 2014), whereas an opposite trend was observed in networks involved in primary information processing, such as the sensorimotor and visual, where the functional connectivity was even found increased with age (Geerligs *et al.*, 2015; Song *et al.*, 2014).

Much less is known about the role played by functional connectome reorganization with aging in laying the groundwork for the gray matter loss. The aim of the present study was to investigate whether and how the brain functional connectome architecture relates with structural brain changes due to aging. We proposed a model that integrates the information of the functional connectome vulnerability, studied through an innovative graph-analysis approach (i.e., stepwise functional connectivity), with the gray matter cortical thinning in aging. This might lead to identify functional temporo-spatial patterns of neuronal dysfunction that might contribute to the cortical brain atrophy in aging.

MATERIALS AND METHODS

For this prospective study, participants were recruited and clinically evaluated at the IRCCS San Raffaele Scientific Institute (Milan, Italy) from 2017 to date in the framework of an observational study. MRI scans were collected from all participants using a Philips Medical Systems Ingenia cx 3T scanner. All MRI data were pre-processed and analyzed at the Neuroimaging Research Unit, Division of Neuroscience, IRCCS San Raffaele Scientific Institute and Vita-Salute San Raffaele University, Milan, Italy.

Participants

One hundred twenty-eight right-handed healthy controls were recruited by word of mouth. None of the participants had any history of psychiatric or neurological disorder, drug or alcohol abuse, or any systemic disease that might compromise cognitive function or blood flow (e.g., diabetes, untreated hypertension, cardiovascular disease). All participants scored in the normal range on the Mini Mental Status Exam ($\geq$27) (Folstein *et al*, 1975). Prior to participation, written informed consent was obtained from all participants.

Participants aged 20-85 years and were divided into two groups according to age: 50 young healthy adults ($\leq$ 35 years old) and 78 older healthy adults (> 35 years old). At study entry, both groups performed a neuropsychological and behavioural evaluation (see Table 1 for more details).

Briefly, the common neuropsychological assessment evaluated: global cognition with the Mini-Mental State Examination (MMSE) (Folstein *et al.*, 1975); memory with the Rey Auditory Verbal Learning test (Carlesimo *et al*, 1996), and the delayed recall of a complex figure (Rey–Osterrieth (Caffarra *et al*, 2002) or Benson (Possin *et al*, 2011) (Possin *et al.*, 2011)); attention and executive functions with the Trail Making Test (Giovagnoli *et al*, 1996) and the Modified Card Sorting Test (Caffarra *et al*, 2004); visuospatial abilities with the copy of a complex figure (Rey–Osterrieth (Caffarra *et al.*, 2002) or Benson (Possin *et al.*, 2011)); and mood with the Beck Depression Inventory (Beck *et al*, 1961).

In addition, in older adults we further assessed memory with the digit and spatial span forward (Orsini *et al*, 1987); attention and executive functions with the attentive matrices (Tognoni, 1987), the Raven coloured progressive matrices (Basso *et al*, 1987), the digit

span backward (Monaco *et al*, 2013), and the phonemic and semantic fluencies (Novelli, 1986); visuospatial abilities with the freehand copying drawings with or without guiding landmarks(Carlesimo *et al.*, 1996); language with the Token Test (De Renzi & Vignolo, 1962); and behaviour with the apathy rating scale (Marin *et al*, 1991).

On the other hand, in young adults we also assessed attention and executive functions with the Pasat 2" test (Amato *et al*, 2006); visuospatial abilities with the Benton line orientation test (Benton *et al*, 1978); language with naming in response to an oral description (CaGi) (Catricala *et al*, 2013); and physical and mental wellness with the Symptom Check List-90-Revised (SCL-90-R).(Derogatis & Savitz, 2000)

Finally, each participant underwent a brain MRI scan, including 3D T2-weighted, 3D fluid-attenuated inversion recovery, 3D high resolution T1-weighted sequences and T2* weighted (GE-EPI) as resting-state functional sequence (see Table 2 for more details).

Statistical analysis: Demographic, clinical and cognitive data

Demographic and cognitive data were compared between young healthy adults and old healthy adults using one-way ANOVA models (for continuous variables) or Chi-squared test (for categorical variables). Cognitive data analysis was corrected for age, sex and education. Two-sided p-value <0.05 was considered for statistical significance. P-values were adjusted for Bonferroni multiple comparisons. Analyses were performed using R Statistical Software (version 4.0.3; R Foundation for Statistical Computing, Vienna, Austria).

MRI ANALYSIS

The study framework is reported in Figure 1. First, *(i)* we identified highly functionally connected regions with 8 *a priori* selected hubs. Then, *(ii)* functional connectivity alterations among hubs themselves and highly connected regions were compared between young and old healthy adults. Subsequently *(iii)* we modelled cortical thickness trajectories over time and finally, *(iv)* gray matter loss of highly connected regions was investigated.

(i) Identification of highly functionally connected regions with hubs

rs-fMRI Pre-processing. Preprocessing of the rs-fMRI data was performed with Data Processing Assistant for Resting-State toolbox (DPARSFA, http://rfmri.org/ DPARSF, (Chao-Gan & Yu-Feng, 2010) based on Statistical Parametric Mapping (SPM12, http://www.fil.ion.ucl.ac.uk/spm), and the rs-fMRI Data Analysis Toolkit [http://www.restfmri.net] (Song *et al*, 2011). Preprocessing included the following steps: removal of the first four volumes of raw rs-fMRI data, slice timing correction (the middle slice was used as the reference point), head motion correction applying a six-parameter (rigid body) linear transformation and a two-step procedure by registering to the first image and then to the mean of the images after the first realignment), spatial normalization to the Montreal Neurological Institute (MNI) atlas template with voxel size set at $5 \times 5 \times 5$ mm^3 for computational efficiency, removal of spurious variance through linear regression. This step included 24 parameters from the head motion correction step [6 head motion parameters, 6 head motion parameters one time point before, and the 12 corresponding squared items] (Friston *et al*, 1996), scrubbing with regression [signal spike regression as well as 1 back and 2 forward neighbors] (Yan *et al*, 2013) at time points with a frame-wise displacement (FD)>0.5mm (Jenkinson *et al*, 2002), linear and quadratic trends, global signal, white matter signal, and the cerebrospinal fluid signal. The last steps of preprocessing included spatial smoothing with a 4 mm FWHM Gaussian Kernel and band-pass temporal filtering (0.01-0.08 Hz) to reduce the effect of low frequency drift and high frequency noise (Biswal *et al*, 1995).

No participant had more than 2 mm/degree of movement in any of the six directions, and no more than 8 volumes removed during scrubbing (1/3 of the total volumes), ensuring at least 5 minutes and 30 seconds of functional data per individual.

Functional connectome reconstruction. As input to the SFC analysis, we first computed the individual association matrices for each participant by computing the Pearson correlation of each voxel to every other voxel time course within a mask covering cortical grey matter. To perform this analysis, the pre-processed rs-fMRI data of each participant were previously converted to an N-by-M matrix, where N was the image voxels in MNI space, and M was the 320 acquisition time points. From this step, a 11705x11705 matrix of Pearson correlation coefficients (i.e., r-values) was obtained per each participant. Fisher z transformation was applied to r-values. Then, all negative correlations and positive correlations that did not reach any false discovery rate (FDR) correction

threshold of p<0.05 were excluded from further analyses (Benjamini *et al*, 2001). Only positive correlations of the association matrix were taken into account, as positive connectivity has been proved to drive functional connectivity network topology in the human brain (Qian *et al*, 2018).

Stepwise functional connectivity analysis. SFC analysis is a graph-theory-based method that aims to characterize regions that connect to specific seed brain areas at different levels of "link-step" distances. Therefore, it allows to detect both direct and indirect functional couplings of a given seed region to other regions in the brain (Qian *et al.*, 2018; Gao *et al*, 2018; Sepulcre *et al*, 2012). With such a framework, a step refers to the number of links (edges) that belongs to a path connecting a node to the seed (or target) area. Accordingly, link step and path length are analogous concepts.

In SFC analysis, the degree of stepwise connectivity of a voxel j for a given step distance l and a seed area i (A_{ji}^{l}) is computed from the count of all paths that (1) connect voxel j and any voxel in seed area i, and (2) have an exact length of l.

Each SFC matrix A_l of size m-by-m can be recursively represented as follows:

Equation 1:

$$A_l(i,j) = \begin{cases} A(i,j) \ [i \neq j, l = 1] \\ \sum_{k=1}^{m} \dfrac{A_{l-1}(i,k) - \min(A_{l-1})}{\max(A_{l-1}) - \min(A_{l-1})} \dfrac{A(k,j) - \min(A)}{\max(A) - \min(A)} \ [i \neq j, l \geq 2] \end{cases}$$

Here, A_l is the functional connectivity matrix with a step distance of l, and A is the correlation matrix after Fisher transformation. Matrices were then normalized between 0 and 1, keeping the final distribution of values intact while making them comparable across step distances. In this sense, a larger SFC degree under the step distance l indicates stronger paths connecting two voxels via link one, while a smaller degree indicates weaker connectivity paths. We explored a wide range of link-step distances, from 1 to 20, to characterize the progression of the derived maps. Although the amount of overlap between consecutive steps is expected to be high, we aimed to see meaningful relative changes between pairs of maps. The SFC patterns are topographically dissimilar between consecutive maps from steps one to three and become stable for link-step distances above four. Based on this analysis, in our results we show only maps up to four steps. Furthermore, we refer to functional connectivity at one-link step as direct connectivity and for the functional connectivity at subsequent steps (2-4) as indirect connectivity.

SFC analysis uses a priori selected seed voxels of interest. Since the aim of this study was to investigate whether and how the functional rearrangement took hold with aging, we selected the following eight seed regions as hubs in healthy brain: middle frontal, inferior parietal, precuneus, middle temporal, posterior cingulate, rostral anterior cingulate (DMN hubs) and pericalcarine and lingual (occipital hubs) (Oldham & Fornito, 2019; van den Heuvel & Sporns, 2013; Zuo *et al*, 2012).

All maps across different link-step distances from one to four (i.e., SFC maps 1 to 4) were used in the characterization of functional connectivity alterations between young healthy adults and older healthy adults (see section *ii* for details).

In order to identify highly connected regions with the eight hubs, four SFC maps for each of the four steps were obtained averaging all the young healthy subject maps. Consequently, SFC maps were projected onto the cerebral hemispheres of the Population-Average Landmark and Surface-based (PALS) surface (PALS-B12) provided with Caret software (Van Essen & Dierker, 2007) using the "enclosing voxel algorithm" and "multifiducial mapping" settings.

(ii) Functional connectivity alterations among hubs themselves and highly connected regions

All maps across different link-step distances from one to four (*i.e.*, SFC maps 1 to 4) were used in the characterization of connectivity alterations between young healthy adults and older healthy adults.

Voxel-wise analyses were performed using general linear models as implemented in SPM12. Whole-brain two-sample t-test comparisons between groups were performed, including age, sex and education as covariates. A threshold-free cluster enhancement method, combined with nonparametric permutation testing (5000 permutations) as implemented in the Computational Anatomy Toolbox 12 (CAT12, http://www.neuro.uni-jena.de/cat/) was used to detect statistically significant differences at $p<0.05$, family-wise error (FWE) corrected. These analyses allowed the identification of specific regions that demonstrated between-group differences in stepwise connectivity.

As a final step, all resulting maps from statistical analysis were projected onto the cerebral hemispheres of the PALS surface (Van Essen & Dierker, 2007) using the "enclosing voxel algorithm" and "multifiducial mapping" settings.

(iii) Modelling of cortical thickness trajectories

Cortical thickness. We estimated cortical thickness on 3D T1-weighted using FreeSurfer (version 5.3) image analysis suite (http://surfer.nmr.mgh.harvard.edu/). The process involved registration to Talairach space, normalization of intensity and an automatic skull stripping to remove extra-cerebral structures. After such processing, images were segmented into gray matter (GM), white matter (WM) and cerebrospinal fluid (CSF). The cerebral hemispheres were separated. Subcortical regions were not included in such analysis due to the low accuracy of such framework for deep cerebral structures. The WM/GM boundary was automatically delineated, and the surface was deformed following the intensity gradients to optimally recognize WM/GM and GM/CSF borders. Thus, WM and pial surface was obtained. The segmentation results were visually inspected, and if necessary, edited manually. Finally, the cerebral cortex was parcellated into 68 cortical regions based on Desikan atlas (Desikan et al., 2006) and mean cortical thickness was calculated per each region as the average shortest distance between WM borders and pial surface.

Modelling regional cortical. To assess cortical thickness changes over time, for each cortical region we modelled the relationship between individuals age and cortical thickness using a supervised learning method, the Gaussian Process Regression (GPR). GPR is a nonparametric Bayesian approach for the probabilistic prediction of continuous variables (CKI & Williams, 2006). The advantages of such methods lie on the probabilistic nature of the prediction and its interpolation with the observed data. Previous studies (Ball *et al*, 2020; Cole *et al*, 2018; Ziegler *et al*, 2014) confirmed its potential to model relationship between age and MRI-derived metrics. GPR was implemented using Matlab 17. Per each cortical region, we obtained predicted age cortical trajectories ranging from 20.5 to 84.6 years, including sex and years of education as covariates. To identify the regional cortical thinning, the relative change over time was assessed starting from the predicted cortical trajectories. Thus, we performed a rank transformation on cortical regions based on their relative thickness at either the end of the observed timeframe (20.5 and 84.6 years) to account for nonnormally distribution of cortical thicknesses. Regions that showed to be thinner compared to other cortical regions were attributed to a higher rank. Then, we evaluated the rank variation per each region by

subtracting the starting rank value (at 20.5 year) of each cortical region to its final rank value (at 84.6 years): *rank variation = final rank – starting rank.* As such, positive values of change reflected regions with the highest change rate over time, while negative values present regions with less change. Based on such rank variation, cortical regions were ordered by the region that varies the least to that which varies the most. Finally, rank variation was Z-scored and correlated with regional mean thickness to assess the relationship between the degree of variation and the cortical thickness of cortical regions.

(iv) Gray matter loss of highly connected regions

In order to identify gray matter loss of highly connected regions with hubs, we investigated spatial similarity between functional pattern and cortical atrophy. The hypothesis is that brain regions highly functionally connected with hubs are those that change with aging and become atrophic first. Therefore, we computed per each seed region the combined version of SFC maps from 1 to 4 into one single map (combined SFC maps) within young adult group. Specifically, we considered the SFC maps from 1 to 4 that were previously calculated per each subject and seed. We identified the highest functional connectivity of each voxel among the four values of each map (from 1 to 4) and set the values of each voxel with the number of step (from 1 to 4) in which the functional connectivity resulted maximized. Thus, we obtained a SFC combined map for each subject and seed whose values ranged from 1 to 4 steps (1=closer to the seed; 4=far from the seed). A mean combined SFC map of young healthy subjects was obtained averaging all the healthy subject maps.

In order to evaluate gray matter loss, regional cortical thickness of old adults has been considered. Regional cortical thickness values per each subject of old adult group were normalized relative to the mean and the standard deviation of regional values of young adults group. Subsequently, we obtained a mean value of cortical thickness per each region by averaging all the normalized values of older subjects.

Correlation analysis between combined SFC maps and mean cortical thickness was performed in order to evaluate spatial similarity between functional pattern and cortical atrophy during aging. Finally, the functionally closest regions to each seed (combined version of SFC maps <1.5) were selected and the distribution of cortical thickness values within older adult group was visually reported. Finally, cortical thickness in such regions

were compared between the two groups using ANOVA models, Bonferroni-corrected for multiple comparisons at level of 0.05 adjusted for sex and years of education.

RESULTS

(i) Identification of highly functionally connected regions with hubs

Investigating the average maps of functional connectivity within the young healthy adults, we found that all seed regions exhibited a dense and predominant regional-local direct functional connectivity (Figure 2). All seed regions, expect for the two occipital seeds (lingual and pericalcarine), revealed a common pattern of direct connections, reaching firstly superior frontal gyrus, supramarginal gyrus, superior and inferior parietal, isthmus and posterior cingulate and precuneus (Figure 2). On the other hand, pericalcarine and lingual regions shared a pattern of dense direct connections within occipital lobe (lateral occipital gyrus, cuneus, lingual, pericalcarine) and the sensorimotor areas (precentral, postcentral and paracentral gyri) (Figure 2). Of note, the precuneus hub is the only seed region directly connected to occipital hubs (lingual and pericalcarine) and the other selected hubs (middle frontal gyrus, rostral anterior cingulate, inferior parietal gyrus, posterior cingulate and middle temporal gyrus) (Figure 2).

At indirect connectivity (intermediate steps), all seed regions, except for the occipital seeds, revealed a common pattern reaching occipital regions (cuneus, lingual and fusiform), the superior temporal and the sensorimotor areas (paracentral, precentral and postcentral gyri) more prominently in the third and the fourth step. The occipital seeds (pericalcarine and lingual) indirectly connected to the superior frontal, the caudal anterior cingulate and the superior temporal (Figure 2).

(ii) Functional connectivity alterations among hubs themselves and highly connected regions

Middle frontal gyrus seed (Figure 3A)*.* Older healthy adults showed decreased direct functional connectivity in frontal lobe (superior frontal gyri, right rostral middle frontal gyrus and medial orbitofrontal cortex), parietal lobe (right inferior parietal and right supramarginal gyrus) and temporal lobe (right middle and inferior temporal gyri) relative to young healthy adults. Decreased indirect functional connectivity was observed in frontal lobe (superior frontal gyri, medial orbitofrontal cortex and right caudal anterior cingulate), right inferior parietal cortex, left insula in older adults compared to young. Concerning the opposite contrast, older subjects exhibited a significantly increased direct functional connectivity in superior parietal cortex, temporal lobe (superior temporal

gyrus, fusiform, right entorhinal cortex, right parahippocampal gyrus and left hippocampus), and occipital lobe (lingual gyrus, left pericalcarine, left cuneus, and left lateral occipital cortex). Enhanced indirect connectivity was also observed in sensorimotor cortex (precentral and postcentral gyri), parietal lobe (superior parietal cortex and right supramarginal gyrus), temporal lobe (right superior temporal gyrus, right fusiform and left hippocampus) and occipital lobe (lingual gyri, left pericalcarine and left cuneus).

Rostral anterior cingulate seed (Figure 3B). Decreased direct connectivity in the frontal lobe (superior frontal gyri, medial orbitofrontal cortex and rostral anterior cingulate cortex), temporal lobe (left entorhinal cortex and right hippocampus) and right isthmus cingulate cortex was found in older adults relative to young adults. Reduced indirect functional connectivity was found in frontal lobe (superior frontal gyri, medial orbitofrontal cortex, rostral anterior cingulate and right caudal anterior cingulate), temporal lobe (left entorhinal cortex and right hippocampus), parietal lobe (precuneus, right posterior cingulate and right isthmus cingulate), and left insula. Moreover, with regard to the opposite contrast, older adults exhibited significant increased direct connectivity in frontal lobe (caudal medial superior frontal gyri, left rostral middle frontal gyrus, left pars opercularis and right caudal anterior cingulate), postcentral gyri, and parietal lobe (superior parietal cortex and supramarginal gyri) relative to young subjects. Additional enhanced indirect connectivity was found in occipital regions (right lingual gyrus, right fusiform gyrus and right lateral occipital cortex) in older subjects relative to young controls.

Precuneus seed (Figure 3C)*.* Older adults presented lower direct functional connectivity in frontal lobe (superior frontal gyri, medial orbitofrontal cortex, rostral anterior cingulate), parietal lobe (precuneus, isthmus cingulate and posterior cingulate), left insula and occipital lobe (pericalcarine and cuneus) relative to young adults. Older healthy adults showed additional lower indirect connectivity in right inferior parietal cortex and left inferior temporal gyrus. Referring to the opposite contrast, older group exhibited enhanced direct functional connectivity from precuneus seed to sensorimotor (precentral and postcentral gyri), parietal lobe (superior parietal cortex and supramarginal gyri), temporal lobe (superior temporal gyri and right fusiform) and occipital lobe (right lateral occipital cortex) compared to young subjects. Across subsequent steps, additional

enhanced indirect connectivity was found in occipital lobe (lateral occipital cortex, lingual gyri, left pericalcarine, left cuneus).

Posterior cingulate seed (Figure 3D). When comparing older subjects with young adults, direct connectivity starting from the posterior cingulate seed revealed decreased functional connectivity in frontal lobe (right superior frontal gyrus, medial orbitofrontal cortex and caudal anterior cingulate) and right insula. Older adults showed lower indirect functional connectivity in frontal lobe (superior frontal gyri, medial orbitofrontal cortex and right caudal anterior cingulate), insular cortex and left transverse temporal cortex relative to young subjects. Referring to the opposite contrast, older group exhibited enhanced direct connectivity from posterior cingulate seed to sensorimotor cortex (precentral and postcentral gyri), superior parietal cortex, and left middle temporal gyrus. Moreover, older subjects also showed enhanced indirect functional connectivity in sensorimotor cortex (precentral and postcentral gyri), superior parietal cortex, right fusiform gyrus and occipital lobe (lingual gyri, pericalcarine and cuneus).

Inferior Parietal cortex seed (Figure 3E). Older adults showed decreased direct functional connectivity compared to young adults in frontal lobe (rostral middle frontal gyri, medial orbitofrontal cortex and pars orbitalis), parietal lobe (right inferior parietal lobule) and left insula, while decreased indirect connectivity was detected within the frontal lobe (superior frontal gyri, medial orbitofrontal cortex and right caudal anterior cingulate) and insula. Regarding the opposite contrast, older adults exhibited a significant increased direct functional connectivity when compared to young subjects in sensorimotor cortex (precentral and postcentral gyri), superior parietal cortex, temporal lobe (right fusiform gyrus and right parahippocampal gyrus) and occipital lobe (lingual gyrus). Additionally, from the inferior parietal seed we observed enhanced indirect connectivity with the parietal lobe (superior parietal cortex and right supramarginal), temporal (right superior temporal gyrus and right fusiform gyrus) and occipital lobe (right lingual gyrus, left pericalcarine and left cuneus) in older group.

Middle temporal gyrus seed (Figure 3F). Starting from middle temporal gyrus, older adults showed decreased direct connectivity in frontal lobe (superior frontal gyri and medial orbitofrontal cortex), right inferior parietal cortex and temporal lobe (middle temporal and inferior temporal gyri). Additionally, older adults were characterized by decreased indirect functional connectivity within left insula, right caudal anterior and

right posterior cingulate relative to the young counterparts. Furthermore, older subjects showed enhanced direct connectivity relative to young adults within the left rostral middle frontal gyrus and left paracentral lobule, along with parietal lobe (superior parietal gyri, supramarginal gyri), right insula, temporal lobe (right transverse temporal gyrus, superior temporal gyri) and lateral occipital cortex. Finally, increased indirect functional connectivity was found within sensorimotor cortex (precentral and postcentral gyri), parietal lobe (superior parietal gyrus and right supramarginal gyrus), superior temporal gyri, and occipital lobe (lingual gyrus, left pericalcarine and left cuneus).

Lingual gyrus seed (Figure 3G). Regarding direct functional connectivity from the lingual seed, older adults showed decreased connectivity relative to the young group in frontal lobe (superior frontal gyri and medial orbitofrontal cortex), isthumus cingulate cortex and lingual gyri. Moreover, older group were characterized by decreased indirect connectivity within frontal lobe (superior frontal gyri, medial orbitofrontal cortex and right caudal anterior cingulate), parietal lobe (precuneus and right posterior cingulate) and left insula. Referring to the opposite contrast, older healthy adults showed increased direct functional connectivity relative to young subjects within the right caudal middle frontal gyrus, the sensorimotor cortex (precentral and postcentral gyri), parietal lobe (superior parietal cortex and right supramarginal gyrus), insula and temporal lobe (right superior temporal gyrus and inferior temporal gyri). Regarding indirect connectivity, older subjects were characterized by additional increased functional connectivity in right fusiform gyrus and occipital lobe (lingual gyri, pericalcarine and cuneus).

Pericalcarine cortex seed (Figure 3H). Older subjects showed decreased direct connectivity relative to yound adults in frontal lobe (superior frontal gyri, medial orbitofrontal cortex and rostral anterior cingulate), insular cortex, left transverse temporal gyrus, isthmus cingulate cortex, occipital cortex (lingual gyri and cuneus), while reduced indirect connectivity was found in frontal lobe (superior frontal gyri, medial orbitofrontal cortex, left rostral anterior cingulate and right caudal anterior cingulate), parietal lobe (precuneus and posterior cingulate), left insula. Regarding the opposite contrast, older healthy adults exhibited significant enhanced direct connectivity in sensorimotor cortex (precentral and postcentral gyri), parietal lobe (superior parietal cortex and right supramarginal gyrus) and temporal lobe (right superior temporal gyrus) and right lateral occipital cortex). Additionally, enhanced indirect functional connectivity was found in

older adults in sensorimotor cortex (precentral and postcentral gyri), parietal lobe (superior parietal cortex and right supramarginal gyrus), temporal lobe (right superior temporal gyrus and right fusiform gyrus), occipital lobe (lingual gyri, pericalcarine, cuneus and lateral occipital cortex) relative to young adults.

(iii) Modelling of cortical thickness trajectories

We modelled the regional change in cortical thickness through GPR on the entire cohort (n=128) between ages 20.5 and 84.6 years. The 97% of cortical regions showed decreasing thickness with advancing age (Figure 4A). Calculating the relative change over time, through the rank transformation, the highest cortical thinning was observed in the majority of DMN hubs (right middle frontal gyrus, rostral anterior cingulate, precuneus, right posterior cingulate, inferior parietal cortex and middle temporal gyrus) and in regions belonging to the temporal lobe (parahippocampal, superior temporal gyrus, transverse temporal gyrus and fusiform), the frontal lobe (lateral orbitofrontal, superior and inferior frontal including pars triangularis, pars opercularis), the parietal lobe (the isthmus of cingulate and supramarginal) and in the insular cortex (Figure 4B and Table 3). On the other hand, occipital hubs (lingual gyrus and pericalcarine cortex), as well as other occipital regions (cuneus and lateral occipital) and all the motor and premotor areas (precentral, postcentral and paracentral regions), showed the lowest cortical thickness change in relation to the whole brain across lifespan (Figure 4B and Table 3). Finally, positive correlation was found between regional mean thickness and regional relative change over time (r=0.32, p=0.01) (Figure 4C).

(iv) Gray matter loss of highly connected regions

Correlation analysis between combined SFC maps of each hub in the young group and mean regional cortical thickness of older healthy adults was performed to evaluate spatial similarity between functional pattern and cortical atrophy during aging. Significant positive correlation between functional pattern of middle frontal hub in young adults and the cortical thinning in older adults (Figure 5A) was found. Whereas, significant negative correlation emerged between the functional network organization of lingual and pericalcarine hubs and the cortical thinning in older adults (Figure 5B-C). Functionally closest regions to hubs were obtained (combined SFC maps regions <1.5). Considering

DMN hubs, frontal pole, caudal middle frontal, pars orbitalis and temporal pole bilaterally and left isthmus cingulate, left pars triangularis and right supramarginal (DMN-linked regions) were selected. Whereas the functionally closest regions to occipital hubs were the hubs themselves (lingual gyrus and pericalcarine cortex) and cuneus (OCC-linked regions). Comparing mean regional cortical thickness in DMN- and OCC-linked regions between the two groups, older healthy adults showed significant reductions in mean regional cortical thickness relative to young adults (Figure 6 and Table 4). However, investigating the distribution of normalized cortical thickness value in older adults, DMN-linked regions showed a greater mean cortical thinning than OCC-linked regions (Figure 6).

DISCUSSION

Brain can be depicted as a highly efficient anatomical and functional organization that can be approached for investigation as a complex and comprehensive network (van den Heuvel & Sporns, 2013). Within this network, hubs are pivotal brain regions with substantial role in integration, enabling efficient neuronal signaling and communication, and they represent potential vulnerability 'stations' preferentially affected by aging (Zhang *et al.*, 2020). Aging is an inherent process of neurodegeneration determined by an accumulation of molecular and cellular damages (Lopez-Otin *et al.*, 2013) that reflects in functional and structural alterations of the brain.

For such reason, we selected, based on existing literature, eight human brain hubs (middle frontal gyrus, rostral anterior cingulate cortex, inferior parietal cortex, precuneus, posterior cingulate cortex, middle temporal gyrus – DMN hubs – , lingual and pericalcarine cortex – OCC hubs), which are also demonstrated to be compromised in different age-related neurodegenerative disorders (Agosta *et al*, 2013; Canu *et al*, 2017).

Our aim was to evaluate as aging affects functional connectivity of these pivotal regions and how such effects influence the vulnerability and structural changes of the whole brain. Overall, DMN hubs showed a highly direct functional connectivity with themselves and among each other, while OCC hubs showed a direct functional connectivity within occipital regions and somatosensory. Investigating cortical thickness changing over time in healthy subjects, we observed that DMN hubs were among the brain regions that changed the most. On the contrary, OCC hubs showed a quite spared cortical thickness across lifespan. The combination of multimodal information of hubs atrophy and their functional connectivity pattern allowed us to delineate the vulnerability of the remaining brain regions. We observed that regions highly functionally connected to DMN hubs were characterized by greater cortical thinning relative to those brain regions highly functionally connected to OCC hubs, which, even though showing mild cortical thinning, resulted more spared.

The evaluation of the functional connectivity average maps of young adults provided the possibility to identify *in vivo* the functional pathways starting from the selected hubs. Identifying the optimal functional topological organization, we observed that each of the DMN hubs was densely and directly (one-step link) connected: (i) within themselves; (ii) with other hubs (inferior parietal gyrus, posterior cingulate cortex and precuneus); and

(iii) with superior frontal gyrus, isthmus cingulate cortex, supramarginal gyrus and superior parietal gyrus. These results are quite expected, since they are regions belonging to a common network (DMN) (Raichle, 2015). Furthermore, in recent studies in which SFC has been applied, it has been demonstrated that seeds regions are always directly connected with themselves (Sepulcre *et al.*, 2012). Moreover, our results highlighted direct connections between some of DMN hubs and regions belonging to the salience network (i.e., anterior insula, dorsal anterior cingulate cortex), supporting the functional link between DMN and salience network, widely reported in literature (Menon, 2015).

On the other hand, the evaluation of healthy functional organization starting from OCC hubs as seeds pointed out that these hubs were densely and directly connected within the occipital local regions, sensorimotor regions (precentral, postcentral and paracentral gyri) and precuneus, in line with recent studies (Sepulcre *et al.*, 2012). Of note, the occipital areas have a deep interconnectivity with primary motor and somatosensory cortices suggesting an early integration of somatomotor and visual processing for oculomotor functions (Sepulcre *et al.*, 2012).

An intriguing result regarded the functional connectivity of the precuneus, which appeared especially central in linking the other DMN hubs and the OCC hubs, serving as functional communication bridge. This is in line with previous studies, which highlighted the role of the precuneus as connector hub (Bagarinao *et al*, 2020; Gordon *et al*, 2018; van den Heuvel & Sporns, 2013). Moreover, this region might play an active role as specific node during disease processes.

Focusing on the indirect connections (intermediate step-link), common connectivity patterns at intermediate step-link distances across all seeds was observed. A whole-brain stable map of connectivity was identified, where all the selected cortical hubs converge, supporting global functional integration properties of the healthy brain (Sporns, 2013).

Subsequently, investigating topological organization changes during aging, we hypothesized that the pattern of functional reorganization with aging primarily affects directly connected regions, and then spreads to indirectly connected regions. In support of our hypothesis, we found functional connectivity alterations in older adults among hubs themselves and areas that were found highly connected at one-step distance. Indeed, the direct functional connections within hubs themselves and towards regions, whcih are mainly distributed within the DMN, were found significantly decreased with aging. These

findings find wide acceptance with previous studies, suggesting that hubs DMN regions are more vulnerable to aging effect and easily affected by neurodegenerative disorders (Crossley *et al*, 2014; Damoiseaux, 2017; Siman-Tov *et al*, 2016; Song *et al.*, 2014). In literature, there is a bunch of evidence reporting functional alterations in hub properties in the main age-related neurodegenerative diseases as Alzheimer's disease (Toussaint *et al*, 2014) and frontotemporal dementia (Agosta *et al.*, 2013). In addition, neuropathologically, Aβ deposition has been found to preferentially accumulate in precuneus and posterior cingulate cortex in Alzheimer's disease, known to be DMN hubs (Buckner *et al*, 2009).

In regards with OCC hubs, decreased direct connectivity was found within themselves and in the cuneus, highlighting a local reduction within the occipital lobe that might be explained by the already seen strong local direct connectivity in the average maps. Decreased connectivity within the visual occipital network has been reported in the literature and might be related with a deficit of sensory processing in aging (Onoda *et al.*, 2012).

Besides decreased direct connectivity, hyperconnectivity was also found in older adults compared to young. Particularly, precuneus, superior parietal lobule and sensorimotor network are the areas that showed increased functional connectivity with both DMN and OCC hubs, respectively. Hyperconnectivity in somatosensory networks is in line with previous studies (Geerligs *et al.*, 2015; Song *et al.*, 2014; Tomasi & Volkow, 2012). The pattern of increasing functional connectivity among regions belonging to different networks could be interpreted as the attempt to compensate for the functional decline within network, which may reflect decreased segregation properties.

This is in keeping with previous studies showing that within-network connectivity weakens during normal aging, while between-network connectivity increases to balance the modular structure in the functional brain network (Spreng *et al.*, 2016).

Intrigued by the functional rearrangement of the hubs in a healthy young brain, we then focused on the structural changes of the hubs, firstly, and of the other brain regions that occur in aging. As well-established in previous literature, we found that cortical thickness decreased across the majority (97%) of the cortex between 20 and 85 years (Fjell & Walhovd, 2010; Salat *et al*, 2004; Shaw *et al*, 2016). We also found that high cortical thinning is centered on DMN hubs and regions within frontal (lateral

orbitofrontal, superior and inferior frontal, including pars triangularis and opercularis), temporal (parahippocampal, entorhinal, superior temporal and fusiform), parietal (the isthmus of cingulate and supramarginal) lobes and insular cortex (Fjell *et al*, 2014b). In contrast, we found that slowest thinning is restricted to OCC hubs and motor and pre-motor cortex (Shaw *et al.*, 2016). Present findings are consistent with the "last in, first out" hypothesis, according to which the prefrontal-inferior parietal-temporal brain areas, that are late-maturing regions, are preferentially the first to be vulnerable to aging (Raz *et al*, 2005).

Finally, some interesting observations can be drawn regarding how the grey matter atrophy and the functional connectivity pattern of the selected hubs strike the remaining brain regions in aging. We observed that regions highly functionally connected to DMN hubs were characterized by greater cortical thinning relative to those brain regions highly functionally connected to OCC hubs, that, even though they showed mild cortical thinning, resulted more spared. This suggests that cortical regions functionally close to the DMN hubs, but far from the occipital hubs, became the more atrophic during aging, finding, one again, consistency in the 'last in, first out' theory (Raz *et al.*, 2005). In agreement with our findings, Douaud and colleagues (Douaud *et al*, 2014) demonstrated that transmodal cortex, almost overlapping with DMN and which develops late in adolescence, showed accelerated degeneration in old age compared with the rest of the brain. Moreover, our results find their consent in a previous study (Vidal-Pineiro *et al*, 2014), where dysfunctional DMN connectivity was related to structural changes in brain aging, suggesting maladaptive plasticity mechanisms during the lifespan in the DMN.

The study is not without limitations. Although the neuropsychological characterization of our sample was very comprehensive, there is a lack of information about lifestyle risk factors (i.e., smoking, obesity, lifestyle, health risk factors), which might modulate the brain aging changes. Another limitation lies in the cross-sectional nature of the study. Our findings may relate to the nature of the aging profiles, which represent snapshots in time. In this context, longitudinal studies are warranted to verify the trajectories of functional changes, assessing the evolution of alterations over time. Regarding methodological concerns, computational constraints required us to downsample data to relatively large voxels (5 mm^3). Finally, due to methodological limitations of thickness measurement in

subcortical regions, we restricted our analysis to the cortical regions, only. Further investigations are warranted to evaluate the aging effect on subcortical areas.

Our findings revealed potential patterns of vulnerability to aging, pointing out how functional network rearrangements of brain hubs and their structural change trajectories across lifespan influence the functional and structural trend of changes of the remaining brain regions.

REFERENCES

Agosta F, Sala S, Valsasina P, Meani A, Canu E, Magnani G, Cappa SF, Scola E, Quatto P, Horsfield MA *et al* (2013) Brain network connectivity assessed using graph theory in frontotemporal dementia. *Neurology* 81: 134-143

Amato MP, Portaccio E, Goretti B, Zipoli V, Ricchiuti L, De Caro MF, Patti F, Vecchio R, Sorbi S, Trojano M (2006) The Rao's Brief Repeatable Battery and Stroop Test: normative values with age, education and gender corrections in an Italian population. *Mult Scler* 12: 787-793

Bagarinao E, Watanabe H, Maesawa S, Mori D, Hara K, Kawabata K, Ohdake R, Masuda M, Ogura A, Kato T *et al* (2020) Identifying the brain's connector hubs at the voxel level using functional connectivity overlap ratio. *NeuroImage* 222: 117241

Ball G, Seidlitz J, Beare R, Seal ML (2020) Cortical remodelling in childhood is associated with genes enriched for neurodevelopmental disorders. *NeuroImage* 215: 116803

Basso A, Capitani E, Laiacona M (1987) Raven's coloured progressive matrices: normative values on 305 adult normal controls. *Functional neurology* 2: 189-194

Beck AT, Ward CH, Mendelson M, Mock J, Erbaugh J (1961) An inventory for measuring depression. *Arch Gen Psychiatry* 4: 561-571

Benjamini Y, Drai D, Elmer G, Kafkafi N, Golani I (2001) Controlling the false discovery rate in behavior genetics research. *Behav Brain Res* 125: 279-284

Benton AL, Varney NR, Hamsher KD (1978) Visuospatial judgment. A clinical test. *Arch Neurol* 35: 364-367

Bertolero MA, Yeo BT, D'Esposito M (2015) The modular and integrative functional architecture of the human brain. *Proc Natl Acad Sci U S A* 112: E6798-6807

Biswal B, Yetkin FZ, Haughton VM, Hyde JS (1995) Functional connectivity in the motor cortex of resting human brain using echo-planar MRI. *Magn Reson Med* 34: 537-541

Buckner RL, Sepulcre J, Talukdar T, Krienen FM, Liu H, Hedden T, Andrews-Hanna JR, Sperling RA, Johnson KA (2009) Cortical hubs revealed by intrinsic functional connectivity: mapping, assessment of stability, and relation to Alzheimer's disease. *J Neurosci* 29: 1860-1873

Caffarra P, Vezzadini G, Dieci F, Zonato F, Venneri A (2002) Rey-Osterrieth complex figure: normative values in an Italian population sample. *Neurol Sci* 22: 443-447

Caffarra P, Vezzadini G, Dieci F, Zonato F, Venneri A (2004) Modified Card Sorting Test: normative data. *Journal of clinical and experimental neuropsychology* 26: 246-250

Canu E, Agosta F, Mandic-Stojmenovic G, Stojkovic T, Stefanova E, Inuggi A, Imperiale F, Copetti M, Kostic VS, Filippi M (2017) Multiparametric MRI to distinguish early onset Alzheimer's disease and behavioural variant of frontotemporal dementia. *Neuroimage Clin* 15: 428-438

Cao M, Wang JH, Dai ZJ, Cao XY, Jiang LL, Fan FM, Song XW, Xia MR, Shu N, Dong Q *et al* (2014) Topological organization of the human brain functional connectome across the lifespan. *Dev Cogn Neurosci* 7: 76-93

Carlesimo GA, Caltagirone C, Gainotti G (1996) The Mental Deterioration Battery: normative data, diagnostic reliability and qualitative analyses of cognitive impairment. The Group for the Standardization of the Mental Deterioration Battery. *Eur Neurol* 36: 378-384

Catricala E, Della Rosa PA, Ginex V, Mussetti Z, Plebani V, Cappa SF (2013) An Italian battery for the assessment of semantic memory disorders. *Neurol Sci* 34: 985-993

Chao-Gan Y, Yu-Feng Z (2010) DPARSF: A MATLAB Toolbox for "Pipeline" Data Analysis of Resting-State fMRI. *Frontiers in systems neuroscience* 4: 13

CKI RC, Williams (2006) Gaussian processes for machine learning. *International Journal of Neural Systems* 14

Coelho A, Fernandes HM, Magalhaes R, Moreira PS, Marques P, Soares JM, Amorim L, Portugal-Nunes C, Castanho T, Santos NC *et al* (2021) Reorganization of brain structural networks in aging: A longitudinal study. *J Neurosci Res* 99: 1354-1376

Cole JH, Ritchie SJ, Bastin ME, Valdes Hernandez MC, Munoz Maniega S, Royle N, Corley J, Pattie A, Harris SE, Zhang Q *et al* (2018) Brain age predicts mortality. *Molecular psychiatry* 23: 1385-1392

Crossley NA, Mechelli A, Scott J, Carletti F, Fox PT, McGuire P, Bullmore ET (2014) The hubs of the human connectome are generally implicated in the anatomy of brain disorders. *Brain* 137: 2382-2395

Damoiseaux JS (2017) Effects of aging on functional and structural brain connectivity. *NeuroImage* 160: 32-40

Damoiseaux JS, Beckmann CF, Arigita EJS, Barkhof F, Scheltens P, Stam CJ, Smith SM, Rombouts SARB (2007) Reduced resting-state brain activity in the "default network" in normal aging. *Cerebral Cortex* 18: 1856-1864

De Renzi E, Vignolo LA (1962) The token test: A sensitive test to detect receptive disturbances in aphasics. *Brain* 85: 665-678

Derogatis LR, Savitz KL (2000) The SCL–90–R and Brief Symptom Inventory (BSI) in primary care. In: *Handbook of psychological assessment in primary care settings*, pp. 297-334. Lawrence Erlbaum Associates Publishers: Mahwah, NJ, US

Douaud G, Groves AR, Tamnes CK, Westlye LT, Duff EP, Engvig A, Walhovd KB, James A, Gass A, Monsch AU *et al* (2014) A common brain network links development, aging, and vulnerability to disease. *Proc Natl Acad Sci U S A* 111: 17648-17653

Fjell AM, McEvoy L, Holland D, Dale AM, Walhovd KB, Alzheimer's Disease Neuroimaging I (2014a) What is normal in normal aging? Effects of aging, amyloid and Alzheimer's disease on the cerebral cortex and the hippocampus. *Prog Neurobiol* 117: 20-40

Fjell AM, Walhovd KB (2010) Structural brain changes in aging: courses, causes and cognitive consequences. *Rev Neurosci* 21: 187-221

Fjell AM, Westlye LT, Grydeland H, Amlien I, Espeseth T, Reinvang I, Raz N, Dale AM, Walhovd KB, Alzheimer Disease Neuroimaging I (2014b) Accelerating cortical thinning: unique to dementia or universal in aging? *Cereb Cortex* 24: 919-934

Folstein MF, Folstein SE, McHugh PR (1975) "Mini-mental state". A practical method for grading the cognitive state of patients for the clinician. *J Psychiatr Res* 12: 189-198

Friston KJ, Williams S, Howard R, Frackowiak RS, Turner R (1996) Movement-related effects in fMRI time-series. *Magn Reson Med* 35: 346-355

Gao Q, Yu Y, Su X, Tao Z, Zhang M, Wang Y, Leng J, Sepulcre J, Chen H (2018) Adaptation of brain functional stream architecture in athletes with fast demands of sensorimotor integration. *Hum Brain Mapp*

Geerligs L, Renken RJ, Saliasi E, Maurits NM, Lorist MM (2015) A Brain-Wide Study of Age-Related Changes in Functional Connectivity. *Cereb Cortex* 25: 1987-1999

Giovagnoli AR, Del Pesce M, Mascheroni S, Simoncelli M, Laiacona M, Capitani E (1996) Trail making test: normative values from 287 normal adult controls. *Ital J Neurol Sci* 17: 305-309

Gordon EM, Lynch CJ, Gratton C, Laumann TO, Gilmore AW, Greene DJ, Ortega M, Nguyen AL, Schlaggar BL, Petersen SE *et al* (2018) Three Distinct Sets of Connector Hubs Integrate Human Brain Function. *Cell Rep* 24: 1687-1695 e1684

Jenkinson M, Bannister P, Brady M, Smith S (2002) Improved optimization for the robust and accurate linear registration and motion correction of brain images. *NeuroImage* 17: 825-841

Li W, Yang C, Shi F, Wang Q, Wu S, Lu W, Li S, Nie Y, Zhang X (2018) Alterations in Normal Aging Revealed by Cortical Brain Network Constructed Using IBASPM. *Brain Topogr* 31: 577-590

Lopez-Otin C, Blasco MA, Partridge L, Serrano M, Kroemer G (2013) The hallmarks of aging. *Cell* 153: 1194-1217

Marin RS, Biedrzycki RC, Firinciogullari S (1991) Reliability and validity of the Apathy Evaluation Scale. *Psychiatry Res* 38: 143-162

Menon V (2015) Large-scale functional brain organization. *Brain mapping: An encyclopedic reference* 2: 449-459

Monaco M, Costa A, Caltagirone C, Carlesimo GA (2013) Forward and backward span for verbal and visuo-spatial data: standardization and normative data from an Italian adult population. *Neurol Sci* 34: 749-754

Novelli G, Laiacona M, Papagno C, Vallar G, Capitani E, Cappa SF (1986) Three clinical tests to research and rate the lexical performance of normal subjects. *Arch Psicol Neurol Psichiatr* 47: 477-506

Oldham S, Fornito A (2019) The development of brain network hubs. *Dev Cogn Neurosci* 36: 100607

Onoda K, Ishihara M, Yamaguchi S (2012) Decreased functional connectivity by aging is associated with cognitive decline. *J Cogn Neurosci* 24: 2186-2198

Orsini A, Grossi D, Capitani E, Laiacona M, Papagno C, Vallar G (1987) Verbal and spatial immediate memory span: normative data from 1355 adults and 1112 children. *Ital J Neurol Sci* 8: 539-548

Possin KL, Laluz VR, Alcantar OZ, Miller BL, Kramer JH (2011) Distinct neuroanatomical substrates and cognitive mechanisms of figure copy performance in Alzheimer's disease and behavioral variant frontotemporal dementia. *Neuropsychologia* 49: 43-48

Power JD, Schlaggar BL, Lessov-Schlaggar CN, Petersen SE (2013) Evidence for hubs in human functional brain networks. *Neuron* 79: 798-813

Qian J, Diez I, Ortiz-Teran L, Bonadio C, Liddell T, Goni J, Sepulcre J (2018) Positive Connectivity Predicts the Dynamic Intrinsic Topology of the Human Brain Network. *Frontiers in systems neuroscience* 12: 38

Raichle ME (2015) The brain's default mode network. *Annu Rev Neurosci* 38: 433-447

Raz N, Lindenberger U, Rodrigue KM, Kennedy KM, Head D, Williamson A, Dahle C, Gerstorf D, Acker JD (2005) Regional brain changes in aging healthy adults: general trends, individual differences and modifiers. *Cereb Cortex* 15: 1676-1689

Salat DH, Buckner RL, Snyder AZ, Greve DN, Desikan RS, Busa E, Morris JC, Dale AM, Fischl B (2004) Thinning of the cerebral cortex in aging. *Cereb Cortex* 14: 721-730

Sepulcre J, Sabuncu MR, Yeo TB, Liu H, Johnson KA (2012) Stepwise connectivity of the modal cortex reveals the multimodal organization of the human brain. *J Neurosci* 32: 10649-10661

Shaw ME, Sachdev PS, Anstey KJ, Cherbuin N (2016) Age-related cortical thinning in cognitively healthy individuals in their 60s: the PATH Through Life study. *Neurobiol Aging* 39: 202-209

Siman-Tov T, Bosak N, Sprecher E, Paz R, Eran A, Aharon-Peretz J, Kahn I (2016) Early Age-Related Functional Connectivity Decline in High-Order Cognitive Networks. *Front Aging Neurosci* 8: 330

Song J, Birn RM, Boly M, Meier TB, Nair VA, Meyerand ME, Prabhakaran V (2014) Age-related reorganizational changes in modularity and functional connectivity of human brain networks. *Brain connectivity* 4: 662-676

Song XW, Dong ZY, Long XY, Li SF, Zuo XN, Zhu CZ, He Y, Yan CG, Zang YF (2011) REST: a toolkit for resting-state functional magnetic resonance imaging data processing. *PLoS One* 6: e25031

Sporns O (2013) Structure and function of complex brain networks. *Dialogues Clin Neurosci* 15: 247-262

Spreng RN, Stevens WD, Viviano JD, Schacter DL (2016) Attenuated anticorrelation between the default and dorsal attention networks with aging: evidence from task and rest. *Neurobiol Aging* 45: 149-160

Terribilli D, Schaufelberger MS, Duran FL, Zanetti MV, Curiati PK, Menezes PR, Scazufca M, Amaro E, Jr., Leite CC, Busatto GF (2011) Age-related gray matter volume changes in the brain during non-elderly adulthood. *Neurobiol Aging* 32: 354-368

Tognoni HSaG (1987) *Standardizzazione e Taratura Italiana di Test Neuropsicologici*

Tomasi D, Volkow ND (2012) Aging and functional brain networks. *Molecular psychiatry* 17: 471, 549-458

Toussaint PJ, Maiz S, Coynel D, Doyon J, Messe A, de Souza LC, Sarazin M, Perlbarg V, Habert MO, Benali H (2014) Characteristics of the default mode functional connectivity in normal ageing and Alzheimer's disease using resting state fMRI with a combined approach of entropy-based and graph theoretical measurements. *NeuroImage* 101: 778-786

van den Heuvel MP, Hulshoff Pol HE (2010) Exploring the brain network: a review on resting-state fMRI functional connectivity. *Eur Neuropsychopharmacol* 20: 519-534

van den Heuvel MP, Sporns O (2013) Network hubs in the human brain. *Trends Cogn Sci* 17: 683-696

Van Essen DC, Dierker DL (2007) Surface-based and probabilistic atlases of primate cerebral cortex. *Neuron* 56: 209-225

Vidal-Pineiro D, Valls-Pedret C, Fernandez-Cabello S, Arenaza-Urquijo EM, Sala-Llonch R, Solana E, Bargallo N, Junque C, Ros E, Bartres-Faz D (2014) Decreased Default Mode Network connectivity correlates with age-associated structural and cognitive changes. *Front Aging Neurosci* 6: 256

Yan CG, Craddock RC, He Y, Milham MP (2013) Addressing head motion dependencies for small-world topologies in functional connectomics. *Front Hum Neurosci* 7: 910

Zhang Y, Wang Y, Chen N, Guo M, Wang X, Chen G, Li Y, Yang L, Li S, Yao Z *et al* (2020) Age-Associated Differences of Modules and Hubs in Brain Functional Networks. *Front Aging Neurosci* 12: 607445

Ziegler G, Ridgway GR, Dahnke R, Gaser C, Alzheimer's Disease Neuroimaging I (2014) Individualized Gaussian process-based prediction and detection of local and global gray matter abnormalities in elderly subjects. *NeuroImage* 97: 333-348

Zuo XN, Ehmke R, Mennes M, Imperati D, Castellanos FX, Sporns O, Milham MP (2012) Network centrality in the human functional connectome. *Cereb Cortex* 22: 1862-1875

Table 1. Sociodemographic data and comprehensive neuropsychological evaluation in young and older healthy adults.

Sociodemographic data			
	Young healthy adults	**Older healthy adults**	**p-value**
Age [years]	25.44 ± 3.01 (20.48 – 31.69)	62.82 ± 9.35 (36.82 – 84.59)	**<0.001**
Sex [M/W]	27/23	22/56	**0.01**
Education [years]	15.56 ± 2.98 (8.00 – 24.00)	12.04 ± 3.75 (5.00 – 20.00)	**<0.001**
Neuropsychological data			
Global cognition — MMSE	29.82 ± 0.39 (29.00 – 30.00)	29.38 ± 0.82 (27.00 – 30.00)	**0.002**
Memory — Digit Span, forward	-	5.96 ± 1.00 (4.00 – 8.00)	-
RAVLT [immediate recall]	57.54 ± 6.74 (43.00 – 70.00)	48.99 ± 7.37 (31.00 – 67.00)	**<0.001**
RAVLT [delayed recall]	12.79 ± 1.80 (8.00 – 15.00)	10.64 ± 2.44 (4.00 – 15.00)	**<0.001**
RAVLT [recognition]	14.88 ± 0.44 (13.00 – 15.00)	14.30 ± 1.38 (6.00 – 15.00)	**0.03**
RAVLT [false positives]	0.62 ± 2.00 (0.00 – 13.00)	0.68 ± 1.71 (0.00 – 13.00)	0.77
Spatial span, forward	-	5.29 ± 1.10 (3.00 – 7.00)	-
Rey's figure [delayed recall]	23.19 ± 5.48 (1.00 – 33.00)	15.00 ± 5.76 (6.50 – 23.00)	**<0.001**
Benson's figure [delayed recall]	-	11.12 ± 3.16 (4.00 – 17.00)	-
Benson's figure [recognition]	-	1.00 ± 0.00 (1.00 – 1.00)	-
Attention and executive functions — Trail Making Test (B-A)	36.07 ± 14.47 (14.01 – 105.40)	64.62 ± 38.03 (19.99 – 209.69)	**<0.001**
Digit Span, backward	-	4.77 ± 1.24 (3.00 – 8.00)	-
Attentive matrices	-	51.77 ±8.46 (4.00 – 60.00)	-
Phonemic fluency	-	37.60 ± 8.18 (18.00 – 59.00)	-
Semantic fluency	-	47.48 ± 9.26 (27.00 – 70.00)	-
Raven CPM	-	32.00 ± 3.29 (17.00 – 36.00)	-
MCST, categories	5.52 ± 0.88	4.42 ± 1.34	**<0.001**

		(3.00 – 6.00)	(1.00 – 6.00)	
	MCST, perseverations	1.30 ± 2.32 (0.00 – 10.00)	3.57 ± 3.51 (0.00 – 16.00)	**<0.001**
	Pasat 2"	40.83 ± 10.17 (18.00 – 58.00)	-	-
Language	Token Test	-	34.14 ± 1.70 (28.00 – 36.00)	-
	Naming to oral description [CaGi]	47.13 ± 1.19 (43.00 – 48.00)	-	-
Visuospatial	Rey's figure [copy]	32.86 ± 2.12 (26.00 – 36.00)	28.79 ± 3.75 (19.50 – 33.00)	**<0.001**
	Benson's figure [copy]	-	15.72 ± 0.77 (14.00 – 17.00)	-
	Copy of drawings [freehand]	-	10.27 ± 1.63 (4.00 – 12. 00)	-
	Copy of drawings with landmarks	-	67.37 ± 3.60 (51.00 – 70.00)	-
	Benton line orientation [30 lines]	27.40 ± 2.61 (18.00 – 30.00)	-	-
Mood and behavior	BDI	5.40 ± 4.68 (0.00 – 24.00)	7.26 ± 4.94 (0.00 – 23.00)	0.31
	Apathy Rating Scale	-	6.33 ± 5.10 (0.00 – 19. 00)	-
	SCL-90-R [Total]	28.95 ± 30.64 (2.00 – 163.00)	-	-

Values are reported as mean ± standard deviation (range). Differences in sociodemographic data were assessed using ANOVA models or Chi-squared test (p<0.05). On the other hand, differences in neuropsychological profile between young and older healthy adults were assessed using one-way ANOVA corrected for age, sex and education (p<0.05). P values were adjusted for Bonferroni- multiple comparison. *Abbreviations*: BDI= Beck Depression Inventory; CPM= coloured progressive matrices; MCST= Modified Card Sorting test; M= Men; MMSE= Mini Mental State Examination; RAVLT= Rey Auditory Verbal Learning Test; SCL-90-R=Symptom Checklist-90-Revised, W= Women.

Table 2. MRI acquisition parameters.

Milan	Philips Medical System Intera 3T scan				
	3D T2-weighted SE	3D FLAIR	3D T1-weighted TFE	Diffusion weighted sequence	T2*-weighted single-shot EPI sequence (RS fMRI)
Repetition time (msec)	2500	4800	7	5900	1567
Echo time (msec)	330	267	3.2	78	35
Flip angle	-	90°	9°	-	70°
Section thickness (mm)	1	1	1	2.3	3
No. of sections	192	192	204	56	48 for 320 volumes
Matrix	256x256	256x256	256x240	112x85	-
Field of view (mm^2)	256x256	256x256	256x240	240x232	240x240
Diffusion gradient directions	-	-	-	6/30/60	-
b value sec/mm^2	-	-	-	700/1000/2855	-

Abbreviations: FFE= fast field echo; FLAIR= fluid-attenuated inversion recovery; MRI= magnetic resonance imaging; msec= millisecond; mm= millimeter; No= number; RS fMRI= resting state functional MRI; SE=spin echo; sec=second.

Table 3. Rank of the cortical regions based on their cortical thinning across lifespan.

Desikan regions	Final Rank	Desikan regions	Final Rank
L parahippocampal	66	L inferior parietal	33
R pars triangularis	65	R rostral anterior cingulate	32
R superior temporal	64	R lateral occipital	31
R middle temporal	63	L pars triangularis	30
R superior frontal	62	L lateral occipital	29
L middle temporal	61	R precentral	28
L superior temporal	60	R pars orbitalis	27
R pars opercularis	59	L lateral orbitofrontal	26
L transverse temporal	58	L lingual	25
R parahippocampal	57	L precentral	24
R precuneus	56	R inferior temporal	23
R insula	55	L medial orbitofrontal	22
R bankssts	54	L frontal pole	21
L fusiform	53	L posterior cingulate	20
L pars opercularis	52	R paracentral	19
L isthmus cingulate	51	R lingual	18
R isthmus cingulate	50	L superior parietal	17
R supramarginal	49	L postcentral	16
L bankssts	48	R entorhinal	15
R posterior cingulate	47	R postcentral	14
R fusiform	46	L inferior temporal	13
L insula	45	R superior parietal	12
L temporal pole	44	L paracentral	11
L supramarginal	43	R temporal pole	10
R transverse temporal	42	L cuneus	9
L precuneus	41	R medial orbitofrontal	8
L superior frontal	40	R caudal anterior cingulate	7
L pars orbitalis	39	L middle frontal	6
L entorhinal	38	R cuneus	5
R middle frontal	37	R frontal pole	4
R lateral orbitofrontal	36	L pericalcarine	3
L rostral anterior cingulate	35	R pericalcarine	2
R inferior parietal	34	L caudal anterior cingulate	1

Considered cortical regions were ordered by the region that varies the least (position 1) to that which varies the most (position 66), based on rank variation of each brain region. The rank variation has been calculated as the difference between the rank position at the end of the observed timeframe and the rank position at the beginning of the observed timeframe. *Abbreviations*: L=left; R=right.

Table 4. Differences in cortical thickness of brain regions highly functionally connected to DMN and OCC hubs between young adults and older adults.

Highly functionally connected regions to	Young healthy adults	Older healthy adults	p value
DMN hubs			
R frontal pole	2.91 ± 0.27	2.71 ± 0.27	<0.001
L frontal pole	2.88 ± 0.20	2.70 ± 0.24	0.001
R caudal middle frontal	2.61 ± 0.11	2.46 ± 0.12	<0.001
L caudal middle frontal	2.56 ± 0.12	2.46 ± 0.14	0.02
R pars orbitalis	2.79 ± 0.18	2.62 ± 0.18	<0.001
L pars orbitalis	2.84 ± 0.21	2.66 ± 0.20	<0.001
R temporal pole	4.05 ± 0.20	3.84 ± 0.26	0.001
L temporal pole	3.99 ±0.23	3.78 ±0.28	0.002
L isthmus cingulate	2.55 ± 0.17	2.36 ± 0.21	<0.001
L pars triangularis	2.52 ±0.15	2.35 ± 0.17	<0.001
R supramarginal	2.66 ± 0.11	2.49 ± 0.12	<0.001
Occipital hubs			
R cuneus	1.83 ± 0.14	1.75 ± 0.13	0.01
L cuneus	1.86 ± 0.17	1.76 ± 0.13	0.01
R lingual	2.00 ± 0.11	1.92 ± 0.13	0.01
L lingual	2.00 ± 0.13	1.91 ± 0.13	0.001
R pericalcarine	1.48 ± 0.13	1.45 ± 0.13	0.04
L pericalcarine	1.52 ± 0.14	1.45 ± 0.13	0.003
L lateral occipital	2.25 ± 0.10	2.18 ±0.15	0.13

Values are means ± standard deviation. P values referred to analysis of variance models, followed by post-hoc pairwise comparisons (Bonferroni-corrected for multiple comparisons). Education and sex were included as covariates. *Abbreviations*: L=left; R=right.
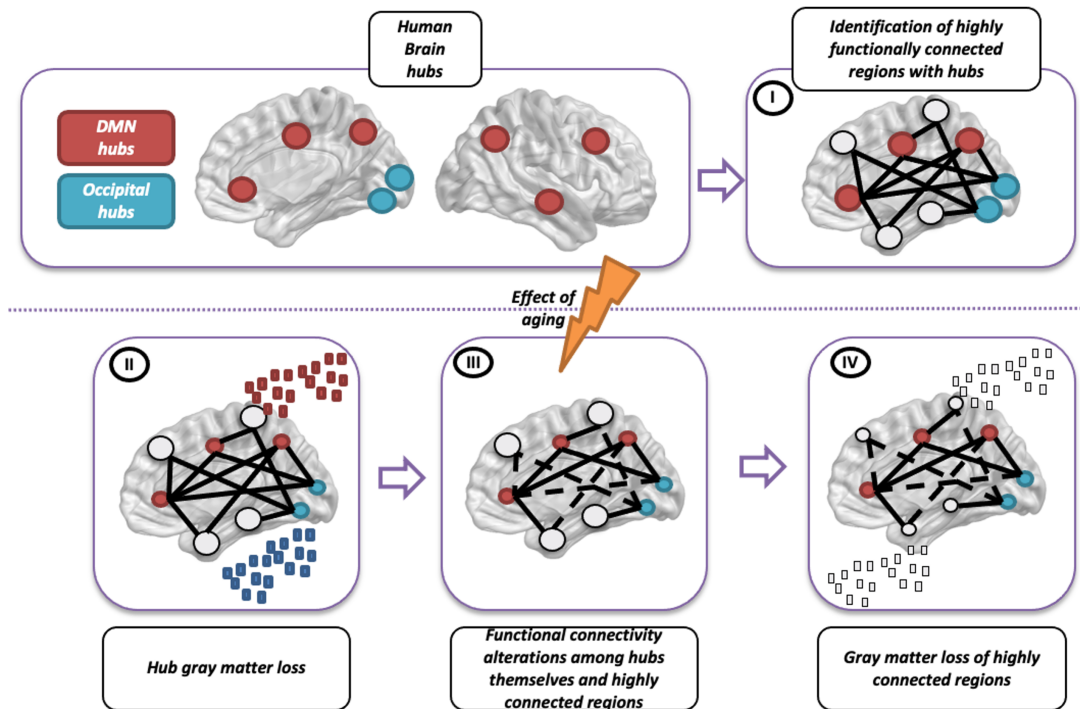
Figure 1. Study framework. Selection of hubs as pivotal regions of the functional brain network (Top row). **I.** Characterization of functional connectivity patterns of each hub to identify regions highly functionally connected to hubs. **II.** Hub grey matter loss: evaluation of cortical thickness changes over time for selected hubs and the remaining brain regions. **III.** Evaluation of functional connectivity alterations among hubs and highly connected regions during aging **IV.** The effect of functional vulnerability and atrophy of hubs on highly connected regions.
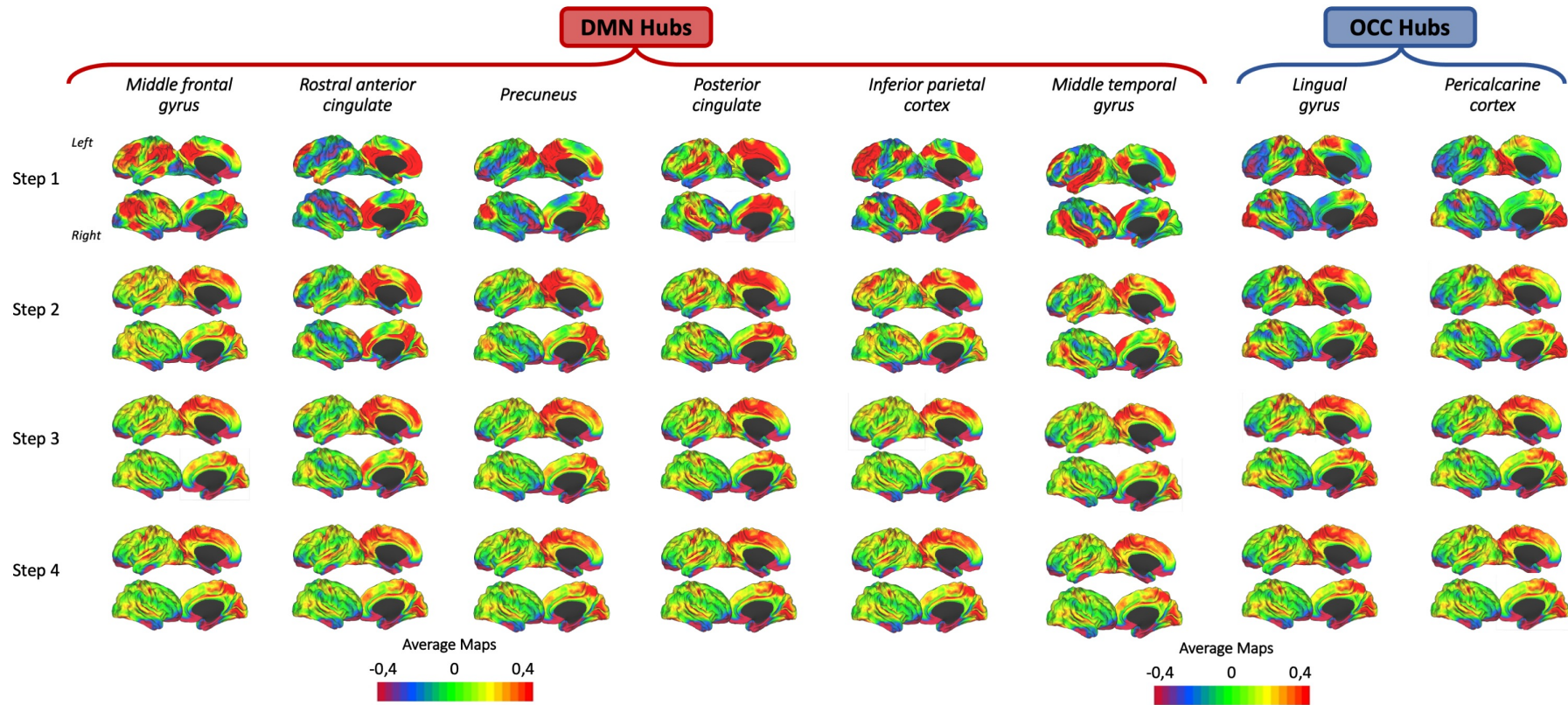
Figure 2. Stepwise functional connectivity average maps of young healthy adults. Cortical maps represent characterization of stepwise connectivity analysis from the DMN the OCC hubs in healthy young adults. Results are depicted in surface space per each of the eight well-known hubs. Yellow/red areas represent strong functional connectivity with the considered hub, whereas blue/violet areas represent weak functional connectivity.
Abbreviations: DMN = Default Mode Network; OCC = occipital.
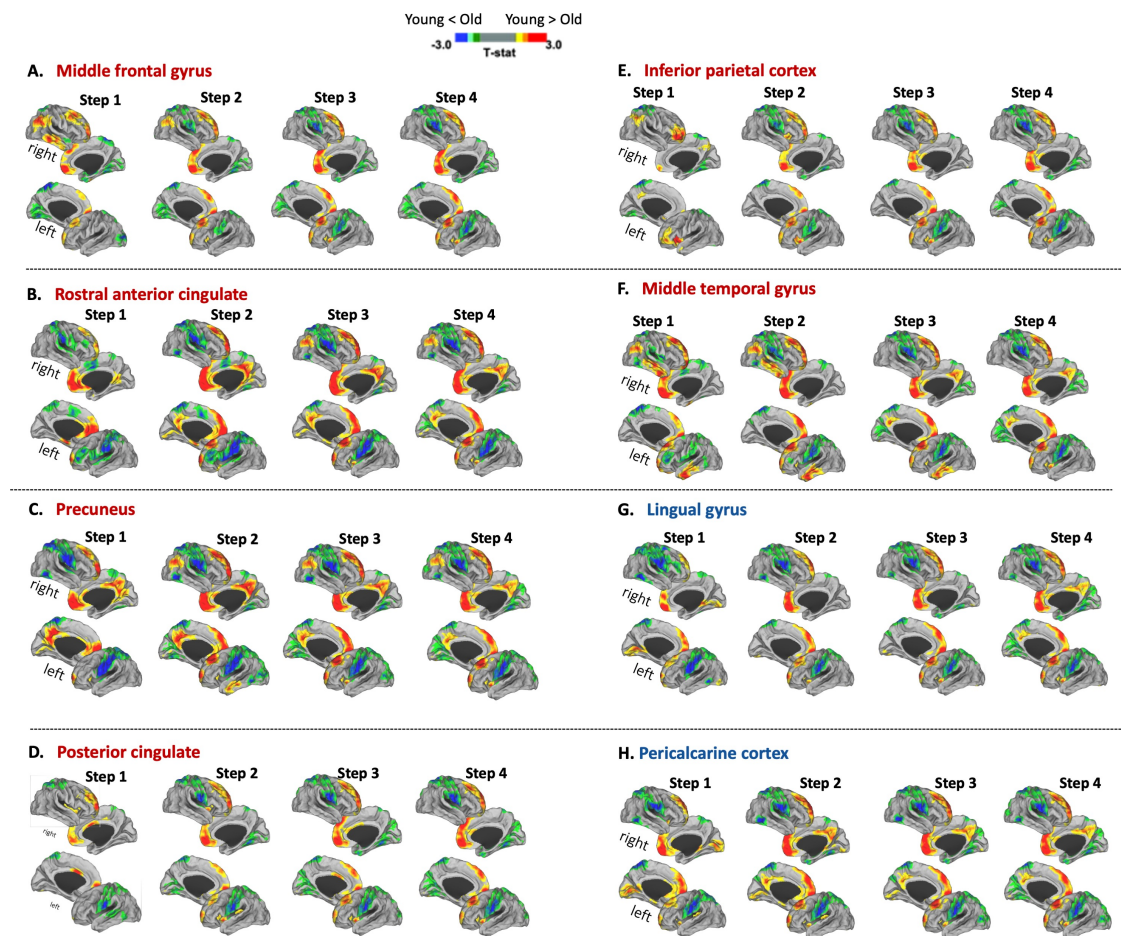
Figure 3. Differences between young and old healthy adults in stepwise functional connectivity of the eight hubs. Cortical maps represent the significant differences in stepwise functional connectivity values between young healthy adults and older healthy adults. Statistical analysis was adjusted for gender and education. Results were corrected for multiple comparisons using a threshold-free cluster enhancement method combined with nonparametric permutation testing at p<0.05 FWE-corrected. Color bars show the t-statistic applicable to the image. Red-yellow areas represent decreased functional connectivity in older adults relative to young adults, whereas blue/green areas represent enhanced functional connectivity in older adults compared to young.
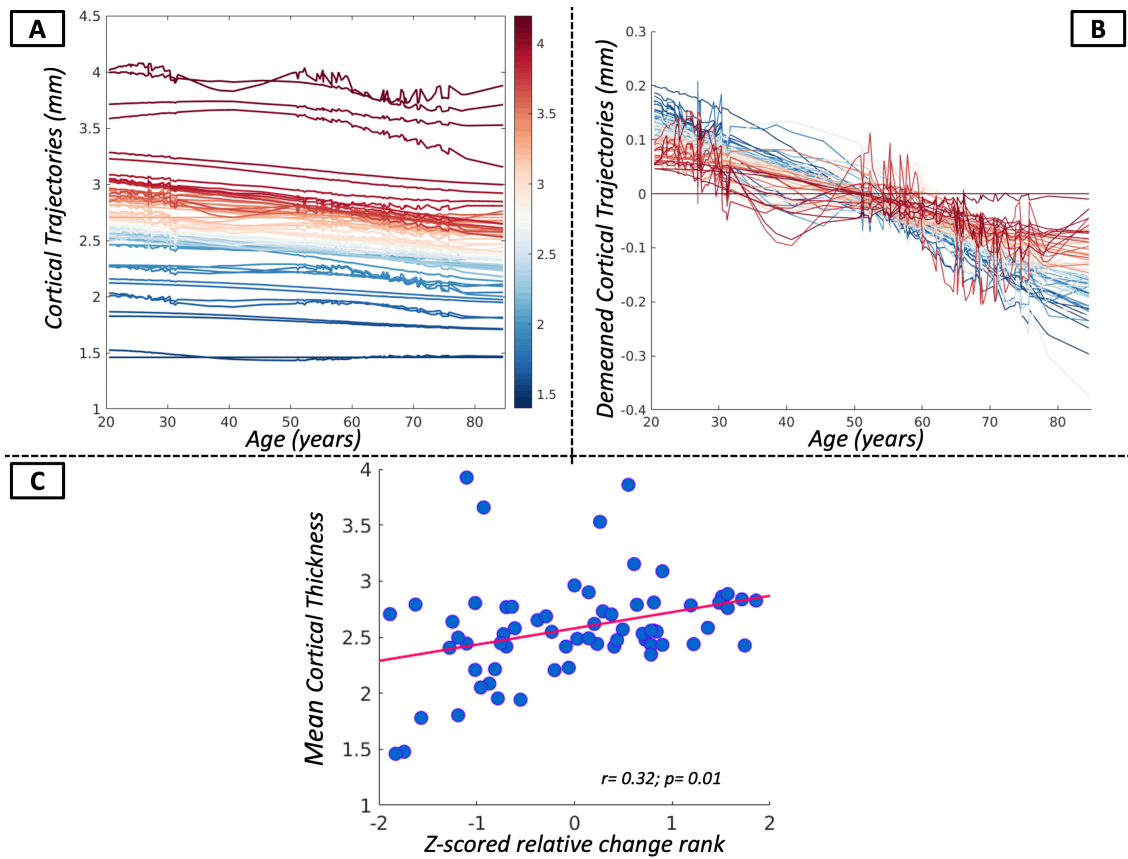
Figure 4. Modelling of cortical thickness trajectories over time. A. The estimated trajectories for each cortical region in the observed timeframe are reported, colored by mean cortical thickness (red= the highest value, blue= the lowest value). **B.** The demeaned estimated cortical trajectories for each region are reported (blue = greater change). **C.** Correlation between regional mean cortical thickness and the relative change over time.
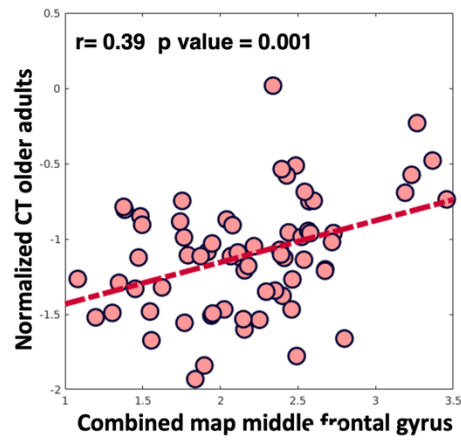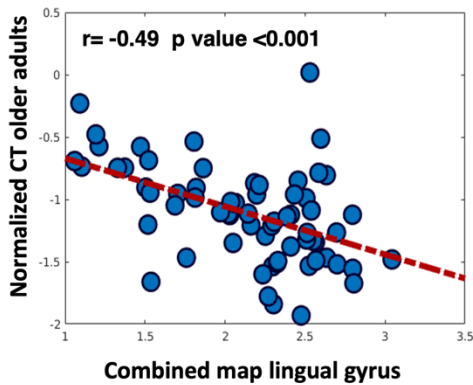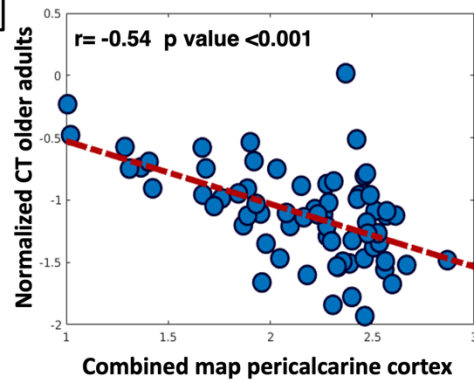
Figure 5. Correlation analysis between combined SFC maps of young group and normalized cortical values in older adults. Relationship between combined SFC maps middle frontal gyrus (DMN hub) **[A]** and OCC hubs **[B, C]** and the cortical thickness of older adults normalized relative to young adults. Abbreviations: DMN= Default Mode Network; OCC=occipital; SFC= Stepwise Functional Connectivity.
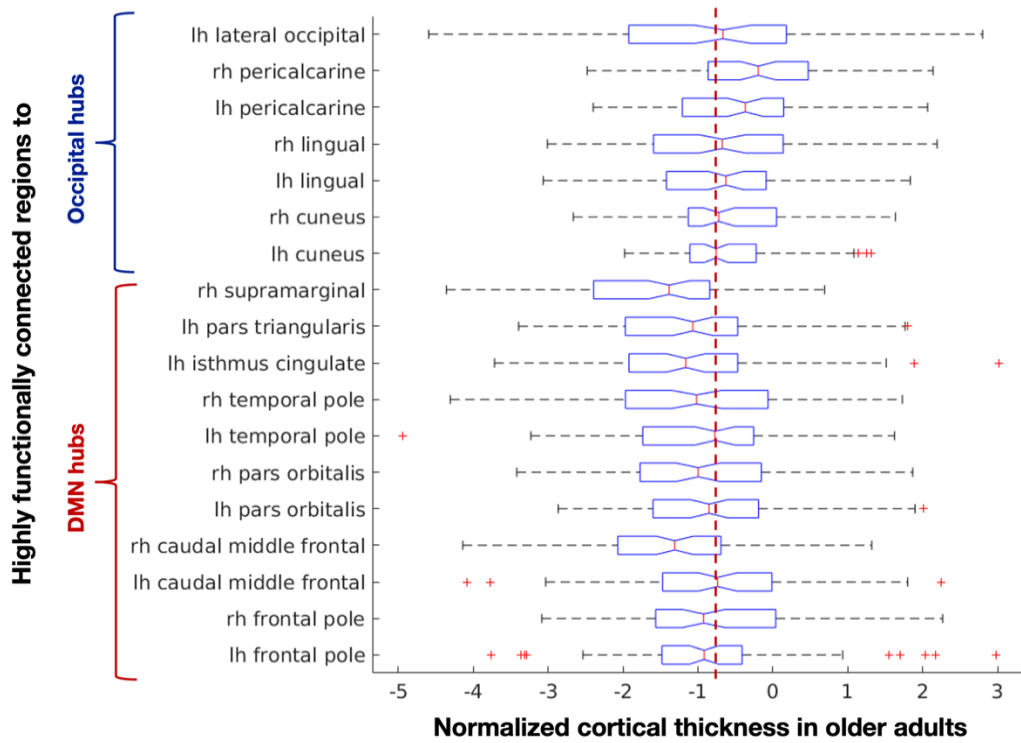
Figure 6. Boxplot of normalized cortical thickness values of hubs highly connected regions in older healthy adults. Cortical thickness value distribution of brain regions highly functionally connected to DMN hubs and OCC hubs. The red dotted line qualitatively highlights that cortical thickness values of the DMN-linked regions are lower than those of OCC-linked regions. *Abbreviations:* DMN= Default Mode Network; OCC=Occipital.

5.2 WHITE MATTER MICROSTRUCTURAL CHANGES IN HEALTHY AGING: A DTI AND NODDI STUDY *(preliminary data)*

INTRODUCTION

An accurate investigation of structural alterations in healthy aging plays a crucial role for detecting the major age-related effects on the complex brain microstructural architecture. The identification of such changes might help to understand the substrate and the regional variability of age-related degeneration. The goal of this preliminary study was to assess white matter (WM) integrity using different diffusion metrics able to identify the tracts affected during aging in a cohort of young and older adults.

METHODS

Participants

Forty-eight young healthy subjects, aged 20-31 years, and 65 older healthy adults, aged 40-85 years, were enrolled and underwent MRI scan.

Diffusion tensor (DT) MRI analysis

The diffusion-weighted data were skull-stripped using the Brain Extraction Tool implemented in FSL and were corrected for distortions caused by eddy currents and movements. The diffusion tensor was estimated on a voxel-by-voxel basis using diffusion-tensor imaging fit provided by the FMRIB Diffusion Toolbox. Maps of fractional anisotropy (FA) and mean diffusivity (MD) were computed.

Furthermore, using the NODDI Matlab Toolbox, Intra-cellular Volume Fraction (ICVF), Orientation Dispersion Index (ODI) and Isotropic Volume Fraction (ISO) maps were estimated using the Neurite Orientation Density and Dispersion Imaging (NODDI) model, providing a direct quantification of neurite morphology and its integrity.

To assess significant variability of the quantified metrics between the two groups of participants, a whole-brain Tract-Based Spatial Statistic (TBSS) analysis ($p<0.05$, family-wise error corrected, 5000 permutations) was conducted. The analysis was adjusted for sex and years of education.

RESULTS

A widespread age-related reduction of FA was detected in supratentorial regions in older healthy adults relative to young adults. On the other hand, a more focal decrease of ICVF was found in older adults relative to young adults in the WM frontal fibers,

specifically in the anterior sub-regions of corpus callosum, anterior corona radiata, frontal fibers of the superior longitudinal fasciculus, inferior fronto-occipital fasciculus and uncinate fasciculus. When the MD and the ISO maps were compared between the two groups, a widespread increase of MD and ISO was observed in older adults relative to young adults replicating the widespread WM alteration pattern obtained by FA results. Furthermore, an increased ODI of the WM fibers in older adults relative to young subjects was identified, involving not only the supratentorial regions but also the cerebellar architecture.

DISCUSSION

Thanks to the NODDI model, it was possible to identify a reduction of intra-neuritic volume (i.e., a loss of axon integrity) with aging, measured by the ICVF metric, specifically in the main frontal WM pathways. These findings suggest that the fibers of frontal regions are characterized by greater damage and are the most vulnerable to aging, followed by the parietal and temporal fibers. The information provided by multi-shell acquisition and multi-model reconstruction allowed us to better quantify the extent of WM architecture deterioration with aging, in terms of density and orientation dispersion. Considering multiple diffusion metrics may lead to a reliable profiling of the healthy brain aging.

6. GENERAL DISCUSSION

6.1 Discussion

I have applied graph theory-based approaches and connectomics to explore brain structural and functional changes across the ALS-FTD spectrum, as a model of neurodegeneration, with the goal of mapping spatiotemporal patterns of degeneration in these conditions. Moreover, I applied novel advanced MRI techniques on healthy aging to identify specific structural and functional brain changes in order to answer the question of whether neurodegeneration-related patterns of damage represent accelerated aging or a distinct process.

In **chapter 4,** we firstly investigated structural and functional brain network architecture in MND clinical phenotypes (chapter 4.1). Subsequently, I focused on the specific and more common phenotype of MND (i.e., ALS), exploring structural and functional network correlates of cognitive/behavioral impairment in patients within the ALS-FTD continuum. In particular, in **chapter 4.1**, we explored brain network structural and functional properties in the clinical variants of MND spectrum, using graph analysis and connectomics. Although graph theory-based approaches have been already used in patients with ALS, this was the first study to apply them in patients with PLS and PMA. Moreover, this methodology provides the potential to bridge the gap of the anatomo-functional link thanks to (1) the application of the same parcellation system, (2) the connectome reconstruction framework and (3) the applied statistical approach.

With such framework, different patterns of brain network changes per each clinical phenotype were revealed. ***Characterization of ALS***. ALS patients were characterized by altered structural global and lobar network properties and regional connectivity, with a great involvement of sensorimotor network, basal ganglia, frontal and temporal lobes. Furthermore, structural connectivity damage correlated with clinical measures of motor impairment. Such findings are consistent with previous DT MRI studies that reported as structural 'signatures' in ALS the involvement of primary motor regions, supplementary motor areas and basal ganglia (Buchanan *et al*, 2015). Moreover, functional connectivity alterations were found in sensorimotor, basal ganglia and frontal areas, consistent with the existing literature (Geevasinga *et al*, 2017; Zhou *et al*, 2016) and suggesting, possibly, a maladaptive role. Such functional disruptions were mostly related to executive dysfunctions and behavioral disturbances. Finally, patients with ALS showed more widespread structural than functional damage relative to healthy controls, in support of

the hypothesis that structural alterations may be earlier in the course of the disease compared with functional network abnormalities (Jucker & Walker, 2013). These findings were independent of the presence of full-blown dementia, since the analysis was re-run excluding the eight ALS-FTD patients. ***Characterization of PLS***. Patients with PLS were characterized by widespread structural and functional alterations encompassing both motor and extra-motor areas with a pattern resembling classic ALS patients (Agosta *et al*, 2014b; Muller *et al*, 2018; Agosta *et al*, 2014a). ***Characterization of PMA.*** PMA patients showed preserved structural and functional connectomes. Such findings are consistent with previous studies (Rosenbohm *et al*, 2016; Spinelli *et al*, 2016) that could not demonstrate central nervous system damage in PMA patients, even using highly sensitive technique to local disruptions in the brain networks.

Based on the abovementioned findings that highlighted structurally and functionally extra-motor impairment in ALS, in **chapter 4.2** I applied multiparametric MRI techniques in order to provide a comprehensive characterization of the neural correlates of the cognitive impairment across the spectrum of ALS-FTD clinical presentations. A connectome-based approach was adopted, first, to identify the structural and functional connectivity signatures of ALS-cn and bvFTD (i.e., the two ends of this spectrum) and then, to characterize the alterations underlying mild cognitive/behavioral deficits and full-blown dementia in ALS patients, with the aid of mathematical models and single-subject analysis. An ALS-cn-like pattern was defined by a focused structural damage within the motor areas, confirming a "signature" pattern of frank decline in FA of the motor subnetworks (Illan-Gala *et al*, 2020; Muller *et al*, 2021). Such "signature" pattern supports the current view of this network as the epicenter of degenerative process of the disease (Brettschneider *et al*, 2013; Meier *et al*, 2020). By contrast, a bvFTD-like pattern was delineated by a widespread structural damage and decreased functional connectivity, specifically in frontal, temporal and parietal areas, in line with the current literature (Agosta *et al*, 2015; Filippi *et al*, 2017; Whitwell *et al*, 2011). Once delineated the ALS-cn-like and the bvFTD-like patterns of damage, the focus of the current study was on elucidating MRI connectomic underpinnings of mild or full-blown cognitive deficits in ALS, possibly addressing the long-standing debate on the nature of cognitive deficits in the course of the disease, as an early or, rather, a late-stage feature.

Regarding the structural brain network, the presence of mild cognitive and/or behavioral impairment in ALS patients did not contribute significantly to an additional microstructural damage relative to ALS-cn with otherwise comparable clinical characteristics – including measures of motor impairment and disease duration. Indeed, the study highlighted shared structural damage between ALS-ci/bi and ALS-cn patients, involving mainly the motor networks. By contrast, the analysis of functional connectivity alterations played an important role for the differentiation of ALS-ci/bi from ALS-cn. ALS-ci/bi patients showed a rearrangement of the functional networks, revealing enhanced functional connectivity within motor areas and decreased connectivity in the frontotemporal networks. Such findings support the maladaptive role of such functional rearrangements in ALS-ci/bi, as previously hypothesized (Menke *et al*, 2018). Therefore, ALS-ci/bi might be considered as a phenotypic variant of ALS, rather than a consequence of disease worsening (Chio *et al*, 2019; Lule *et al*, 2018), in agreement with one of the few longitudinal studies (Elamin *et al*, 2013). In contrast with ALS-ci/bi cases, when ALS patients had co-occurrent dementia (ALS-FTD), our study has outlined not only a pattern of microstructural damage involving the motor networks (i.e., the characteristic ALS-cn-like pattern), but also a disruption of frontal, temporal, parietal and striatal circuits, both from a structural and a functional point of view – therefore, resembling the bvFTD-like pattern (Saxon *et al*, 2020). In this study, multiparametric connectome-based approaches provided novel pathophysiological insights and biomarkers of cognitive dysfunction in the context of ALS-FTD. Although connectivity data alone cannot fully address the homogeneity or heterogeneity of this spectrum, our findings suggest a maladaptive role of functional rearrangements in ALS-ci/bi concomitantly with similar structural alterations compared to ALS-cn, supporting the hypothesis that ALS-ci/bi might be considered as a phenotypic variant of ALS, rather than a consequence of disease worsening.

In **Chapter 5**, advanced and novel MRI techniques have been applied to understand the role played by healthy aging, studying the age-related vulnerability of the human brain connectome. The aim was to evaluate as aging affects functional connectivity of hubs, pivotal regions in the human connectome, and how such effects influence the vulnerability and structural changes of the whole brain. I found decreased functional connectivity alterations in older adults among hubs themselves and regions, which are

mainly distributed within the DMN. These findings find wide acceptance with previous studies, suggesting that hubs DMN regions are more vulnerable to aging effect and easily affected by neurodegenerative disorders (Crossley *et al*, 2014; Damoiseaux, 2017; Siman-Tov *et al*, 2016; Song *et al*, 2014). Moving to structural changes, decreased cortical thickness across the majority of the cortex was found, in agree with the current literature (Fjell & Walhovd, 2010; Salat *et al*, 2004; Shaw *et al*, 2016). I also observed that DMN hubs were among the brain regions that changed the most (Fjell *et al*, 2014), whereas OCC hubs showed a quite spared cortical thickness across lifespan, in line with previous study(Shaw *et al.*, 2016). The combination of multimodal information of hubs atrophy and their functional connectivity pattern allowed us to delineate the vulnerability of the remaining brain regions. I observed that regions highly functionally connected to DMN hubs were characterized by greater cortical thinning relative to those brain regions highly functionally connected to OCC hubs, that, even though they showed mild cortical thinning, resulted more spared. Present findings are consistent with the "last in, first out" hypothesis, according to which the prefrontal-inferior parietal-temporal brain areas, that are late-maturing regions, are preferentially the first to be vulnerable to aging (Douaud *et al*, 2014; Raz *et al*, 2005).

Finally, in **chapter 5.2** I assessed white matter integrity using novel and advanced diffusion metrics, able to identify the tracts affected during aging. The identification of such changes might help to understand the substrate and the regional variability of age-related degeneration. The NODDI model was applied on multi-shell diffusion-weighted data of young and older healthy subjects. Such model provided a direct quantification of neurite morphology and its integrity. The information provided by multi-shell acquisition and multi-model reconstruction allowed us to better quantify the extent of WM architecture deterioration with aging, in terms of density and orientation dispersion. Such preliminary results suggest that the fibers of frontal regions are characterized by greater damage and are the most vulnerable to aging, followed by the parietal and temporal fibers, once again, in support of the theory of "last in, first out" (Raz *et al.*, 2005).

6.2 Conclusions

In summary, the studies included in this thesis provide novel information about neurodegenerative diseases, including MND and FTD, and healthy aging.

We have shown that graph analysis and connectomics may help in mapping structural and functional brain network organization in healthy conditions and in detecting alterations in different pathological conditions. Such tools helped also in characterizing differences between clinical variants of the MND spectrum and in elucidating the neural correlates of the cognitive impairment in the ALS-FTD clinical spectrum. Furthermore, by applying up-to-date MRI techniques, I proposed a model that integrated the information of the functional connectome vulnerability with gray matter cortical thinning and explored white matter integrity in healthy aging.

We have observed disease-specific patterns of functional and structural network topology and connectivity alterations in ALS, PLS and PMA, through a multimodal neuroimaging approach. Moreover, combining mathematical models and multimodal connectomic techniques, I showed disease-specific functional and structural patterns in ALS with the only motor impairment and in the bvFTD, which are considered the two opposite ends of a clinical continuum. I might have even contributed significantly to the long-standing debate on the nature of cognitive deficits in the course of the ALS disease, as an early or, rather, a late-stage feature. Finally, I assessed the role of healthy aging, reveling potential patterns of vulnerability and pointing out how functional network rearrangements of brain hubs and their grey matter change trajectories across lifespan influence the functional and structural trend of changes of the remaining brain regions. In conclusion, thanks to NODDI model, it was possible to identify a reduction of intra-neuritic volume (i.e., a loss of axon integrity) with aging, as preliminary data. This may hold the promises to better elucidating the additive risk effect of the aging in neurodegeneration.

Albeit promising, the present findings need to be expanded by future studies aimed at clarifying even further the relationship between healthy aging and neurodegenerative diseases. Indeed, the study of the brain mechanisms underpinning healthy aging will help in delineating comprehensively mathematical models for predicting clinical evolution and allowing prompt intervention for patients.

REFERENCES

Agosta F, Canu E, Inuggi A, Chio A, Riva N, Silani V, Calvo A, Messina S, Falini A, Comi G *et al* (2014a) Resting state functional connectivity alterations in primary lateral sclerosis. *Neurobiol Aging* 35: 916-925

Agosta F, Galantucci S, Magnani G, Marcone A, Martinelli D, Antonietta Volonte M, Riva N, Iannaccone S, Ferraro PM, Caso F *et al* (2015) MRI signatures of the frontotemporal lobar degeneration continuum. *Hum Brain Mapp* 36: 2602-2614

Agosta F, Galantucci S, Riva N, Chio A, Messina S, Iannaccone S, Calvo A, Silani V, Copetti M, Falini A *et al* (2014b) Intrahemispheric and interhemispheric structural network abnormalities in PLS and ALS. *Hum Brain Mapp* 35: 1710-1722

Brettschneider J, Del Tredici K, Toledo JB, Robinson JL, Irwin DJ, Grossman M, Suh E, Van Deerlin VM, Wood EM, Baek Y *et al* (2013) Stages of pTDP-43 pathology in amyotrophic lateral sclerosis. *Annals of neurology* 74: 20-38

Buchanan CR, Pettit LD, Storkey AJ, Abrahams S, Bastin ME (2015) Reduced structural connectivity within a prefrontal-motor-subcortical network in amyotrophic lateral sclerosis. *Journal of magnetic resonance imaging : JMRI* 41: 1342-1352

Chio A, Moglia C, Canosa A, Manera U, Vasta R, Brunetti M, Barberis M, Corrado L, D'Alfonso S, Bersano E *et al* (2019) Cognitive impairment across ALS clinical stages in a population-based cohort. *Neurology* 93: e984-e994

Crossley NA, Mechelli A, Scott J, Carletti F, Fox PT, McGuire P, Bullmore ET (2014) The hubs of the human connectome are generally implicated in the anatomy of brain disorders. *Brain* 137: 2382-2395

Damoiseaux JS (2017) Effects of aging on functional and structural brain connectivity. *NeuroImage* 160: 32-40

Douaud G, Groves AR, Tamnes CK, Westlye LT, Duff EP, Engvig A, Walhovd KB, James A, Gass A, Monsch AU *et al* (2014) A common brain network links development, aging, and vulnerability to disease. *Proc Natl Acad Sci U S A* 111: 17648-17653

Elamin M, Bede P, Byrne S, Jordan N, Gallagher L, Wynne B, O'Brien C, Phukan J, Lynch C, Pender N *et al* (2013) Cognitive changes predict functional decline in ALS: a population-based longitudinal study. *Neurology* 80: 1590-1597

Filippi M, Basaia S, Canu E, Imperiale F, Meani A, Caso F, Magnani G, Falautano M, Comi G, Falini A *et al* (2017) Brain network connectivity differs in early-onset neurodegenerative dementia. *Neurology* 89: 1764-1772

Fjell AM, Walhovd KB (2010) Structural brain changes in aging: courses, causes and cognitive consequences. *Rev Neurosci* 21: 187-221

Fjell AM, Westlye LT, Grydeland H, Amlien I, Espeseth T, Reinvang I, Raz N, Dale AM, Walhovd KB, Alzheimer Disease Neuroimaging I (2014) Accelerating cortical thinning: unique to dementia or universal in aging? *Cereb Cortex* 24: 919-934

Geevasinga N, Korgaonkar MS, Menon P, Van den Bos M, Gomes L, Foster S, Kiernan MC, Vucic S (2017) Brain functional connectome abnormalities in amyotrophic lateral sclerosis are associated with disability and cortical hyperexcitability. *Eur J Neurol* 24: 1507-1517

Illan-Gala I, Montal V, Pegueroles J, Vilaplana E, Alcolea D, Dols-Icardo O, de Luna N, Turon-Sans J, Cortes-Vicente E, Martinez-Roman L *et al* (2020) Cortical microstructure in the amyotrophic lateral sclerosis-frontotemporal dementia continuum. *Neurology* 95: e2565-e2576

Jucker M, Walker LC (2013) Self-propagation of pathogenic protein aggregates in neurodegenerative diseases. *Nature* 501: 45-51

Lule D, Bohm S, Muller HP, Aho-Ozhan H, Keller J, Gorges M, Loose M, Weishaupt JH, Uttner I, Pinkhardt E *et al* (2018) Cognitive phenotypes of sequential staging in amyotrophic lateral sclerosis. *Cortex; a journal devoted to the study of the nervous system and behavior* 101: 163-171

Meier JM, van der Burgh HK, Nitert AD, Bede P, de Lange SC, Hardiman O, van den Berg LH, van den Heuvel MP (2020) Connectome-Based Propagation Model in Amyotrophic Lateral Sclerosis. *Annals of neurology* 87: 725-738

Menke RAL, Proudfoot M, Talbot K, Turner MR (2018) The two-year progression of structural and functional cerebral MRI in amyotrophic lateral sclerosis. *Neuroimage Clin* 17: 953-961

Muller HP, Agosta F, Gorges M, Kassubek R, Spinelli EG, Riva N, Ludolph AC, Filippi M, Kassubek J (2018) Cortico-efferent tract involvement in primary lateral sclerosis and amyotrophic lateral sclerosis: A two-centre tract of interest-based DTI analysis. *Neuroimage Clin* 20: 1062-1069

Muller HP, Lule D, Roselli F, Behler A, Ludolph AC, Kassubek J (2021) Segmental involvement of the corpus callosum in C9orf72-associated ALS: a tract of interest-based DTI study. *Ther Adv Chronic Dis* 12: 20406223211002969

Raz N, Lindenberger U, Rodrigue KM, Kennedy KM, Head D, Williamson A, Dahle C, Gerstorf D, Acker JD (2005) Regional brain changes in aging healthy adults: general trends, individual differences and modifiers. *Cereb Cortex* 15: 1676-1689

Rosenbohm A, Muller HP, Hubers A, Ludolph AC, Kassubek J (2016) Corticoefferent pathways in pure lower motor neuron disease: a diffusion tensor imaging study. *J Neurol* 263: 2430-2437

Salat DH, Buckner RL, Snyder AZ, Greve DN, Desikan RS, Busa E, Morris JC, Dale AM, Fischl B (2004) Thinning of the cerebral cortex in aging. *Cereb Cortex* 14: 721-730

Saxon JA, Thompson JC, Harris JM, Richardson AM, Langheinrich T, Rollinson S, Pickering-Brown S, Chaouch A, Ealing J, Hamdalla H *et al* (2020) Cognition and behaviour in frontotemporal dementia with and without amyotrophic lateral sclerosis. *J Neurol Neurosurg Psychiatry* 91: 1304-1311

Shaw ME, Sachdev PS, Anstey KJ, Cherbuin N (2016) Age-related cortical thinning in cognitively healthy individuals in their 60s: the PATH Through Life study. *Neurobiol Aging* 39: 202-209

Siman-Tov T, Bosak N, Sprecher E, Paz R, Eran A, Aharon-Peretz J, Kahn I (2016) Early Age-Related Functional Connectivity Decline in High-Order Cognitive Networks. *Front Aging Neurosci* 8: 330

Song J, Birn RM, Boly M, Meier TB, Nair VA, Meyerand ME, Prabhakaran V (2014) Age-related reorganizational changes in modularity and functional connectivity of human brain networks. *Brain connectivity* 4: 662-676
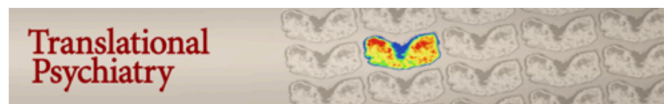
Spinelli EG, Agosta F, Ferraro PM, Riva N, Lunetta C, Falzone YM, Comi G, Falini A, Filippi M (2016) Brain MR Imaging in Patients with Lower Motor Neuron-Predominant Disease. *Radiology* 280: 545-556

Whitwell JL, Jack CR, Jr., Parisi JE, Knopman DS, Boeve BF, Petersen RC, Dickson DW, Josephs KA (2011) Imaging signatures of molecular pathology in behavioral variant frontotemporal dementia. *J Mol Neurosci* 45: 372-378

Zhou C, Hu X, Hu J, Liang M, Yin X, Chen L, Zhang J, Wang J (2016) Altered Brain Network in Amyotrophic Lateral Sclerosis: A Resting Graph Theory-Based Network Study at Voxel-Wise Level. *Frontiers in neuroscience* 10: 204

7. ADDITIONAL STUDIES

1) Harrewijn A, Cardinale EM, Groenewold NA, Bas-Hoogendam JM, Aghajani M, Hilbert K, Cardoner N, Porta-Casteràs D, Gosnell S, Salas R, Jackowski AP, Pan PM, Salum GA, Blair KS, Blair JR, Hammoud MZ, Milad MR, Burkhouse KL, Phan KL, Schroeder HK, Strawn JR, Beesdo-Baum K, Jahanshad N, Thomopoulos SI, Buckner R, Nielsen JA, Smoller JW, Soares JC, Mwangi B, Wu MJ, Zunta-Soares GB, Assaf M, Diefenbach GJ, Brambilla P, Maggioni E, Hofmann D, Straube T, Andreescu C, Berta R, Tamburo E, Price RB, Manfro GG, Agosta F, Canu E, **<u>Cividini C</u>**, Filippi M, Kostić M, Munjiza Jovanovic A, Alberton BAV, Benson B, Freitag GF, Filippi CA, Gold AL, Leibenluft E, Ringlein GV, Werwath KE, Zwiebel H, Zugman A, Grabe HJ, Van der Auwera S, Wittfeld K, Völzke H, Bülow R, Balderston NL, Ernst M, Grillon C, Mujica-Parodi LR, van Nieuwenhuizen H, Critchley HD, Makovac E, Mancini M, Meeten F, Ottaviani C, Ball TM, Fonzo GA, Paulus MP, Stein MB, Gur RE, Gur RC, Kaczkurkin AN, Larsen B, Satterthwaite TD, Harper J, Myers M, Perino MT, Sylvester CM, Yu Q, Lueken U, Veltman DJ, Thompson PM, Stein DJ, Van der Wee NJA, Winkler AM, Pine DS. Cortical and subcortical brain structure in generalized anxiety disorder: findings from 28 research sites in the ENIGMA-Anxiety Working Group. Transl Psychiatry. 2021 Oct 1;11(1):502. doi: 10.1038/s41398-021-01622-1. PMID: 34599145; PMCID: PMC8486763.

Cortical and subcortical brain structure in generalized anxiety disorder: findings from 28 research sites in the ENIGMA-Anxiety Working Group

ABSTRACT

The goal of this study was to compare brain structure between individuals with generalized anxiety disorder (GAD) and healthy controls. Previous studies have generated inconsistent findings, possibly due to small sample sizes, or clinical/analytic heterogeneity. To address these concerns, we combined data from 28 research sites worldwide through the ENIGMA-Anxiety Working Group, using a single, pre-registered mega-analysis. Structural magnetic resonance imaging data from children and adults (5-90 years) were processed using FreeSurfer. The main analysis included the regional and vertex-wise cortical thickness, cortical surface area, and subcortical volume as dependent variables, and GAD, age, age-squared, sex, and their interactions as independent variables. Nuisance variables included IQ, years of education, medication use, comorbidities, and global brain measures. The main analysis (1020 individuals with GAD and 2999 healthy controls) included random slopes per site and random intercepts per scanner. A secondary analysis (1112 individuals with GAD and 3282 healthy controls) included fixed slopes and random intercepts per scanner with the same variables. The main analysis showed no effect of GAD on brain structure, nor interactions involving GAD, age, or sex. The secondary analysis showed increased volume in the right ventral

diencephalon in male individuals with GAD compared to male healthy controls, whereas female individuals with GAD did not differ from female healthy controls. This mega-analysis combining worldwide data showed that differences in brain structure related to GAD are small, possibly reflecting heterogeneity or those structural alterations are not a major component of its pathophysiology.

2) Spinelli EG, Ghirelli A, Basaia S, **Cividini C**, Riva N, Canu E, Castelnovo V, Domi T, Magnani G, Caso F, Caroppo P, Prioni S, Rossi G, Tremolizzo L, Appollonio I, Silani V, Carrera P, Filippi M, Agosta F. Structural MRI Signatures in Genetic Presentations of the Frontotemporal Dementia/Motor Neuron Disease Spectrum. Neurology. 2021 Oct 19;97(16):e1594-e1607. doi: 10.1212/WNL.0000000000012702. Epub 2021 Sep 20. PMID: 34544819; PMCID: PMC8548958.

Structural MRI Signatures in Genetic Presentations of the Frontotemporal Dementia/Motor Neuron Disease Spectrum

Edoardo Gioele Spinelli, MD, Alma Ghirelli, MD, Silvia Basaia, PhD, Camilla Cividini, MSc, Nilo Riva, MD, PhD, Elisa Canu, PhD, Veronica Castelnovo, MSc, Teuta Domi, PhD, Giuseppe Magnani, MD, Francesca Caso, MD, PhD, Paola Caroppo, MD, PhD, Sara Prioni, MSc, Giacomina Rossi, PhD, Lucio Tremolizzo, MD, Ildebrando Appollonio, MD, Vincenzo Silani, MD, Paola Carrera, BSc, Massimo Filippi, MD, and Federica Agosta, MD, PhD[✉]

ABSTRACT

Background and objectives: To assess cortical, subcortical, and cerebellar gray matter (GM) atrophy using MRI in patients with disorders of the frontotemporal lobar degeneration (FTLD) spectrum with known genetic mutations.

Methods: Sixty-six patients carrying FTLD-related mutations were enrolled, including 44 with pure motor neuron disease (MND) and 22 with frontotemporal dementia (FTD). Sixty-one patients with sporadic FTLD (sFTLD) matched for age, sex, and disease severity with genetic FTLD (gFTLD) were also included, as well as 52 healthy controls. A whole-brain voxel-based morphometry (VBM) analysis was performed. GM volumes of subcortical and cerebellar structures were obtained.

Results: Compared with controls, GM atrophy on VBM was greater and more diffuse in genetic FTD, followed by sporadic FTD and genetic MND cases, whereas patients with sporadic MND (sMND) showed focal motor cortical atrophy. Patients carrying C9orf72 and GRN mutations showed the most widespread cortical volume loss, in contrast with GM sparing in SOD1 and TARDBP. Globally, patients with gFTLD showed greater atrophy of parietal cortices and thalami compared with sFTLD. In volumetric analysis, patients with gFTLD showed volume loss compared with sFTLD in the caudate nuclei and thalami, in particular comparing C9-MND with sMND cases. In the cerebellum, patients with gFTLD showed greater atrophy of the right lobule VIIb than sFTLD. Thalamic volumes of patients with gFTLD with a C9orf72 mutation showed an inverse correlation with Frontal Behavioral Inventory scores.

Discussion: Measures of deep GM and cerebellar structural involvement may be useful markers of gFTLD, particularly C9orf72-related disorders, regardless of the clinical presentation within the FTLD spectrum.

3) Cecchetti G, Agosta F, Basaia S, **Cividini C**, Cursi M, Santangelo R, Caso F, Minicucci F, Magnani G, Filippi M. Resting-state electroencephalographic biomarkers of Alzheimer's disease. Neuroimage Clin. 2021;31:102711. doi: 10.1016/j.nicl.2021.102711. Epub 2021 May 29. PMID: 34098525; PMCID: PMC8185302.
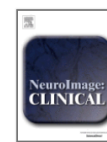
Resting-state electroencephalographic biomarkers of Alzheimer's disease

Giordano Cecchetti [a, b, c, d, e, 1], Federica Agosta [a, d, e, 2], Silvia Basaia [d, 3], Camilla Cividini [d, e, 4], Marco Cursi [b, 5], Roberto Santangelo [a, b], Francesca Caso [a, 6], Fabio Minicucci [b], Giuseppe Magnani [a], Massimo Filippi [a, b, c, d, e] [7] ✉

ABSTRACT

Objective: We evaluated the value of resting-state EEG source biomarkers to characterize mild cognitive impairment (MCI) subjects with an Alzheimer's disease (AD)-like cerebrospinal fluid (CSF) profile and to track neurodegeneration throughout the AD continuum. We further applied a resting-state functional MRI (fMRI)-driven model of source reconstruction and tested its advantage in terms of AD diagnostic accuracy.

Methods: Thirty-nine consecutive patients with AD dementia (ADD), 86 amnestic MCI, and 33 healthy subjects enter the EEG study. All ADD subjects, 37 out of 86 MCI patients and a distinct group of 53 healthy controls further entered the fMRI study. MCI subjects were divided according to the CSF phosphorylated tau/β amyloid-42 ratio (MCIpos: $\geq$ 0.13, MCIneg: < 0.13). Using Exact low-resolution brain electromagnetic tomography (eLORETA), EEG lobar current densities were estimated at fixed frequencies and analyzed. To combine the two imaging techniques, networks mostly affected by AD pathology were identified using Independent Component Analysis applied to fMRI data of ADD subjects. Current density EEG analysis within ICA-based networks at selected frequency bands was performed. Afterwards, graph analysis was applied to EEG and fMRI data at ICA-based network level.

Results: ADD patients showed a widespread slowing of spectral density. At a lobar level, MCIpos subjects showed a widespread higher theta density than MCIneg and healthy subjects; a lower beta2 density than healthy subjects was also found in parietal and occipital lobes. Evaluating EEG sources within the ICA-based networks, alpha2 band distinguished MCIpos from MCIneg, ADD and healthy subjects with good accuracy. Graph analysis on EEG data showed an alteration of connectome configuration at theta frequency in ADD and MCIpos patients and a progressive disruption of connectivity at alpha2 frequency throughout the AD continuum.

Conclusions: Theta frequency is the earliest and most sensitive EEG marker of AD pathology. Furthermore, EEG/fMRI integration highlighted the role of alpha2 band as potential neurodegeneration biomarker.

4) De Micco R, Agosta F, Basaia S, Siciliano M, **Cividini C**, Tedeschi G, Filippi M, Tessitore A. Functional Connectomics and Disease Progression in Drug-Naïve Parkinson's Disease Patients. Mov Disord. 2021 Jul;36(7):1603-1616. doi: 10.1002/mds.28541. Epub 2021 Feb 27. PMID: 33639029.

Functional Connectomics and Disease Progression in Drug-Naïve Parkinson's Disease Patients

Rosa De Micco MD, PhD, Federica Agosta MD, PhD, Silvia Basaia PhD, Mattia Siciliano PhD, Camilla Cividini MSc, Gioacchino Tedeschi MD, Massimo Filippi MD, PhD, Alessandro Tessitore MD, PhD ✉

ABSTRACT

Background: Functional brain connectivity alterations may be detectable even before the occurrence of brain atrophy, indicating their potential as early markers of pathological processes.

Objective: We aimed to determine the whole-brain network topologic organization of the functional connectome in a large cohort of drug-naïve Parkinson's disease (PD) patients using resting-state functional magnetic resonance imaging and to explore whether baseline connectivity changes may predict clinical progression.

Methods: One hundred and forty-seven drug-naïve, cognitively unimpaired PD patients were enrolled in the study at baseline and compared to 38 age- and gender-matched controls. Non-hierarchical cluster analysis using motor and non-motor data was applied to stratify PD patients into two subtypes: 77 early/mild and 70 early/severe. Graph theory analysis and connectomics were used to assess global and local topological network properties and regional functional connectivity at baseline. Stepwise multivariate regression analysis investigated whether baseline functional imaging data were predictors of clinical progression over 2 years.

Results: At baseline, widespread functional connectivity abnormalities were detected in the basal ganglia, sensorimotor, frontal, and occipital networks in PD patients compared to controls. Decreased regional functional connectivity involving mostly striato-frontal, temporal, occipital, and limbic connections differentiated early/mild from early/severe PD patients. Connectivity changes were found to be independent predictors of cognitive progression at 2-year follow-up.

Conclusions: Our findings revealed that functional reorganization of the brain connectome occurs early in PD and underlies crucial involvement of striatal projections. Connectomic measures may be helpful to identify a specific PD patient subtype, characterized by severe motor and non-motor clinical burden as well as widespread functional connectivity abnormalities.

5) Castelnovo V, Canu E, Riva N, Poletti B, **Cividini C**, Fontana A, Solca F, Silani V, Filippi M, Agosta F. Progression of cognitive and behavioral disturbances in motor neuron diseases assessed using standard and computer-based batteries. Amyotroph Lateral Scler Frontotemporal Degener. 2021 May;22(3-4):223-236. doi: 10.1080/21678421.2020.1867179. Epub 2021 Jan 19. PMID: 33463386.

Progression of cognitive and behavioral disturbances in motor neuron diseases assessed using standard and computer-based batteries

Veronica Castelnovo, Elisa Canu, Nilo Riva, Barbara Poletti , Camilla Cividini, Andrea Fontana, Federica Solca, Vincenzo Silani , Massimo Filippi & **Federica Agosta** ...show less

ABSTRACT

Objective: Detecting and monitoring cognitive and behavioral deficits in motor neuron diseases (MND) is critical due to their considerable clinical impact. In this scenario, computer-based batteries may play an important role. In this study, we investigated the progression of cognitive and behavioral deficits in MND patients using both standard and computer-based neuropsychological batteries.

Methods: This is a retrospective study on 74 MND patients (52 amyotrophic lateral sclerosis [ALS], 12 primary lateral sclerosis [PLS], and 10 progressive muscular atrophy [PMA]) who were followed up for 12 months and underwent up to three cognitive/behavioral assessments, 6 months apart, including standard and/or computerized based (the Test of Attentional Performance [TAP]) batteries. Behavioral/cognitive changes were investigated over time using generalized linear model for longitudinal data accounting for time and revised-ALS Functional Rating Scale.

Results: Over 12 months, ALS patients showed a global cognitive decline (Mini Mental State Examination) at the standard battery and reduced performance in the alertness, sustained and divided attention, go/nogo, cross-modal and incompatibility TAP tasks. Most of these findings remained significant when ALSFRS-R changes over time were included as covariate in the analyses. ALS patients did not show significant behavioral abnormalities over time. No cognitive and behavioral changes were found in PLS and PMA cases.

Conclusions: Computer-based neuropsychological evaluations are able to identify subtle cognitive changes in ALS, unique to this condition. This study highlights the need of specific, accurate and well-tolerated tools for the monitoring of cognitive deficits in MND.

6) Filippi M, <u>**Cividini C**</u>, Agosta F. Deep learning: a turning point in acute neurology. Lancet Digit Health. 2020 Jun;2(6):e273-e274. doi: 10.1016/S2589-7500(20)30106-0. Epub 2020 May 14. PMID: 33328119.
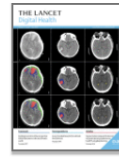
Comment

Deep learning: a turning point in acute neurology

Massimo Filippi [a, b, c, d] ✉, Camilla Cividini [c, d], Federica Agosta [c, d]

- [a] Neurology Unit, Institute of Experimental Neurology, Division of Neuroscience, IRCCS San Raffaele Scientific Institute, Milan, Italy
- [b] Neurophysiology Unit, Institute of Experimental Neurology, Division of Neuroscience, IRCCS San Raffaele Scientific Institute, Milan, Italy
- [c] Neuroimaging Research Unit, Institute of Experimental Neurology, Division of Neuroscience, IRCCS San Raffaele Scientific Institute, Milan, Italy
- [d] Vita-Salute San Raffaele University, Milan, Italy

7) Canu E, Bessi V, Calderaro D, Simoni D, Castelnovo V, Leocadi M, Padiglioni S, Mazzeo S, **Cividini C**, Nacmias B, Sorbi S, Filippi M, Agosta F. Early functional MRI changes in a prodromal semantic variant of primary progressive aphasia: a longitudinal case report. J Neurol. 2020 Oct;267(10):3100-3104. doi: 10.1007/s00415-020-10053-9. Epub 2020 Jul 10. PMID: 32651673.

Early functional MRI changes in a prodromal semantic variant of primary progressive aphasia: a longitudinal case report

Elisa Canu, Valentina Bessi, Davide Calderaro, David Simoni, Veronica Castelnovo, Michela Leocadi, Sonia Padiglioni, Salvatore Mazzeo, Camilla Cividini, Benedetta Nacmias, Sandro Sorbi, Massimo Filippi & Federica Agosta ✉

ABSTRACT

Objective: To assess longitudinal patterns of brain functional MRI (fMRI) activity in a case of prodromal semantic variant of a primary progressive aphasia (svPPA).

Methods: Clinical, cognitive and neuroimaging data (T1-weighted and task-based fMRI during silent naming [SN] and object knowledge [OK]) were obtained at baseline, month 8 and month 16 from a 49-year-old lady presenting with anomias and evolving to overt svPPA in 8 months.

Results: At baseline, the patient showed isolated anomias and mild left anterior temporal pole atrophy. During SN-fMRI, she showed bilateral temporal and left inferior frontal gyri (iFG) activations. During OK-fMRI, we observed normal performance and the recruitment of bilateral posterior hippocampi, iFG and left middle orbitofrontal gyrus (mOFG). At month 8, the patient received a diagnosis of svPPA and showed isolated right iFG activity during SN-fMRI, and a borderline performance during OK-fMRI together with a disappearance of mOFG recruitment. At the last visit (after 7-month language therapy), the patient showed a stabilization of naming disturbances, and, compared to previous visits, an increased left iFG recruitment during SN-fMRI. During OK-fMRI, she performed abnormally and did not show the activity of mOFG and iFG. Across all visits, brain atrophy remained stable.

Conclusions: This case report showed longitudinal fMRI patterns during semantic-related tasks from prodromal to overt svPPA. Frontal brain recruitment may represent a compensatory mechanism in patients with early svPPA, which is likely to be reinforced by language-therapy. Brain fMRI is more sensitive compared with structural MRI to detect progressive brain changes associated with disease and treatment.

8) Zugman A, Harrewijn A, Cardinale EM, Zwiebel H, Freitag GF, Werwath KE, Bas-Hoogendam JM, Groenewold NA, Aghajani M, Hilbert K, Cardoner N, Porta-Casteràs D, Gosnell S, Salas R, Blair KS, Blair JR, Hammoud MZ, Milad M, Burkhouse K, Phan KL, Schroeder HK, Strawn JR, Beesdo-Baum K, Thomopoulos SI, Grabe HJ, Van der Auwera S, Wittfeld K, Nielsen JA, Buckner R, Smoller JW, Mwangi B, Soares JC, Wu MJ, Zunta-Soares GB, Jackowski AP, Pan PM, Salum GA, Assaf M, Diefenbach GJ, Brambilla P, Maggioni E, Hofmann D, Straube T, Andreescu C, Berta R, Tamburo E, Price R, Manfro GG, Critchley HD, Makovac E, Mancini M, Meeten F, Ottaviani C, Agosta F, Canu E, **Cividini C**, Filippi M, Kostić M, Munjiza A, Filippi CA, Leibenluft E, Alberton BAV, Balderston NL, Ernst M, Grillon C, Mujica-Parodi LR, van Nieuwenhuizen H, Fonzo GA, Paulus MP, Stein MB, Gur RE, Gur RC, Kaczkurkin AN, Larsen B, Satterthwaite TD, Harper J, Myers M, Perino MT, Yu Q, Sylvester CM, Veltman DJ, Lueken U, Van der Wee NJA, Stein DJ, Jahanshad N, Thompson PM, Pine DS, Winkler AM. Mega-analysis methods in ENIGMA: The experience of the generalized anxiety disorder working group. Hum Brain Mapp. 2020 Jun 29. doi: 10.1002/hbm.25096. Epub ahead of print. PMID: 32596977.

Mega-analysis methods in ENIGMA: The experience of the generalized anxiety disorder working group

André Zugman ✉, Anita Harrewijn, Elise M. Cardinale, Hannah Zwiebel, Gabrielle F. Freitag, Katy E. Werwath, Janna M. Bas-Hoogendam, Nynke A. Groenewold, Moji Aghajani ... **See all authors** ⌄

ABSTRACT

The ENIGMA group on Generalized Anxiety Disorder (ENIGMA-Anxiety/GAD) is part of a broader effort to investigate anxiety disorders using imaging and genetic data across multiple sites worldwide. The group is actively conducting a mega-analysis of a large number of brain structural scans. In this process, the group was confronted with many methodological challenges related to study planning and implementation, between-country transfer of subject-level data, quality control of a considerable amount of imaging data, and choices related to statistical methods and efficient use of resources. This report summarizes the background information and rationale for the various methodological decisions, as well as the approach taken to implement them. The goal is to document the approach and help guide other research groups working with large brain imaging data sets as they develop their own analytic pipelines for mega-analyses.

9) Migliaccio R, Agosta F, Basaia S, **Cividini C**, Habert MO, Kas A, Montembeault M, Filippi M. Functional brain connectome in posterior cortical atrophy. Neuroimage Clin. 2020;25:102100. doi: 10.1016/j.nicl.2019.102100. Epub 2019 Nov 20. PMID: 31865020; PMCID: PMC6931188.

ELSEVIER

NeuroImage: Clinical

Volume 25, 2020, 102100

NeuroImage: CLINICAL

Functional brain connectome in posterior cortical atrophy

Raffaella Migliaccio [a, b] ✉, Federica Agosta [c], Silvia Basaia [c], Camilla Cividini [c], Marie-Odile Habert [d, e], Aurélie Kas [d, e], Maxime Montembeault [f], Massimo Filippi [c, g]

ABSTRACT

This study investigated the functional brain connectome architecture in patients with Posterior Cortical Atrophy (PCA). Eighteen PCA patients and 29 age- and sex- matched healthy controls were consecutively recruited in a specialized referral center. Participants underwent neurologic examination, cerebrospinal fluid (CSF) examination for Alzheimer's disease (AD) biomarkers, cognitive assessment, and brain MRI. For a smaller subset of participants, FDG-PET examination was available. We assessed topological brain network properties and regional functional connectivity as well as intra- and inter-hemispheric connectivity, using graph analysis and connectomics. Supplementary analyses were performed to explore the association between the CSF AD profile and the connectome status, and taking into account hypometabolic, atrophic, and spared regions (nodes). PCA patients showed diffuse functional connectome alterations at both global and regional level, as well as a connectivity breakdown between the posterior brain nodes. They had a widespread loss of both intra- and inter-hemispheric connections, exceeding the structural damage, and including the frontal connections. In PCA, connectome alterations were identified in all the brain nodes irrespectively of their structural and metabolic classification and were associated with a connectivity breakdown between damaged and spared areas. Taken together, these findings suggest the potentially high sensitivity of graph-analysis and connectomic in capturing the progression and maybe early signs of neurodegeneration in PCA patients.

10) Filippi M, Spinelli EG, **Cividini C**, Agosta F. Resting State Dynamic Functional Connectivity in Neurodegenerative Conditions: A Review of Magnetic Resonance Imaging Findings. Front Neurosci. 2019 Jun 20;13:657. doi: 10.3389/fnins.2019.00657. PMID: 31281241; PMCID: PMC6596427.

Resting State Dynamic Functional Connectivity in Neurodegenerative Conditions: A Review of Magnetic Resonance Imaging Findings

Massimo Filippi[1,2,3*], Edoardo G. Spinelli[1], Camilla Cividini[1] and Federica Agosta[1,3]

[1]Neuroimaging Research Unit, Institute of Experimental Neurology, Division of Neuroscience, IRCCS San Raffaele Scientific Institute, Milan, Italy
[2]Neurology Unit, IRCCS San Raffaele Scientific Institute, Milan, Italy
[3]Vita-Salute San Raffaele University, Milan, Italy

ABSTRACT

In the last few decades, brain functional connectivity (FC) has been extensively assessed using resting-state functional magnetic resonance imaging (RS-fMRI), which is able to identify temporally correlated brain regions known as RS functional networks. Fundamental insights into the pathophysiology of several neurodegenerative conditions have been provided by studies in this field. However, most of these studies are based on the assumption of temporal stationarity of RS functional networks, despite recent evidence suggests that the spatial patterns of RS networks may change periodically over the time of an fMRI scan acquisition. For this reason, dynamic functional connectivity (dFC) analysis has been recently implemented and proposed in order to consider the temporal fluctuations of FC. These approaches hold promise to provide fundamental information for the identification of pathophysiological and diagnostic markers in the vast field of neurodegenerative diseases. This review summarizes the main currently available approaches for dFC analysis and reports their recent applications for the assessment of the most common neurodegenerative conditions, including Alzheimer's disease, Parkinson's disease, dementia with Lewy bodies, and frontotemporal dementia. Critical state-of-the-art findings, limitations, and future perspectives regarding the analysis of dFC in these diseases are provided from both a clinical and a technical point of view.